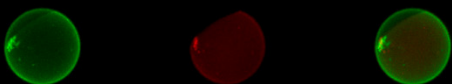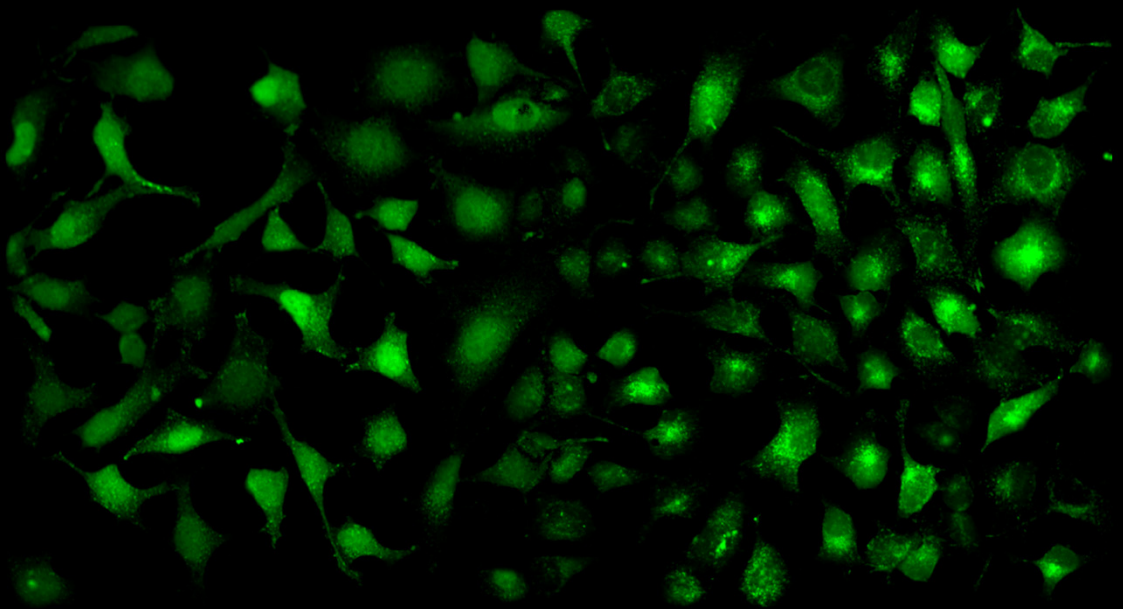# Delivery of small nucleic acids by conjugation to carbohydrates and lipids as novel research and therapeutic tools
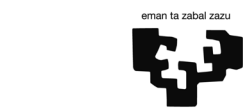
Begoña Ugarte Uribe

Doctoral Thesis, Leioa 2012

Doctoral thesis

Delivery of small nucleic acids
by conjugation to carbohydrates and lipids
as novel research and therapeutic tools

Begoña Ugarte Uribe

Supervisor: Prof. Miren Itziar Alkorta Calvo

Leioa, 2012

Acknowledgements / Esker onak:

First and foremost, I would like to thank my tutor, Prof. Itziar Alkorta, for providing me with numerous opportunities to enhance my knowledge and professional skills. I am thankful for her guidance, support and patience throughout the duration of my research. I would like to express my deep and sincere gratitude to Prof. Félix Mª Goñi and Prof. Alicia Alonso Izquierdo for giving me the chance to enter the world of Science when I was still a Biochemistry student and for their understanding and valuable assistance during the thesis.

I am deeply grateful to Dr. Juan Carlos Morales (Instituto de Investigación Biomédica, Sevilla, Spain), Prof. Ramón Eritja and Dr. Santiago Grijalvo (Instituto de Química Avanzada de Cataluña, Barcelona, Spain) for their continuous help, support and productive collaboration. I would also like to thank Dr. Alfredo Berzal Hérranz, Dr. Cristina Romero and Dr. José Reyes (Instituto de Parasitología y Biomedicina "López-Neyra"-CSIC, Granada, Spain) for teaching me cell culture techniques and for their contribution to this project.

I am also very grateful to Prof. Cesar Martín and Dr. Jon Busto for aiding me in the development of my experiments and for their advice, thoughtful comments, suggestions and wonderful friendship.

"...iragan hau guztia betiko izango genuela aurretik…"

Gorka Urbizu

Contents

iii

Index of figures

Index of tables

Abbreviations

2'-MOE-RNA	2'-O-methoxyethyl RNA
2'-OMe-RNA	2'-O-methyl RNA
3'UTR	3'-untranslated region
AAV	adeno-associated virus
AFM	atomic force microscopy
Ago2	Argonaute 2 protein
AIDS	acquired immunodeficiency syndrome
Alexa 488	Alexa Fluor 488
AMO	anti-miRNA oligonucleotide
AntiGEM91	Complementary sequence to GEM91
ASGP-R	asialoglycoprotein receptor
AS-ON	antisense oligonucleotide
BSA	bovine serum albumin
Chol	cholesterol
Clathrin HC	clathrin heavy chain
CMV	cytomegalovirus
COC	carbohydrate-oligonucleotide conjugate
CpG	cytosine phosphate guanine motif
CPP	cell-penetrating peptides
CPZ	chlorpromazine
Cy5	Cyanine dye 5
Cyt D	cytochalasin D
DB	double dendrimer
DMA	5-(N,N-dimethyl)amiloride

DMEM	Dulbecco's modified Eagle's medium
DMSO	dimethyl sulfoxide
DNA	deoxyribonucleic acid
dNMP	deoxyribonucleoside-5'-monophosphate
DOPC	1,2-dioleyl-L-α-phosphatidylcholine
DOPE	1,2-dioleoyl-*sn*-glycero-3-phosphatidylethanolamine
DOTAP	1,2-oleoyl-3-trimethylammonium propane
DOTMA	N-[1-(2,3-dioleoxy)propyl]-N,N,N-trimethylammonium chloride
DPBS	Dulbecco's Phosphate Buffered Saline
dsRNA	double-stranded RNA
EDTA	ethylenediaminetetraacetic acid
ER	endoplasmic reticulum
eSM	egg sphingomyelin
FBS	fetal bovine serum
FDA	Food and Drug Administration
FL	fluorescent detector
FSC	forward scatter
G-4	G-quadruplex
GAPDH	Glyceraldehyde 3-phosphate dehydrogenase
GEM91	gene-expression modulator 91
GLUT	glucose transporter
GMFI	geometric mean of fluorescence intensity
GUV	giant unilamellar vesicle
HIV-1	human immunodeficiency virus type 1
HRP	horseradish peroxidise

HSC	hepatic stellate cell
L$_d$	liquid-disordered lamellar lipid phase
LNA	locked nucleic acids
L$_o$	liquid-ordered lamellar lipid phase
LOC	lipid-oligonucleotide conjugate
LUV	large unilamellar vesicle
M6P/IGF-II	mannose 6-phosphate/insulin-like growth factor II
M6PR	mannose 6 phosphate receptor
miRNA	microRNA
MLV	multilamellar vesicle
MOD	morphological domain
mRNA	messenger RNA
MTS	3-(4,5-dimethylthiazol-2-yl)-5-(3-carboxymethoxyphenyl)-2-(4-sulfophenyl)-2H-tetrazolium
ODN	oligodeoxynucleotide
pAMAM	polyamidoamine
PAMP	pathogen-associated molecular pattern
PBS	phosphate buffered saline
PCR	polymerase chain reaction
PDMAEMA	poly(dimethylamino-ethylmethacrylate)
PEG	polyethyleneglycol
PEI	poly(ethyleneimine)
PFA	paraformaldehyde
PLGA	poly(lactic-*co*-glycolic acid)
PLL	poly-L-lysine

PMO	morpholino phosphoroamidates
PMS	phenazine methosulfate
PMSA	prostate-specific membrane antigen
PNA	peptide nucleic acids
pre-miRNA	precursor miRNA
pre-mRNA	precursor mRNA
PS	phosphorothioate
PTMAEMA	poly(trimethylaminoethylmethacrylate)
RGD motif	arginine-glycine-aspartic acid motif
RISC	RNA-induced silencing complex
RNA	ribonucleic acid
RNAi	RNA interference
RT	room temperature
SDS-PAGE	SDS polyacrylamide gel electrophoresis
SE	stabilising element
shRNA	short hairpin RNA
siRNA	small interfering RNA duplex
s-Lex	syalyl Lewis X
SPB	supported planar bilayer
SSC	side scatter
ssDNA	single-stranded DNA
ssRNA	single-stranded RNA
SUV	small unilamellar vesicle
TA	translational activator
TBS	Tris-buffered saline

TBST	TBS supplemented with 0.1% (w/v) Tween 20
TF	transcription factor
TF-FITC	transferrin-FITC
TFO	triple helix forming oligonucleotides
TLR9	Toll-like Receptor

Abstract

Abstract

The ability of small nucleic acids to silence specific genes or inhibit the biological activity of specific proteins has generated great interest in their use as research tools and therapeutic agents. Unfortunately, biological applications of oligonucleotides meet with a huge limitation: their poor cellular accessibility. Thus, there is a big challenge for developing an appropriate delivery system in order to achieve their efficient cellular uptake.

Conjugation of appropriate molecules to small nucleic acids is advantageous over structural modifications because it could not only promote target specificity, but also improve their pharmacokinetic behaviours and cellular uptake efficiencies, endowing them with entirely new properties. In the present work different carbohydrate- and lipid-oligonucleotide conjugates have been studied as novel tools for targeted delivery and enhancement of cellular permeability.

According to the results obtained in this work, it was concluded that keeping a certain distance (15 to 18 atoms) between DNA and sugar modification could be important for a better incorporation of this type of conjugates into the target cell, being a useful requirement for further promising conjugate design. It was also confirmed that long or double-tailed lipid modifications are preferred for an enhanced incorporation into membrane-model and cell systems, being dual saturated lipid neighbouring modification (C_{28}) capable of inserting into both liquid-disordered and liquid-ordered phases of lipid bilayer systems. Interestingly, C_{28} lipid moiety provided efficient cellular incorporation mainly by macropinocytosis, without causing cytotoxicity in cells or altering the binding properties of the oligonucleotide part, thereby enabling binding to different molecules. All these features make C_{28} moiety a good conjugation candidate to be analysed in a wide range of nucleic acid-based molecules for improving oligonucleotide delivery.

3

Chapter 1:

General introduction and objectives

Chapter 1: General introduction and objectives

1.1 DNA molecule

DNA is the universal molecule responsible for genetic information storage. This information is faithfully passed on to the next generation of cells or organisms by a process called replication, where the double helical DNA unwinds and creates a copy of itself. Subsequently, this genetic information is transferred through two consecutive steps from DNA to RNA and finally to proteins through a process known as gene expression. The passage from DNA to RNA is called transcription, a process where an enzyme system converts the genetic information from a segment of double-stranded DNA into an RNA strand with a base sequence complementary to one of the DNA strand (Nelson and Cox, 2008). The degree of complexity increases from prokaryotic to eukaryotic cells where the new synthesised RNA molecule (precursor mRNA) suffers intron splicing in order to remove these non-coding regions to produce the mature RNA. Then, during the second step named translation, mRNA is decoded by the ribosome in the cytoplasm to produce a specific amino acid chain, or polypeptide, that will later fold into a mature protein (Klug *et al.*, 2008) (Figure 1.1).
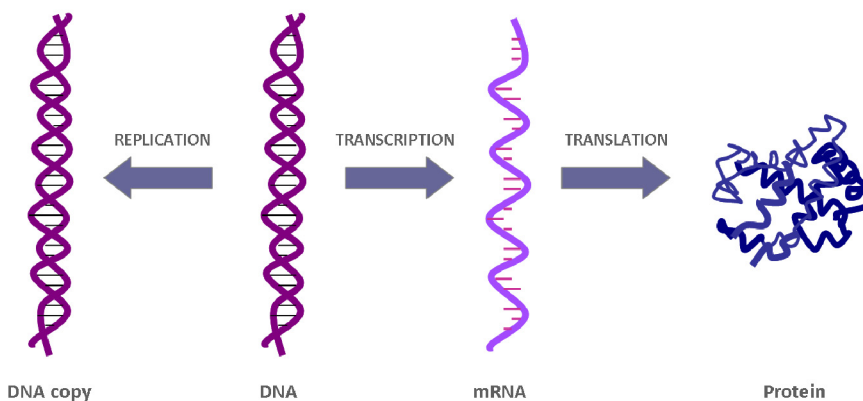
Figure 1.1 Processing of genetic information in biological systems. This figure was modified from Singh *et al.* (2010).

1.1.1 A walk through history: Revolutionary discoveries in DNA/RNA field

In 1977, Paterson and co-workers showed that an exogenous oligodeoxynucleotide (a short fragment of DNA) with a complementary sequence of targeted mRNA was able to stop the protein translation process in a very specific manner, uncovering a novel mechanism to modify gene expression (Paterson *et al.*, 1977). Only a year later, Zamecnik and Stephenson demonstrated that short oligodeoxynucleotides could be used to inhibit the development of Rous sarcoma virus in viral infected cell cultures, either at viral RNA translation level (Stephenson and Zamecnik, 1978) or at virus replication level (Zamecnik and Stephenson, 1978). Since then, many studies were carried out using synthetic oligodeoxynucleotides (ODNs) in order to inhibit protein synthesis of a targeted mRNA and in many occasions successful data were obtained (Coppelli and Grandis, 2005).

Prior to 1980, RNA was still viewed as a mere inert nucleic acid intermediate for protein production. But a dramatic change in its perception came about in the early 1980s with the discovery of catalytic RNAs or ribozymes, capable of cleaving the target sequence without the need of additional enzymes (Cech *et al.*, 1981; Guerrier-Takada *et al.*, 1983). Regarding these data, in 1994 catalytic DNAs or DNAzymes were also found to cleave specific RNA molecules (Breaker and Joyce, 1994).

In 1998, Fire and co-workers discovered another naturally occurring biological strategy for targeting mRNA when they injected long double-stranded RNA (dsRNA) into *Caenorhabditis* elegans, which lead to efficient sequence-specific gene silencing (Fire *et al.*, 1998). As a result of this work, they coined the term RNA interference (RNAi) that was particularly notable because it represented the first identification of the causative agent for the phenomenon. These data were useful to explain earlier observations in petunias which turned white rather than purple upon the introduction of the gene responsible for the purple colour in form

of dsRNA (Napoli *et al.*, 1990). In 2001, Elbashir and collaborators reported that small interfering RNA duplexes (siRNAs) were able to knockdown the expressed gene target specifically in either *Drosophila melanogaster* embryo lysate or in cultured mammalian cells (Elbashir *et al.*, 2001a, 2001b). Indeed, they demonstrated that siRNA was the effector molecule in RNAi inside the cell (Figure 1.2).
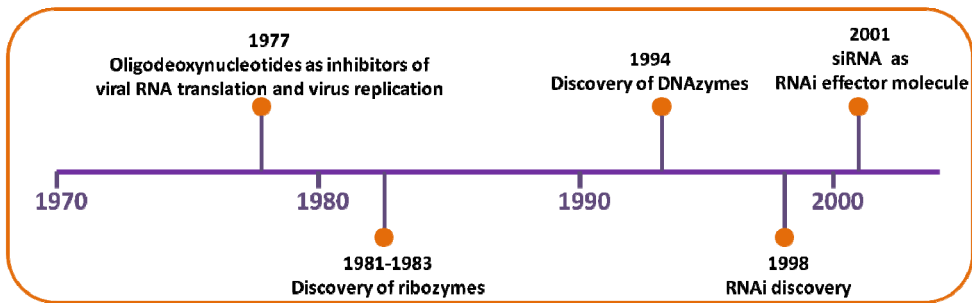
Figure 1.2 Representative timeline based on revolutionary discoveries in DNA/RNA field.

1.2 Nucleic acid based strategies

All the aforementioned revolutionary findings have led to the design of various classes of oligonucleotides which focus in different nucleic-acid based strategies such as modulation of gene expression, silencing miRNA, inhibition of protein function and immunostimulation.

1.2.1 Modulation of gene expression

To date, there are several promising nucleic acid based strategies for modulating gene expression. These gene silencing strategies can be divided in two groups, depending on the target molecule, which can be the genomic DNA or mRNA (Kalota *et al.*, 2004).

1.2.1.1 Genomic DNA as target molecule

This strategy also known as <u>antigene mechanism</u> is based on disrupting the transcription of genes targeting the genomic DNA, using either triple helix forming oligonucleotides or DNA decoys.

<u>Triple helix forming oligonucleotides</u>

<u>Triple helix forming oligonucleotides</u> (TFOs) are single-stranded oligonucleotides (10-30 nucleotides in length) that hybridise to the purine or pyrimidine-rich region in the major groove of double-helical DNA in a sequence-specific manner, forming triple helices through Hoogsteen base pairing. Thus, they either prevent the unwinding of the double-stranded DNA, necessary for transcription of the targeted region or block the binding of transcription factor complexes (Praseuth *et al.*, 1999) (Figure 1.3A). In fact, it has been observed that TFOs are able to inhibit the transcription of specific genes either *in vitro* or *in vivo* (Cooney *et al.*, 1988; Postel *et al.*, 1991; Grigoriev *et al.*, 1993; Kim and Miller, 1995; Kim *et al.*, 1998).

<u>DNA decoys</u>

<u>DNA decoys</u> are short double-stranded oligodeoxynucleotides that compete with endogenous DNA for attracting specific transcription factors. Consequently, the transcription factor that is retained by these molecules is unable to execute its function, which results in a decrease in the rate of transcription of genes dependent on the sequestered transcription factor (Morishita *et al.*, 1998; Tomita *et al.*, 2003) (Figure 1.3B).
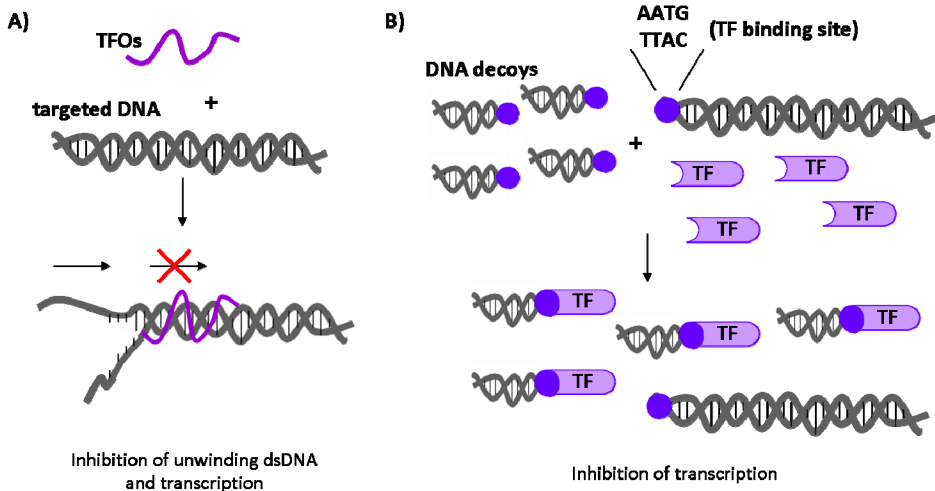
Figure 1.3 Strategies to disrupt the transcription of genes by targeting the genomic DNA in the nucleus. A) Triple helix forming oligonucleotides (TFOs) can bind to dsDNA thereby blocking its unwinding and subsequent transcription. B) DNA decoys can bind to transcription factors (TF) and inhibit transcription by decreasing the accessibility of TF for genomic DNA. This figure was modified from Kalota *et al.* (2004).

1.2.1.2 mRNA as target molecule

The second group of gene silencing strategies is based on destabilising mRNA or preventing its translation by direct targeting mRNA. It comprises three different mechanisms of action, depending on the effector molecule used.

<u>RNA decoys</u>

The first mechanism is similar to the strategy of DNA decoys, in fact <u>RNA decoys</u> (short double-stranded oligonucleotides) are designed to provide alternative competing binding sites for proteins that act as mRNA-stabilising elements or translational activators. As a result, target protein synthesis is hindered and there is an induction of instability that ends up with the destruction of the mRNA (Opalinska and Gewirtz, 2002) (Figure 1.4).
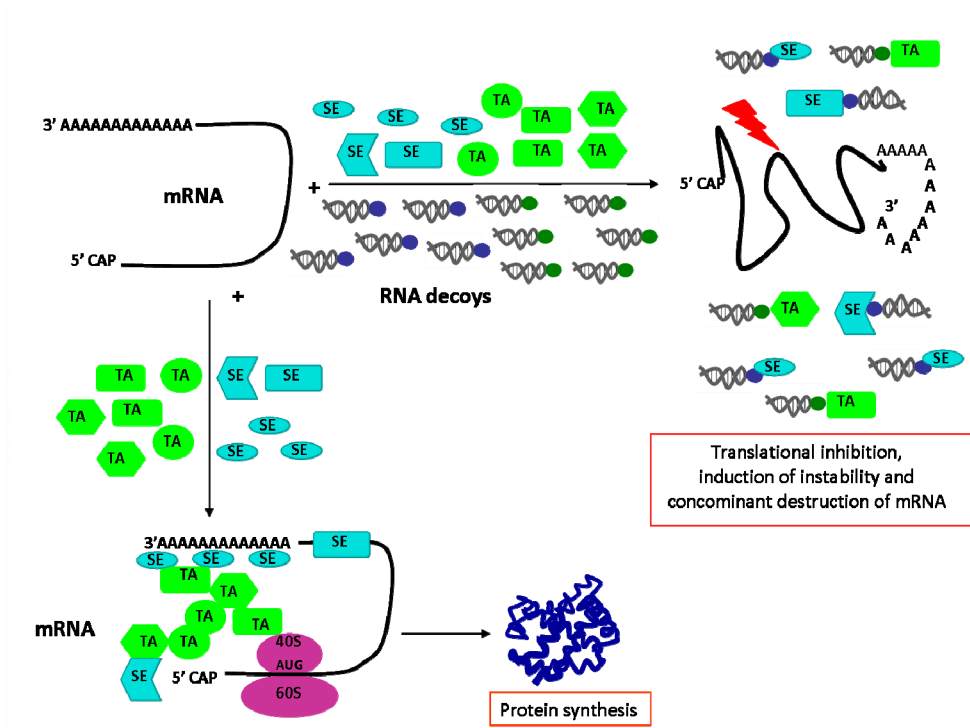
Figure 1.4 Mechanism of action of RNA decoys. RNA decoys can bind to mRNA stabilising elements (SE) or translational activators (TA), inducing translation inhibition and mRNA instability, associated with subsequent destruction of the mRNA. In this diagram RNA decoys in blue have specific binding sites for SE and RNA decoys in green have specific binding sites for TA. In the figure the ribosome subunits are represented as 40S and 60S and translation initiation point as AUG codon.

Antisense oligonucleotides

The second mechanism is also known as antisense mechanism and is the most investigated approach (Figure 1.5). It is based on the recognition of a specific region of mRNA by so-called antisense oligonucleotides (AS-ON), leading to a translation arrest through a complementary Watson-Crick base pair hybridisation (Juliano *et al.*, 2008). These AS-ONs can be composed of DNA or RNA molecules which are typically 15-30 nucleotides in length (Mahato *et al.*, 2005). At the

moment, there are two main hypotheses to explain the mechanism of action of AS-ONs. The first hypothesis suggests that after complementary hybridisation between AS-ON and target mRNA, expression is blocked by a steric hindrance effect that interferes with the translation machinery. In this theory it is assumed that the 40S ribosomal subunit is blocked by the heteroduplex, obstructing the progression of the ribosome along the mRNA. In fact, this effect has been mostly observed when the target region of the mRNA is the 5' untranslated region (Augustine, 1997). In the nucleus of eukaryotic cells, these steric-blocker oligonucleotides can also physically prevent or inhibit the progression of the splicing machinery which is necessary to mature precursor mRNA (pre-mRNA). On the contrary, the second hypothesis defends the idea of an enzyme-mediated mRNA degradation through RNase H dependent mechanism. When the heteroduplex is formed by the specific hybridisation between AS-ON and the specific region of the mRNA, RNase H is able to recognise this heteroduplex, thereby causing its cleavage in a specific manner with the subsequent degradation of the RNA strand. In cells, this enzyme plays a pivotal role during DNA replication since it is responsible for the degradation of the Okazaki's fragments (Donis-Keller, 1979) (Figure 1.5B).

Moreover, AS-ONs can be designed to contain catalytic activity, where the oligomers of RNA form ribozymes and the oligomers of DNA yield DNAzymes (Gewirtz, 2000). These catalytic molecules can also bind to their target transcript through Watson-Crick base pairing and cleave it in a sequence-specific manner without the aid of protein-enzymes (Opalinska and Gewirtz, 2002). Noteworthy, once the RNA strand is cleaved, the resulting products dissociate from the active complex and the ribozyme or DNAzyme is then free and ready to bind to another target sequence, repeating the same mechanism of action (Usman and Blatt, 2000). In particular, ribozymes are the most studied catalytic nucleic acids. Their catalytic moiety recognises a specific nucleotide sequence, GUX, where X= C, U or A (Ruffner *et al.*, 1989) or in some cases, NUX, where N is any nucleotide (Xing and Whitton, 1992). At least five major catalytic motifs are derived from naturally occurring ribozymes, but only two of them, hammerhead and hairpin, have

attracted attention since they are relative small and simple and are capable to bind to a number of flanking sequence motifs without changing site-specific cleavage capacities (Sun *et al.*, 2000) (Figure 1.5C).
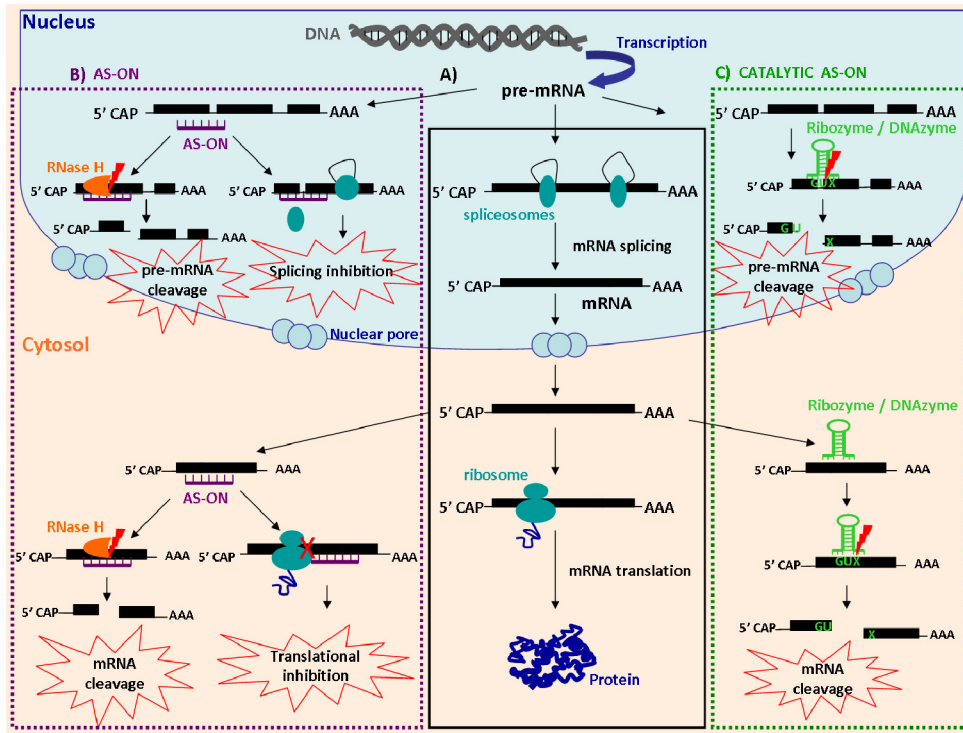
Figure 1.5 Some of the mechanisms of action implicated in the specific inhibition of gene expression in eukaryotic cells: A) Steps required for protein synthesis; B) AS-ON molecules recognise their target and (i) activate RNase H to cleave it in a specific manner or (ii) produce an steric hindrance effect interfering with slicing or translational machinery; C) Catalytic AS-ONs: Ribozymes and DNAzymes recognise and cleave their target molecule without the need of auxiliary enzymes.

RNA interference

Finally, the third mechanism is RNA interference (RNAi) which has hitherto generated the most interest (Figure 1.6). This natural process that occurs in eukaryotic cells can be roughly divided into two phases, that is, the initiation phase and the effector phase. The initiation phase starts with the recognition of long dsRNA (500-1000 nucleotides) by an enzyme termed Dicer (RNase III protein), which is the responsible for cleaving this substrate into duplexes of 21-23 nucleotides (Hamilton and Baulcombe, 1999; Zamore *et al.*, 2000; Bernstein *et al.*, 2001; Elbashir *et al.*, 2001a). Dicer can also recognise and cleave short hairpin RNAs (shRNAs) that are synthesised by RNAi expression vectors rendering also RNA duplexes of 21-23 nucleotides. These RNA products are called small interfering RNAs (siRNAs) that contain a symmetric two nucleotides overhang at the 3'-ends as well as a 5'-phosphate group and unphosphorylated hydroxyl groups at the 2' and 3'-sites (Elbashir *et al.*, 2001b; Elbashir *et al.*, 2001c; Putnam and Doody, 2006). The siRNA structure is characteristic of Dicer-like pattern and plays a crucial role in its recognition by other RNAi components. In the next phase, these effector siRNAs are incorporated to the RNA-induced silencing complex (RISC). Due to thermodynamic conditions, only one of the strands of siRNA, so-called the guide strand or antisense strand, interacts with RISC. In mammalian cells, the protein Argonaute 2 (Ago2) is the catalytic component of RISC that cleaves target mRNA (Liu *et al.*, 2004; Meister *et al.*, 2004). In the RISC assembly process, siRNA duplexes are initially loaded to Ago2 and then this protein cuts the passenger strand (or sense strand), thereby producing active RISC ready to cleave its target (Matranga *et al.*, 2005; Leuschner *et al.*, 2006). The guide strand retained by RISC serves as a template for specific recognition of the targeted mRNA based on complementary Watson-Crick base-pairing mechanism.

Depending on the complementarity degree between the nucleotide sequences of the guide strand and the target mRNA, two post-transcriptional events can occur. When the <u>guide strand matches exactly</u> with its target, RISC cleaves the mRNA between bases 10 and 11 relative to the 5'-base of the guide strand thanks to the endonucleolytical activity of Ago2 (Elbashir *et al.*, 2001a). Thus, the generation of unprotected RNA ends results in the rapid degradation of the mRNA molecule (Figure 1.6A). In this case, RISC can undergo several cycles of mRNA slicing because the template is not affected by this reaction, leading to a net reduction of the specific mRNA levels and hence to the decreased expression of the corresponding gene (Elbashir *et al.*, 2001c; Meister and Tuschl, 2004). In fact, it has been observed that siRNA molecules can silence their target mRNA almost 100 times more effectively than single-stranded AS-ONs (Miyagishi *et al.*, 2003), even though only the antisense strand of siRNA is incorporated in RISC (Martinez *et al.*, 2002).

Nevertheless, when the <u>guide strand presents mismatches</u> there is an induction of translation arrest which is not followed by mRNA cleavage. This event named bypass pathway is known to occur in cell foci implicated in the turnover of mRNA termed P-bodies (Tolia and Joshua-Tor, 2007; Kim and Rossi, 2007). Furthermore, it is typically induced by endogenous expression of small regulatory RNAs so-called microRNAs (miRNAs) which associate with RNAi machinery and suppress gene expression by binding to their target mRNAs, preferentially to the 3'-untranslated region (3'UTR) with a partial base-paring mechanism, inducing mRNA degradation and/or by preventing mRNA translation (Jackson *et al.*, 2003; Bartel, 2004, Baek *et al.*, 2008; Selbach *et al.*, 2008; Chekulaeva and Filipowicz, 2009) (Figure 1.6B). Apart from cell foci known as P-bodies, miRNAs have also been found in GW-bodies, exosomes, nucleus and mitochondria (Hwang *et al.*, 2007; Valadi *et al.*, 2007; Gibbings *et al.*, 2009; Kren *et al.*, 2009; Kulkarni *et al.*, 2010; Torres *et al.*, 2012).
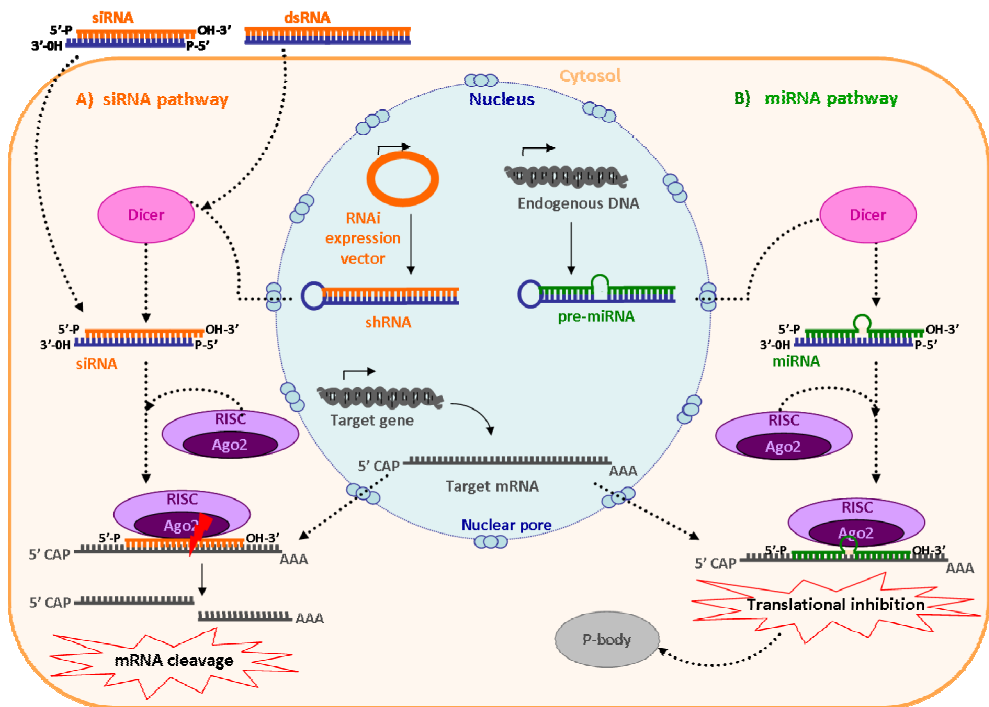
Figure 1.6 Mechanism of RNA interference (RNAi) in mammalian systems. A) RNAi expression vector produces short hairpin RNA (shRNA) which is cleaved by Dicer to generate small interference RNA (siRNA). Dicer can also cleave incorporated exogenous dsRNA to create siRNA. This step can be avoided introducing directly siRNA molecules into the cell. The RNA-induced silencing complex (RISC) can interact with the guide strand of siRNA (the orange strand) and recognise target mRNA. In this case, there is a total complementarity degree between the guide strand and target mRNA, leading to mRNA cleavage by a component of RISC named Ago2; B) Precursor microRNA (pre-miRNA) is synthesised endogenously and it is cleaved by Dicer to generate miRNA. Then, RISC uses the guide strand of miRNA (the green strand) to recognise target mRNA. The imperfect complementarity between the guide strand and target mRNA leads to a translational inhibition which is associated with the turnover of mRNA termed P-bodies.

Depending on the degree of complementarity with the target mRNA, siRNAs and miRNAs are found to be functionally interchangeable. Unfortunately, this is one of the reasons for the undesired down regulation of non-targeted transcripts by siRNAs, termed off-target effects (Jackson *et al.*, 2003; Bartel, 2004). These off-target effects can also be produced because not only the guide strand but also the passenger strand of an siRNA can direct gene silencing of non-target genes, since it has been documented to happen when as few as 15 bp of complementarity exists between them. These findings suggest a strong mechanistic parallelism between siRNA off-targeting and miRNA-mediated gene regulation (Jackson *et al.*, 2003).

When dsRNA is longer than 30 bp, it generally activates the interferon response in differentiated cells via the Protein Kinase-R pathway, which ends up promoting a widespread shut-off of protein synthesis, as well as non-specific mRNA degradation (Manche *et al.*, 1992; Elbashir *et al.*, 2001b; Kim and Rossi, 2007; Sen and Sarkar, 2007). This obstacle can be bypassed delivering siRNAs directly into the target cell, thereby omitting the initiation phase produced by Dicer.

1.2.2 Silencing miRNA: Anti-miRNA oligonucleotides

A novel class of chemically engineered oligonucleotides termed anti-miRNA oligonucleotides (AMOs) have also been designed to silence miRNA in a specific manner (Weiler *et al.*, 2006; Lennox and Behlke, 2011). As mentioned above, miRNAs are an abundant class of endogenous non-coding RNA ranging from 20 to 23 nt of length that are post-transcriptional regulators of gene expression. Antagomirs, a type of AMOs, are single-stranded RNA analogs that harbor several modifications for RNase protection and pharmacologic properties such as enhanced tissue and cellular uptake. They differ from normal RNA by complete 2'-O-methylation of sugar, phosphothioate backbone and a cholesterol moiety at 3'-end. Although antagomirs are complementary to their miRNA sequence, they can discriminate between single nucleotide mismatches of the

targeted miRNA. Owing to the specific binding between antagomir and its target miRNA, miRNA function is inhibited, thereby downregulating the translation of proteins specifically predicted to be controlled by the respective silencing miRNA (Figure 1.7). Degradation of different chemically protected miRNA/antagomir duplexes in mouse livers and localisation of antagomirs in a cytosolic compartment that is distinct from P-bodies indicates a degradation mechanism independent of the RNAi pathway (Krützfeldt *et al.*, 2005, 2007).
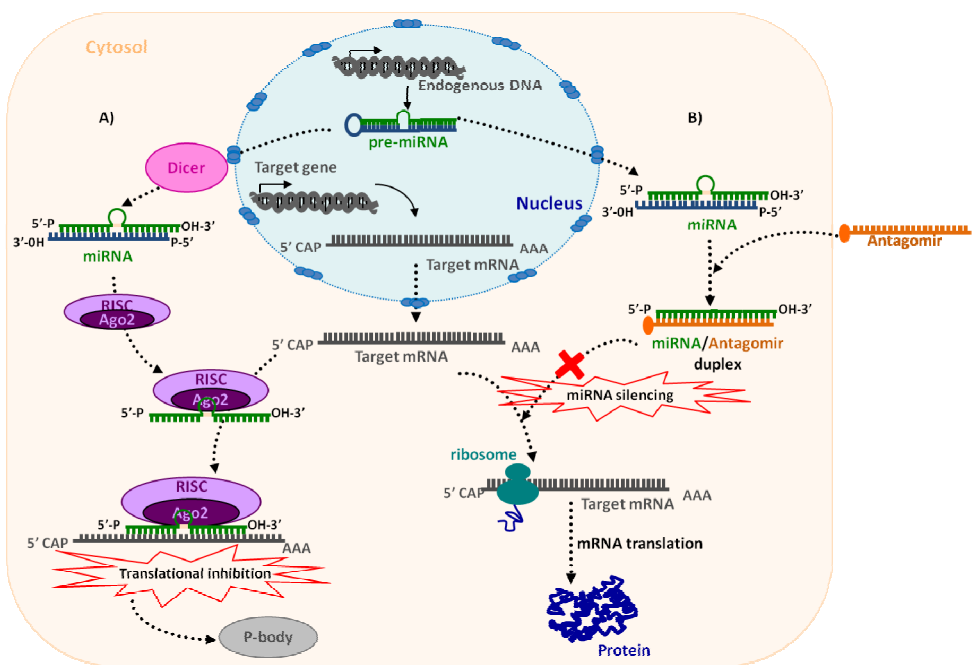
Figure 1.7 Silencing miRNA with a type of AMOs termed antagomirs. In general, mRNA levels are regulated by miRNA in the cell. A) Pre-miRNA is synthesised endogenously and it is cleaved by Dicer to generate miRNA. Then, RISC uses the guide strand of miRNA (the green strand) to recognise target mRNA. The imperfect complementarity between the guide strand and target mRNA leads to a translational inhibition which is associated with the turnover of mRNA termed P-bodies. B) Antagomirs bind to target miRNA, inducing miRNA silencing and providing mRNA translation to protein. Degradation of miRNA/antagomir duplex is RNAi independent.

1.2.3 Inhibition of protein function: Aptamers

The mechanism of <u>aptamers</u> is based on the capability of these molecules to form complex three-dimensional structures which efficiently recognise and bind targets from small molecules to proteins or nucleic acid structures in a very selective manner, thereby interfering with their biological activity (Figure 1.8). Aptamers are DNA or RNA-based oligonucleotides, 15-40 nucleotides in length, which are isolated from large combinatorial oligonucleotide libraries by *in vitro* selection (Famulok *et al.*, 2000). Like antibodies, they exhibit high specificity and affinity for target binding. Among several architectures, the G-quadruplex (G-4) is one of the most interesting structures adopted by aptamers, consisting in planar arrays of four guanines, where each guanine pairs with two neighbours by Hoogsteen bonding.
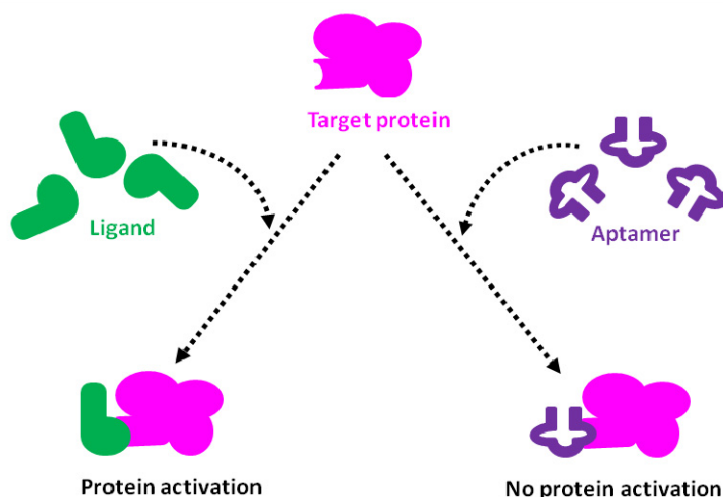
Figure 1.8 Binding mechanism of aptamer to its target protein. Aptamer binds to a domain on target protein's surface by its tertiary structure, interfering in protein's biological function.

1.2.4 Immunostimulation: CpG oligodeoxynucleotides

In the late 90's, several studies showed that short single-stranded DNA molecules (ssDNAs) that contained unmethylated cytosine phosphate guanosine (CpG) motifs could act as immunostimulants (Krieg *et al.*, 1995; Weiner *et al.*, 1997). Surprisingly, bacterial genome differs from vertebrate genome in that it contains an increased number of unmethylated CpG dinucleotides (Bauer and Wagner, 2002). Since CpG motifs are considered pathogen-associated molecular patterns (PAMPs), synthetic CpG ODNs have been developed to be used as adjuvants to induce robust humoral and cellular immune responses (Wagner, 2001; Krieg, 2002). These synthetic compounds have several modifications in order to enhance nuclease resistance and cellular uptake [partially or completely phosphorothioated (PS) backbone instead of the typical phosphodiester backbone and a poly G tail at either 3'-end or 5'-end, or both] (Dalpke *et al.*, 2002). This immunostimulatory effect is based on the interaction between CpG ODNs and Toll-like Receptor 9 (TLR9), which directly affects the function of macrophages, B cells, NK cells and dendritic cells, leading to the Type I pro-inflammatory response (Chu *et al.*, 1997; Trieu *et al.*, 2006).

1.3 Potential therapeutic agents for biological applications

The ability of some of these molecules to silence specific genes or inhibit the biological activity of specific proteins has generated great interest in their use as a research tool and therapeutic agent (Elsabahy *et al.*, 2011). Indeed, innapropriate gene expression is related to several pathologies which may include expression of genes that are "silent" or absent in normal cell, such as viral oncogenes, or overexpression of one or multiple genes, as in cancer (Takeshita and Ochiya, 2006; Whitehead *et al.*, 2009), infection and inflammation (Ponnapa, 2009), respiratory diseases (Garbuzenko *et al.*, 2009), neurological diseases (Davidson and Paulson, 2004) and autoimmune diseases (Hou *et al.*, 2009).

Moreover, miRNAs are proposed to regulate up to one-third of all human genes at the post-transcriptional level through a repression of protein from mature mRNA (Lewis *et al.*, 2005) and their role is gradually emerging in physiological and pathological processes such as differentiation and maintenance of cell identity in the hematopoietic system (Monticelli *et al.*, 2005; Garzon *et al.*, 2006), morphogenesis control of epithelial tissues (Yi *et al.*, 2006), regulation of organogenesis (Lu *et al.*, 2005; Zhao *et al.*, 2005) and metabolic processes (Krützfeldt *et al.*, 2005; Esau *et al.*, 2006). It has also been observed that viruses are able to encode miRNAs which seem to evolve rapidly and regulate both the viral life cycle and the interaction between viruses and their hosts (Nair and Zavolan, 2006). Overall, it is not surprising that different abnormal miRNA signatures have been identified in numerous disease states, as cancer, hepatitis C and diabetes, which could be used as important diagnostic and/or prognostic markers (Gregory and Shiekhattar, 2005; Lu *et al.*, 2005; Yanaihara *et al.*, 2006). Indeed, the modulation of miRNA activity by AMOs may contribute to the dissection of miRNA functions and putative roles in human disease processes, thereby providing therapeutic benefit (Esau *et al.*, 2006; Czech, 2006; Qi *et al.*, 2006; Shi *et al.*, 2011).

According to nucleic acid three-dimensional structure, it has been observed that the formation of quadruplex structures in telomeres (G-rich regions) as well as in non-telomeric regions, such as gene promoters, recombination sites and DNA tandem repeats, plays an important role in key biological processes as maintenance of telomeres and regulation of gene transcription (Sannohe and Sugiyama, 2010). G-quadruplex structures that form near or in promoter regions of several proto-oncogenes or in telomeres have particular interest in the development of anticancer therapies since these structures could be useful to block transcription of oncogenes or to decrease the activity of telomerase enzyme, which is responsible for maintaining the length of telomeres and is involved in around 85% of all cancers

(Siddiqui-Jain *et al.*, 2002; Sun *et al.*, 2005; Fernando *et al.*, 2006; Guo *et al.*, 2007; Palumbo *et al.*, 2008).

On the other hand, it is also known that CpG ODNs act as immunostimulants. As a result, these synthetic compounds can be used as potent vaccine adjuvants, as well as therapeutic agents for the treatment of autoimmune diseases or cancers (Fonseca and Kline, 2009; Lubaroff and Karan, 2009; Weiner, 2009; Goodchild, 2011).

Even with our current extensive information regarding the human transcriptome, development of nucleic acid-based therapeutics represents an enormous challenge, and only a few candidate compounds have made it to clinical trials (Singh *et al.*, 2010). The limited application of these therapeutic agents in clinics has been attributed to their unfavourable pharmacokinetic and pharmacodynamic properties (Crooke, 2004). Indeed, biological applications of oligonucleotides meet with two main limitations, which are stability and accessibility.

1.4 Main problems in nucleic acid based therapies

Stability problem is associated with nuclease sensitivity as natural oligonucleotides can be rapidly degraded either in biological fluids or inside the cell before reaching their intended target. Exonucleases and endonucleases can cleave these compounds at the phosphodiester bonds, usually via $3' \rightarrow 5'$ activity (Wickstrom, 1986; Akhtar *et al.*, 1991; Eder *et al.*, 1991). Besides, generated degradation products, deoxyribonucleoside-5'-monophosphate (dNMP) mononucleotides, may show cytotoxic and antiproliferative effects (Vaerman *et al.*, 1997). The latter consequence can be correlated with mononucleotide dephosphorylation by the cell surface enzyme ecto-5'-nucleotidase which dephosphorylates dNMP to the corresponding nucleoside, leading to the functional inhibition of critical proteins involved in cell growth (Koziolkiewicz *et al.*, 2001).

23

Although native oligonucleotides show very short half-lives *in vivo*, there are stability differences depending on the type of sugar or the number of strands present in the molecule. For instance, the phosphodiester backbone of RNA is more sensitive to hydrolysis than in DNA and also siRNA duplexes are much more stable than single-stranded RNAs (ssRNAs) due to intramolecular hybridisation (Chen *et al.*, 2005; De Paula *et al.*, 2007).

The second and most important obstacle is cellular accessibility. Phospholipid bilayers represent a strong barrier for the highly negative charged phosphodiester backbone of the oligonucleotides. As a result, they show an extremely poor penetration across the cell membrane mainly induced by a large charge repulsion derived from their polyanionic nature. This is a crucial step since these molecules have to reach the nucleus or the cytoplasm to meet their target and guarantee a correct and successful antisense activity (Lemaitre *et al.*, 1987; Alahari *et al.*, 1998).

1.5 Improvements in nuclease resistance: Chemical modifications

To date, a variety of chemical modifications have been performed in the nucleotide moiety in order to resolve the problem of nuclease degradation, thereby improving oligonucleotide stability in biological media. According to this approach, these modifications range from changes in the overall electronic charge of the molecule to the incorporation of non-phosphate oligonucleotide backbones. In addition, they can be used to control pharmacokinetic profiles of the molecules and reduce non-specific effects without affecting their biological activity. In general, they are commonly classified into three generations (Figure 1.9): i) analogs with altered phosphate backbones, ii) modified sugars (especially at the 2'position of the ribose), and iii) unnatural bases (Kurreck, 2003).
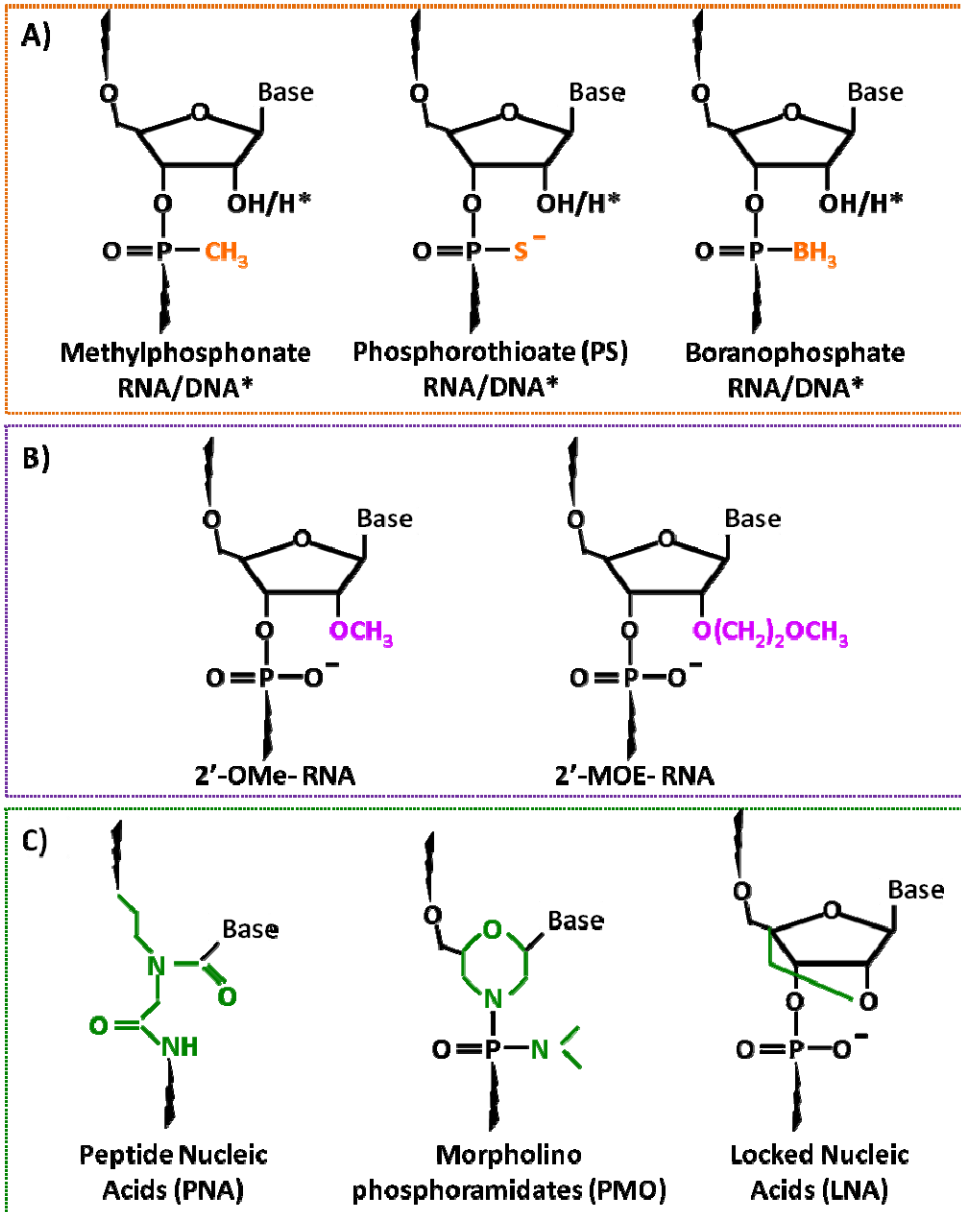
Figure 1.9 Three generations of chemical modifications. A) First generation oligonucleotides; B) Second generation oligonucleotides; C) Third generation oligonucleotides.

The principal representatives of first generation DNA/RNA analogs are phosphorothioate (PS) oligonucleotides. In PS linkages one of the two non-bridging oxygen atoms in the phosphodiester bond is replaced by a sulfur atom. They were first synthesised in the 1960s by Eckstein and colleagues and were first used to inhibit HIV replication by Matsukura and co-workers (De Clercq *et al.*, 1969; Matsukura *et al.*, 1987). They provide relative nuclease resistance, negative charge, regular Watson-Crick base pairing, activation of RNase H and attractive pharmacokinetic properties (Crooke, 2000).

Furthermore, PS oligonucleotides have been studied in several disease models, both *in vivo* and *in vitro*, with promising results (Crooke, 2000). The first PS antisense drug approved by Food and Drug Administration (FDA) was Formivirsen (Vitravene) from Isis (Carlsbad, CA, USA) and it was used in the treatment of inflammatory viral infection of the eye (retinitis) caused by cytomegalovirus (CMV) in immunocomprised patients, including those with acquired immunodeficiency syndrome (AIDS), but it was later withdrawn from the market (Opalinska and Gewirtz, 2002).

Despite PS oligonucleotides are widely used in several laboratory settings and outgoing clinical trials, they have many properties which render them suboptimal antisense effector molecules. This is due to their ability to bind to numerous cellular proteins, especially heparin-binding growth factors, which in turn induces non-specific effects and may cause cytotoxicity (Brown *et al.*, 1994; Fennewald and Rando, 1995; Guvakova *et al.*, 1995; Benimetskaya *et al.*, 1997; Rockwell *et al.*, 1997; Gewirtz *et al.*, 1998; Hogrefe, 1999; Levin, 1999; Amarzguioui *et al.*, 2003; Manoharan, 2004; Mahato *et al.*, 2005). Another shortcoming of PS oligonucleotides is the fact that they present a slightly reduced affinity towards complementary target molecule, although it is compensated by an enhanced specificity of hybridisation, compared with unmodified oligonucleotides (Crooke, 2000).

Another backbone modification of first generation is <u>boranophosphonate</u> linkage where the non-bridging oxygen is substituted by an isoelectronic borane (-BH$_3$) moiety. As a result, there is a polarity change in the resultant molecule which makes it more hydrophobic. As PS linkage, boranophosphonate modification improves stability of the molecule against nuclease degradation. Additionally, it has been observed that the activity of boranophosphonate oligonucleotides exceeds that of PS or unmodified oligonucleotides, regardless of the base or strand modified (Hall *et al.*, 2004).

1.5.2 Second generation molecules

In an attempt to overcome the various non-specific problems associated with first generation oligonucleotides, new chemical modifications were developed and classified as <u>second generation</u> oligonucleotides. The strategy for this generation of modified molecules is based on a wide variety of sugar modifications. The common modification is a replacement of the hydrogen at the 2' position of ribose by an O-alkyl, being the most important representatives <u>2'-O-methyl</u> (OMe) and <u>2'-O-methoxyethyl</u> (MOE) RNAs (Figure 1.9B). These compounds are more resistant to nuclease degradation and less toxic than PS oligonucleotides. They can even form high melting heteroduplex with their target inducing an RNase H independent antisense effect, probably as a result of interference with ribosomal assembly (Monia *et al.*, 1993; Baker *et al.*, 1997) or splicing machinery. The latter event can be an interesting approach since blocking of a splice site can increase the expression of an alternatively spliced protein variant, which is being developed for example to treat the genetic blood disorder β-thalassemia (Sierakowska *et al.*, 1996).

Nevertheless, for most antisense approaches, target RNA cleavage by RNase H was considered necessary to achieve desired antisense potency. Therefore, mixed backbone oligonucleotides were synthesised which comprise a PS modified deoxyribose core with 2'-OMe ribonucleosides at each end (Agrawal

and Zhao, 1998; Shen *et al.*, 1998). While the end blocks prevent nucleolytic degradation, the PS core of at least four or five deoxy residues is sufficient for activation of RNase H (Monia *et al.*, 1993; Crooke *et al.*, 1995; Wu *et al.*, 1999). These chimeric compounds were called gapmer oligonucleotides.

1.5.3 Third generation molecules

The latter category of modified nucleotides was designed in order to improve some important properties of the antisense oligonucleotides, such as nuclease resistance, target affinity and pharmacokinetics. These compounds were classified as third generation of antisense oligonucleotides and in their design the concept of conformational restriction was widely used to enhance binding affinity and biostability. These are DNA and RNA analogs with modified phosphate linkages, riboses or nucleotides with a completely different chemical moiety replacing the furanose ring. Peptide nucleic acids (PNA), morpholino phosphoroamidates (PMO) and locked nucleic acids (LNA) are the most promising candidates of this class (Figure 1.9C).

Instead of the natural phosphate-ribose backbone, PNAs possess an uncharged, flexible, polyamide backbone consist of repeating N-(2-aminoethyl)glycine units to which the nucleobases are bound via methylene carbonyl linkers (Nielsen *et al.*, 1991; Egholm *et al.*, 1993). They can also form very stable duplexes or triplexes, depending on the type of target molecule (single- or double-stranded DNA or RNA) (Jensen *et al.*, 1997).

In PMOs the riboside moiety of each subunit is converted to a morpholine moiety and the negative charged phosphodiester intersubunit linkage is replaced by uncharged phosphorodiamidate linkages (Summerton *et al.*, 1997; Heasman, 2002). They are very stable in biological systems and also form tight bonds with their target molecule (Hudziak *et al.*, 1996).

Both PNAs and PMOs represent a more radical approach to nuclease resistance problem since the phosphodiester linkage is completely replaced by a polyamide or phosphoramidate backbone. Due to their uncharged backbone they are unlikely to form undesired interactions with proteins that normally recognise polyanions, which are a major source of non-specific effects. In addition, it has been observed effective gene knock-down by PNA and PMO antisense molecules *in vivo* and they seem to be non-toxic (Summerton and Weller, 1997; Taylor *et al.*, 1998; Braasch and Corey, 2002). The disadvantage of these molecules is that they are unable to activate RNase H or other RNases and their effects only depend on steric hindrance (Dias *et al.*, 1999; Mologni *et al.*, 1999; Hudziak *et al.*, 2000). Nonetheless, the greatest potential of PNAs might not be their use as antisense agents but their application to modulate gene expression via strand invasion of chromosomal duplex DNA (Ray and Norden, 2000).

Another type of third generation modified oligonucleotides is LNA, also known as bridged nucleic acids. They have a methylene bridge connecting the 2'-oxigen of the ribose with the 4'-carbon. This bridge locks the ribose ring in the 3'-endo conformation characteristic of RNA (Bondensgaard *et al.*, 2000; Braasch and Corey, 2001; Elayadi and Corey, 2001; Orum and Wengel, 2001). They improve binding to complementary DNA or RNA sequences and are compatible with siRNA intracellular machinery, preserving molecule integrity (Braasch and Corey, 2001; Braasch *et al.*, 2003; Elmen *et al.*, 2005).

However, they are unable to activate RNase H, enzyme responsible for cleaving target mRNA. Owing to gapmer technology mentioned above, there is the possibility of designing chimeric molecules which comprise a central DNA portion flanked by LNA. As a result, these chimeric LNA-containing oligonucleotides present desired properties as high affinity of LNA binding and ability of DNA core to recruit RNase H. Moreover, it has been observed that LNA oligonucleotides provide an efficient gene knock-down *in vivo* (Wahlestedt *et al.*, 2000; Fluiter *et al.*, 2003).

1.6 Improvements in cellular accessibility

In general, any drug molecule must reach its intended site of action to exert its therapeutic effect and its efficiency depends especially on intracellular delivery and access to the target side, issues that are still relatively poor understood (Shi and Hoekstra, 2004). If this does not occur, the drug will have no therapeutic activity and may even cause non-specific effects through undesired interactions with non-intended targets (Khalil *et al.*, 2006). Therefore, accessibility problem has been considered the major bottleneck in the development of nucleic acids as potential therapeutics (Mintzer and Simanek, 2009).

The first biological barrier that must be overcome is the plasma membrane of living cells, a dynamic structure that is hardly lipophilic in nature, which is the responsible for separating the intracellular components from the extracellular environment (Bally *et al.*, 1999). As a result, it restricts the entry of hydrophilic or charged molecules, such as naked oligonucleotides. Indeed, it has been observed in cultured cells that their uptake is usually inefficient, mainly due to the generated repulsion between the negative charges of the oligonucleotides and the hydrophobic nature of the cell plasma membrane. Since this hurdle makes difficult for them to traverse the plasma membrane on their own, there is a big challenge for developing an appropriate delivery system in order to achieve their efficient cellular uptake. To date, a number of methods have been developed for *in vitro* and *in vivo* delivery of oligonucleotides (Figure 1.10).
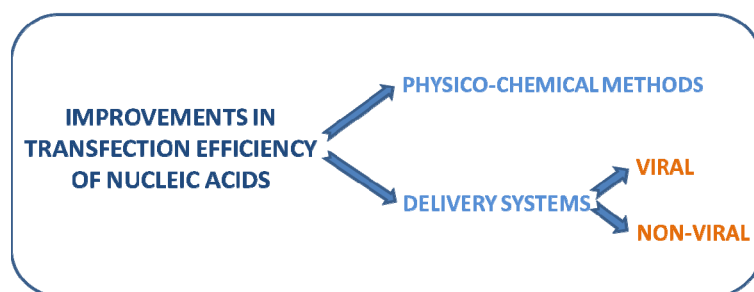
Figure 1.10 Improvements in transfection efficiency of nucleic acids.

1.6.1 Physico-chemical methods

Bypassing the plasma membrane can be accomplished experimentally using physico-chemical methods, such as microinjection, electroporation or membrane permeabilisation with chemical agents. These technologies improve transfection efficacy of the desired molecule *in vitro*, being a useful laboratory tool. Nevertheless, they are still too laborious (microinjection) or harmful to cells (electroporation and permeabilisation), requiring careful adjustments for each cell type employed. In fact, such harsh physical techniques are unlikely to receive wide clinical acceptance, leading to a limited clinical application (Wagner *et al.*, 2004; Kawakami *et al.*, 2008).

1.6.2 Delivery systems

An alternative approach for these compounds to enter cells is to take advantage of the natural uptake strategy that cells have adapted to internalise a variety of molecules which are not capable to cross plasma membrane by themselves. This basic cellular process is called endocytosis. Kinetically, three modes of endocytosis can be defined: fluid-phase, adsorptive and receptor-mediated endocytosis (Amyere *et al.*, 2002). Fluid-phase endocytosis is a low efficiency and non-specific process which refers to the bulk uptake of solutes in the exact proportion to their concentration in the extracellular fluid. Nonetheless, in adsorptive and receptor-mediated endocytosis, macromolecules are bound to the cell surface and concentrated before internalisation. In fact, in adsorptive endocytosis molecules preferentially interact with generic complementary binding sites in a non-specific manner (*i.e.*, by charged interaction) and once bound to these sites, largely follow the fate of plasma membrane. In receptor-mediated endocytosis, there is an affinity based binding between specific ligands and their receptors on the cell surface, then ligand-receptor complex is concentrated before internalisation (Khalil *et al.*, 2006).

Although a prerequisite for any endocytic pathway is a budding structure from the plasma membrane, there are some differences in the mechanisms involved and in the final destination of each route (Doherty and McMahon, 2009).

Over the past twenty years, many mechanisms of entry have been identified for nucleic acids, including fluid-phase, adsorptive and receptor-mediated endocytosis, and even trafficking through cell membrane nucleic acid channels, which are typically involved in the transport of small molecules (Stein *et al.*, 1993; Wu-Pong *et al.*, 1994; Hanss *et al.*, 1998; Hanss *et al.*, 2002; Chelobanov *et al.*, 2006). Furthermore, the intracellular fate of nucleic acids varies depending on the mechanism of entry. However, it is widely thought that cellular uptake of gene-silencing molecules, such as AS-ONs and siRNAs, occurs especially via non receptor-mediated endocytosis (Akhtar and Benter, 2007). When nucleic acids are internalised in vesicles called endosomes, these structures tend to fuse with some organelles present in the cell. If endosomes fuse with organelles known as lysosomes, then these nucleic acid molecules need to escape from these membranes to avoid degradation and reach their target compartments. In addition, when endosomes fuse with other subcellular compartments, nucleic acids can also leak from endosomes in order to reach their target compartments and exert their function. Thus, the innate activity of oligonucleotides taken up by cells is likely due to a modest amount of continuous leakage from endomembrane compartments that spontaneously occurs during intracellular trafficking (Juliano *et al.*, 2012). For example, the target site of siRNAs is located in the cytoplasm, whereas the target site of AS-ONs is either in the cytoplasm or in the nucleus. Surprisingly, nuclear membrane does not represent a diffusion barrier for small nucleic acids since they can freely pass from the cytoplasm to the nucleus through nuclear pores, as some authors reported in the early 90's when microinjected oligonucleotides in the cytosol were almost immediately transferred into the nucleus (Chin *et al.*, 1990; Leonetti *et al.*, 1991; Fisher *et al.*, 1993). For conventional phosphodiester oligonucleotides, both passive diffusion and active transport have been described as nuclear entry mechanisms (Hartig *et al.*, 1998; Lorenz *et al.*, 2000).

In the case of AS-ONs, Figure 1.11 shows their possible cellular entry pathways and intracellular trafficking.
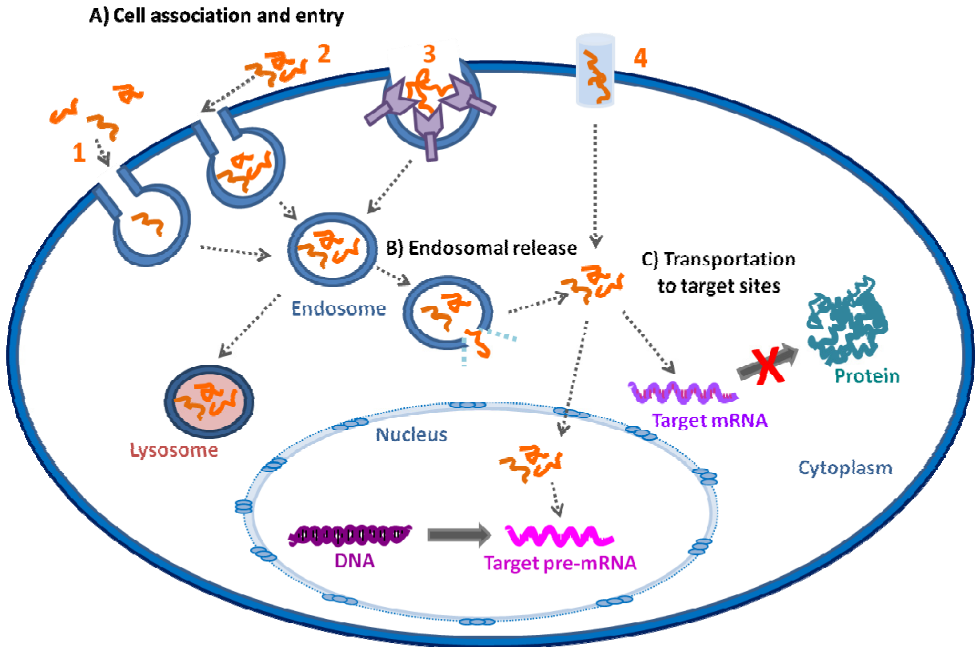
Figure 1.11 Possible cellular entry pathways and intracellular trafficking of AS-ONs. Uptake of AS-ONs is divided in three steps. A) First AS-ONs associate with the membrane. (1) In fluid-phase endocytosis there is no specific interaction with the membrane. (2) In adsorptive endocytosis AS-ONs bind to the membrane by charged interactions. (3) In receptor-mediated endocytosis AS-ONs bind to specific surface receptors. (4) AS-ONs can also penetrate through membrane nucleic acid channels. B) Generated endosomes can fuse with lysosomes, leading to AS-ON degradation, or AS-ONs can escape from endosomes, being released to the cytoplasm. C) Once in the cytoplasm, AS-ONs have to reach their target compartments (nucleus or cytoplasm) in order to bind to their target molecule (pre-mRNA or mRNA, respectively). This figure was modified from Shi and Hoekstra (2004).

As the mechanism of entry used by a molecule is closely related to its intracellular fate, the successful design of a delivery system needs a deep understanding of the multiple endocytic routes and complex trafficking pathways that exist in cells (Juliano *et al.*, 2008).

1.6.2.1 Viral delivery systems

In the past few decades, none of the designed non-viral delivery systems has been capable to equal or even exceed the high transfection rate that viral carriers provide at delivering both DNA and RNA to numerous cell lines or *in vivo* (Figure 1.12). This dramatic outcome has forced the majority of clinical trials to employ viral vectors, such as retroviruses, lentiviruses (a subclass of retroviruses) and adenoviruses (Guo *et al.*, 2009; Xu and Anchordoquy, 2011). However, there are several drawbacks connected with their use (Edelstein *et al.*, 2004, 2007). Among those are safety and toxicity issues related to immunogenicity and insertational mutagenesis (Dewey *et al.*, 1999; Fox, 2000; Schmidt-Wolf and Schmidt-Wolf, 2003).

Although the transfection efficiency of artificial non-viral delivery systems is generally lower than viral vectors, they appear much safer for future applications in humans, being potentially less immunogenic and relatively easy to produce in clinically relevant quantities (de Martimprey *et al.*, 2009).
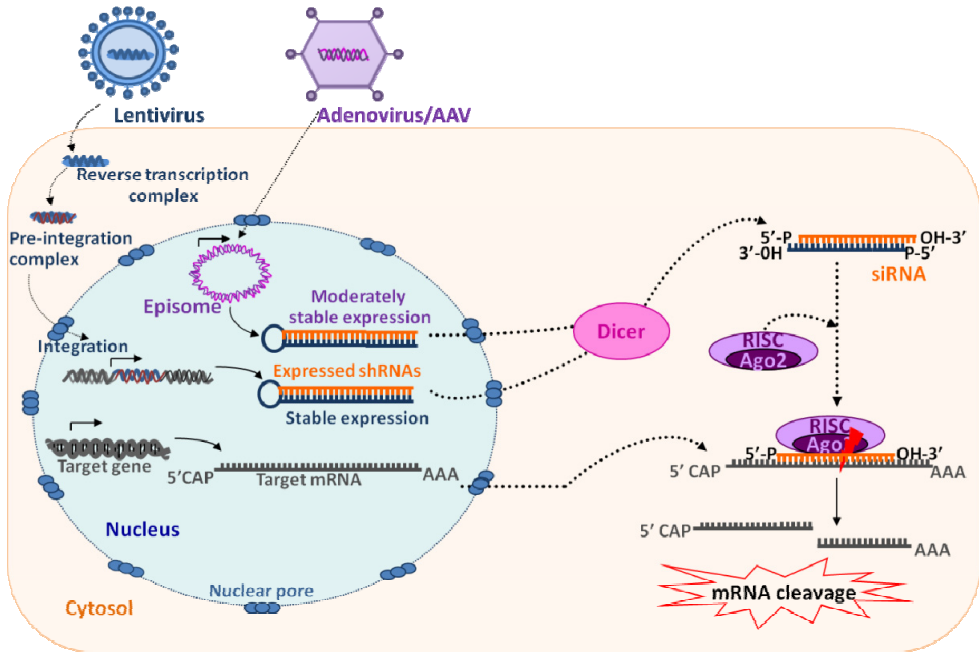
Figure 1.12 Representative picture of viral delivery systems. Lentiviral vectors deliver therapeutic shRNA-expressing transgenes which integrate into the genome for stable shRNA expression. On the other hand, adenoviral and adeno-associated virus (AAV) vectors are not able to integrate their transgenes into the genome but instead express shRNAs episomally for moderately stable levels of shRNA expression. Then, shRNA is processed by Dicer, generating siRNA that is recognised by RISC in order to target mRNA and cleave it. This figure was modified from Kim and Rossi (2007).

1.6.2.2 Non-viral delivery systems

Yet, no "magic bullet" has emerged that can carry these nucleic acid based compounds universally into a wide range of cultures cell lines, including primary cells. However, progress has been made on the study of several non-viral carriers, such as lipids, polymers and peptides for oligonucleotide delivery. This conception includes an assortment of fairly unrelated approaches yielding various degrees of enhanced cellular uptake of nucleic acids (Laufer and Restle, 2008).

In general, three approaches have been proposed for carrying the cargo, which differ on the association manner between the carrier and the oligonucleotide. These approaches can be classified as encapsulation, complex formation and conjugation.

Encapsulation

The classic definition of the word implies the lack of an interaction with the encapsulating material. In this regard, this definition is consistent with the traditional use of the term in liposomal studies wherein encapsulation refers to molecules that are enclosed within lipid bilayers and reside inside the aqueous interior of liposomes, avoiding exposure to the exterior surface (providing nuclease protection) and diffusing away from the vehicle upon disruption/fusion (Xu and Anchordoquy, 2011). For instance, several anionic liposomes were studied as possible vehicles for oligonucleotide delivery (Loke *et al.*, 1989; Burch and Mahan, 1991; Thierry and Dritschilo, 1992). Nevertheless, these formulations presented a demanding preparation which required very high concentration of lipids in order to obtain high rates of encapsulation (Figure 1.13).
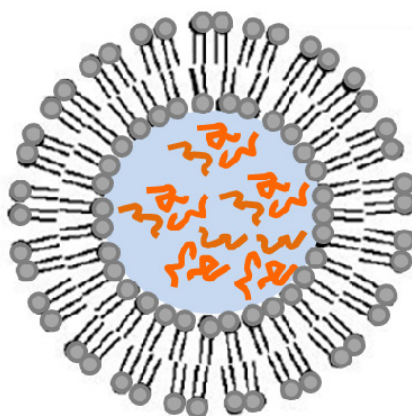
Figure 1.13 Representative picture of a liposome enclosing oligonucleotides in the aqueous cavity.

In the case of polymers, such as poly(lactic-*co*-glycolic acid) (PLGA), the cargo would be embedded in the polymer matrix rather than encapsulated, leading to similar advantages as encapsulation.

Complex formation

This approach is based on the association between cationic carriers and negative charged oligonucleotides through electrostatic interactions. These interactions must be stable enough to sustain the cargo during the carrier pathway, allowing dissociation of it at the delivery site so as to execute therapeutic activity. In the majority of the cases, the cationic part of these carriers is composed by amine groups. The efficiency of successful nucleic acid delivery is dependent on the charge ratio of the complexes. This is known as N/P ratio which is defined as a ratio of the number of amine groups of the cationic agent divided by the number of phosphate groups of the nucleic acid molecule (de Martimprey *et al.*, 2009). In addition, cationic agents can also facilitate interactions with anionic moieties on the cell surface. Regardless, it has been recognised that the positive charged surface of these complexes that promotes cell and serum protein binding is related to cytotoxic problems (Allen and Cullis, 2004).

Cationic lipids

The complexes formed by electrostatic interactions between cationic lipids and negative charge nucleic acids are called lipoplexes (Wolff and Rozema, 2008). The proposed mechanism of formation of lipoplexes is that negatively charged molecules bind to positively charged vesicles (Weisman *et al.*, 2004). Then, additional positively charged vesicles adsorb to the solvent-exposed nucleic acids. Finally, this process causes formation of a multilamellar structure of positively charged lipid bilayers (Bouxsein *et al.*, 2007; Desigaux *et al.*, 2007) (Figure 1.14).
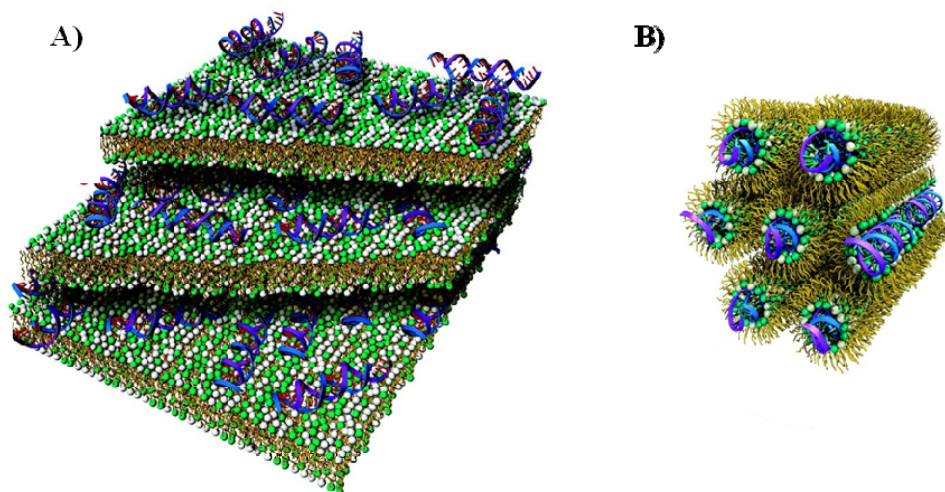
Figure 1.14 Possible lipoplex structures formed with siRNA. A) Lamellar structure; B) inverted hexagonal phase. This figure was adapted from Bouxsein *et al.* (2007).

The first synthetic lipid used to transfer plasmid DNA into mammalian cells was DOTMA (N-[1-(2,3-dioleoxy)propyl]-N,N,N-trimethylammonium chloride) (Felgner and Ringold, 1989), which was later used for oligonucleotide delivery (Bennett *et al.*, 1992). Other cationic lipids commonly used as building blocks for delivery systems are DOTAP (1,2-oleoyl-3-trimethylammonium propane), Transfectam and a lipid-like molecule (lipidoid) termed $98N_{12}$-5 (Table 1.1). Additionally, it has been reported that cationic lipids with multivalent headgroups seem to be more effective for nucleic acid delivery than their monovalent counterparts (Mahato *et al.*, 1998, 1999; Keller, 2003).

Lipid	DOTAP	DOTMA	Transfectam®	98N$_{12}$-5(1)
Chemical name	1,2-di-O-octadecenyl-3-trimethylammonium propane (chloride salt)	1,2-dioleyl-3-trimethylammonium propane (chloride salt)		
Structure				
Tail length: unsaturated bonds	18:1	18:1	17:0	11:0

Table 1.1 Molecular structure and tail configuration of the common cationic lipids used for lipoplex preparations. This table was adapted from de Schroeder *et al.* (2010).

In general, these cationic lipids are formulated with helper or co-lipids, which are frequently added to increase not only the lipoplex fusogenicity but also to decrease their toxicity (Midoux *et al.*, 2009). They are neutral lipids that enhance lipoplex stability, reducing repulsion between similar charges in the bilayer. The main helper lipids used are cholesterol and DOPE (1,2-dioleoyl-*sn*-glycero-3-phosphatidylethanolamine) (Figure 1.15). When cholesterol is incorporated as a co-lipid, it may facilitate cell fusion or endosomal internalisation of the carrier (Schroeder *et al.*, 2010).

Otherwise, the advantage of using DOPE as a co-lipid is that this phospholipid promotes the transition from lamellar to inverted hexagonal phase below pH 8, leading to a destabilisation of endosomal membrane and a release of contents from the endocytosed complexes trapped in endosomes before fusion to lysosomes for cargo degradation.
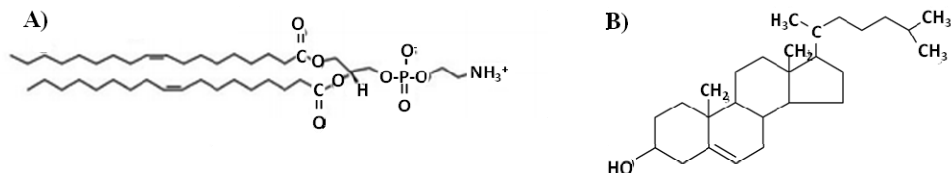
Figure 1.15 Helper lipids commonly used in lipoplex formulations. A) Helper lipid termed DOPE; B) cholesterol.
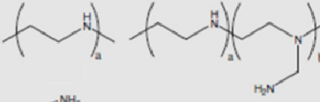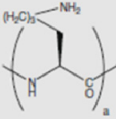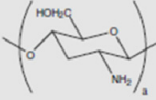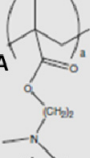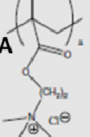
On the other hand, electrostatic interactions between nucleic acids and cationic liposomes may present some disadvantages, such as a relatively uncontrolled interaction process leading to lipoplexes of excessive size and poor stability, or an incomplete encapsulation of the oligonucleotides, exposing them to potential enzymatic or physical degradation before being internalised by cells (De Paula *et al.*, 2007). In addition, it has been reported that cationic liposomes are able to interact with serum molecules (*e.g.*, proteins, lipoproteins), resulting in an aggregation or nucleic acids release from lipoplexes prior to cellular uptake, or even activate the complement system which promotes their rapid clearance by macrophages of the reticuloendothelial systems (Mahato *et al.*, 1997).

Cationic polymers

Like cationic lipids, cationic polymers were initially used for gene delivery but systems were optimised to suit with oligonucleotide delivery, such as AS-ONs and siRNAs (Köping-Höggård *et al.*, 2001; Farrell *et al.*, 2007).

They also form complexes with the cargo spontaneously through electrostatic interactions between positively charged amine groups of the polycations and negatively charged phosphate groups of the nucleic acids. Complexes formed by this process are called <u>polyplexes</u> (De Paula *et al.*, 2007).

Among cationic polymers, the most commonly used for delivery of nucleic acids are PLL (poly-L-lysine), PEI [poly(ethyleneimine)] and pAMAM (polyamidoamine) dendrimers, chitosan, cyclodextrin-based polymers, PDMAEMA [poly(dimethylamino-ethylmethacrylate)] and PTMAEMA [poly(trimethylaminoethylmethacrylate)] (Table 1.2). In most cases, the primary amine groups present on the surface of these polymers are positively charged at physiological pH and enable the complexing of the negative charged nucleic acids through electrostatic interactions, as well as the interaction with the negative charged plasma membrane of cells (De Paula *et al.*, 2007).

Table 1.2 Chemical structure of the common cationic polymers used for nanocarrier preparations. This table was modified from de Martimprey *et al.* (2009).

PLL polymer was the first polymeric carrier chosen for oligonucleotide delivery. Due to the potential toxicity exhibited by PLL, following investigations were carried out using glycosylated PLL polyplexes (Leonetti *et al.*, 1988; Mahato *et al.*, 1997).

PEI is probably the most widely used cationic polymer for delivery of oligonucleotides including AS-ONs and siRNAs. The high transfection efficiency of this linear or branched polymer is attributed to the "proton sponge effect" generated by its secondary and tertiary amines (de Martimprey *et al.*, 2009). The mechanism proposed for this effect starts with the acidification of the endosome during the internalisation of these polyplexes. When the pH of the endosome decreases, the amine groups present in polyplexes, which have a pKa in the range of 7 and 5, are protonated. This is followed by an influx of additional protons and chloride ions. Owing to the osmotic imbalance created by these ions, there is an entrance of water to counter this effect, leading to an inflation of the endosome which ends up this its rupture. Finally, this rupture is the responsible for contents release from the endosome to the cytoplasm (Sonawane *et al.*, 2003; Akinc *et al.*, 2005).

pAMAM dendrimers are a class of highly branched spherical polymers which offer synthesis control in terms of degree and generation of branching. Due to this property, these particles can be produced with a very low degree of polydispersity, being a significant advantage over other polymers, such as PLL. In addition, these dendrimers have been applied in several delivery studies of nucleic acids (Hollins *et al.*, 2004; Santhakumaran *et al.*, 2004; Choi, 2005).

Chitosan is a cationic polysaccharide with biodegradable and biocompatible properties (Kim *et al.*, 2006a). As well as chitosan, cyclodextrins are natural biocompatible cyclic oligosaccharides which can be copolymerised with polycations (Gonzalez *et al.*, 1999; Hwang *et al.*, 2001). Both polyplexes formed

with oligonucleotides presented successful transfection efficiency in numerous reports (You *et al.*, 2006; Bartlett and Davis, 2007; Heidel *et al.*, 2007).

Overall, the downside is that the transfection efficiency of these artificial nanocarriers is generally lower than viral systems. Moreover, intrinsic drawbacks with these cationic polymers, such as solubility and cytotoxicity, have limited their use *in vivo*. In order to increase polymer solubility and reduce toxic effects, these polymers are usually grafted with PEG (polyethyleneglycol), dextran or cholesterol (Allen *et al.*, 2002; Wang *et al.*, 2002; Patil *et al.*, 2005; Sun *et al.*, 2011). These modifications also stabilise nanoparticles *in vivo* and lessen nonspecific interactions with serum elements (Wu *et al.*, 2010).

Conjugation

This promising approach includes a covalent attachment by chemical and biological methods of the cargo to a functional or non-functional molecule. Among them, a wide array of molecules can be used to conjugate directly to small nucleic acids, including aptamers, antibodies or their fragments, liposomal components, lipids, saccharides, hormones, proteins, peptides, toxins, growth factors, vitamins and polymers (Nishina *et al.*, 2008; Singh *et al.*, 2008).

Direct cleavable and non-cleavable conjugation of these molecules to small nucleic acids, such as AS-ONs and siRNAs, is advantageous over structural modifications because it could not only promote target specificity, but also improve their pharmacokinetic behaviours and cellular uptake efficiencies, endowing them with entirely new properties (Jeong *et al.*, 2009; Singh *et al.*, 2010).

With the aim of maximising delivery efficiency of nucleic acid based bioconjugates, several crucial conjugation parameters, such as the conjugation site of oligonucleotide, cleavability, the length of spacer and the nature of molecules to be conjugated (*i.e.*, charge, molecular weight and hydrophobicity) should be carefully considered.

In the case of siRNA, previous reports revealed that the integrity of the 5'-terminus of the antisense strand, rather than that of the 3'-terminus, is necessary for the initiation of RNAi mechanism (Chiu and Rana, 2003; Khvorova *et al.*, 2003; Schwarz *et al.*, 2003; McNamara *et al.*, 2006). Hence, the 3' and 5'-terminus of the sense strand and the 3'-terminus of the antisense strand are especially considered as potential sites for conjugation with minimal influence on RNAi activity. In fact, it has been recently suggested that the conjugation of molecules to the 5'-terminus of the sense strand may enhance biased incorporation of the antisense strand into RISC, resulting in a reduction of the sense strand-directed undesirable off-target effects (Chen *et al.*, 2008).

Related to cleavability, several bioconjugates employ cleavable linkages, such as acid-labile and reducible bonds, between the nucleic acid molecule and the conjugation partner so as to facilitate the release of intact oligonucleotide inside cells. For instance, acid-labile linkages are expected to be cleaved in acidic endosomes while disulfide linkages should be cleaved in the reductive cytosolic space (Jeong *et al.*, 2009).

Targeted delivery

One of the interesting advantages that conjugation provides is targeted delivery of the therapeutic molecules to the desired cells and tissues. It is based on the conjugation of specific antibodies, ligands (*e.g.*, sugar molecules, vitamins, hormones, lipids, proteins) or ligand mimetics (*e.g.*, aptamers) to either the small nucleic acid molecules or to the surface of the carriers (*i.e.*, liposomes, lipoplexes, polyplexes) in order to direct the nanoparticles to specific targets (Soutschek *et al.*, 2004; Pestourie *et al.*, 2005; Ikeda and Taira, 2006; Park *et al.*, 2006; Pirollo *et al.*, 2006; Wu *et al.*, 2007; Kumar *et al.*, 2008; Lares *et al.*, 2010; Schroeder *et al.*, 2010) (Figure 1.16). This specific delivery not only minimises the possibility of undesirable off-target effects, but also decreases the amount of dose required to achieve a maximal therapeutic effect (Peer *et al.*, 2007).

In the majority of the cases, selected antibodies or ligands are specifically recognised by certain receptors in target cells, which mediate their internalisation through receptor-mediated endocytosis.
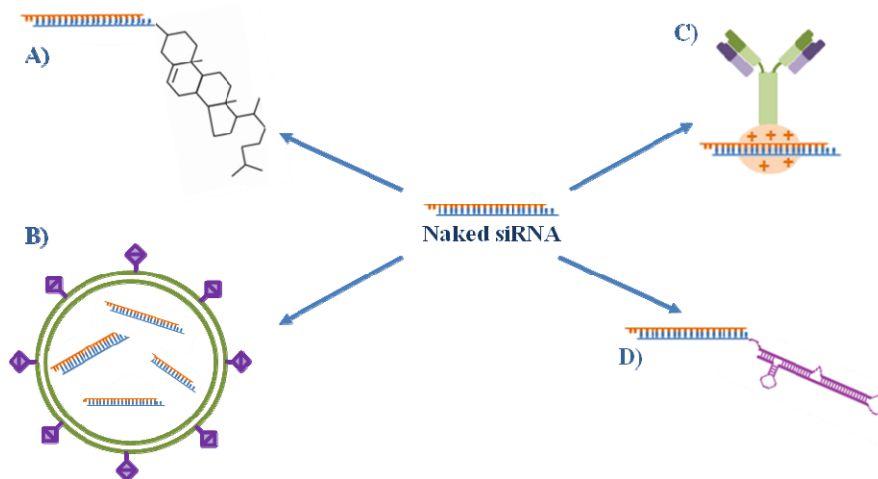
Figure 1.16 Different molecules used to conjugate to siRNA for targeted delivery. A) Cholesterol as specific ligand, directly bound to siRNA; B) A specific ligand bound to the surface of a liposome; C) Specific antibody coupled to positive charged protamine; D) Aptamer. This figure was modified from Dominska and Dykxhoorn (2010).

In this regard, and with the knowledge of specific receptors present in target cells and tissues, several studies have been reported with successful delivery, such as polymeric carriers with galactose and lactose as ligands to bind to asialoglycoprotein receptors expressed on the surface of hepatocytes and human hepatoma Huh-7 cells (Kim *et al.*, 2005; Oishi *et al.*, 2005), mannosylated lipoplexes to bind to mannose receptors and mannose related receptors in dendritic cells (Kawakami *et al.*, 2004), polyplexes with folate as ligand for folate receptor that is expressed on many human tumour cells (Kim *et al.*, 2006b), polymeric carriers with RGD (arginine-glycine-aspartic acid) motif to target tumour

45

neovasculature-expressing integrins (Schiffelers *et al.*, 2004), cyclodextrin-based polymers with human transferrin protein ligand to target solid tumours expressing transferrin receptors (Davis *et al.*, 2010), lipoplexes bearing the anti-transferrin receptor single chain antibody fragment to bind to primary and metastasic tumour cells expressing transferrin receptors (Yu *et al.*, 2004) and PMSA (prostate-specific membrane antigen) specific aptamers conjugated to small nucleic acids or to polymeric carriers to target prostate cancer cells and tumour vascular endothelium which overexpress PSMA cell surface receptor (Farokhzad *et al.*, 2004; McNamara *et al.*, 2006; Chu *et al.*, 2006).

Enhancement of cellular permeability

Additionally, another attractive application that this approach provides is the conjugation of peptides or lipophilic molecules to small nucleic acids which can be an attractive alternate way to solve the cellular permeation problem. In most cases, this effect is not cell specific, but it could avoid the disadvantage that receptor-mediated endocytosis often present, where the oligonucleotides have to trigger endosomal escape to reach their target (Laufer and Restle, 2008).

The idea of using peptides as carriers started about twenty years ago when it was observed that the human immunodeficiency type 1 (HIV-1) transactivating protein Tat was internalised in mammalian cells (Frankel and Pabo, 1988; Green and Loewenstein, 1988). This discovery was followed by a similar action of the Antennapedia homeodomain of *Drosophila melanogaster* (Joliot *et al.*, 1991). Promising results were obtained by peptides derived from Tat and Antennapedia (penetratin) as well as other proteins with the capability of transporting cargoes into cells (Fawell *et al.*, 1994; Allinquant *et al.*, 1995; Schwarze *et al.*, 1999), resulting in a development of expanding field focusing on the so-called CPPs (cell-penetrating peptides). Table 1.3 gives an overview of selected "classical" CPPs.

Commonly, these amphipathic peptides are helical structures of short polycationic sequences of less than 30 amino acids which can translocate nucleic

acids through plasma membrane even at 4ºC by a receptor independent mechanism, thereby transporting nucleic acids directly to the cytoplasm (Derossi *et al.*, 1996). Successful transfection efficiency of AS-ONs and siRNAs by CPPs has been demonstrated in different types of cells (Astriab-Fisher *et al.*, 2002; Simeoni *et al.*, 2003; Chiu *et al.*, 2004; Muratovska and Eccles, 2004; Veldhoen *et al.*, 2006; Yin *et al.*, 2008). However, the mechanisms underlying the cellular translocation of CPPs are still poorly understood and are subject of controversial discussion (Veldhoen *et al.*, 2008).

PEPTIDE	SEQUENCE	REFERENCES
Tat[48-60]	GRKKRRQRRRPPQ	Vives *et al.*, 1997
penetratin (Antp[43-58])	RQIKIWFQNRRMKWKK	Derossi *et al.*, 1994
transportan	GWTLNSAGYLLGKINLKALAALAKKIL	Pooga *et al.*, 1998
TP10	AGYLLGKINLKAALLAKKIL	Soomets *et al.*, 2000
Oligoarginine (R_8)	RRRRRRRR	Futaki *et al.,* 2001
MAP	KLALKLALKALKAALKLA	Oehlke *et al.,* 1998
MPG	GALFLGFLGAAGSTMGAWSQPKKKRKV	Morris *et al.*, 1997
MPGα	GALFLAFLAAALSLMGLWSQPKKKRKV	Deshayes *et al.,* 2004

Table 1.3 Sequences of selected "classical" CPPs. This table was adapted from Laufer and Restle (2008).

On the other hand, conjugation to lipophilic molecules introduces a hydrophobic character in the small nucleic acids which may enhance their cellular uptake not only by increased membrane permeability but also through receptor-mediated endocytosis (Singh *et al.*, 2008). Among them, cholesterol-conjugates have shown to be potential systems for delivery of nucleic acids (Akhtar and Juliano, 1992; Clarenc *et al.*, 1993; Lorenz *et al.*, 2004; Cheng *et al.*, 2006). Indeed, when cholesterol is conjugated to oligonucleotides like AS-ONs and siRNAs, it seems to act as a targeting entity for certain tissues such as liver, allowing membrane fusion through lipid-raft-mediated endocytosis (Soutschek *et al.*, 2004).

In conclusion, despite the progress made on the development of several delivery systems for carrying these nucleic acid based compounds, they still present a number of problems that make them insufficient to be used in therapy. Similarly, while extensive information exists regarding the overall pharmacokinetics and tissue distribution of both classic antisense and siRNA, we lack an equivalent depth of knowledge about behaviour at the cellular and intracellular level. Therefore, there is a need for keeping on searching new potential candidates and investigating their internalisation routes.

1.7 Aims of this study

The present work has been focused particularly on the study of the conjugation approach analysing different modified oligodeoxynucleotides in order to test both applications, namely targeted delivery and enhancement of cellular permeability.

The first objective has been based on the investigation of cellular uptake profiles of glucose-DNA conjugates with different carbohydrate presentation in two different cell lines which have cell-surface carbohydrate receptors.

The second goal has been undertaken by the use of lipid-DNA conjugates with different alkyl chain presentation, which have been tested for the following aspects:

* Examining the interaction between lipid-DNA conjugates and membrane lipid model systems and investigating their cellular uptake and localisation profiles.

* Characterising in depth the most promising lipid-DNA conjugate as a potential candidate for oligonucleotide delivery.

Chapter 2:

Experimental procedures

Chapter 2: Experimental procedures

2.1 Materials

2.1.1 Chemical products

Supplier	Reagents and products
Abcam	Mouse monoclonal antibody to glucose transporter (GLUT)1
	Mouse monoclonal antibody to mannose 6 phosphate receptor (M6PR)
	Rabbit polyclonal antibody to clathrin heavy chain (HC)
	Rabbit polyclonal antibody to caveolin-1
Amersham	Cyanine dye 5
Avanti Polar Lipids	DOPC (1,2-*dioleyl-L-α*-phosphatidylcholine)
	eSM (egg sphingomyelin)
	Chol (cholesterol)
BD Bioscience	96 well-BD Falcon™ Black/Clear, Tissue Culture Treated Imaging Plate, Flat Bottom with lid
	BD FACSFlow™ Sheath Fluid
	BD FACSRinse Solution
BIO-RAD	40% Acrylamide/Bis Solution, 19:1
	BCA assay reagents
	Nitrocellulose membrane
	Precision Plus Protein™ Standards, All Blue
	Transfectin™ Lipid Reagent
Cell Signaling Technology	HRP-linked Goat anti-rabbit IgG antibody
	HRP-linked Goat anti-mouse IgG antibody
eBioscience	Anti-Mouse CD11b FITC antibody
EXBIO	Human Transferrin-FITC
Fermentas	Gene Ruler™ Ultra Low Range DNA Ladder
Gibco (Invitrogen)	0.05% trypsin-EDTA (ethylenediaminetetraacetic acid) (1X) solution
	DMEM (Dulbecco's modified Eagle's medium) No Glucose

	OPTIMEM® I Reduced Serum Media
	Penicillin-Streptomycin, liquid
Invitrogen	1 Kb Plus DNA Ladder
	Geneticin® Selective Antibiotic, powder (G418 Sulphate)
	Oligofectamine™ Reagent
Lonza	Metaphor® Agarose
	FBS (Fetal Bovine Serum)
Minerva Biolabs	Venor® GeM *Mycoplasma* Detection Kit
Molecular Probes	Alexa Fluor 488
(Invitrogen)	Alexa Fluor 546 phalloidin
	Alexa Fluor 546 Donkey anti-mouse IgG (H+L) antibody
	Alexa Fluor 633 Goat anti-rabbit IgG (H+L) antibody
	Hoechst 33258, DNA stain
	DiD dye
	DiO dye
	SYBR® Green I nucleic acid gel stain
	SYBR® Gold nucleic acid gel stain
New England Biolabs	10X Strand Taq Polymerase
	Taq DNA Polymerase (5,000 U/ml)
Novagen	6X DNA Loading Buffer
Nunc	6 well plate
	24 well plate
	8-well Lab-Tek™ Chamber Slides
	T-25 cell culture flask
	T-75 cell culture flask
PAA Laboratories	DMEM Low Glucose
	Mycokill AB
Promega	CellTiter 96® Aqueous MTS Reagent Powder
Santa Cruz Biotechnology,	Caveolin-1 siRNA
Inc.	Clathrin HC siRNA
	Rabbit polyclonal antibody to Glyceraldehyde 3-phosphate dehydrogenase (GAPDH)
	Rabbit polyclonal antibody to GLUT 3

Sarstedt	150 mm dish
	96-well plate
	Cell scraper 16 cm
	Cell scraper 25 cm
Sigma-Aldrich	30% Acrylamide/Bis Solution
	5-(N,N-Dimethyl)amiloride hydrochloride
	BSA (Bovine Serum Albumin)
	Chlorpromazine hydrochloride
	DMSO (Dimethyl sulfoxide)
	Fibrinogen from bovine plasma
	Genistein
	Hygromycin B
	L-glutamine solution (200 mM)
	Nystatin
	PBS (Phosphate Buffered Saline), tablet
	PFA (paraformaldehyde), powder
	PMS (phenazine methosulfate), powder
	Poly-L-lysine solution
	Protease inhibitor cocktail
	Puromycin dihydrochloride solution (10 mg/ml)
	Sucrose
	Tween-20
Thermo Scientific	Super Signal West Femto Maximum Sensitivity Substrate
Other chemicals and reagents	Analytic grade reagents

2.1.2 Oligonucleotide conjugates

All the conjugates used in this work had the same oligodeoxynucleotide phosphodiester sequence, based on GEM91 (gene-expression modulator 91). This antisense phosphorothioate of 25 nucleotides in length was designed to interact with the conserve gag initiation site of HIV-1 and it was shown to be a potent inhibitor of HIV-1 replication in cell culture (Lisziewicz *et al.*, 1994; Yamaguchi *et al.*, 1997; Turner *et al.*, 2006) (Figure 2.1).
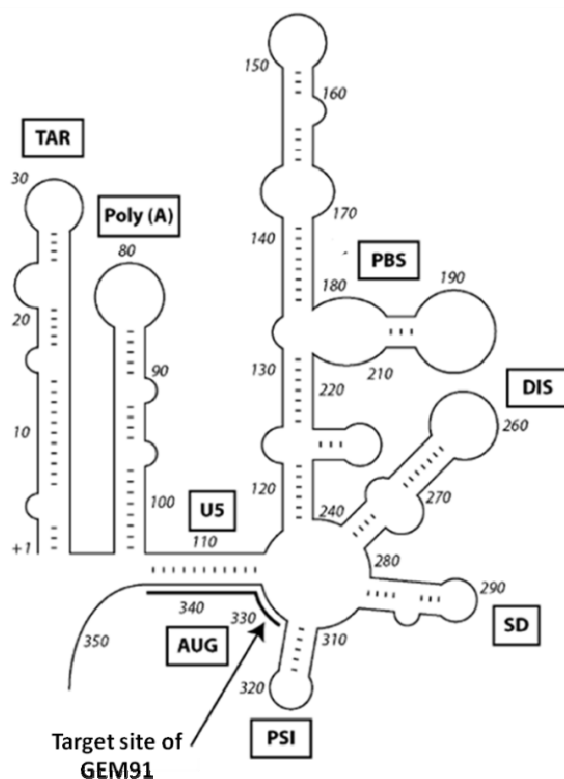
Figure 2.1 Secondary structure schematic model of the HIV-1 leader sequence showing the functional regions and the interaction sites of the clinically investigated phosphorothioate GEM91. This figure was modified from Turner *et al.* (2006).

The only difference between the sequence of the bioconjugates tested in this work and GEM91 model sequence was the phosphate backbone, being phosphodiester and phosphorothioate, respectively. The reason why phosphodiester backbone was chosen for these compounds is that its synthesis is considered to be easier and faster. Additionally, a complementary sequence to GEM91, termed AntiGEM91, was used to obtain double stranded oligodeoxynucleotides. Table 2.1 shows nucleotide sequences of GEM91 and its complementary oligodeoxynucleotide.

Name of oligodeoxynucleotide	DNA Sequence
GEM91	5'-CTCTCGCACCCATCTCTCTCCTTCT-3'
AntiGEM91	5'- AGAAGGAGAGAGATGGGTGCGAGAG-3'

Table 2.1 Oligodeoxynucleotide sequences of GEM91 and its complementary strand AntiGEM91.

Owing to the fact that most of the experimental techniques performed in this work were based on fluorescence, conjugates carrying a fluorescent label at their free end were synthesized. Two different fluorescent labels were used in these studies, *i.e.*, Alexa Fluor 488 (Alexa 488) (Molecular Probes, Invitrogen) and Cyanine dye 5 (Cy5) (Amersham) (Figure 2.2). In particular, a free amine group at the end of the oligonucleotide was needed to couple Alexa 488 dye by an amide linkage.
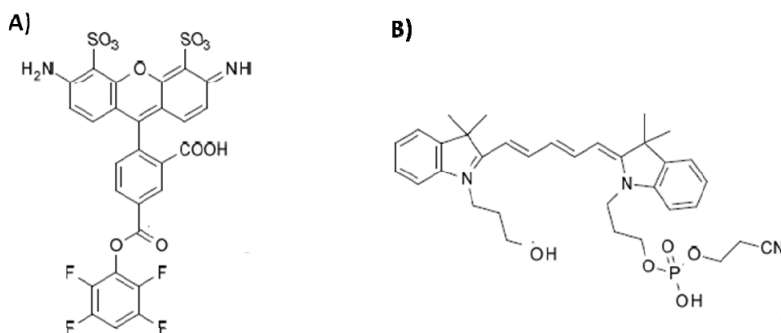
Figure 2.2 Fluorescent dyes for conjugate labelling. A) Alexa Fluor 488; B) Cy5.

As DNA control, GEM91 sequence having a phosphodiester backbone and lacking either sugar or lipid moieties was used. For this purpose two different control sequences were prepared, one of them had an amine group at the 3'-end of the DNA strand, named GEM91-(3')NH$_2$ (**1**) and the other control sequence lacked amine groups (**15**). When fluorescence experiments were carried out, labelled DNA control sequences were needed. Here again two different control sequences were designed: GEM91-(3')Alexa 488 (**8**) and Cy5(5')-GEM91 (**16**).

To form double-stranded oligodeoxynucleotides by hybridization between complementary strands, an AntiGEM91 sequence having a phosphodiester backbone and an amine group at the 5'-end of the DNA strand [NH$_2$(5')-AntiGEM91] was used (**17**). For fluorescence experiments, Alexa 488(5')-AntiGEM91 (**18**) was also prepared.

The following table shows DNA control sequences and complementary strands used in this study.

Compound No.	Oligonucleotide conjugate
1	GEM91-(3')NH$_2$
8	GEM91-(3')Alexa 488
15	GEM91
16	Cy5(5')-GEM91
17	NH$_2$(5')-AntiGEM91
18	Alexa 488(5')-AntiGEM91

Table 2.2 DNA control sequences and complementary strands used in this study.

All the conjugates studied in this project were kindly provided by the group of Dr. Ramón Eritja (Institute for Research in Barcelona, Institute for Advanced Chemistry of Catalonia, IQAC-CSIC, Barcelona, Spain) in collaboration with the group of Dr. Juan Carlos Morales (Instituto de Investigaciones Químicas, CSIC-Universidad de Sevilla, Sevilla, Spain). All oligonucleotide conjugates were provided as lyophilized powder and dissolved in 1X PBS solution (Liu *et al.*, 2010).

2.1.2.1 Carbohydrate-oligonucleotide conjugates (COCs)

Oligodeoxynucleotides carrying carbohydrates at the 5'-end were prepared as described in Ugarte-Uribe *et al.* (2010). Table 2.3 shows the different sugar moieties bound to the 5'-end of the DNA strand, where some of them had a spacer linker or a double dendrimer (DB) between them.

Compound No.	COC	Sugar moiety
1	GEM91-(3')NH$_2$	None
2	Glucose-C2(5')-GEM91-(3')NH$_2$	Glucose
3	Fucose-C2(5)'-GEM91-(3')NH$_2$	Fucose
4	(Glucose-C2)$_2$-DB(5')-GEM91-(3')NH$_2$	Glucose x2
5	(Glucose-C2)$_4$-DB-DB(5')-GEM91-(3')NH$_2$	Glucose x4
6	Maltose-PEG4(5')-GEM91-(3')NH$_2$	Maltose
7	Maltotriose-C2(5')-GEM91-(3')NH$_2$	Maltotriose

Table 2.3 Sequences of the DNA glycoconjugates used in this study presenting different sugar moieties. C2 stands for (-CH$_2$CH$_2$-OPO$_2^-$-); DB stands for the symmetric doubler phosphoramidite; PEG4 stands for [-(OCH$_2$CH$_2$)$_4$-OPO$_2^-$-]. Number **1** refers to DNA control which lacks sugar moiety.

All oligodeoxynucleotides had an amine group in the 3'-end of the DNA strand to bind Alexa 488 for fluorescence experiments, leading to good yields of labelling (67–93%). The following schematic figure shows the DNA glycoconjugates analysed in this work.
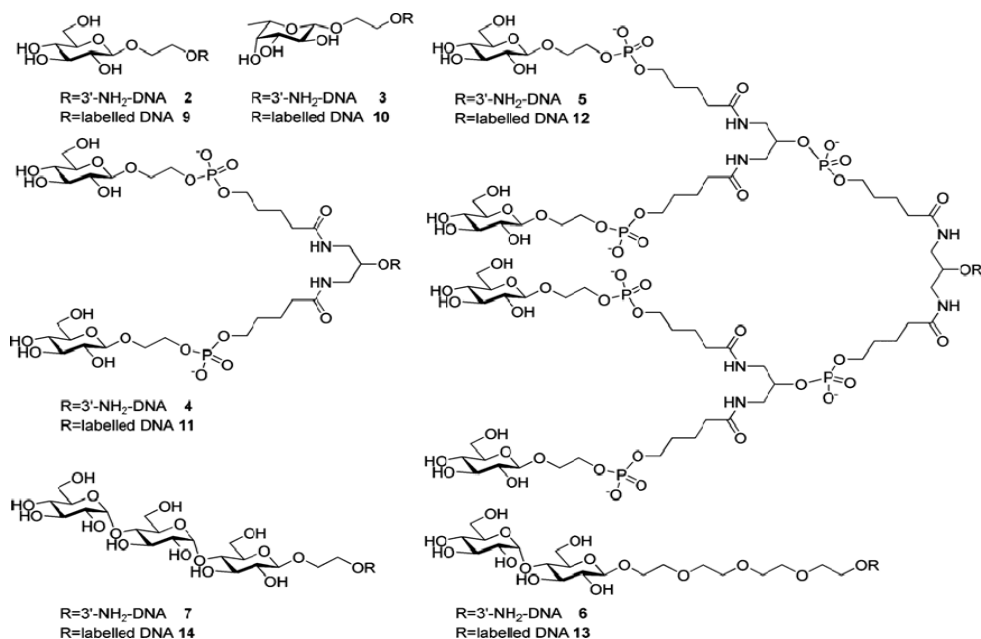
Figure 2.3 Schematic figure of COCs. "3′-NH$_2$-DNA" strands correspond to -OPO$_2^-$-GEM91-3′-NH$_2$ sequence; "Labelled DNA" corresponds to GEM91 strands with Alexa 488 coupled at the 3′-end. This figure was adapted from Ugarte-Uribe *et al.* (2010).

2.1.2.2 Lipid-oligonucleotide conjugates (LOCs)

In this section five lipophilic conjugates differing in the conjugation site of the oligonucleotide and the alkyl moiety were prepared. Some of the selected lipid groups were previously reported by Grijalvo *et al.* (2010, 2011). Three lipid modifications were carried out in the 3'-end of DNA strand and other two lipid modifications in the 5'-termini. All lipid moieties were neutral lipids, except one

lipid conjugated in the 3'-termini which had a polar group at the end of the lipophilic tail ($C_{12}NH_2$). Figure 2.4 shows the different alkyl modifications used for LOCs.
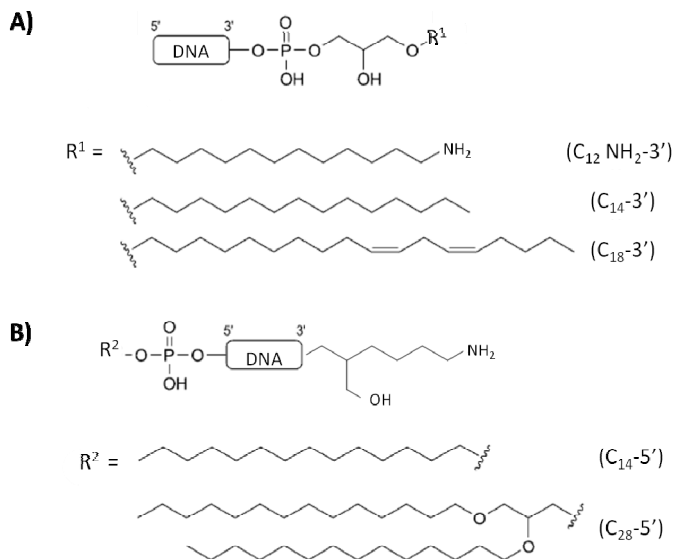
Figure 2.4 Lipid modifications introduced into DNA strand. A) Selected lipids (R^1) were bound to the 3'-end of the DNA strand. B) Selected lipids (R^2) were bound to the 5'-termini. DNA strand corresponds to GEM91 sequence. This figure was modified from Grijalvo *et al.* (2011).

For fluorescent experiments, Alexa 488 fluorescent tag was primarily selected to couple with the LOCs due to its higher photostability and brightness compared to other common fluorescent labels, and also because its higher fluorescent lifetime and hydrolytic stability of the corresponding amine-reactive Alexa 488 derivative. As observed in Figure 2.4, to introduce a free amine group in the 3'-termini of the LOCs bearing a lipid moiety at the 5'-end of the DNA strand the 2-(*N*-[9*H*-fluoren-9-yl-methoxycarbonyl]-4-aminobutyl)propane-1,3-diol linker (Glen Research) was selected, leading to an aliphatic amino group at the 3′-end. On the other hand, in order to introduce an amine group at 5'-termini of the LOCs bearing a lipid moiety at the 3'-end of the DNA strand, commercially available 5'-amine-modifier-C6-Tfa phosphoramidite (Glen Research) was selected.

Unfortunately, labelling with Alexa 488 presented some drawbacks with the oligonucleotides carrying lipid modification at the 3'-end of the DNA strand. In the case of the LOC that contained $C_{12}NH_2$ modification at the 3'-termini, it was not possible to couple Alexa 488 tag specifically to the 5'-termini because of the reactive primary amine presented at the end of the C_{12} moiety. On the other hand, when bioconjugates carrying C_{14} or C_{18} alkyl modifications at the 3'-termini were coupled with Alexa 488 at the 5'-end of the DNA strand, low purity yields were obtained (50% and 30%, respectively). As a result, Cy5 dye was also selected to label the 5'-termini of the aforementioned LOCs.

The following table summarizes the characteristics and the compound number given to the LOCs tested in this project.

Compound No.	Lipid moiety	Label	NH$_2$ termini at opposite site of lipid moiety
19	$C_{12}NH_2$ (3')	No	No
20	C_{14} (3')	No	No
21	C_{18} (3')	No	No
22	C_{14} (5')	No	Yes
23	C_{28} (5')	No	Yes
24	C_{14} (3')	No	Yes
25	C_{18} (3')	No	Yes
26	$C_{12}NH_2$ (3')	Cy5 (5')	No
27	C_{14} (3')	Cy5 (5')	No
28	C_{18} (3')	Cy5 (5')	No
29	C_{14} (5')	Alexa 488 (3')	No
30	C_{28} (5')	Alexa 488 (3')	No
31	C_{14} (3')	Alexa 488 (5')	No
32	C_{18} (3')	Alexa 488 (5')	No

Table 2.4 List of LOCs used in this study, differing in lipid moiety, conjugation position and fluorescent label. All these conjugates had the same DNA sequence: GEM91 sequence (5'-CTCTCGCACCCATCTCTCTCCTTCT-3') with phosphodiester backbone.

2.1.3 Cell lines

HeLa and U87.CD4.CXCR4 cells lines were kindly provided by Prof. Alfredo Berzal-Herranz (Instituto de Parasitología y Biomedicina "López-Neyra", CSIC, Granada, Spain).

PANC-1, C2C12 and RAW 264.7 cell lines were generously donated by Prof. Antonio Gómez-Muñoz (Departamento de Bioquímica y Biología Molecular, EHU/UPV, Leioa, Spain).

CHO K1, CHO CR3+, J774A.1 and J774A.1 CR3- cell lines were kindly provided by Prof. Cesar Martín (Unidad de Biofísica, Centro Mixto CSIC-UPV/EHU and Departamento de Bioquímica y Biología Molecular, EHU/UPV, Leioa, Spain).

2.1.3.1 HeLa cell line

HeLa (cervical adenocarcinoma) cell line is the oldest and most commonly used human cell line in scientific research (Figure 2.5).
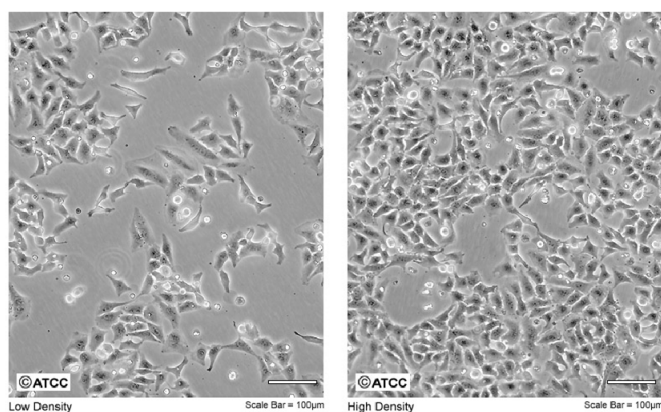
Figure 2.5 HeLa cell culture. This figure was adapted from ATCC (American Type Culture Collection).

2.1.3.2 U87.CD4.CXCR4 cell line

U87 (human glioblastoma-astrocytoma) cell line is formally known as U87 MG (ATCC). It has epithelial morphology and it is usually used as an *in vitro* model of human glioblastoma cells to investigate the cytotoxic effect of chemotherapeutic drugs towards cancer cells (Figure 2.6). In this study U87.CD4.CXCR4 cell line, which expressed CD4 receptor and CXCR4 co-receptor in the cell surface, was used. It is known that these surface molecules are involved in the cellular entry of the most pathogenic variants of HIV in a later stage of disease progression towards AIDS (Penn *et al.*, 1999; Jekle *et al.*, 2003).
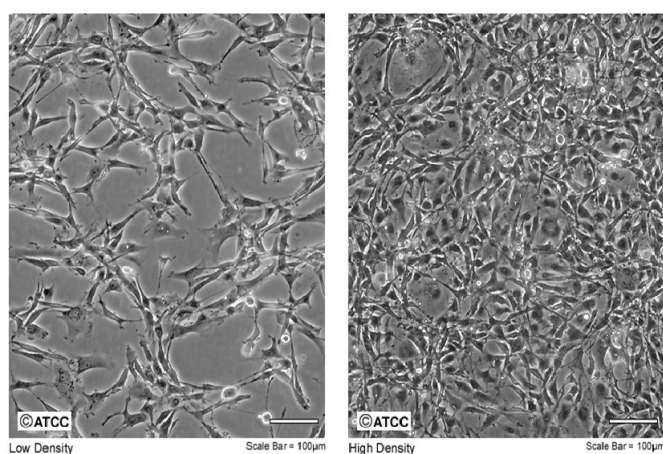
Figure 2.6 U87 MG cell culture. This figure was adapted from ATCC.

2.3.1.3 PANC-1 cell line

This is a human pancreatic carcinoma, epithelial-like cell line which is commonly used as an *in vitro* model of non-endocrine pancreatic cancer for tumorigenicity studies (Figure 2.7).
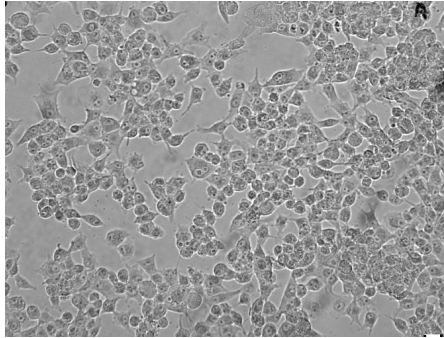
Figure 2.7 PANC-1 cell culture. This image was taken in Leica DMI 4000 B inverted microscope by image acquisition (Hamamatsu C10600 ORCA-R2 digital camera) using a 10X objective.

2.1.3.4 C2C12 cell line

This is a subclone of mouse myoblast which differentiates rapidly, forming contractile myotubes and producing characteristic muscle proteins (Figure 2.8).
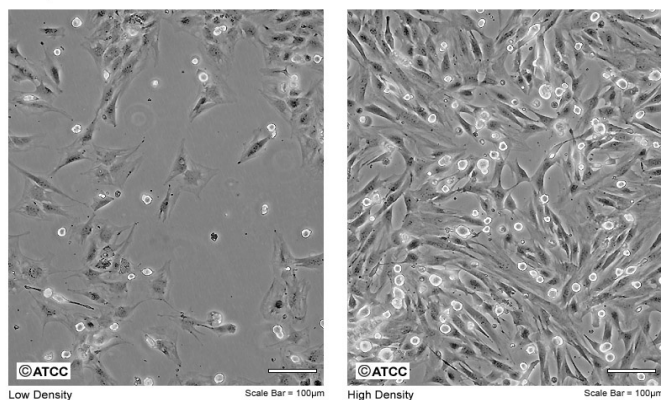
Figure 2.8 C2C12 cell culture. This figure was adapted from ATCC.

2.1.3.5 RAW 264.7 cell line

This is a monocyte/macrophage cell line obtained from Abelson murine leukemia virus-induced tumour of BALB/c mice. This cell line was chosen due to the stable expression of β_2 integrin, CD11b/CD18 (CR3), on its cell surface (Figure 2.9).
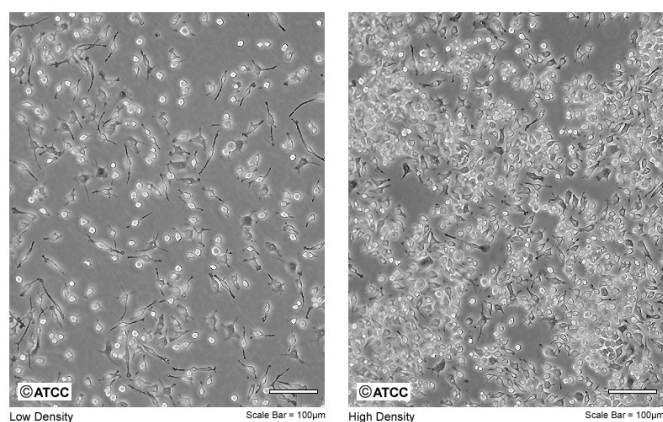
Figure 2.9 RAW 264.7 cell culture. This figure was adapted from ATCC.

2.1.3.6 CHO K1 and CHO CR3+ cell lines

This epithelial-like cell line was derived as a subclone from the parental CHO cell line initiated from a biopsy of an ovary of an adult Chinese hamster. In this study CHO CR3+ cell line was also used, which expressed β_2 integrin, CD11b/CD18 (CR3), in the cell surface (Figure 2.10).
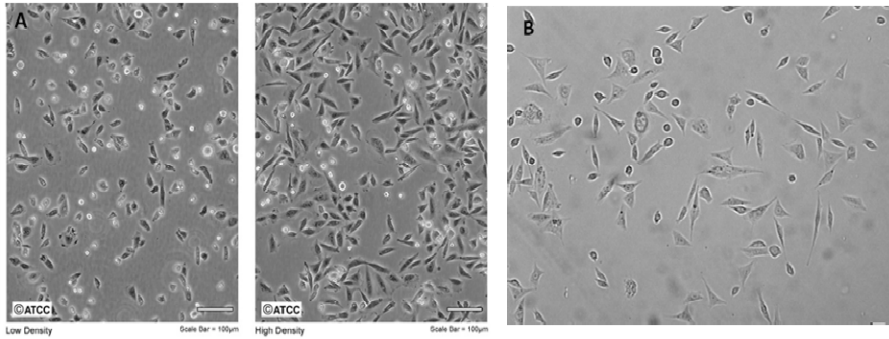
Figure 2.10 (A) CHO K1 and (B) CHO CR3+ cell cultures. Figure A was adapted from ATCC. Figure B was taken in Leica DMI 4000 B inverted microscope by image acquisition (Hamamatsu C10600 ORCA-R2 digital camera) using a 10X objective.

2.1.3.7 J774A.1 and J774A.1 CR3- cell lines

This is a monocyte/macrophage cell line obtained from a BALB/c mice with reticulum-like sarcoma. As RAW 264.7, J774A.1 cell line also presented a stable expression of β_2 integrin, CD11b/CD18 (CR3), on its cell surface. Additionally, J774A.1 CR3- cell line, which did not express β_2 integrin, was also used in this study and presented CHO-like cell morphology (Figure 2.11).
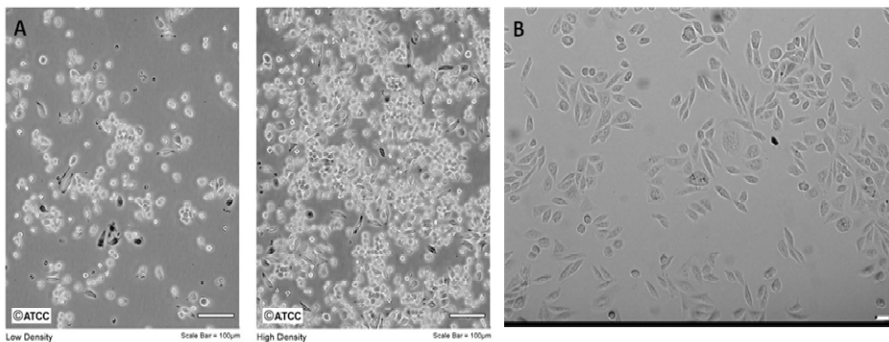
Figure 2.11 (A) J774A.1 and (B) J774A.1 CR3- cell cultures. Figure A was adapted from ATCC. Figure B was taken in Leica DMI 4000 B inverted microscope by image acquisition (Hamamatsu C10600 ORCA-R2 digital camera) using a 10X objective.

2.1.4 Devices and equipment

Device/Equipment	Model	Supplier
Atomic force microscope	NanoWizard II AFM	JPK Instruments
Autoclave	Raypa Steam Sterilizer	Raypa
Bath sonicator	FB-15049	Fisher Scientific Inc.
Cantilever of AFM	MLCT SiN	Veeco Instruments
Cell counter	BIO-RAD TC 10TM	BIO-RAD
Centrifuge	Alegra X-12R	Beckman Coulter
Electric wave generator	TG330 function generator	Thurlby Thandar Ins.
Flow cytometer	FACSCalibur	BDBiosciences
Fluorescence confocal	Olympus IX 81	Olympus
microscopes	Leica TCSSP5	Leica Microsystems
Gel Electrophoresis System	Mini-PROTEAN® 3 Cell	BIO-RAD
Gel Electrophoresis System	Mini-Sub Cell GT Cell	BIO-RAD
Gel Documentation System	Scie-Plas VISION	Scie-Plas
Incubator	Auoflow4950	NuAire
Langmuir balance	µThrough-S equipment	Kibron
Microcentrifuge	Biofuge Fresco	Heraeus
Microplate reader	Powerwave XS	BioTek
Power supply	PowerPac Basic™	BIO-RAD
Sonicator	Soniprep 150	MSE Scientific Ins.
Thermal cycler (PCR)	Mastercycler gradient	Eppendorf
T-controlled water bath	Julabo® F10-MH	Julabo Labortechnik
Tissue Culture Hood	Bio II A	TELSTAR
Ultracentrifuge	Optima™ MAX	Beckman Coulter

2.1.5 Software and internet resources

Software/Internet source	Application
Adobe 9.0 Professional	Adobe Systems
Adobe Photoshop CS	Adobe Systems
CellQuest Pro (Becton-Dickinson)	Flow cytometry software
Endnote X5	Bibliographic analysis
Film Ware 2.30	Langmuir balance data analysis
Fluoview v.50	Image analysis
Gen5	Data analysis
GraphPad Prism 5	Data analysis
JPK Image Processing software	AFM analysis
Leica Application Suite software	Image analysis
Microsoft Office Applications	Microsoft
NCBI (Ntl. Center for Biotech. Information)	www.ncbi.nlm.nih.gov
Quantity One 4.5	Densitometric data analysis
WinMDI 2.9	Flow cytometry analysis

2.2 Cell culture

Cells were cultured as exponentially growing subconfluent monolayers and maintained in DMEM containing glutamate, sodium pyruvate and 1 g/l glucose and supplemented with 10% (v/v) heat inactivated FBS (50 min, 55ºC), 4 mM L-glutamine, Mycokill AB and penicillin/streptomycin (100 U/ml and 100 µg/ml, respectively) in a humidified atmosphere consisting of 5% CO_2 and 95% air at 37ºC. The culture media used for U87.CD4.CXCR4, CHO CR3+ and J774A.1 CR3- cells were also supplemented with 1 µg/ml puromycin and 300 µg/ml Geneticin (G418 sulphate), 150 µg/ml hygromycin B and 500 µg/ml G418, and 1.5 µg/ml puromycin, respectively.

These adherent cells were regularly passaged at subconfluence. More in detail, when subconfluent monolayers were obtained, cells were washed with 1X PBS prior to cell detachment using 0.05% trypsin/EDTA solution. Next, 0.05%

trypsin/EDTA solution was diluted 1:10 by adding new fresh growth medium (DMEM supplemented with the reagents mentioned above) to detached cells. Since the above described trypsin treatment was not suitable for detaching RAW 264.7 and J774A.1 cells these cells were harvested by scrapping. Finally, all cells were plated at 1:2-1:10 dilutions onto culture flasks.

On the other hand, when exact number of cells was needed to seed in each well of 24 and 96-well plates, 10 µl of each cell sample were loaded into a slide that was subsequently inserted in BIO-RAD TC 10TM automated cell counter to measure cell number per ml of cell suspension.

For long-term storage of cell lines, cells were washed with 1X PBS followed by scrapping or trypsin treatment. Then, growth medium was added to detached cells and they were centrifuged at $520 \times g$ for 10 min. The resulting pellet was resuspended in freezing medium [90% (v/v) FBS and 10% (v/v) DMSO containing medium] and aliquots were frozen at −80°C and transferred to liquid nitrogen.

2.2.1 *Mycoplasma* detection assay

It was previously reported that *Mycoplasma* infection could promote accelerated oligonucleotide uptake by cultured cell lines, thereby inducing the expression of a plasma membrane "receptor" involved as an invariant bacterial membrane protein (de Diesbach *et al.*, 2003). In this regard, in order to discard cell cultures contaminated with *Mycoplasma*, Venor®GeM *Mycoplasma* Detection Kit was used.

This kit is based on the polymerase chain reaction (PCR), which was established as the method of choice for highest sensitivity in the detection of *Mycoplasma* and *Acholeplasma* contamination in cell cultures and other cell culture derived biologicals. The primer set is specific to the highly conserved

rRNA operon (*i.e.*, the 16S rRNA coding region in the mycoplasma genome), allowing detection not only of *M. orale, M. hyorhinis, M. arginini, M. fermentas, M. salivarium* and *M. hominis* (usually encountered as contaminants in cell cultures), but also *M. pneumoniae*, *Acholeplasma laidlawii*, *M. synoviae* and *Ureaplasma* species.

Mycoplasma detection kit for conventional PCR

1) Sample preparation: 100 µl supernatant from test culture at 90-100% confluence was transferred to a sterile microcentrifuge tube, boiled at 95ºC for 5 min and briefly centrifuged for 5 s to pellet cellular debris before adding to the PCR mixture.

2) Total volume per reaction used was 25 µl. The following is the pipetting scheme for one reaction and the program of amplification (Table 2.5):

   a. Water   15 µl

   b. 10X Strand Taq Reaction Buffer   2.5 µl

   c. Primer/Nucleotide Mix   2.5 µl

   d. Internal Control   2.5 µl

   e. Taq DNA Polymerase (5,000 U/ml)   0.5 µl

   f. Sample/Negative control/Positive control   2 µl

Cycles	Temperature (ºC)	Time (s)	Process
1	94	120	Initial denaturation
39	94	30	Denaturation
	55	30	Annealing
	72	30	Elongation
1	4-8		Cool down

Table 2.5 Program of amplification used in the Mastercycler gradient thermal cycler.

3) Agarose gel electrophoresis: agarose gel was prepared in a concentration of 1.5% (w/v) agarose in 1X TBE [0.1 M Tris-borate (pH 8.3), 2 mM EDTA] buffer. PCR products were mixed with 6X loading dye prior to loading onto the gel. As a marker 1 Kb Plus DNA Ladder was used. Prepared samples were loaded on agarose gel and run at 100 V for 30 min. Then, DNA bands were stained in SYBR® Green dye containing 1X TBE buffer and visualised by Scie-Plas VISION Gel Documentation System (Figure 2.12).
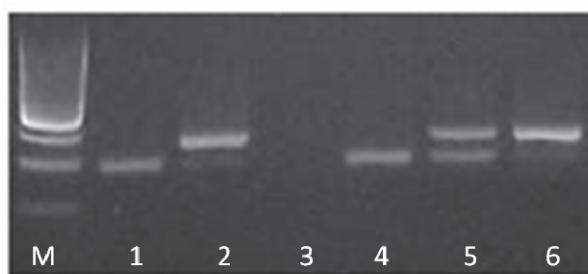
Figure 2.12 Representative image showing possible results of PCR products. M: 100 bp DNA Ladder; 1: negative control; 2: positive control; 3: inhibited sample; 4: negative sample; 5: positive sample, weak contamination; 6: positive sample, strong contamination. This figure was taken from the technical bulletin of Venor®GeM *Mycoplasma* Detection Kit.

2.2.2 Cell cytotoxicity assay

Cytotoxicity assays are widely used by pharmaceutical industry to screen the negative effect of compound libraries. This is a crucial step to assess unwanted cytotoxic effects before studying in depth their development as drugs. According to this, it was essential to perform this kind of assays with selected oligonucleotide conjugates prior to cell surface adsorption and uptake experiments to test whether these compounds were cytotoxic in these cells. Additionally, this assay was also

used to test the cytotoxic effect that endocytic inhibitors could generate in HeLa cells during uptake experiments.

Cell cytotoxicity was measured by CellTiter 96® AQueous Non-Radioactive Cell Proliferation Assay. This colorimetric method, also known as cell viability and proliferation assay, is based on rate of reduction of the tetrazolium dye MTS [3-(4,5-dimethylthiazol-2-yl)-5-(3-carboxymethoxyphenyl)-2-(4-sulfophenyl)-2H-tetrazolium] in the presence of an electron coupling reagent PMS (phenazine methosulfate) [5% (v/v)] by mitochondrial dehydrogenases of metabolically active cells, producing a soluble product called formazan which can be measured at 490 nm. The quantity of generated formazan product, as measured by the amount of 490 nm absorbance, is directly proportional to the number of viable cells in culture (Figure 2.13).
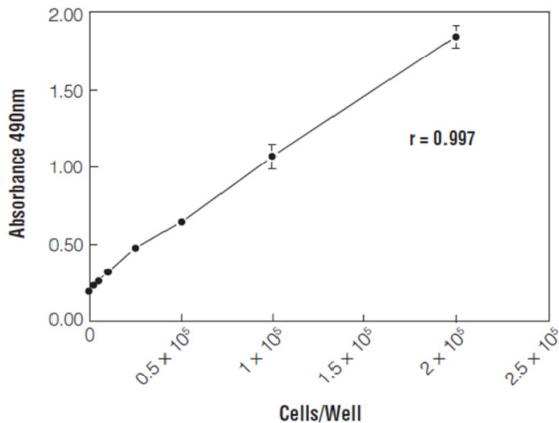
Figure 2.13 Representative figure of the effect of cell number on absorbance at 490 nm measured using CellTiter 96® AQueous assay. Different amounts of K562 (human chronic myelogenous leukemia) cells were plated in the wells of a 96-well plate in appropriate growth medium and equilibrated for 1 h at 37ºC in a humidified 5% CO_2 atmosphere before adding 20 µl/well combined MTS/PMS solution. After incubation for 1 h with combined MTS/PMS solution absorbance was recorded at 490 nm in an ELISA plate reader. The correlation coefficient of the line indicates a linear response between cell number and absorbance at 490 nm. This figure was taken from Promega's technical bulletin of CellTiter 96® AQueous Assay.

MTS and PMS reagents were dissolved in DPBS (Dulbecco's Phosphate Buffered Saline), as described in user's manual.

Cell cytotoxicity assay

1) Cells were seeded in 96-well plates in triplicate and allowed to attach overnight in appropriate growth medium (see section 2.2).

2) The following day cells were washed with DPBS and incubated in 100 µl OptiMEM in the absence or presence of oligonucleotide conjugates or endocytic inhibitors for desired incubation time at 37ºC.

3) Then, 20 µl/well of combined MTS/PMS solution were added.

4) After 2 h of incubation at 37ºC with combined MTS/PMS solution, absorbance was measured at 490 nm in a Biotek Powerwave XS microplate reader. The absorbance of the medium without cells was subtracted to all absorbance values and the control values were considered as 100% of cell viability. Relative cell viability of individual samples was calculated by normalizing their absorbance to that of the corresponding control sample.

5) Statistical analysis were performed using the Student's t-test as appropriate, with the level of significance set at $p < 0.05$. Significance and symbols: $p > 0.05$ non significant (n.s.); $p < 0.05$ significant (*); $p < 0.01$ significant (**); $p < 0.001$ significant (***).

2.2.3 Cell-surface adsorption studies

Cell-surface adsorption experiments were performed with COCs to compare their behaviour in two different incubation media, glucose free or glucose at physiological concentration (5.5 mM glucose).

<u>Cell-surface adsorption assay</u>

1) HeLa and U87.CD4.CXCR4 cells were seeded at 1.25×10^5 cells/well into 24-well plates 48 h before treatment in appropriate growth medium, in the absence or presence of glucose (5.5 mM) (see section 2.2).

2) Then, cells were washed with DPBS and incubated for 1 h on ice with 250 µl serum-free DMEM containing 5 µM of different Alexa 488-labelled COCs, with or without glucose (5.5 mM).

   - The low incubation temperature used in this experiment was sufficient to provide the adsorption or binding of the compounds to the cell surface but avoided their internalisation.

   - Untreated cells were used as negative control.

3) After incubation, cells were washed three times with ice-cold DPBS to remove unbound compound, harvested by scrapping and resuspended in 400 µl ice-cold PBS.

4) These samples were analysed by flow cytometry (see section 2.3).

2.2.4 Cellular uptake studies

Cellular uptake experiments were performed in order to compare *uptake profiles* of the different oligonucleotide conjugates tested.

<u>Cellular uptake assay</u>

1) Cells were seeded at 1.25×10^5 cells/well in 24-well plates and incubated overnight in appropriate growth medium (see section 2.2).

2) Next day cells were washed with DPBS and incubated with 250 µl of appropriate incubation medium [serum-free DMEM with or without glucose (5.5 mM) for COCs and OptiMEM for LOCs] in the presence of Alexa 488-labelled or Cy5-labelled oligonucleotide conjugates for desired incubation time at 37ºC.

   - As negative control untreated cells were used.

   - In LOC uptake experiments unmodified Alexa 488-labelled GEM91 was also mixed with Transfectin™ cationic lipid reagent to compare conjugation and complexation patterns.

3) After incubation, cells were washed three times with 1X PBS to remove unbound compound. Subsequently, cells were harvested by scrapping or completely dissociated in 0.05% trypsin-EDTA solution.

4) Cell samples were centrifuged at $520 \times g$ for 10 min and then resuspended into 200 µl ice-cold 1X PBS, followed by flow cytometric analysis (see section 2.3).

Cellular uptake experiments were also performed in presence of endocytic inhibitors with the LOC that showed the best uptake profile, which was Alexa 488-labelled C_{28}(5')-GEM91 (compound number **30**), to further unravel the *internalisation pathway* used by this molecule.

Cellular uptake assay in presence of endocytic inhibitors

1) HeLa cells were seeded at 1.25×10^5 cells/well in 24-well plates and incubated overnight in appropriate growth medium (see section 2.2).

2) Next day cells were washed with DPBS and preincubated with 250 µl OptiMEM in absence or presence of inhibitors of different endocytic routes for 30 min at 37ºC.

3) Then, 0.5 µM C_{28}(5')-GEM91-(3')Alexa 488 (**30**) was added to each well and incubated for 2 h at 37ºC.

4) After incubation, cells were washed three times with 1X PBS to remove unbound compound. Subsequently, cells were completely dissociated in 0.05% trypsin-EDTA solution.

5) Trypsin treated cells were washed by centrifugation at $520 \times g$ for 10 min and then resuspended into 200 µl ice-cold 1X PBS, followed by flow cytometric analysis (see section 2.3).

Finally, cellular uptake experiments were designed in presence of fibrinogen, a natural ligand for β_2 integrin, with the LOC that showed the best uptake profile, which was Alexa 488-labelled C_{28}(5')-GEM91 (compound number **30**), to further examine *the role of β_2 integrin* in C_{28}(5')-GEM91 uptake by CHO CR3+, J774A.1 and RAW 264.7 cells.

Cellular uptake assay in presence of fibrinogen,

a natural ligand for β_2 integrin

1) CHO K1, CHO CR3+, J774A.1 CR3-, J774A.1 and RAW 264.7 cells were seeded at 1.25×10^5 cells/well in 24-well plates and incubated overnight in appropriate growth medium (see section 2.2).

2) Next day cells were washed with DPBS and preincubated with 250 µl OptiMEM in absence or presence of different concentrations of fibrinogen (100 nM or 500 nM) for 30 min at 37ºC.

3) Then, 100 nM C_{28}(5')-GEM91-(3')Alexa 488 (**30**) was added to each well and incubated for 30 min at 37ºC.

4) After incubation, cells were washed three times with 1X PBS to remove unbound compound. Subsequently, cells were harvested by scrapping or completely dissociated in 0.05% trypsin-EDTA solution.

5) Cells samples were centrifuged at $520 \times g$ for 10 min and then resuspended into 200 µl ice-cold 1X PBS, followed by flow cytometric analysis (see section 2.3).

2.2.5 Subcellular localisation studies

Subcellular localisation experiments were performed in order to analyse the *intracellular destination of internalised LOCs*.

<u>**Cellular uptake assay for localisation studies**</u>

1) HeLa cells were seeded at 5×10^4 cells/well in 8 well-Lab-Tek™ Chamber slides pretreated with Poly-L-lysine solution and incubated overnight in appropriate growth medium (see section 2.2).

2) The following day cells were washed with DPBS and incubated with 250 µl OptiMEM containing 500 nM Alexa 488-labelled or Cy5-labelled LOCs for 4 h at 37ºC.

3) After incubation, cells were washed three times with DPBS to remove unbound compound and fixed with 4% PFA (w/v) for 15 min at room temperature (RT).

4) After fixation, cells were stained with nuclear marker Hoechst 33258 for 10 min at RT and 250 µl 1X PBS was added to each well.

5) Finally, samples were visualized using Olympus IX 81 inverted fluorescence confocal microscope and capture image acquisition with a digital camera (Axiocam NRc5, Zeiss) (see section 2.7).

In particular, localisation studies were also designed for the LOC that showed the best uptake profile, which was Alexa 488-labelled $C_{28}(5')$-GEM91 (compound number **30**), to analyse its *internalisation behaviour in different cell lines*.

Cellular uptake assay for localisation studies in different cell lines

1) Cells were seeded at 2×10^4 cells/well in 96 well-BD Falcon™ Tissue Culture Treated Imaging Plates and incubated overnight in appropriate growth medium (see section 2.2).

2) The following day cells were washed with DPBS and incubated with 100 µl OptiMEM containing 500 nM Alexa 488-labelled $C_{28}(5')$-GEM91 (compound number **30**) for 30 min and 4 h at 37ºC.

3) After incubation, cells were washed three times with DPBS to remove unbound compound and fixed with 4% (w/v) PFA for 15 min at RT.

4) After fixation, cells were stained with nuclear marker Hoechst 33258 for 10 min at RT and 250 µl 1X PBS was added to each well.

5) Finally, samples were visualized using Olympus IX 81 inverted fluorescence confocal microscope and capture image acquisition with a digital camera (Axiocam NRc5, Zeiss) (see section 2.7).

Finally, deeper studies were undertaken with the LOC that showed the best uptake profile, which was Alexa 488-labelled C_{28}(5')-GEM91 (compound number **30**), to further unravel the internalisation pathway used by this molecule. In this case, several endocytic markers were used to analyse *co-localisation profiles* between this compound and different cellular compartments.

Cellular uptake assay for co-localisation studies

1) Cells were seeded at 5×10^4 cells/well in 8 well-Lab-Tek™ Chamber slides pretreated with Poly-L-lysine solution and incubated overnight in appropriate growth medium (see section 2.2).

2) Next day cells were washed with DPBS and pretreated with different endocytic inhibitors for 30 min at 37ºC in OptiMEM, previous to incubation with 100 nM Alexa 488-labelled C_{28}(5')-GEM91 for 2 h at 37ºC.

3) After incubation, cells were washed three times with 1X PBS to remove unbound compound and fixed with 4% (w/v) PFA for 15 min at RT followed by permeabilization with 0.1% (w/v) Triton X-100 dissolved in 1X PBS for 10 min at RT.

4) Next, samples were blocked with 1% (w/v) BSA dissolved in 1X PBS at RT for 30 min to block unspecific binding of the antibodies.

5) After blocking reaction, samples were incubated with the appropriate primary antibodies (1:200 dilution) at RT for 1 h followed by incubation with Alexa Fluor 546 and 633-conjugated secondary antibodies (1:200 dilution) at RT for 1 h.

6) Finally, samples were stained with nuclear marker Hoechst 33258 at RT for 10 min and 100 μl 1X PBS was added to each well before visualizing them in Olympus IX 81 inverted fluorescence confocal microscope (see section 2.7).

2.2.6 RNA interference transfection assay

To further unravel the internalisation route involved in Alexa 488-labelled C_{28}(5')-GEM91 (**30**) uptake by HeLa cells, the expression of clathrin heavy chain and caveolin-1 proteins were silenced. These two proteins are crucial for clathrin dependent endocytosis and caveolae dependent endocytosis, respectively.

This experiment was performed in order to complete cellular uptake studies carried out in presence of endocytic inhibitors (see section 2.2.4).

<u>**siRNA transfection protocol**</u>

1) HeLa cells were seeded at 1.25×10^5 cells/well in 6-well plates, incubated in appropriate growth medium (see section 2.2) and allowed to attach for 6 h. Then, medium was replaced by 800 µl OptiMEM and incubated overnight.

2) Next day desired siRNA was added to each well following manufacturer's instructions (quantities per well):

- Solution A: 4 µl oligofectamine + 100 µl OptiMEM (mixed and incubated for 5-10 min at RT).

- Solution B: 4 µl siRNA (from 10 µM siRNA stock) + 100 µl OptiMEM.

- Once these two solutions were prepared, solution A was added into solution B and mixed gently by pipetting. The mixture was incubated for 15 min at RT and then added into the well. Cells were incubated for 5 h.

3) After incubation, 1 ml OptiMEM supplemented with 20% (v/v) FBS was added to each well without removing transfection mixture. This cell culture was further incubated for 24 h. Then, the medium was replaced by appropriate growth medium and cells were subsequently incubated for another 24 h.

4) 24 h after medium replacement, cells were washed with 1X PBS and completely dissociated in 0.05% trypsin-EDTA solution. Trypsin treated cells were centrifuged at $520 \times g$ for 10 min, resuspended into appropriate growth medium and counted in order to be seeded (1.25×10^5 cells/well) in 24-well plates.

5) The following day some wells were used to perform cellular uptake assays with Alexa 488-labelled C_{28}(5')-GEM91 (**30**), following the same protocol designed for endocytic inhibitors. The remaining wells were used for western blotting experiments in order to test siRNA silencing efficiency obtained by this assay (see section 2.4).

2.2.7 Cell-surface receptor staining assay

This assay was performed in order to determine cell-surface β_2 integrin expression in CHO CR3+, J774A.1 and RAW 264.7 cells and as negative controls CHO and J774A.1 CR3- cells were used. The experiment was designed in parallel to cellular uptake studies carried out in the presence of fibrinogen, a natural ligand of β_2 integrin.

<u>Determination of cell-surface CD11b expression</u>

1) Cells were seeded at 1.25×10^5 cells/well in 24-well plates and incubated overnight in appropriate growth medium.

2) Next day cells were washed twice with 0.1% (w/v) BSA dissolved in 1X PBS, scrapped and collected into microcentrifuge tubes to be centrifuged at $520 \times g$ for 8 min at 4ºC.

3) Cell pellets were resuspended in 200 µl blocking solution [1X PBS containing 0.1% (w/v) BSA and 10% (v/v) FBS] for 15 min on ice to block unspecific binding of the antibody.

4) After blocking reaction, cells were washed twice with 0.1% (w/v) BSA dissolved in 1X PBS and cell pellets were resuspended with 100 µl anti-CD11b FITC conjugated antibody solution [1X PBS containing 0.1% (w/v) BSA and antibody (1:1000 dilution)]. Samples were incubated for 1h on ice.

5) Then, cells were washed twice with 0.1% (w/v) BSA dissolved in 1X PBS and fixed with 200 µl 4% (w/v) PFA for 20 min on ice.

6) After fixing treatment, cells were washed twice with 0.1% (w/v) BSA dissolved in 1X PBS, followed by flow cytometric analysis (see section 2.3).

2.3 Flow cytometry

Flow cytometry is a sophisticated fluorescence technique that enables the characterization and analysis of a particle or cell suspension. Indeed, this technique is able to analyse simultaneously multiple physical and chemical characteristics of each individual suspended particle or cell when this passes in a fluid stream through a beam of laser light. Suitable particle size range for flow cytometry varies between 200 nm and 50 µm, which includes the size of most of cell types.

The principle of flow cytometry is based on a laser light of a single wavelength which is directed onto a hydro-dynamically focused stream of fluid. Three types of detectors are aimed at the point where the stream passes through the light beam:

- FSC (forward scatter) that is in line with the light beam. It correlates with the cell volume.

- SSC (side scatter) that is perpendicular to the light beam. It depends on the inner complexity of the particle (*i.e.*, shape of the nucleus, amount and type of cytoplasmic granules, membrane roughness).

- Fluorescent detectors (FL) that are perpendicular to the light beam. They collect the fluorescence of the particle (*i.e.*, the emission from multiple fluorophores).

Hence, when each suspended particle or cell passes through the beam, it scatters the light (light dispersion) and fluorescent chemicals of the particle or attached to it may be excited into emitting light at a higher wavelength than the light source. The combination of both scattered and fluorescent lights is picked up by the detectors previously mentioned (Figure 2.14).
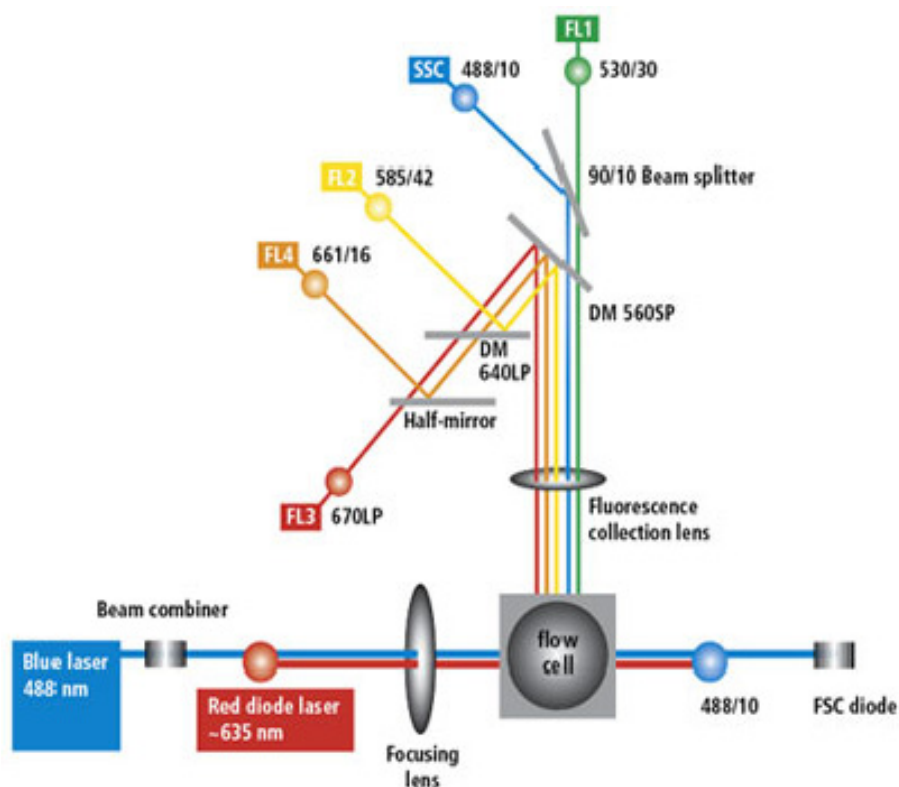
Figure 2.14 Schematic representation of BD FACSCalibur optical path configuration.
This figure was taken from FACSCalibur brochure of BDBiosciences.

The result is a specific distribution of fluorescence for the cell population, which can be depicted as a histogram of fluorescence intensity versus the number of cells. Thus, the fluorescence intensity of different cell populations can be easily compared, such as treated with different oligonucleotide conjugates or different incubation conditions.

In this project, flow cytometry was used in order to analyse cell-surface adsorption and cellular uptake experiments carried out with fluorescent oligonucleotide conjugates. The flow cytometer used in this study was FACSCalibur, BDBiosciences.

Flow cytometry analysis for cell-surface adsorption, cellular uptake and cell-surface receptor staining assays

1) Cell suspensions were obtained from cell-surface adsorption, cellular uptake and cell-surface receptor staining experiments. The fluorescence emitted from Alexa 488-labelled or Cy5-labelled oligonucleotide conjugates and FITC-conjugated antibody was measured by loading these samples onto the flow cytometer. The specific parameters for each cell line were determined by loading untreated cell suspensions and the fluorescence of 10,000 cells was measured from each sample.

2) In cell-surface adsorption and cell-surface receptor staining assays the surface-fluorescence cells was measured. This is due to the fact that at 4ºC internalisation of either Alexa 488-labelled COCs or FITC-conjugated antibody was avoided. By contrast, two different flow cytometry analyses were obtained from cellular uptake assays with Alexa 488-labelled oligonucleotide conjugates, depending on total or intracellular fluorescence of cell populations:

   a. Total fluorescence of cell populations was measured by loading the samples directly onto the flow cytometer. In this case, both internalised and extracellular fluorescence were collected together.

   b. Intracellular fluorescence was assessed by mixing the samples with Trypan Blue [0.2% (v/v) final concentration] before loading them onto the flow cytometer. Trypan Blue was used to quench the fluorescence remaining at the cell surface, thereby measuring only the fluorescence corresponding to internalised compounds (Pils *et al.*, 2006). Unfortunately, Trypan Blue was not a suitable quencher for Cy5 fluorescence and only total fluorescence could be measured from Cy5-containing samples.

85

3) Alexa 488 and FITC fluorescence were measured using an air-cooled 488 nm argon-ion laser, collecting emission signals by FL1 detector. In the case of Cy5, an air-cooled 633 helium-neon ion laser was used and Cy5 emission was collected by FL4 detector.

GMFI (Geometric Mean Fluorescence Intensity) data of histograms were used for analysis comparison (Figure 2.15). Statistical analysis were performed using the Student's t-test as appropriate, with the level of significance set at $p < 0.05$. Significance and symbols: $p > 0.05$ non significant (n.s.); $p < 0.05$ significant (*); $p < 0.01$ significant (**); $p < 0.001$ significant (***).
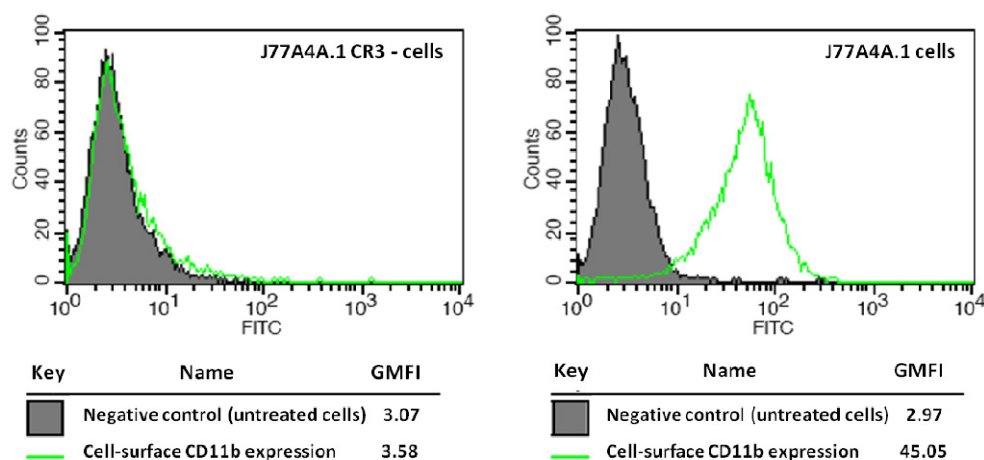
Figure 2.15 Representative picture of various histograms showing GMFI data obtained for FITC fluorescence in cell-surface CD11b receptor staining experiments using anti-CD11b FITC conjugated antibody. J774A.1 CR3- cells (left) are used as negative control since they do not express CD11b receptor on the cell-surface. J774A.1 cells (right) present a stable expression of CD11b receptor on the cell-surface.

2.4 Western blotting

This widely used analytical technique is suitable for detecting specific proteins of tissue homogenate or cell extract samples. It is based on protein separation by SDS polyacrylamide gel electrophoresis (SDS-PAGE) followed by electrophoretic transfer and immobilization of these proteins on PVDF or nitrocellulose membranes. Then, either specific monoclonal or polyclonal antibodies can be used to recognise desired target proteins. Finally, these primary antibodies are detected by a second antibody which is usually linked to biotin or to a reporter enzyme such as alkaline phosphatase or horseradish peroxidase. This means that several secondary antibodies will bind to one primary antibody and enhance the signal (Towbin et al., 1979; Hempelmann et al., 1987). In this case, horseradish peroxidase (HRP)-linked secondary antibodies were used to cleave a chemiluminescent agent, producing luminescence in proportion to the amount of protein.
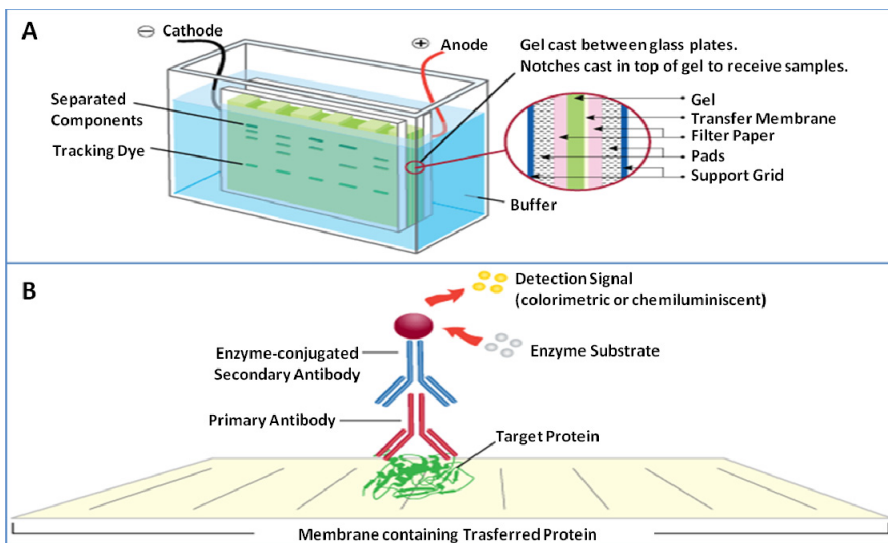
Figure 2.16 Representative picture of western blotting. Illustrations of western blotting set up (A) and target protein detection (B). These figures were taken from Leinco technologies, Inc.

This technique was used to determine GLUT 1 and GLUT 3 glucose transporters expression in HeLa and U87.CD4.CXCR4 cell lines in absence or presence of glucose (5.5 mM). For this purpose, plasma membrane was also separated from these samples in order to compare the two experimental conditions mentioned above.

<u>**GLUT 1 and GLUT 3 detection by western blotting**</u>

1) HeLa and U87.CD4.CXCR4 cells were seeded at 5×10^5 cells/dish in 150 mm diameter dishes and incubated in appropriate growth medium overnight (see section 2.2).

2) Next day cells were washed with DPBS and incubated for 48 h with appropriate incubation medium in the absence or presence of glucose (5.5 mM).

3) After incubation, cells were washed with ice-cold DPBS, scrapped and harvested with ice-cold homogenisation buffer [50 mM HEPES (pH 8.0), 137 mM NaCl, 1 mM $MgCl_2$, 1 mM $CaCl_2$, 1% (v/v) NP-40, 10% (v/v) glycerol, 2.5 mM EDTA, 10 mM NaP_2O_7, 1 µl/ml protease inhibitor cocktail] as described (Hundal *et al.*, 2003).

4) Then, cells were homogenised by passing the samples through a 26G needle 10 times at 4ºC. The homogenate was centrifuged at $520 \times g$ for 10 min at 4ºC to remove nuclei and cell debris (Torres *et al.*, 2012).

5) The supernatant was collected and ultracentrifuged at $100,000 \times g$ for 30 min at 4ºC to separate membrane-bound compartments (pellet) and the remaining cytoplasm (supernatant).

6) These two remaining samples were sonicated and their protein concentration was determined by BioRad commercial kit (BCA assay).

7) Protein samples (20 µg protein/sample) were mixed with 4X loading buffer [125 mM Tris (pH 6.8), 50% (v/v) glycerol, 4% (w/v) SDS, 0.08% (w/v) bromophenol blue, 50 µl/ml β-mercaptoethanol] and heated at 70ºC for 10 min.

8) These samples were loaded onto 12% polyacrylamide gels to perform protein separation by SDS-PAGE. As protein-marker Precision Plus Protein™ Standards were used. Electrophoresis was run (120 V for 2 h) in electrophoresis buffer [25 mM Tris-HCl (pH 8.3), 192 mM glycine, 0.1% (w/v) SDS].

9) After that, gel proteins were transferred onto nitrocellulose membrane. Transference was run (400 mA for 75 min) in ice-cold transfer buffer [25 mM Tris (pH 8.3), 192 mM glycine, 20% (v/v) methanol]. In order to avoid unspecific antibody bindings, nitrocellulose membrane was blocked for 1 h with 5% (w/v) skim milk dissolved in Tris-buffered saline (TBS) [50 mM Tris (pH 7.6), 150 mM NaCl] containing 0.01% (w/v) NaN_3 and 0.1% (w/v) Tween 20.

10) Blocking solution was then removed and the nitrocellulose membrane was incubated overnight with the primary antibody (1:5000 dilution for anti-GLUT 1 antibody; 1:1000 dilution for anti-GLUT 3 and anti-GAPDH antibodies) in TBS supplemented with 0.1% (w/v) Tween 20 (TBST) at 4ºC. Since GAPDH is considered a housekeeping protein, in this work it was used as loading control for western blotting analysis and further protein normalisation. After incubation with the primary antibody, the membrane was washed three times with TBST and subsequently incubated with HRP-conjugated secondary antibody (1:4000 dilution) in TBST for 1 h at RT.

11) After incubation with the secondary antibody, the membrane was washed three times with TBST and the chemiluminescent reaction was performed. Bands were visualized by enhancing chemiluminescence and exposed films were analysed by Quantity One 4.5 software in order to measure arbitrary units.

Additionally, western blotting was also used to confirm an efficient siRNA silencing effect in the expression of clathrin heavy chain and caveolin-1 proteins.

Measurement of clathrin heavy chain and caveolin-1 expression
by western blotting

1) After siRNA treatment (see section 2.2.6), HeLa cells were washed with ice-cold DPBS, scrapped and harvested with ice-cold homogenisation buffer [50 mM HEPES (pH 8.0), 137 mM NaCl, 1 mM $MgCl_2$, 1 mM $CaCl_2$, 1% (v/v) NP-40, 10% (v/v) glycerol, 2.5 mM EDTA, 10 mM NaP_2O_7, 1 µl/ml protease inhibitor cocktail] as described (Hundal *et al.*, 2003).

2) Samples were then lysed by sonication and protein concentration was determined by BioRad commercial kit (BCA assay).

3) Protein samples (20 µg protein/sample) were mixed with 4X loading buffer [125 mM Tris (pH 6.8), 50% (v/v) glycerol, 4% (w/v) SDS, 0.08% (w/v) bromophenol blue, 50 μl/ml β-mercaptoethanol] and heated at 90ºC for 10 min.

4) The following steps were performed using the protocol designed for "GLUT 1 and GLUT 3 detection by western blotting", starting from step 8. Here, primary antibody dilution used was 1:1000 (anti-clathrin heavy chain; anti-caveolin-1; GAPDH) and secondary antibody dilution was 1:4000.

2.5 Formation of DNA duplexes

After studying the interesting properties that C_{28} lipid moiety provided to single stranded oligodeoxynucleotide GEM91, double stranded C_{28} conjugate species were prepared to analyse whether these properties were present in a similar manner with double-stranded compounds.

Preparation of DNA duplexes

1) Double stranded C_{28} conjugates were prepared by mixing C_{28}-conjugated GEM91 with complementary strand AntiGEM91 in equimolar ratio. For fluorescence experiments, one strand of the duplex was labelled with Alexa 488.

2) The annealing procedure was performed by incubating samples dissolved in 1X PBS at 95ºC for 2 min, followed by a cooling step at 1ºC/min to RT in a temperature-controlled water circulating bath Julabo® F10-MH (Bene *et al.*, 2004; Ohrt *et al.*, 2006; Chung *et al.*, 2011).

3) Then, formation of DNA duplexes was checked by either polyacrylamide or agarose gel electrophoresis.

2.5.1 Polyacrylamide gel electrophoresis

Non-denaturing polyacrylamide gel electrophoresis was performed using 15% (w/v) polyacrylamide gels (19:1 monomer/bis ratio) in 1X TBE running buffer. Samples (single and double stranded species) were mixed with 6X loading dye before loading in each pocket. Polyacrylamide gel was run at 120 V for 3 h followed by staining with SYBR® Gold dye. Finally, DNA bands were analysed by Scie-Plas VISION Gel Documentation System.

For staining of single and double DNA bands SYBR® Gold nucleic acid gel stain was chosen since it is considered as the most sensitive fluorescent stain available for detecting either single or double stranded DNA or RNA in electrophoretic gels, using standard ultraviolet transilluminators, even surpassing the sensitivity of SYBR® Green gel stains for this application (Tuma *et al.*, 1999).

As a marker GeneRuler™ Ultra Low Range DNA Ladder was used in either polyacrylamide or agarose gels, which contained a mix of 11 chromatography-purified individual DNA fragments (in base pairs) where a 50 bp fragment was used as reference band for easy orientation (Figure 2.17).
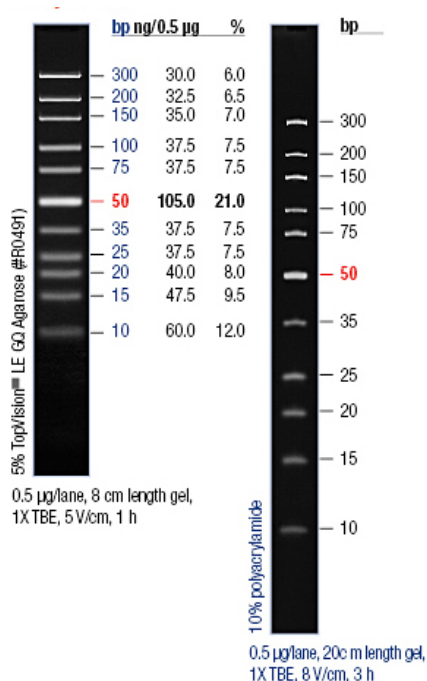
Figure 2.17 GeneRuler™ Ultra Low Range DNA Ladder in 5% (w/v) agarose gel (left) and 10% (w/v) polyacrylamide gel (right). A 50 bp fragment is shown in red and it was used as reference band for easy orientation. This figure was adapted from Fermenta's technical bulletin of GeneRuler™ Ultra Low Range DNA Ladder.

2.5.2. Agarose gel electrophoresis

RNA/DNA fragments identical in size are indistinguishable on agarose gels but on polyacrylamide gels even slight differences in DNA sequence can lead to noticeably different migration rates. In this regard, fragments of the same size do not always run the same on acrylamide gels. This is attributed more to the limitations of polyacrylamide gel technology than to a problem with the ladder composition. As defined in most molecular biology lab manuals and as acknowledged by the manufacturers of polyacrylamide gels, applications requiring precise sizing of DNA fragments should be performed using agarose gels whenever possible (Sambrook *et al.*, 1989).

In order to avoid those differences on migration rates associated with polyacrylamide gels, Metaphor® agarose gels were also performed. This high resolution agarose is known to challenge polyacrylamide since it can resolve PCR products and small DNA fragments that differ in size by 2%.

For agarose gel electrophoresis of DNA duplexes a special high resolving Metaphor® agarose was used. All agarose gels had a 4% (w/v) concentration and were used with 1X TBE running buffer (Liu *et al.*, 2010). Samples (single and double stranded species) were mixed with 6X loading dye before loading in each pocket. Agarose gel was run at 75 V for 75 min followed by staining with SYBR® Gold dye. Finally, DNA bands were analysed by Scie-Plas VISION Gel Documentation System**.**

2.6 Membrane lipid model systems

In this work three types of model membranes were used: i) lipid monolayers, ii) lipid vesicles or liposomes and iii) supported planar bilayers.

2.6.1 Lipid monolayers

This model system was used to study the interactions between lipids and LOCs. The system is based on monomolecular films at the air-water interface termed lipid monolayers. One interesting advantage of using lipid monolayers is that neither curvature nor fluctuation effects are present. Thus, there is an accurate control of the lateral pressure, molecular packing and lipid composition at every time. Unfortunately, its principal drawback appears to be the application of data from lipid monolayers to bilayers or more complex biological membranes. Nevertheless, very valuable information can be obtained about the interaction behaviour between lipids and LOCs using a combination of lipid monolayer and bilayer model system studies, which can be used as a prediction of their behaviour in cell membranes.

Lipid solutions were dissolved in chloroform/methanol (2:1) mixture, a highly volatile organic solution. For the generation of lipid monolayers, so-called Langmuir films, a desired lipid solution was spread on top of an aqueous solution. This process was easy and simple to prepare owing to the amphipatic nature of the lipids. In this manner, lipid self-organised by orienting their polar headgroups in close contact with the aqueous environment and moving their acyl chains towards the air. Once the lipid monolayer was formed and the solvent evaporated, a number of measurements within the monolayer were performed by the use of a Langmuir balance. This process was undertaken based on the Wilhelmy method, where a suspended probe was immersed in the air-water interface in order to measure any deviation from water surface tension (Figure 2.18).
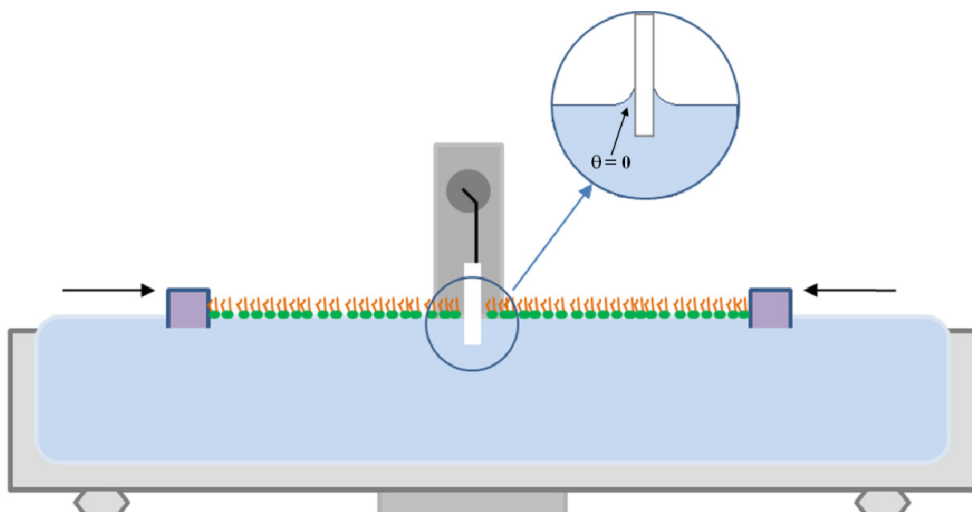
Figure 2.18 A lipid monolayer formed at the air-aqueous interface of a Langmuir trough. Zoomed area shows the contact angle on the Wilhelmy plate, which is slightly introduced into the gas-liquid interface. This figure was modified from NIMA Technology.

2.6.1.1 Langmuir balance: surface pressure measurement

This technique is based on the measurement of the water surface tension by means of a suspended solid probe that is slightly introduced into the gas-liquid interface (typically a filter paper or a platinum probe) (see Figure 2.18). This probe is also known as "Wilhelmy plate" since Ludwig Wilhelmy was the first author who provided a way for measuring surface tension back in 1863 (Wilhelmy, 1863). This probe is capable of measuring surface tension, which arises from the excess of free cohesive energy of water molecules present at the gas-liquid interface. More in detail, water molecules are exposed to forces from surrounding molecules, which are balanced in the bulk of a water solution due to the equal attraction in every direction. Nevertheless, on the surface water molecules are not subjected to attractive forces in every direction where their interactions with the neighbouring molecules are limited and weaker, leading to a reduced intermolecular hydrogen bonding of the molecules and a higher free energy termed surface free energy (Figure 2.19).

95
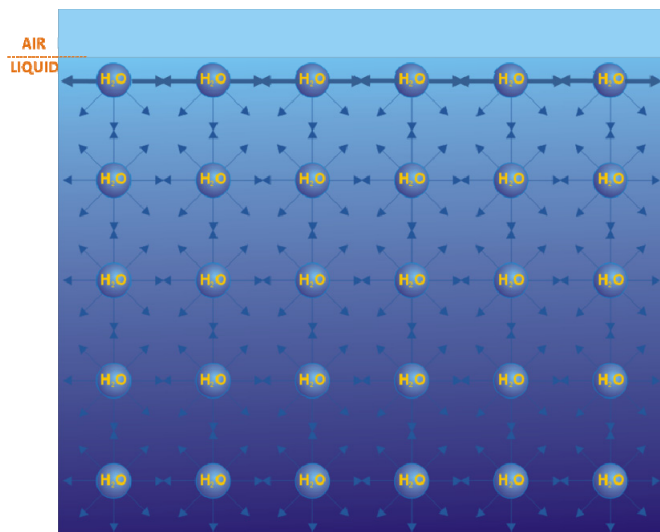
Figure 2.19 Free cohesive energy of water molecules at air-liquid interface. This figure was adapted from Kibron Inc.

This excess energy can be related to surface tension as force/length by means of the forces detected by the probe, which can be further related with surface pressures. The overall forces that the solid probe detects are:

Total force = Probe weight + probe buoyancy + surface tension

Before measuring the sample, the pressure detected by the probe must be adjusted to zero, thereby discarding the weight force. In addition, since probe buoyancy reflects the applied force of displaced water molecules upon probe immersion acting upwards, it must be also discarded as the probe is maintained at a constant depth during the measurement. In this regard, the overall force can be reduced to surface tension, which is represented in the following equation:

$$F = 2(w + t)(\gamma)(\cos \theta)$$

where: w and t represent the width and thickness of the probe, respectively; γ is the surface tension and θ is the contact angle.
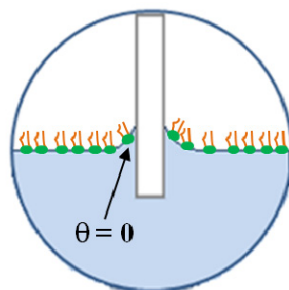
Figure 2.20 Generated meniscus and contact angle at an air-liquid interface when the probe is slightly immersed in the aqueous solution. This figure was adapted from Figure 2.17.

Owing to the meniscus formed by the probe when this is introduced in the aqueous solution (Figure 2.20), the contact angle value obtained is zero degrees, reducing the equation to:

$$\gamma = \text{Force/Perimeter}$$

This is also known as force/length and its units are mN/m (dynes/cm). In the case of water molecules, they present one of the highest surface tension in nature because of their high intermolecular attractive forces (72.8 mN/m at 22ºC and 1 atmosphere). When amphipathic molecules are found at the air-water interface, the cohesive energy of water molecules is disrupted, leading to a decrease in the water surface tension. This reduction is called surface pressure (π) which is given in the same units but opposite sign.

$$\pi = \gamma_o - \gamma$$

Taken together, all Langmuir balance measurements are carried out following surface pressure changes. Commonly, lipids are dissolved in a highly volatile organic solvent and the prepared lipid solution is spread onto the surface of an aqueous solution (the gas-liquid interface).

While the solvent is evaporated the lipids organise themselves with the hydrophilic headgroup towards the aqueous solution and the hydrophobic chain towards the air, thereby generating a lipid monolayer at an air-aqueous interface. Accordingly, while the lipids spread over the available surface area, the water surface tension is decreased. In this regard, for lipid-specific molecule interaction experiments, a lipid at a desired controlled surface pressure is initially prepared followed by the injection of the specific molecule into the subphase, leading to changes in surface pressure which are related to the incorporation or adsorption of the specific molecule into the monolayer (Figure 2.21). Of note, it is to be underscored that cell membranes are proposed to have a surface pressure of around 30 mN/m (Janmey and Kinnunen, 2006), though this value can largely vary.
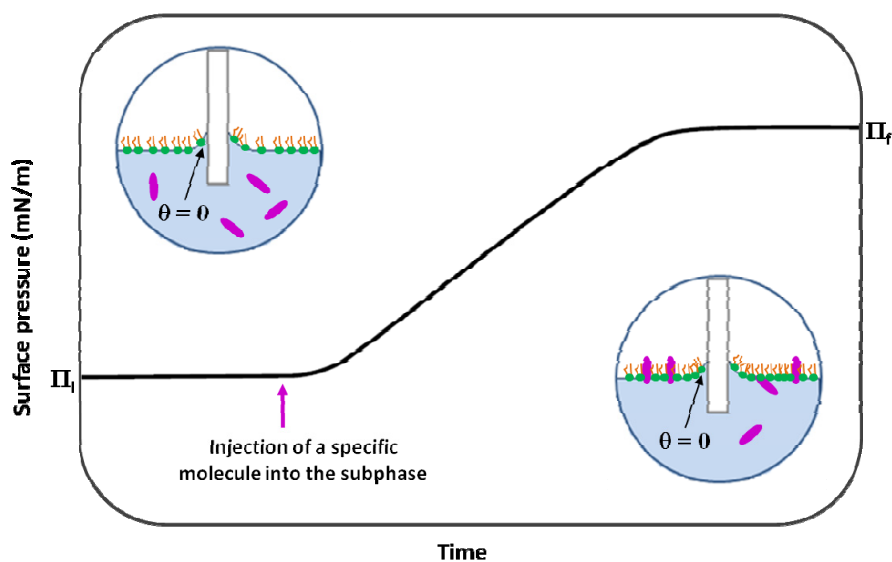
Figure 2.21 An increase of surface pressure in a Langmuir monolayer at an air-liquid interface after adsorption or incorporation of a specific molecule into the monolayer. This figure was adapted from Figure 2.17.

Particularly, in this work the Langmuir balance was used to study LOC-lipid interaction as follows. First, the surface-active properties of LOCs at an air-aqueous interface were analysed to test whether LOC monolayers were formed. This is generally performed to control the possible tensoactivity of the tested molecules and to look for the optimal concentration to be used with a lipid monolayer. Second, the desired lipid monolayers were prepared (ideally at surface pressures above those obtained by pure LOCs at the air-liquid interface, to avoid for data misunderstanding due to surface pressure changes originated from LOC tensoactivity and not by pure lipid-LOC interaction) and LOCs added to subphase (at the minimum concentration giving maximum surface-activity) to study their possible lipid interaction. The interaction studies were carried out at increasing initial lipid monolayer surface pressures, allowing for later determination of maximum pressures at which LOCs could interact with the lipids. All the experiments were performed at 22ºC using µThrough-S equipment (Kibron Inc., Finland) consisting in a small 2-cm rounded multi-well plate that allowed for 1 ml subphase measurements.

<u>Studies of surface-active properties of LOCs</u>

1) 1 mL 1X PBS was added to a well of the Langmuir balance as the aqueous solution.

2) Then, a titration with increasing concentrations of LOC dissolved in 1X PBS were injected into the subphase through an adjusted hole, following LOC transition to the interface in terms of changes in surface pressure. These changes in surface pressure (π) were recorded for 4,000 s in order to obtain equilibrium values where π remained constant.

Lipid-LOC interaction studies

1) 1 mL 1X PBS was added to a well of Lagmuir balance as aqueous solution.

2) Pure lipid stocks of DOPC (1,2-*dioleyl-L-α*-phosphatidylcholine), eSM (egg sphingomyelin) and Chol (cholesterol) were prepared by diluting commercially available lipids in powder into a chloroform/methanol [2:1 (v/v)] organic solution to the desired concentration. Monolayers were formed by spreading a small amount (typically 1-2 μl) of lipid in chloroform/methanol [2:1 (v/v)] solution over assaying buffer until reaching the desired controlled surface pressure (mN/m). Monolayers at increasing surface pressures (mN/m) were analysed.

3) After allowing for solvent evaporation, a defined LOC concentration was injected into the subphase through an adjusted hole and the changes in surface pressure (π) were recorded for 4,000 s in order to follow incorporation or adsorption of the LOC into the monolayer.

2.6.2 Lipid vesicles

A lipid vesicle or liposome is a lipid structure in a bilayer configuration which encloses an aqueous solution. These specific lipid structures represent a fast source of lipid-model systems since they can be spontaneously formed by diluting cylindrical shaped lipids (approximately equal cross sectional area of the hydrophilic polar headgroup and the hydrophobic tail) in aqueous environment. Depending on the treatment used for the preparation of liposomes, two types of lipid vesicles can be generated, such as multilamellar vesicles (which have several bilayers or lamellas) and unilamellar vesicles (which only have one bilayer) (Figure 2.22).

Multilamellar vesicles (MLVs) can be generated in a very easy and fast way. Unfortunately, their disadvantage is that they become a complicated tool for binding studies of a specific molecule because only the effects of interaction with lipids on the external bilayer can be achieved, leading to difficult data analysis and interpretation.

To further overcome this drawback, unilamellar vesicles are commonly prepared. Three types of unilamellar vesicles are known, differing in their size and preparation method: small unilamellar vesicles (SUVs), large unilamellar vesicles (LUVs) and giant unilamellar vesicles (GUVs).
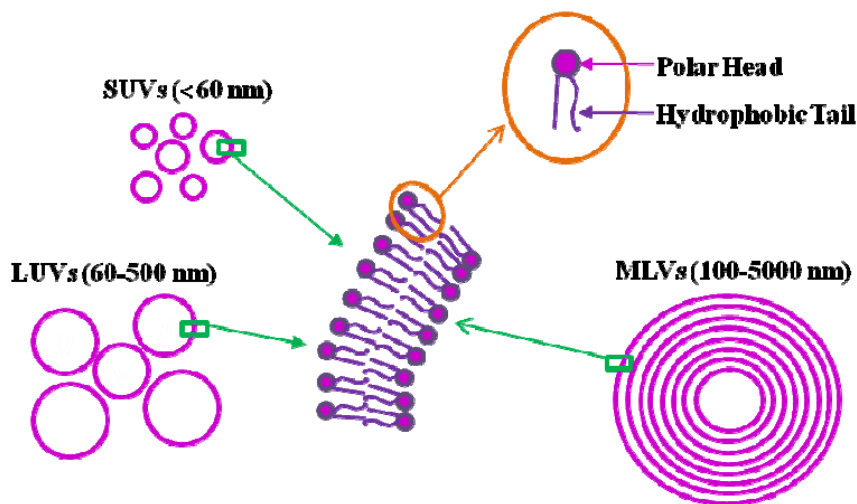
Figure 2.22 Representative figure of lipid organisation into different sized multilamellar (MLV) and unilamellar vesicles (SUVs and LUVs). Giant unilamellar vesicles (GUVs), which are not represented in the figure, have a diameter of 5-100 µm. This figure was modified from Avanti Polar lipids.

2.6.2.1 Preparation of multilamellar vesicles (MLVs)

MLV preparation is the simplest and fastest way of all liposome formation methods. These vesicles are spontaneously generated after lipid hydration and sample shaking. Generated MLVs commonly contain between 7 and 10 concentric bilayers, each of them separated by a thin aqueous layer. However, they are very heterogeneous in size, resulting in a diameter range from 100 to 5,000 nm.

In this work MLVs were generated as a previous step for the preparation of SUVs, to further form supported planar bilayers.

<u>Preparation of MLVs</u>

1) Pure lipid stocks of DOPC, eSM and Chol were prepared by diluting commercially available lipids in powder into a chloroform/methanol [2:1 (v/v)] organic solution to the desired concentration. The desired amount of lipid was pipetted from the stock solution into a glass test tube. Additionally, 0.4 mol % of the lipophilic fluorescent probes DiO or DiD in chloroform/methanol [2:1 (v/v)] were pipetted into the lipid mixture.

2) Samples were dried by evaporating the solvent under a stream of nitrogen and introduced into a high vacuum desiccator for 2 h in order to completely remove any traces of organic solvent. As a result, a dried lipid film at the bottom of the test tube was obtained.

3) Then, samples were hydrated with 500 µl 1X PBS solution at a temperature above that of the lipid with the highest main phase transition temperature (specifically for eSM which presents a gel-fluid phase transition near 40ºC, and for the eSM/Chol liquid-ordered phase generated in ternary mixtures) and vortexed vigorously for complete lipid detachment from the bottom of the test tube, resulting in the generation of MLVs.

4) Owing to the high temperature selected, the lipid was faster hydrated and a more homogeneous lipid composition was expected because lipids of the lipid mixture were maintained in the fluid phase state.

2.6.2.2 Preparation of small unilamellar vesicles (SUVs)

These lipid vesicles of small size (60 nm) present a high curvature which induces lipid enrichment in the external monolayer comparing with the inner one (Szoka and Papadjopoulos, 1980). Due to their curvature stress, they are an ideal tool for studying membrane fusion and/or fission related processes (Nieva *et al*., 1989). Their preparation is usually performed by probe-sonication of MLVs.

In this work, SUVs were prepared for making supported planar bilayers (SPBs) to be measured under atomic force microscopy and fluorescence confocal microscopy. SUVs were generated by bath sonication, which is not ideal for a homogeneous small vesicle population to be formed but enough for planar bilayers to be generated.

Preparation of SUVs

1) MLV suspensions were introduced in a bath sonicator and kept for 1 h with intermittent vortex at a temperature above that of the lipid with the highest gel-fluid main phase transition temperature, resulting in the generation of a heterogeneous SUV population.

2.6.2.3 Preparation of giant unilamellar vesicles (GUVs)

Giant unilamellar vesicles are hitherto considered the most promising model systems for studying membrane heterogeneity. Due to size similarity between cells and giant vesicles (from 5 to 100 µm as prepared by electroformation), direct microscopy of individual vesicles can be easily performed.

To date, the most commonly applied procedure for the generation of giant vesicles is based on the method developed by Dimitrov and co-workers in 1986 (Figure 2.23) where dry lipid films are exposed to an aqueous solution under electric fields (Angelova and Dimitrov, 1986; Angelova *et al.*, 1992). At present, the method that is used for generation of giant vesicles has been improved in order to be much faster and obtain a higher amount of homogeneous size vesicles, but the aqueous solution is still kept at temperatures higher than that of the lipid with the highest main phase transition.
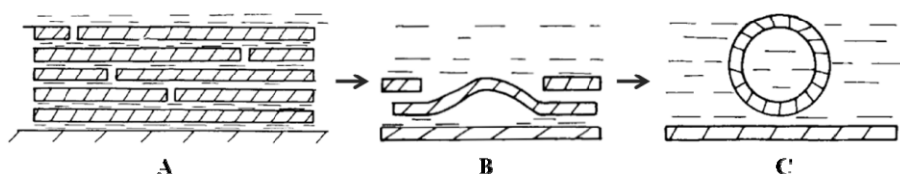
Figure 2.23 Generation of GUVs by electroformation. The electric field allows lipid film growth (A) and detachment (B), resulting in GUV formation (C). This figure was taken from Angelova and Dimitrov (1986).

On the other hand, the generation of giant vesicles under electric fields strongly depends on lipid composition, aqueous solution ionic strength and pH, electric voltage and frequency conditions (Bagatolli, 2003). According to these conditions, buffers with very low ionic strength are exclusively used to form GUVs under this method, although new developments have been made, rendering possible the generation of giant vesicles from erythrocyte membranes in physiological salt solutions (Montes *et al.*, 2007).

In this work giant unilamellar vesicles were prepared in order to examine the interaction between this lipid model system and different LOCs by fluorescence confocal microscopy.With this aim, GUVs based on a ternary DOPC/eSM/Chol mixture were used.

104

These are commonly used as a very simple model system of raft-containing vesicles, presenting a DOPC-enriched fluid liquid-disordered and an eSM/Chol-enriched liquid-ordered phase. Thus, we studied the incorporation behaviour of each LOC in GUVs presenting these phases. Independently, GUVs in pure liquid-disordered and liquid-ordered phase states were analysed.

Preparation of GUVs in solution

1) Pure lipid (DOPC) or lipid mixture [DOPC/eSM/Chol (2:2:1); eSM/Chol (2:1)] stocks were prepared by diluting commercially available lipids in powder into a chloroform/methanol [2:1 (v/v)] organic solution to a final 0.2 g/ml concentration. Additionally, 0.4 mol % of the lipophilic fluorescent probes DiO or DiD in chloroform/methanol [2:1 (v/v)] were pipetted into the stock lipid solutions.

2) 3 µl of the appropriate stock solution were added onto the surface of platinum electrodes in a specially designed chamber of four wells with two electrodes each.

3) Then, the chamber was introduced into a high vacuum desiccator for at least 2 h to completely remove any traces of organic solvent.

4) After that, the chamber was equilibrated to the temperature above that of the lipid with the highest gel-fluid main phase transition temperature, by an incorporated water bath for 15 min.

5) When the chamber was equilibrated to the desired temperature, the platinum wires were covered with a 300 mM sucrose solution previously equilibrated at the same temperature.

6) Next, the chamber wells were covered with a glass held in place with vacuum grease, thereby avoiding evaporation during electroformation.

7) The platinum electrodes were connected to an electric wave generator under AC field conditions (10 Hz, 0.9 V) for approximately 2 h. During this process vesicles were generated enclosing sucrose while keeping the temperature above that of the lipid of main phase transition temperature.

8) Then, the applied frequency was decreased (1 Hz, 0.9 V) for 10 min to induce vesicle detachment from the electrodes.

9) Generator and water bath were switched off and vesicles were left to equilibrate for 30 min.

10) Finally, vesicle solution was collected and 50 µl added to 250 µl of an equiosmolar PBS buffer placed into each well of 8 well-Lab-Tek™ Chamber slides pretreated with BSA (to avoid vesicle rupture).

11) Sucrose-containing vesicles sedimented at the bottom of each well due to the higher density of the enclosed sucrose, thus allowing a better observation under Leica TCSSP5 inverted fluorescence confocal microscope for fluorescent experiments.

2.6.3 Supported planar bilayers (SPBs)

This type of membrane lipid model system is considered a powerful tool for studying lipid domains or lateral phase segregation by means of scanning atomic force microscopy (AFM). In addition, recently approaches have evolved, providing combination with other techniques such as fluorescence confocal microscopy. In this regard, incorporation of a specific molecule into a certain lipid domain can be also monitored by fluorescence techniques.

There are different methods for generating SPBs on top of lipid supports. Particularly, in the present work SPB generation was performed through liposome adsorption. Formed SPBs were used to obtain topographical images by AFM, discerning lateral domain segregation by height differences due to their lipid

packing. In addition, these SPBs were also prepared to analyse incorporation behaviours of LOCs into different domains by fluorescence confocal microscopy.

The method of SPB generation through liposome adsorption is based on the spontaneous liposome adsorption upon incubation with a specific solid support such as glass or mica (Jass *et al.*, 2000). During incubation process, liposomes adsorb to the solid support, get deformed and break down, generating a single planar bilayer. The precise mechanism by which such energetically unfavourable phenomenon happens is still unknown. Jass and co-workers described a possible explanation for this process, where adsorbed vesicles could suffer a strong deformation followed by a superposition of bilayer areas from opposing poles on the vesicle, leading to a breakage at the edges because of the high curvature stress. In this manner, a superposition of two bilayers would be formed, where the upper bilayer would then slide through the bilayer on the bottom towards the solid support, resulting in a homogeneous single bilayer patch on top of the solid support (Figure 2.24).
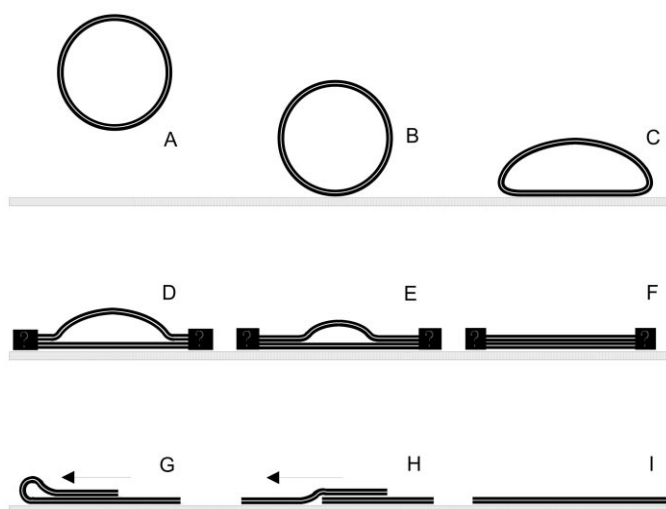
Figure 2.24 Representative picture describing step by step the proposed hypothesis for the generation of SPBs. This figure was taken from Jass *et al.* (2000).

The liposomes commonly used for generation of SPBs are either SUVs or LUVs with high diameters. Owing to the high curvature stress that SUVs present, they provide a high instability upon contact with the solid support, enabling a good adsorption and bilayer extension. Especially, in this work SUVs were used to form SPBs.

Preparation of SPBs

1) A sheet of muscovite mica (1.5×1.5 cm) was adhered with epoxy glue into a glass slide fitting the liquid cell for AFM measurements. This step was done at least 3 days before measurements to ensure perfect glue sticking to the glass slide.

2) The mica surface was cleaved with a common scotch tape, mounted onto a BioCell coverslip-based liquid-cell specially designed for AFM measurements (JPK Instruments, Berlin, Germany) and covered with 1X PBS supplemented with 3 mM $CaCl_2$. Divalent ions were used in order to favour adsorption and further spreading of vesicles.

3) Then, a small SUV aliquot in 1X PBS without $CaCl_2$ [prepared with pure DOPC, DOPC/eSM/Chol (2:2:1) or eSM/Chol (2:1)] was added on top of the mica to a final lipid concentration of 150 µM, at a temperature higher than that of the lipid with the highest main phase transition temperature and left adsorb for 30 min at a constant temperature.

4) After the incubation period, the Biocell was switched off and the sample left to cool down to RT for 30 min. Thereafter, non-adsorbed vesicles were discarded by several washing steps with 1X PBS in the absence of divalent ions at RT. During washing steps, a small amount of buffer was always left on top of the substrate, avoiding dehydration of SPBs.

5) 350 µl 1X PBS were finally added to the SPBs at RT and further left to equilibrate at RT for 45 min before measuring under AFM or fluorescence confocal microscopy.

2.6.3.1 Atomic force microscopy

Atomic force microscopy (AFM), also known as scanning force microscopy, is a high-resolution type of scanning probe microscopy that was developed by Binnig and co-workers to overcome the disadvantage that the scanning tunnelling microscope presented, where scanning was restricted only for conducting surfaces (Binnig *et al.*, 1986). In this regard, AFM provides scanning any kind of surface, either conductive or not, allowing the characterisation of biological samples in aqueous solutions. At present, AFM is considered one of the foremost tools for imaging, measuring and manipulating matter at nanoscale, covering from topographical analysis of biological membranes to scanning of individual macromolecules at physiological conditions (Connell and Smith, 2006).
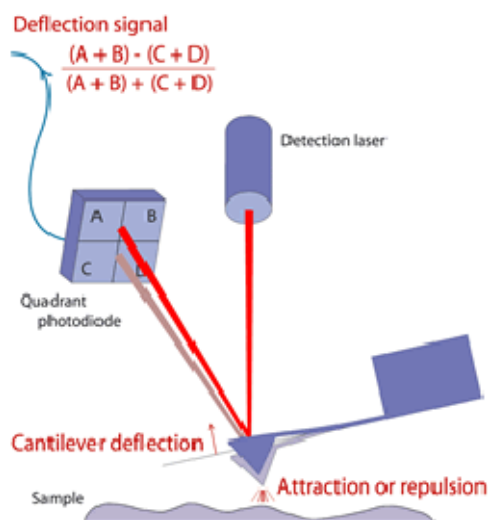
Figure 2.25 Basic principles of AFM measurements. This figure was taken from JPK Instruments.

As shown in Figure 2.25, AFM consists of a flexible cantilever, typically made of nitride or silicon nitride, with a sharp tip at its end to scan the desired surface. The cantilever reflects the laser beam focused into a position-sensitive for quadrant photodetector by the use of a mirror. For measuring a sample, the tip is moved across the x-y axis within selected area where it can meet a structure with height differences, leading to a deflection of the cantilever in the z axis, which is detected by the microscope as a movement of the laser beam within photodetector. Thus, the movement of the laser through the different quadrants is controlled by means of voltage and correlated in order to obtain subnanometric high-resolution topographic images. There are two ways for measuring the sample. The first one is maintaining a constant force through the sample to analyse height information, and conversely, the second one is maintaining a constant height to analyse force information. These measurements are possible due to a piezoelectric scanner that moves up and down as the tip scans the surface in a proportional way to the applied voltage, recording height distribution, and to a feedback mechanism that provides to control the force and distance between tip and sample, thereby preventing crashing.

Furthermore, these measurements can be commonly performed under contact mode or intermittent contact mode (Figure 2.26).
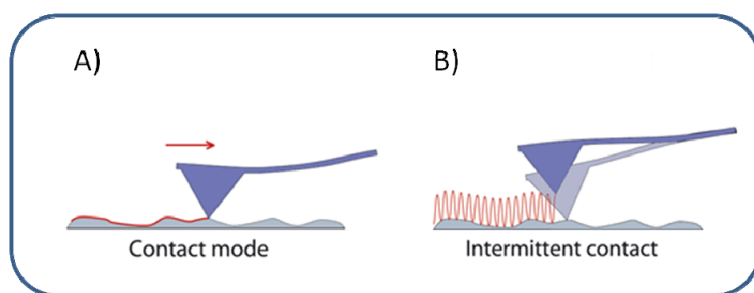
Figure 2.26 Common scanning modes used for AFM measurements. A) Contact mode. B) Intermittent mode. This figure was taken from JPK Instruments.

Contact mode, also known as static mode, is based on the continuous physical contact between the tip and the sample because the tip never leaves the surface (Figure 2.26A). Here, a constant force is maintained through the scan and the topography of the sample is obtained by changes of the vertical deflection of the cantilever that are subsequently converted to length units so as to build the height image. This is the common scanning mode used for very high-resolution imaging, although it may be aggressive for measuring soft samples. Also, lateral deflection is measured, which gives information about the friction between tip and sample that is mainly dependent on the sample's physical properties. Likewise, distinct areas can be distinguished that have the same height but different chemical properties (Figure 2.27).
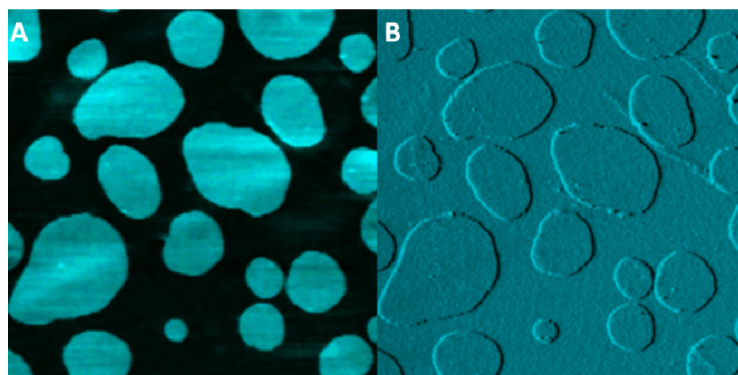
Figure 2.27 Height image (A) and deflection image (B) of a phase-separated lipid bilayer (DOPC/SM/cholesterol) in liquid. The background liquid disordered phase is around 1 nm lower than the liquid ordered islands. AFM and fluorescence imaging in liquid in-situ on a Zeiss LSM 510 Meta. Scan-field: 15 µm × 15 µm. Z-range: 2 nm. Images courtesy of Dr S. Chiantia, group of Prof. Schwille, TU Dresden. This figure was taken from JPK Instruments.

On the contrary, intermittent contact mode, also denoted as dynamic or tapping mode, is based on the oscillation of the cantilever at its resonance frequency close to the sample surface, resulting in a less aggressive scanning procedure (Figure 2.26B). During the phase of cantilever oscillation, there is a unique contact between tip and sample surface, followed by a retraction to the neighbouring position for the next oscillation cycle. Hence, the topographic image is obtained by changes of resonance frequency or signal amplitude. Owing to this method, the phase of oscillation signal can be obtained, providing attractive information about the properties of the sample, including stiffness and mechanical information or adhesion.

In this work, this technique was used to analyse SPBs, particularly lipid domain generation within them and their height differences. The measurements were performed on a NanoWizard II AFM at 22°C. MLCT SiN cantilevers with a spring constant of 0.1 N/m were used in contact mode scanning (constant vertical deflection) to measure the generated SPBs. Resolution images measuring 256×256 pixels were collected at a scanning rate between 1 and 1.5 Hz and line-fitted using the JPK Image Processing software as required (Busto *et al.*, 2010).

2.7 Fluorescence confocal microscopy

This technique offers a number of advantages over epifluorescence microscopy, including controllable depth of field, elimination of image degrading out-of-focus information resulting in high resolution and contrast, and the possibility of collecting serial sections of the sample enabling the reconstruction of three-dimensional structures from the images obtained. Indeed, the key to the confocal approach consists in the use of a pinhole next to the detector where only fluorescence coming from the in-focus plane can reach the detector, thereby discarding fluorescence coming from out-of-focus planes.

The following figure shows the main components of a fluorescence confocal microscope (Figure 2.28). Briefly, a laser beam is focused into a dichroic mirror, selecting the light to be directed through an objective into a small spot within the sample. Then, fluorescent molecules are excited by the selected light and their emitted fluorescence is recovered and directed across the dichroic mirror into a pinhole which selects the emitted fluorescence to reach the photodetector. In this way, only fluorescence coming from the focal plane can pass through the pinhole whereas fluorescence from out-of-focus planes is blocked. For the construction of three dimensional images special mirrors are also needed to scan the laser beam on the x-y plane and control the z sample movement in an accurate manner. Thus, the corresponding term for this special confocal microscopy is laser scanning confocal microscopy.
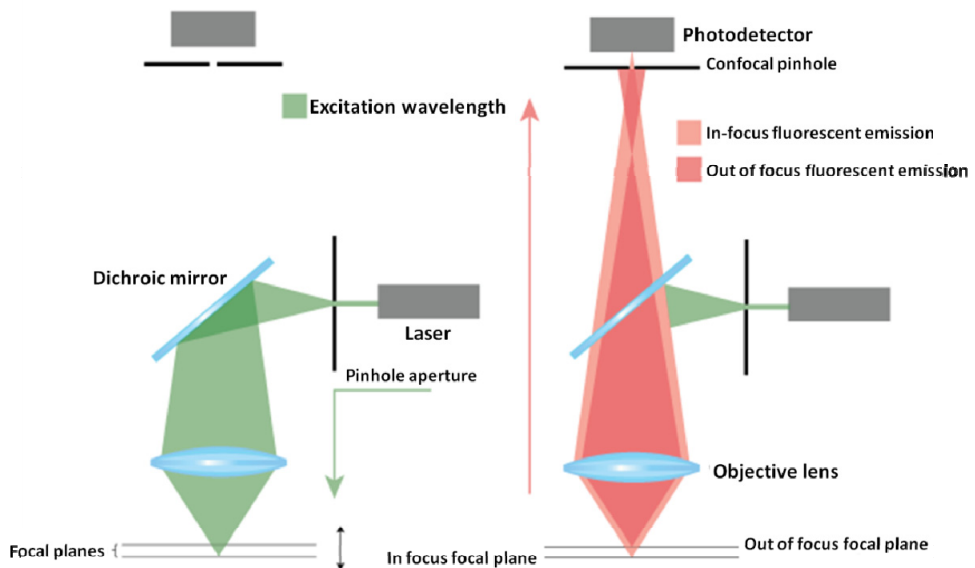
Figure 2.28 Representative picture showing the main components of a fluorescence confocal microscopy. Owing to the confocal pinhole, only fluorescence from in-focus focal plane is collected by the photodetector. This figure was adapted from BIOimaging sponsored by Olympus.

113

Thanks to this technique, extremely high-quality images can be achieved from a wide variety of samples, leading to several applications in many areas of current research interest which are in part related to the rapid advances that have been undertaken in synthetic fluorophore technology.

For instance, in fluorescence experiments cell samples are commonly incubated with fluorescent molecules such as fluorophore-labelled primary or secondary antibodies in order to mark specific molecules within the cell (Opas, 1999) (Figure 2.29). Interestingly, the use of a number of antibodies labelled with different fluorescent dyes which present well-separated excitation wavelengths within single cell samples provides a deeper analysis of the samples, where different subcellular localisation profiles can be obtained including co-localisation analysis (Miyashita, 2004). In addition, cellular uptake and internalisation route and destiny of a specific molecule can also be studied by directly coupling to a fluorescent tag, as in the present work, followed by incubation with different fluorophore-labelled cellular markers.
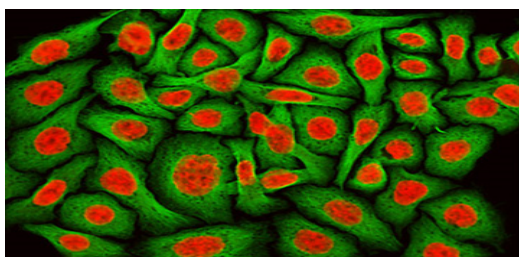
Figure 2.29 Representative subcellular localisation picture showing different cellular compartments by the use of fluorescent antibodies. An adherent monolayer culture of HeLa cells was fixed, permeabilised, blocked, and then treated with mouse primary antibodies that target *alpha*-tubulin, a major component of the microtubule network. The primaries were labelled with goat anti-mouse secondary antibodies conjugated to Alexa Fluor 488 (green) in a solution containing nuclear marker TO-PRO-3 to simultaneously stain DNA (red). Images were recorded with sequential scanning with the 488-nanometer spectral line of an argon-ion laser and the 633-nanometer line of a red helium-neon laser. This figure was adapted from Olympus confocal microscopy image gallery.

Another attractive approach is the use of lipophilic fluorescent dyes in membrane lipid model systems as GUVs and SPBs (Bagatolli, 2006; García-Sáez and Schwille, 2010). Here, the use of either fluorescently labelled lipids or pure hydrophobic fluorescent probes, such as DiO and DiD, enables the study of lipid domains generated in those model systems due to a different partition of the probes within phases with different chemical compositions, allowing the study of lateral segregation in GUVs and SPBs (Figure 2.30). For example, time series can be performed to follow the incorporation behaviour of a fluorescent molecule to a specific lipid domain, as in the studies carried out with LOCs.
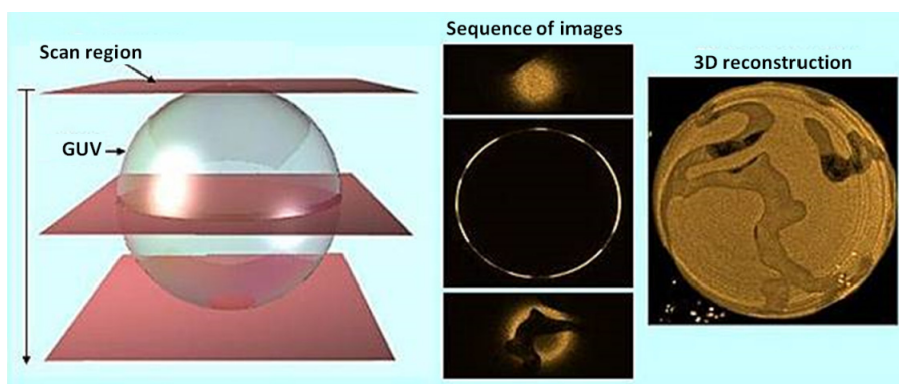
Figure 2.30 Laser scanning of a GUV (left) through a series of multiple planes. Each plane emits a fluorescent contour (middle). It can be reconstructed into a three-dimensional (3D) picture (right) by collecting each plane. This figure was adapted from BIOimaging sponsored by Olympus.

Concerning to this work, laser scanning confocal microscopy was used for a number of purposes, including subcellular localisation of Alexa 488-labelled or Cy5-labelled LOCs with different cellular compartments and characterisation of lipid domains in GUVs and SPBs followed by the study of incorporation profiles that Alexa 488-labelled or Cy5-labelled LOCs showed in these membrane lipid model systems. Particularly, two types of inverted fluorescence confocal microscopes were used in this work.

115

According to the subcellular localisation studies performed with cells, samples were visualised using Olympus IX 81 inverted fluorescence confocal microscope with sequential excitation and capture image acquisition with a digital camera (Axiocam NRc5, Zeiss). Here, Alexa 488-labelled or Cy5-labelled oligonucleotide conjugates were used, as well as, Hoechst 33258 and Alexa 546/633-labelled secondary antibodies as different markers for cellular compartments. As mentioned in section 2.2.5, these experiments were carried out using 8 well-Lab-Tek™ Chamber slides or 96 well-BD Falcon™ Tissue Culture Treated Imaging plates. The slides and plates were placed on top of the microscope followed by image acquisition with a 20X objective and zoom factor of 2X or a 60X oil immersion objective, using an excitation wavelength of 405, 488, 543 and 633 nm for Hoechst 33258, Alexa 488, Alexa 546 and Cy5 or Alexa 633, respectively. The emission was recovered between 430-460 nm for Hoechst 33258, 505-525 nm for Alexa 488, 560-600 nm for Alexa 546, 660-IF nm for Cy5 or Alexa 633. Image treatment was performed using Fluoview v.50 software.

On the other hand, in experiments performed with GUVs and SPBs, images were achieved in Leica TCSSP5 inverted fluorescence confocal microscope. Briefly, 8 well-Lab-Tek™ Chamber slides where GUVs were sedimented at the bottom of each well, or biocell-liquid-cell containing SPBs were placed on top of the microscope followed by image acquisition with a 40X LD objective using an excitation wavelength of 488 and 633 nm for DiO and DiD, respectively, and the emission was recovered between 505-540 nm for DiO and 655-795 nm for DiD. Binding of Alexa 488-labelled and Cy5-labelled LOCs to fluorescently labelled GUVs or SPBs was observed under the microscope in sequential mode imaging, using the same excitation and emission wavelengths for Alexa 488 and Cy5 as for DiO and DiD, respectively. Image treatment was performed using Leica Application Suite software.

Chapter 3:

Carbohydrate-oligonucleotide
conjugation approach
for targeted delivery

Chapter 3: Carbohydrate-oligonucleotide conjugation approach for targeted delivery

3.1 Introduction

Targeted delivery of drugs or nucleic acids to their site of action has clear therapeutic advantages by maximising their therapeutic efficiency and minimising their systemic toxicity, thereby directing these delivery systems to specific cell or tissue with the help of specific targeting ligands (Zhang *et al.*, 2010). Indeed, these delivery systems are decorated with biorecognitive ligands, which possess high affinity to receptors at or close to the desired site of action (Gabor *et al.*, 2004). In this regard, this interesting area focuses mainly on receptor mediated endocytosis.

Recent emergences of glycobiology, glycotechnology and glycomics have been clarifying enormous roles of carbohydrates in both physiological and pathological recognition systems. Thus, it has been recognised that carbohydrates represent the third informational biomolecules. On that account, the studies based on carbohydrate-protein interactions reveal promising medical applications of carbohydrates since it has been observed that certain oligosaccharide sequences can mediate cell-cell interactions and cell-routing. This strategy was termed glycotargeting and focused on the use of carbohydrates as "magic bullets" in order to enhance cellular uptake of drugs or nucleic acids in specific target cells or tissues (Monsigny *et al*., 1999).

In particular, regarding nucleic acid delivery, a carbohydrate moiety can be covalently or non-covalently associated with nucleic acids, either directly or through a carrier molecule. These carbohydrate residues can be recognised by cell surface carbohydrate-binding proteins called lectins. The interaction between lectins and carbohydrates then mediates the internalisation of nucleic acids through receptor mediated endocytosis, thereby enhancing the cellular uptake of nucleic acids (Yan and Tram, 2007).

Lectins are proteins that recognise and bind to carbohydrates with high specificity. These carbohydrates can be a sugar itself, but they can also be the glycan moiety of glycosylated molecules. Lectins are found actively to direct their specific ligands to intracellular compartments, including endosomes, lysosomes and Golgi apparatus. Fortunately, since lectins recognise the terminal sugar residues of glycosylated ligands, endocytosis is not substantially influenced by the size and composition of the aglycone moiety of the ligand (Yan and Tram, 2007).

In the context of targeted delivery systems, several approaches have been developed using carbohydrates as ligands for specific lectins (Davis *et al.*, 2002; Lönnberg, 2009; Zhang *et al.*, 2010). For instance, asialoglycoprotein receptor (ASGP-R) is a very attractive target in the liver due to its high density on the hepatocyte surfaces. This receptor can bind specifically to ligands with terminal galactose or N-acetylgalactosamine residues, including asialofetuin and synthetic ligands with galactosylated or lactosylated residues (Wu *et al.*, 1998; Nag and Ghosh, 1999; Shinoda *et al.*, 1999; Sliedregt *et al.*, 1999; Cho *et al.*, 2001; Kawakami *et al.*, 2001; Wu *et al.*, 2002; Kunath *et al.*, 2003; Morimoto *et al.*, 2003; Kim *et al.*, 2007; Jiang *et al.*, 2008; Letrou-Bonneval *et al.*, 2008). Additionally, hepatic stellate cells (HSC), which represent a hallmark of liver fibrosis, highly express mannose 6-phosphate/insulin-like growth factor II (M6P/IGF-II) receptor on their cell-surface. Thus, this receptor can also be a potential target by of mannose 6-phosphate conjugated drugs (Beljaars *et al.*, 1999; Ye *et al.*, 2006; Yang *et al.*, 2009). Moreover, macrophages are believed to be important targets for drug delivery because they accumulate at pathological sites, such as infections, tumours, atherosclerotic plaques and arthritic joints. In this way, alveolar macrophages as well as macrophages in liver and spleen, express macrophage-mannose receptor on their cell-surface, which could bind to mannosylated delivery systems, leading to their internalisation mediated by mannose-receptor endocytosis (Erbacher *et al.*, 1996; Hattori *et al.*, 2005; Hashimoto *et al.*, 2006). Another successful example is based on the surface

expression of different types of adhesive glycoproteins, such as E-selectin and P-selectin, in endothelial cells that are known to take part in processes including chronic inflammation, injury, repair, angiogenesis and atherogenesis. A number of studies have been reported for targeting these glycoproteins by the use of specific ligands such as syalyl Lewis X (s-Lex) (Stahn *et al.*, 2001; Yamazaki *et al.*, 2005; Hirai *et al.*, 2007; Hashida *et al.*, 2008). Besides, galactose-binding lectins (galectins) are commonly expressed on the surface of certain types of cancer cells and could be an interesting target for nucleic acid based delivery (Katav *et al.*, 2008).

Most importantly, among the carbohydrates present in nature, glucose (β-D-glucose) serves as the major and essential energy source for cell survival and its transport is facilitated by members of the GLUT (glucose transporter) protein family. To date, there are 14 GLUT family members described.

GLUT1 is undoubtedly one of the most intensively studied of all membrane transport proteins and is the most frequently isoform over-expressed in fast-growing and metastatic tumours, although other GLUT isoforms, including GLUT3 and GLUT5, not usually found in the original tissue, may also be over-expressed (Higashi *et al.*, 1997; Medina and Owen, 2002; Rodríguez-Enríquez *et al.*, 2009). In this way, different types of tumour cells show an increase in glucose uptake directly associated with elevated levels of these GLUT isoforms (Watanabe *et al.*, 2010). Moreover, a number of investigations support the idea that GLUT1 may participate in the transport of D-glucose-derived drugs even through the blood-brain barrier (Dufes *et al.*, 2000; Guo *et al.*, 2005). In the case of GLUT3, this isoform has a high affinity for glucose and has the highest calculated turnover number of the GLUT isoforms, thereby ensuring efficient glucose uptake (Thorens and Mueckler, 2010). Indeed, GLUT3 only takes up extracellular glucose, avoiding the release of intracellular glucose to the extracellular space even if the intracellular glucose concentration is higher than the extracellular concentration (Iwabuchi and Kawahara, 2011).

Taken together, the above mentioned GLUT isoforms can be potential targets in cancer and blood-brain barrier transfer, mediating the internalisation of nucleic acid based delivery systems by the use of glucose moieties as specific ligands for GLUT membrane proteins.

In particular, since it is long known that maltose molecules are also capable to bind at the extracellular face of GLUT proteins, in this work we studied oligonucleotides modified at the 5′-end with glucose and glucose-containing saccharides (maltose and maltotriose) at the nonreducing end (Figure 3.1). Two types of spacers [*i.e.*, ethyleneglycol (C2) and tetraethyleneglycol (PEG4)] and a dendron scaffold, which is a symmetric doubler (DB), were used to probe a diversity of sugar presentations. Also a COC containing a fucose unit was also prepared as a negative control. The carbohydrate moieties were covalently bound to a single-stranded ODN antisense sequence termed GEM91 and finally the Alexa 488 fluorescence tag was added when needed. The corresponding labelled COCs were used to study their cell-surface binding and their cellular uptake in HeLa and U87.CD4.CXCR4 cell lines using flow cytometric analysis (Ugarte-Uribe *et al.*, 2010).
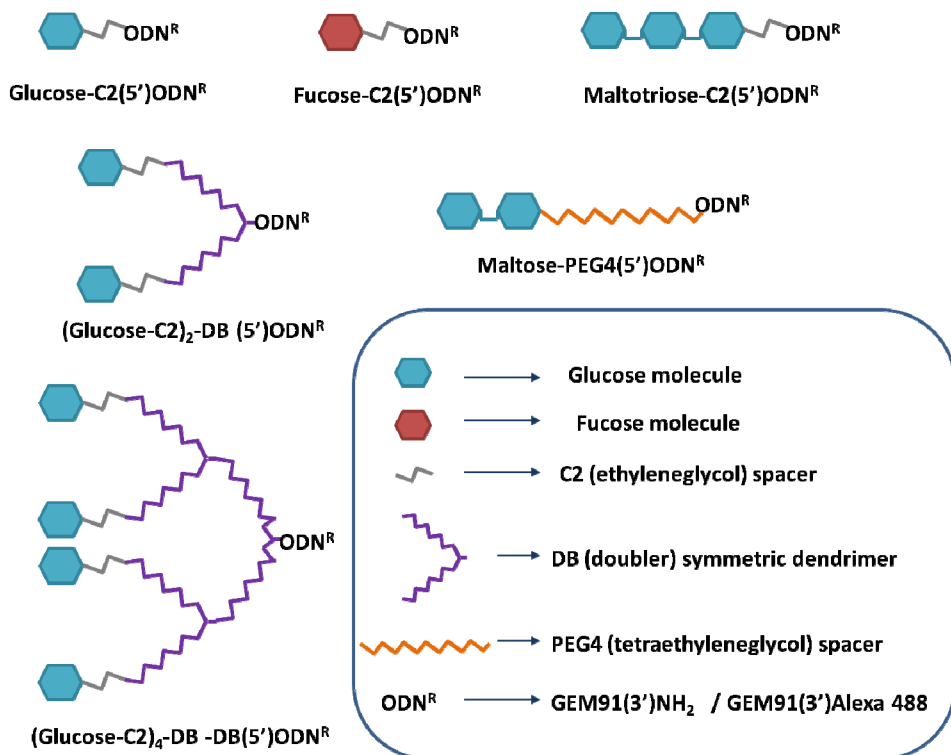
Figure 3.1 Schematic figure of COCs. This guidance scheme is explained in a very basic manner in order to show easily the different carbohydrate presentations chosen in this study.

3.2 Results

It has been previously mentioned that *Mycoplasma* infection could change cell membrane properties and consequently oligonucleotide uptake could be accelerated (de Diesbach *et al.*, 2003). Thus, it was necessary to maintain *Mycoplasma*-free cultures. The first step then was to set up a rutine procedure to check whether HeLa and U87.CD4.CXCR4 cell cultures were contaminated or not by *Mycoplasma*. To do so, Venor®GeM *Mycoplasma* Detection Kit was applied regularly in order to ensure the reliability of our results (Figure 3.2).
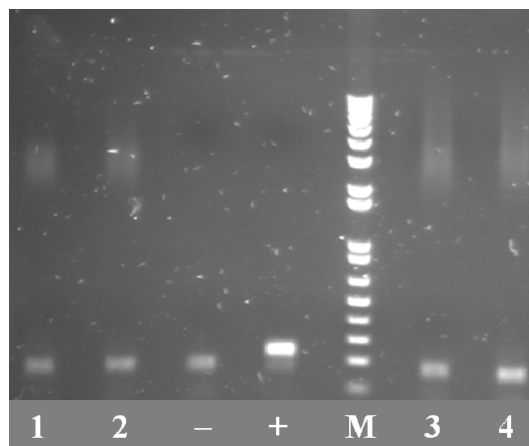
Figure 3.2 PCR products obtained from Mycoplasma detection kit. 1-2: HeLa culture samples; -: negative control; +: positive control; M: 1 Kb Plus DNA Ladder; 3-4: U87.CD4.CXCR4 culture samples.

Once we tested that HeLa and U87.CD4.CXCR4 cell cultures were not contaminated by *Mycoplasma*, we then examined whether COCs or control-oligonucleotide [GEM91-(3')NH$_2$] were cytotoxic at concentrations that would further be used to perform cell-surface adsorption and cellular uptake studies. This cytotoxicity assay was designed under physiological conditions (5.5 mM glucose) and in the absence of serum in order to avoid COC degradation.
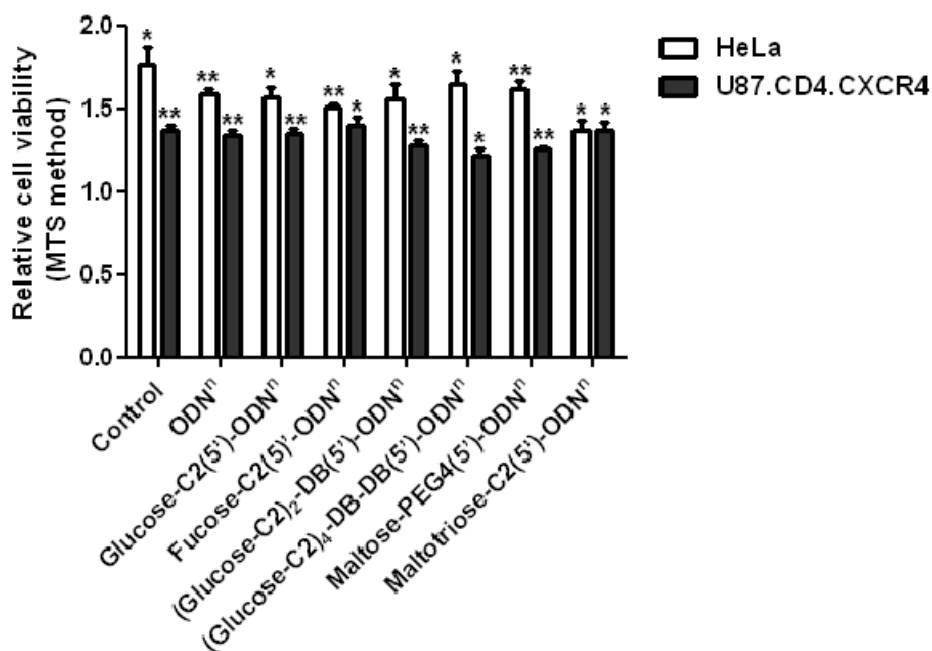
Figure 3.3 Cell cytotoxicity assay performed in HeLa and U87.CD4.CXCR4 cells in the presence of control-oligonucleotide [GEM91-(3')NH2] and COCs. Cells were seeded (5×10^3 cells/well) in 96 well plates and incubated overnight in appropriate growth medium. The next day cells were washed with DPBS and incubated in 100 µl OptiMEM in the absence or presence of the control-oligonucleotide [GEM91-(3')NH$_2$] or COC (5 µM) for 24 h at 37ºC. Untreated cells were used as negative control (Control); ODN^n stands for GEM91-(3')NH$_2$. Data were normalised to the control value (untreated cells at 0 h of incubation) and are expressed as the mean ± SEM of 3 independent experiments performed in triplicate (*p<0.05; **p<0.01).

In Figure 3.3 it can be observed that the concentration of COC chosen (5 µM) had neither cytotoxic nor antiproliferative effect in both HeLa and U87.CD4.CXCR4 cells during 24 h of incubation, since COC treated cells presented similar growth compared to untreated cells, which were only incubated with OptiMEM. Therefore, from this point onwards 5 µM COC concentrations were used for cell-surface adsorption assays.

125

Analysis of the levels of GLUT expression

In the present study the internalisation strategy of COCs is based on the capability of GLUT protein family to bind these carbohydrate modified oligonucleotides. In particular, GLUT1 which is the most frequently over-expressed isoform in fast-growing and metastatic tumours. Importantly, previous work reported that U87 cells presented very low level of GLUT1 protein expression on the cell surface, as well as low abundance of GLUT1 mRNA, compared to HeLa cells (Jin *et al.*, 2006). In this regard, to confirm the expression of GLUT1 in both cell lines and to examine whether GLUT1 expression was dependent on extracellular glucose concentration, we performed western blotting assays in the absence and presence of physiological glucose concentration (5.5 mM). We also tested the possible expression of GLUT3 in both cell lines under the same conditions due to the presence of high GLUT3 protein levels in tumorigenic HeLa cell hybrids and in human astrocytic tumours (Nagamatsu *et al.*, 1993; Sakyo *et al.*, 2007).

Cellular fractionation by ultracentrifugation was carried out in both cell lines in order to separate membrane-bound compartments from the remaining cytoplasm. Since GAPDH is considered a housekeeping protein, in this work this protein was used as loading control for western blotting analysis and further protein normalisation.
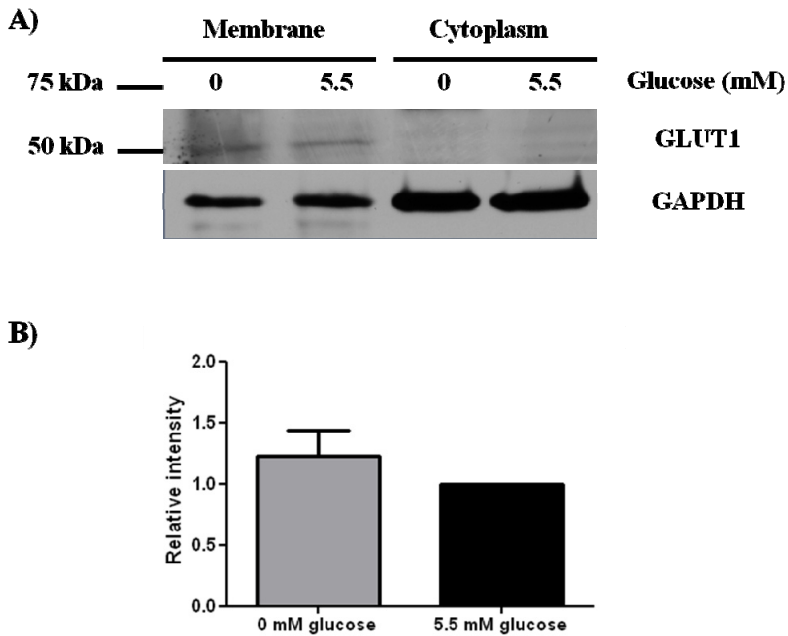
Figure 3.4 GLUT1 protein expression in HeLa cells. Cells were incubated in appropriate growth medium in the absence or presence of glucose (5.5 mM). After 48 h of incubation, cells were harvested in ice-cold homogenisation buffer. Membrane-bound compartments were separated from the remaining cytoplasm fraction as described in Experimental procedures section. (A) Western blotting assay. The presence of GLUT1 was analysed using an antibody specific to GLUT1 protein. Equal loading of protein was monitored using a specific antibody to GAPDH protein. Results are representative of one experiment and were confirmed in two additional experiments. (B) Results of scanning densitometry of the exposed films corresponding only to the membrane-bound fractions. Data are expressed as arbitrary units of intensity relative to control value which is the physiological glucose concentration (5.5 mM glucose) and results are the mean ± SEM of 3 independent experiments.

Figure 3.5 GLUT1 protein expression in U87.CD4.CXCR4 cells. Cells were incubated in appropriate growth medium in the absence or presence of glucose (5.5 mM). After 48 h of incubation, cells were harvested in ice-cold homogenisation buffer. Membrane-bound compartments were separated from the remaining cytoplasm fraction as described in Experimental procedures section. (A) Western blotting assay. The presence of GLUT1 was analysed using an antibody specific to GLUT1 protein. Equal loading of protein was monitored using a specific antibody to GAPDH protein. Results are representative of one experiment and were confirmed in two additional experiments. (B) Results of scanning densitometry of the exposed films corresponding only to the membrane-bound fractions. Data are expressed as arbitrary units of intensity relative to control value which is the physiological glucose concentration (5.5 mM glucose) and results are the mean ± SEM of 3 independent experiments.

As observed in Figures 3.4 and 3.5, both HeLa and U87.CD4.CXCR4 cell lines presented low expression of GLUT1, which was only noticeable in the membrane-bound fraction. There was no significant difference in GLUT1 expression between both experimental conditions, cells incubated in the absence of glucose, or cells incubated under physiological glucose concentration (5.5 mM).

A)

B)
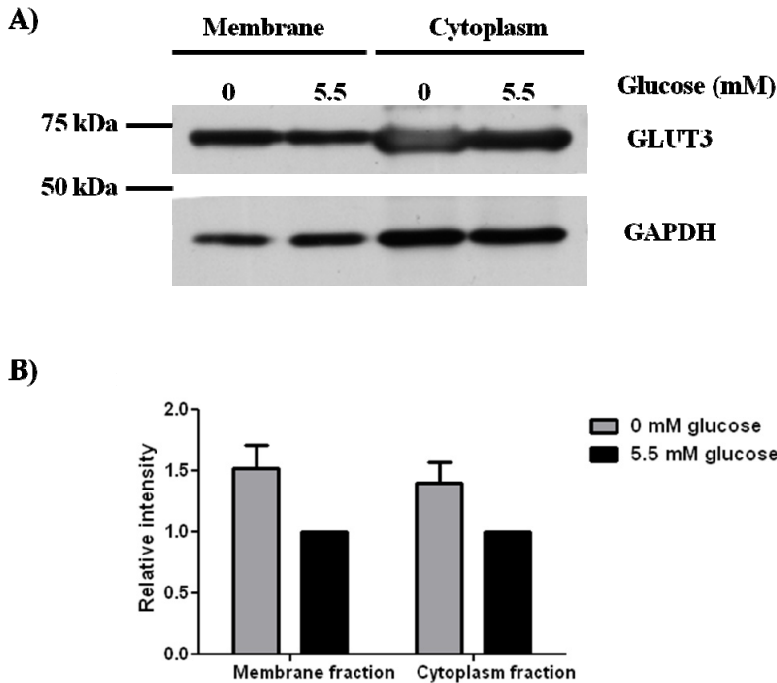
Figure 3.6 GLUT3 protein expression in HeLa cells. Cells were incubated in appropriate growth medium in the absence or presence of glucose (5.5 mM). After 48 h of incubation, cells were harvested in ice-cold homogenisation buffer. Membrane-bound compartments were separated from the remaining cytoplasm fraction as described in Experimental procedures section. (A) Western blotting assay. The presence of GLUT3 was analysed using an antibody specific to GLUT3 protein. Equal loading of protein was monitored using a specific antibody to GAPDH protein. Results are representative of one experiment and were confirmed in two additional experiments. (B) Results of scanning densitometry of the exposed films. Data are expressed as arbitrary units of intensity relative to control value which is the physiological glucose concentration (5.5 mM glucose) and results are the mean ± SEM of 3 independent experiments.

As seen in Figures 3.6 and 3.7, HeLa and U87.CD4.CXCR4 cell lines presented higher expression of GLUT3 than the observed expression for GLUT1 receptors (Figures 3.3 and 3.4), which was noticeable not only in the membrane-bound fraction but also in the cytoplasm fraction. Surprisingly, the apparent molecular mass of the GLUT3 protein was about 70 kDa compared to the

theoretical molecular mass of the GLUT transporter (50-55 kDa) (Suzuki *et al.*, 1999), indicating that this protein was expressed as a larger form. Furthermore, these results point out that in the absence of glucose, there is not only an induction of GLUT3 transport to the cell-surface, but also a slight increase in GLUT3 expression.
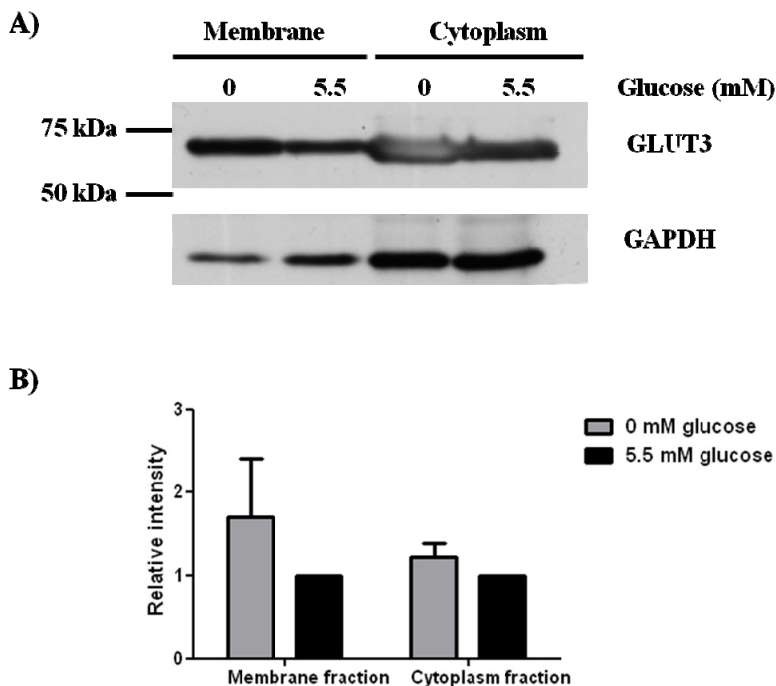
Figure 3.7 GLUT3 protein expression in U87.CD4.CXCR4 cells. Cells were incubated in appropriate growth medium in the absence or presence of glucose (5.5 mM). After 48 h of incubation, cells were harvested in ice-cold homogenisation buffer. Membrane-bound compartments were separated from the remaining cytoplasm fraction as described in Experimental procedures section. (A) Western blotting assay. The presence of GLUT3 was analysed using an antibody specific to GLUT3 protein. Equal loading of protein was monitored using a specific antibody to GAPDH protein. Results are representative of one experiment and were confirmed in two additional experiments. (B) Results of scanning densitometry of the exposed films. Data are expressed as arbitrary units of intensity relative to control value which is the physiological glucose concentration (5.5 mM glucose) and results are the mean ± SEM of 3 independent experiments.

130

Taking into account the differences observed in GLUT3 expression in both HeLa and U87.CD4.CXCR4 cell lines in the absence or presence of glucose, we further examined if these experimental conditions would alter the cell-surface adsorption of control-oligonucleotide [GEM91-(3')NH$_2$] and COCs.

Analysis of cell-surface adsorption of COCs

To avoid endocytosis-dependent cellular internalization, cell-surface adsorption experiments were performed at 4ºC (Nishi and Saigo, 2007).
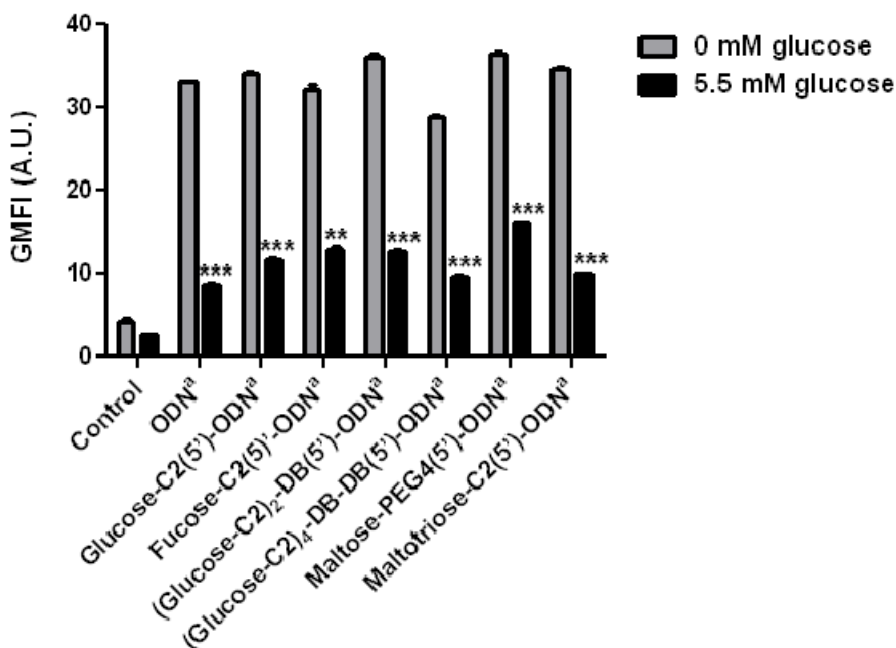
Figure 3.8 Cell-surface adsorption of Alexa 488-labelled control-oligonucleotide and COCs in HeLa cells. Cells were cultured in the absence or presence of glucose (5.5 mM) for 48 h at 37ºC. Then, the medium was replaced and cells were incubated with 5 μM bioconjugate for 1 h at 4ºC in the absence or presence of glucose. After incubation, cells were washed three times, resuspended in ice-cold PBS, and analysed by flow cytometry. Control stands for untreated cells, representing cell basal fluorescence intensity; ODN[a] stands for GEM91-(3')Alexa 488. GMFI corresponds to Geometric Mean of Fluorescence Intensity. Results are expressed as GMFI ± SD of 2 independent experiments for 0 mM glucose condition and GMFI ± SEM of 3 independent experiments for 5.5 mM glucose condition (**p<0.01; ***p<0.001).

As observed in Figure 3.8, when HeLa cells were incubated in the absence of glucose, cells present better cell-surface adsorption not only of COCs, but also of control-oligonucleotide. Moreover, in the absence of glucose COCs containing two branched glucoses [(glucose-C2)$_2$-DB], maltose-PEG4 and maltotriose-C2 were slightly better adsorbed to the surface than the remaining oligonucleotides. In the presence of glucose, there was a slight increase of fluorescence again for COCs bearing two branched glucoses [(glucose-C2)$_2$-DB] and maltose-PEG4. By contrast, tetravalent COC [(glucose-C2)$_4$ -DB-DB] showed worse adsorption than the other COCs either in the absence or presence of glucose.
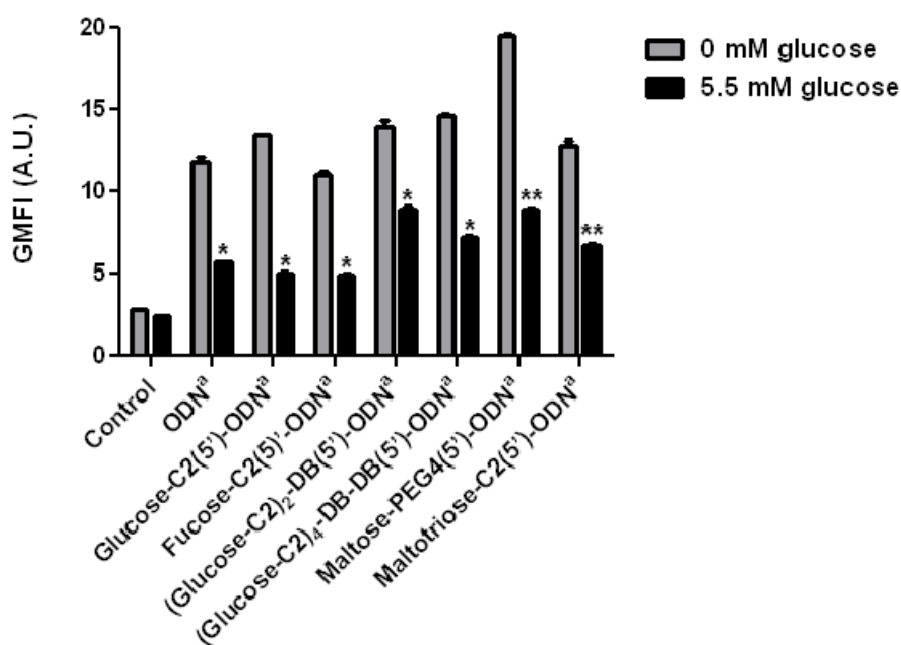
Figure 3.9 Cell-surface adsorption of Alexa 488-labelled control-oligonucleotide and COCs in U87.CD4.CXCR4 cells. Cells were cultured in the absence or presence of glucose (5.5 mM) for 48 h at 37ºC. Then, the medium was replaced and cells were incubated with 5 μM bioconjugate for 1 h at 4ºC in the absence or presence of glucose. After incubation, cells were washed three times, resuspended in ice-cold PBS, and analysed by flow cytometry. Control stands for untreated cells, representing cell basal fluorescence intensity; ODN[a] stands for GEM91-(3')Alexa 488. GMFI corresponds to Geometric Mean of Fluorescence Intensity. Results are expressed as GMFI ± SD of 2 independent experiments (*p<0.05; **p<0.01).

Figure 3.9 shows that as with HeLa cells, U87.CD4.CXCR4 cells also present better cell-surface adsorption for all the compounds tested when cells were incubated in the absence of glucose. Surprisingly, in the absence of glucose all glucose-containing COCs showed a better cell-surface adsorption than control-oligonucleotide or fucose-containing COC, with a strong adsorption for the COC presenting maltose-PEG4 moiety. In the presence of glucose, there was a slight increase of fluorescence again for COCs bearing two branched glucoses [(glucose-C2)$_2$-DB] and maltose-PEG4.

It is noteworthy that in the absence of glucose an overall increase in fluorescence intensity is observed for all oligonucleotides analysed in comparison to the data observed when glucose was present in the incubation medium. This behaviour was similar in both HeLa and U87.CD4.CXCR4 cell lines. In general, the differences found in cell-surface adsorption of these compounds were small, where COCs containing two branched glucoses [(glucose-C2)$_2$-DB] and maltose-PEG4 moieties showed a slight increase in fluorescence, for both cell types either in the absence or presence of glucose.

Analysis of cellular uptake of COCs

After performing cell-surface adsorption assays under these two experimental conditions (in the absence or presence of glucose), we continued with the study of cellular uptake of COCs in order to evaluate the influence of glucose units in the oligonucleotide and the relevance of the different spatial presentation in the cellular uptake by HeLa and U87.CD4.CXCR4 cells.
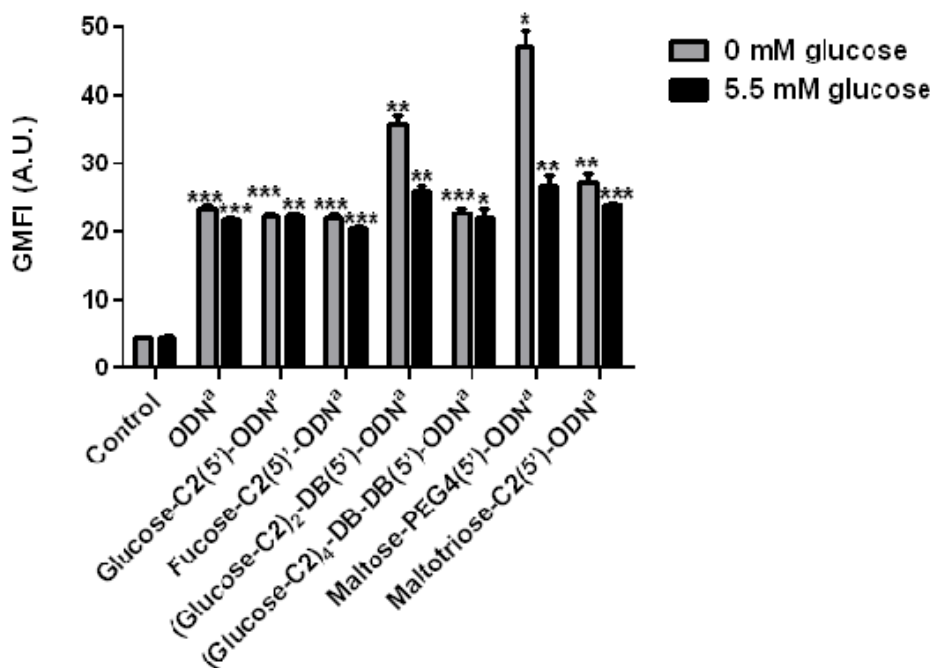
Figure 3.10 Cellular uptake of Alexa 488-labelled control-oligonucleotide and COCs in HeLa cells. Cells were seeded (1.25×10^5 cells/well) in 24 well plates and cultured overnight in appropriate growth medium. The next day cells were washed with DPBS and incubated with 2 µM bioconjugate for 2 h at 37°C in the absence or presence of glucose (5.5 mM). After incubation, cells were washed three times, resuspended in ice-cold PBS, and analysed by flow cytometry. Control stands for untreated cells, representing cell basal fluorescence intensity; ODN[a] stands for GEM91-(3')Alexa 488. GMFI corresponds to Geometric Mean of Fluorescence Intensity. Results are expressed as GMFI ± SEM of 3 independent experiments performed in duplicate (*$p<0.05$; **$p<0.01$; ***$p<0.001$).

The results shown in Figure 3.10 reveal that COCs containing two branched glucoses [(glucose-C2)$_2$-DB] and maltose-PEG4 moiety presented better incorporation into HeLa cells in both experimental conditions, with a higher fluorescence difference in the absence of glucose compared to that of control-oligonucleotide or other COCs.

134
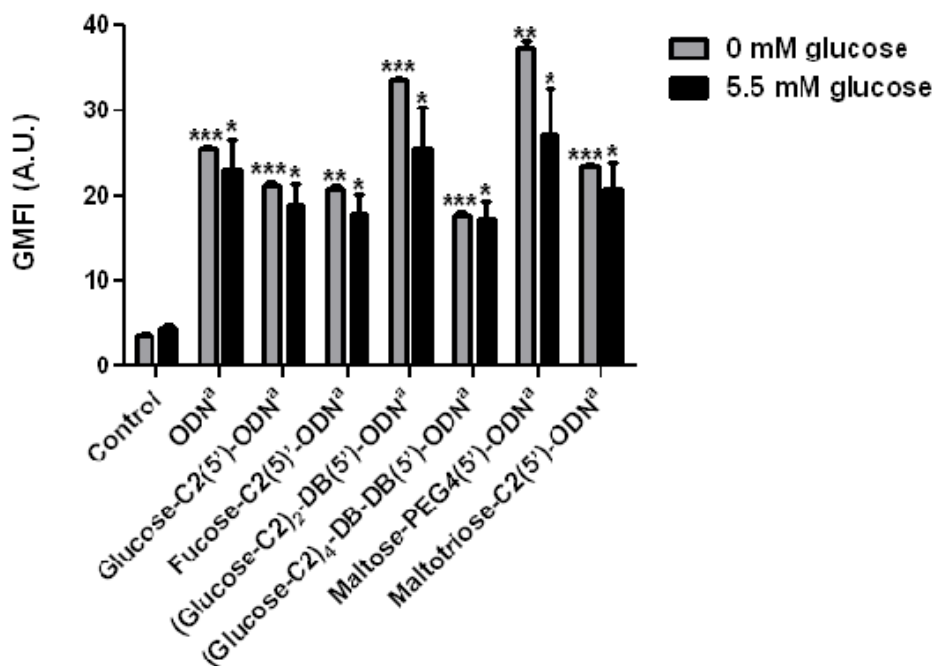
Figure 3.11 Cellular uptake of Alexa 488-labelled control-oligonucleotide and COCs in U87.CD4.CXCR4 cells. Cells were seeded (1.25×10^5 cells/well) in 24 well plates and cultured overnight in appropriate growth medium. The next day cells were washed with DPBS and incubated with 2 µM bioconjugate for 2 h at 37ºC in the absence or presence of glucose (5.5 mM). After incubation, cells were washed three times, resuspended in ice-cold PBS, and analysed by flow cytometry. Control stands for untreated cells, representing cell basal fluorescence intensity; ODN[a] stands for GEM91-(3')Alexa 488. GMFI corresponds to Geometric Mean of Fluorescence Intensity. Results are expressed as GMFI ± SEM of 3 independent experiments performed in duplicate (*p<0.05; **p<0.01; ***p<0.001).

As observed in Figure 3.11 similar results were obtained when cellular uptake of these compounds in U87.CD4.CXCR4 cells was analysed, showing the best incorporation profiles in both experimental conditions those COCs bearing two branched glucoses [(glucose-C2)$_2$-DB] and maltose-PEG4 moiety. This result was more remarkable in the absence of glucose.

135

3.3 Discussion

A safe and efficient system of delivering oligonucleotides is still a difficult challenge for the development of nucleic acid based therapy. Apart from their instability, naked oligonucleotides also have to deal with the problem of nonspecific cellular uptake. To overcome this latter difficulty, glycoconjugation approach appears to be a promising tool because of the biologically important properties that carbohydrates confer, such as signalling capability and tissue specificity (Ikeda *et al.*, 2010).

To date, several nucleic acid based delivery methods have been reported using molecules modified with a carbohydrate, including glycosylated polyamines and streptavidin (Lemarchand *et al.*, 2004). In these systems, which are known to be difficult to characterise and toxic at concentrations above 100 μM, the glycosylated molecules form complexes with nucleic acids via noncovalent interactions. In contrast to noncovalent interactions, covalent carbohydrate-oligonucleotide conjugates present a number of advantages, such as the structural homogeneity of each starting material and product, the low toxicity of the components of the conjugates even at elevated concentrations and the fact that the components of the conjugate are in defined relative proportions to each other (Zatsepin and Oretskaya, 2004). Indeed, it has been already reported that covalent carbohydrate-oligonucleotide conjugates exhibit an increased biological activity compared to the noncovalent complexes (Maier *et al.*, 2003).

In this work and according to the results obtained in the cytotoxicity assay, it can be assumed that the carbohydrate-oligonucleotide conjugates (COCs) and the control-oligonucleotide [GEM91-(3')NH$_2$] are not cytotoxic at the concentration tested (5 μM). This is not surprising since most carbohydrates (*i.e.*, glucose and glucose derivatives) are electrically neutral and ubiquitous in living systems.

Different type of tumour cells show an increase in glucose uptake, which is often associated with elevated levels of GLUT family members including GLUT1 and GLUT3 (Watanabe *et al.*, 2010). In particular, GLUT1 and GLUT3 share many similarities in structure and function. About 65% of their amino acid sequences are identical, but their C-terminal domains and the extracellular loops are distinctive. Also, these isoforms have a high affinity for D-glucose when they are expressed at the cell surface (Dwyer, 2001; Sakyo *et al.*, 2007). These features can be exploited to develop delivery strategies into tumour cells based on the design of glucose-derived conjugate oligonucleotides. In this regard, glucose-containing conjugates could be potential candidates to be used as delivery systems to target specifically tumour cells expressing GLUT1 and GLUT3 proteins on the cell surface (Rodríguez-Enríquez *et al.*, 2009).

When the expression levels of both GLUT1 and GLUT3 were analysed, according to the results obtained by western blotting (Figures 3.4, 3.5, 3.6 and 3.7), GLUT3 seems to be the majority GLUT isoform expressed in both studied HeLa and U87.CD4.CXCR4 cell lines in this work. Indeed, GLUT3 protein appeared in either membrane-bound fraction or cytoplasm fraction, with a higher molecular mass (about 70 kDa) compared to the theoretical molecular mass of the glut transporter (50-55 kDa) (Suzuki *et al.*, 1999), suggesting that GLUT3 might be expressed as a larger form, probably due to modifications of N-glycosylation. Furthermore, in the absence of glucose it can be observed not only an induction of GLUT3 transport to the cell-surface, but also a slight increase in GLUT3 expression. Although the fractionation procedure chosen did not separate endoplasmic reticulum (ER)/Golgi and plasma membrane fractions, the occurrence of matured N-glycosylation of GLUT3 protein indicates that their targeting to at least the post ER/Golgi fraction within the cells was completed (Suzuki *et al.*, 1999).

GLUT3 band present in the cytoplasm fraction also has higher molecular mass, underscoring that this protein has already passed the N-glycosylation procedure. From the latter results it can be postulated that GLUT3 could have an inducible expression and therefore, it could be retained in intracellular vesicles, waiting for the correct stimuli to be translocated to the cell surface, as reported by other authors (Hiraki *et al.*, 1988; Heijnen *et al.*, 1997; Thoidis *et al.*, 1999; Watanabe *et al.*, 2010; Iwabuchi *et al.*, 2011).

In cell-surface adsorption and cellular uptake assays similar results were obtained in both HeLa and U87.CD4.CXCR4 cell lines. A dramatic increase in cell-surface fluorescence was observed for all COCs, as well as for the control-oligonucleotide, when cells were incubated in the absence of glucose, which could be due to the starving conditions suffered by the cells during long periods of time (*i.e.*, 48 h).

On the other hand, tetravalent glucose oligonucleotide conjugate [(glucose-C2)$_4$-DB-DB] behaved differently for each type of cell, showing worse adsorption than the other compounds tested in HeLa cells, whereas in U87.CD4.CXCR4 cells, its adsorption was better than the control-oligonucleotide. However, the results obtained for this tetravalent COC in cellular uptake assays, reveals that high multivalency of glucose seems to hinder cellular uptake, probably due to the high structural volume of this compound. Similarly, Aviñó and co-workers observed that branching somehow reduces the inhibitory properties of siRNA duplex in HeLa cells (Aviñó *et al.*, 2011). In contrast with these observations, some authors reported that multivalent carbohydrate clusters moieties are preferred to be used as ligands for targeting lectins, pinpointing the term "cluster effect" (Sliedregt *et al.*, 1999; Maier *et al.*, 2003).

Flow cytometry studies revealed that the differences found in cell-surface adsorption of all the compounds were generally small. It can be observed that COCs containing terminal glucose units linked through just one doubler dendrimer [(glucose-C2)$_2$-DB] or a long tetraethylene glycol spacer (maltose-PEG4) showed the best adsorption profiles for both HeLa and U87.CD4.CXCR4 cell lines, either in the absence or presence of glucose. Likewise, in cellular uptake assays higher fluorescence intensity was also obtained for these two COCs in comparison to other COCs and the unconjugated control-oligonucleotide, being this behaviour more remarkable in the absence of glucose. Unfortunately, the differences in fluorescence intensity diminished quite considerably when glucose was present in the incubation medium, most probably due to the large difference in concentration between glucose (5.5 mM) and the COCs (2 μM). A possible explanation for these results is that GLUT3 protein could be involved in the incorporation of these two COCs into HeLa and U87.CD4.CXCR4 cell lines, suggesting that free glucose molecules present in the medium could play as competitors in the binding sites of GLUT proteins.

In sum, these results indicate that keeping a certain distance (15 to 18 atoms) between DNA and sugar modification could be important for a better incorporation of oligonucleotide conjugate into the target cell. Similar observations have been reported by other authors who pointed out that elongation of the spacer from 4 to 20 Å had a great influence on the binding, leading to the tightening of binding to lectins (Maier *et al.*, 2003; Zatsepin and Oretskaya, 2004). In agreement with these results, it seems to be a necessary requirement to pinpoint a defined distance (15 to 18 atoms) between the DNA molecule and the sugar moiety for further promising COC design.

Chapter 4:

Study of lipid-oligonucleotide conjugates with different lipid tails in membrane lipid model systems and HeLa cells

Chapter 4: Study of lipid-oligonucleotide conjugates with different lipid tails in membrane lipid model systems and HeLa cells

4.1 Introduction

Cell membranes act as selective barriers and regulate the entry of molecules into the cells. In this regard, these hydrophobic barriers prevent the entry of hydrophilic molecules into the cell (Singh *et al.*, 2010). In particular, oligonucleotides are hydrophilic molecules by virtue of their phosphate and sugar backbone. Although the nucleobase is hydrophobic, hydrophilicity dominates because of the extensive hydrogen bonding resulting from the phosphate and sugar residues. In addition, this intrinsic hydrophilicity is increased by the anionic nature of the backbone. Thus, the hydrophilic and polyanionic character of these compounds leads to a reduction in cellular permeation. Unfortunately, simple elimination of the anionic charges does not improve cellular uptake, as evidenced by chemically modified neutral backbone-containing oligonucleotides, such as methylphosphonates and PNA oligomers (Manoharan, 2002). Therefore, it is quite natural that the use of lipid based systems has long received the interest as a possible method to solve cell permeation problems (Lönnberg, 2009).

Delivery of oligonucleotides relying on conjugation with lipophilic molecules rather than lipid based complex formation (*i.e.*, lipoplexes) provides an attractive strategy to avoid some undesired effects associated with complexes (Ye *et al.*, 2007). Indeed, covalent attachment of fatty acids provides a soluble molecule with sufficient hydrophobic character for cell membrane interaction and insertion (Bunge *et al.*, 2007). To optimise the type and placement of lipophilic groups on oligonucleotides in order to facilitate cell uptake and intracellular trafficking, it is important to consider how natural biomolecules are tagged by lipophilic groups (Laing *et al.*, 2010).

To date, several lipophilic molecules, including cholesterol, phospholipids, α-tocopherol and alkyl chains, have been used to conjugate with oligonucleotides in order to confer them more "drug-like" properties (MacKellar *et al.*, 1992; Crooke *et al.*, 1996; Manoharan, 2001; Herbert *et al.*, 2005; Nishina *et al.*, 2008; Chan *et al.*, 2009). In this regard, the main goal of these lipophilic compounds is to improve oligonucleotide delivery and enhance their cellular uptake via receptor-mediated endocytosis or by an increased membrane permeability, without altering the potential properties of the nucleic acid molecule in order to achieve desired inhibition of gene expression (Boutorin *et al.*, 1989; Shea *et al.*, 1990; Lorenz *et al.*, 2004; De Paula *et al.*, 2007; Jeong *et al.*, 2009; Lönnberg, 2009). Lipophilic oligonucleotides reported in a number of studies have shown a greatly improved cellular uptake, compared to the unmodified oligonucleotides. Moreover, such compounds seem to display a higher resistance toward nucleases, being the increase in resistance proportional to the size of the aliphatic chain. However, the antisense efficiency does not always correlate with the lipophilicity (Singh *et al.*, 2010).

From all the lipophilic moieties used for conjugation, cholesterol is perhaps the best characterised, having been studied by several groups for the past two decades (Maru *et al.*, 2004; Pfeiffer and Höök, 2004; Beales and Vanderlick, 2007). In particular, it has been reported to increase binding of oligonucleotides to lipoproteins, thereby enhancing cellular association and transport as well as influencing tissue distribution and cellular uptake behaviours (Wolfrum *et al.*, 2007). Consequently, cholesterol conjugates can be recognised by hepatic cells and internalised by lipoprotein-mediated endocytosis (Bijsterbosch *et al.*, 2000, 2001). Also, it has been shown that conjugation with cholesterol increases the silencing effect of antisense oligonucleotide and siRNA either *in vitro* or *in vivo* (Alahari *et al.*, 1996; Epa *et al.*, 1998; Lorenz *et al.*, 2004; Soutschek *et al.*, 2004; Cheng *et al.*, 2006).

In this work, we studied five lipid-oligonucleotide conjugates (LOCs) differing in the conjugation site of the oligodeoxynucleotide (ODN) and in the alkyl moiety (Figure 4.1). We used three membrane lipid model systems (*i.e.*, monolayers, GUVs and SPBs) and a cell system (*i.e.*, HeLa cell line) in order to analyse the interaction between lipids and LOCs and the cellular uptake behaviours, respectively. As shown in Figure 4.1, three lipid modifications were carried out in the 3'-end of ODN and other two lipid modifications in the 5'-termini. All lipid modifications were neutral lipids based on SNALP formulations, except one lipid conjugated in the 3'-termini which had a polar group at the end of the lipophilic tail ($C_{12}NH_2$), mimicking the effect produced by lipoplex complexes. Indeed, four of the selected lipid groups were previously tested in the passenger strand of siRNA molecules by Grijalvo and co-workers, who reported that these lipid moieties did not disrupt RNAi machinery (Grijalvo *et al.*, 2010, 2011). As observed in Figure 4.1, the LOCs bearing a lipid moiety at the 5'-end of the DNA strand presented an aliphatic amine group at the 3′-end in order to bind the Alexa 488 fluorophore, as described in the Experimental procedures section. By contrast, in the LOCs bearing a lipid moiety at the 3'-end of the DNA strand no linker was needed to incorporate a free amine group at the 5'-termini to bind to Alexa 488 since in their synthesis the 5'-amine-modifier-C6-Tfa phosphoramidite (Glen Research) was used. Further structure information of control-ODN and LOC is given in the Appendix section (Tables A.1-A.3).
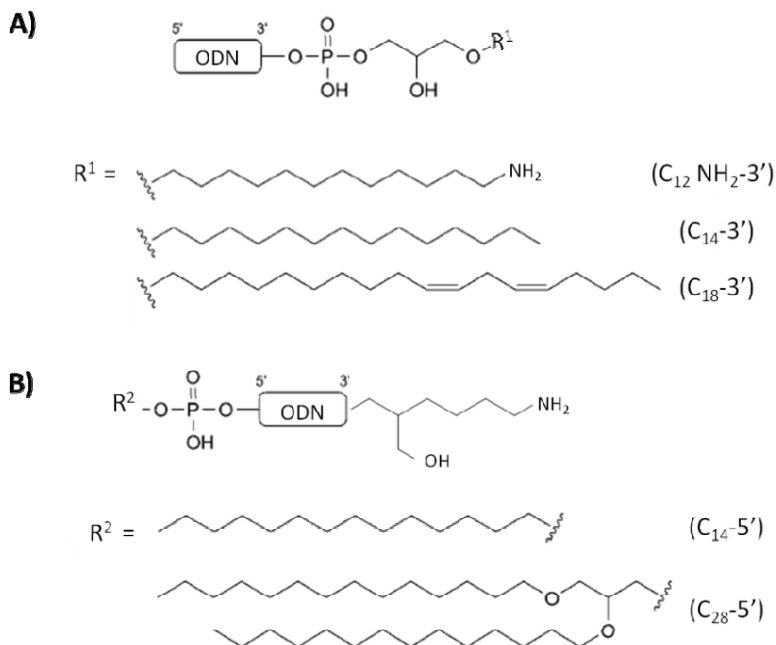
Figure 4.1 Lipid modifications introduced into the oligodeoxynucleotide (ODN). A) Selected lipids (R^1) were bound to the 3'-end of the ODN. B) Selected lipids (R^2) were bound to the 5'-termini. ODN corresponds to GEM91 sequence. This figure was modified from Grijalvo *et al.* (2011).

4.2 Results

4.2.1 Membrane lipid model systems

4.2.1.1 Lipid monolayers

We first investigate the interfacial behaviour of LOCs at the free air-water interface. To study this issue we used a Langmuir balance. LOCs suspended in 1X PBS were injected into the subphase, and the change in surface pressure (π) was recorded during 4,000 s. All LOCs caused a dose-dependent increase in surface pressure at the air-water interface, except the LOC bearing $C_{12}NH_2$ at the 3' termini, which did not cause any change in surface pressure, as ODN itself.

Similarly, in the case of C_{14} moiety, very slight changes in surface pressure were detectable, the conjugation site of the lipid chain apparently not showing remarkable differences, even when the LOC presented or not a free amine group on the other side of lipid conjugation (Figure 4.2). After a certain time, which decreased with increasing concentration of LOC, π remained constant, except for $C_{28}(5')$-GEM91-$(3')NH_2$, which caused a dramatic increase in surface pressure changes at longer time periods when higher concentrations (up to 5 µM) were used. This constant value was operationally defined as an equilibrium value in this context. In order to compare the behaviour of LOCs under the same experimental conditions, π at 4,000 s was chosen as an equilibrium value, which was a constant value for all LOCs, except for $C_{28}(5')$-GEM91-$(3')NH_2$.
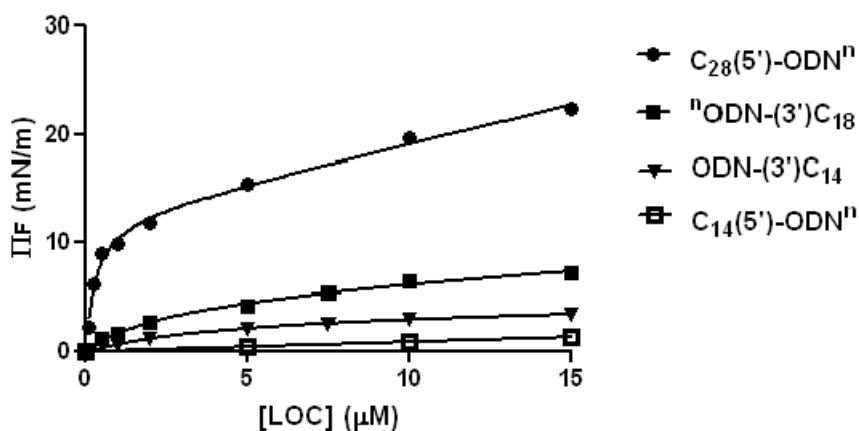
Figure 4.2 Changes in surface pressure at the air-water interface induced by LOCs. Final π values obtained from LOCs at 4,000 s of incubation with constant stirring. ODN^n, ^nODN and ODN stand for GEM91-$(3')NH_2$, $NH_2(5')$-GEM91 and GEM91, respectively. Average values ± SD (n=2). Subphase composition was 1X PBS. LOCs were injected into the subphase.

The LOCs that caused changes in surface pressure at the air-water interface were used to further examine their insertion into phospholipid monolayers using again the Langmuir balance, with preformed monolayers solely composed of the zwitterionic DOPC lipid at the air-water interface, and LOCs injected into the subphase. As observed in Figure 4.2, the π_F vs. LOC concentration curves reached a plateau at specific LOC concentration, which was different for each LOC. The minimum LOC concentrations rendering maximum surface-activity were used to test LOC insertion into DOPC monolayers at varying initial π values (Figure 4.3).
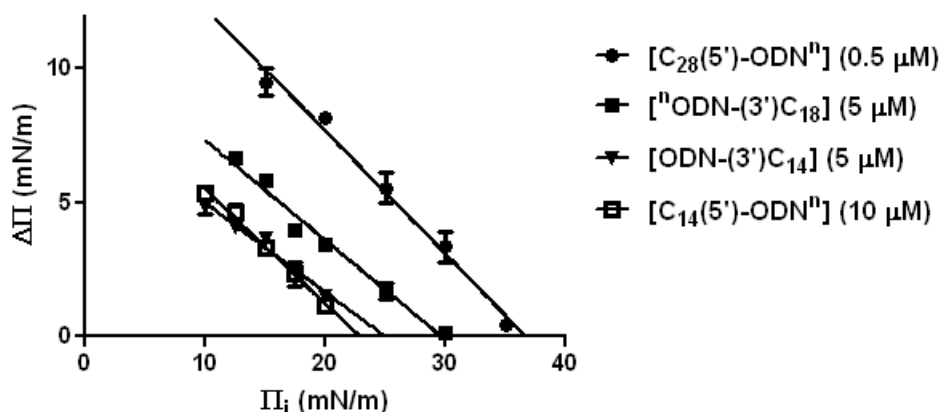
Figure 4.3 Changes in surface pressure of DOPC monolayers oriented at the air-water interface as a result of LOC insertion, at varying initial pressures. The plateau values of surface pressure increases ($\Delta\pi$) after LOC insertion are plotted as a function of the initial π (π_i). ODN^n, ^{n}ODN and ODN stand for GEM91-(3')NH$_2$, NH$_2$(5')-GEM91 and GEM91, respectively. Average values ± SD (n=2). Subphase was 1X PBS. LOCs were injected into the subphase with constant stirring.

LOC derived increases in surface pressures of DOPC monolayers depended strongly on the initial π value (π_i). The data were fitted to a straight line, whose extrapolation to $\Delta\pi=0$ gives an idea of the maximum monolayer surface pressure allowing LOC insertion.

As seen in Figure 4.3, LOCs containing the C_{14} moiety in either 3' or 5'-termini could not be inserted into monolayers at initial π above 25 mN/m, whereas LOCs containing longer or double alkyl chain could. Nevertheless, the LOC bearing C_{18} moiety at the 3' termini and a free amine group at the 5'-termini could not be inserted into monolayers at initial π above 30 mN/m, compared to C_{28}(5')-GEM91-(3')NH$_2$, which could become inserted into monolayers at initial π up to 35 mN/m, even at lower concentrations (0.5 μM) than the other LOCs. These observations are important because the cell membranes are considered to support a lateral pressure $\pi \approx 30$ mN/m, albeit large fluctuations around this average value (Marsh, 1996; Busto *et al.*, 2007).

Given the results above described and based on the assumption of 30 mN/m as an average membrane pressure, it could be postulated that from all the LOCs tested only C_{28}(5')-GEM91-(3')NH$_2$ should easily insert into cell membranes. This information may be relevant for further cellular uptake studies in HeLa cells.

4.2.1.2 Lipid bilayers

The plasma membrane can be considered as a flat plane devoid of curvature stress, in the size scale of the phospholipid bilayer width ($\approx$4-6 nm). The absence of curvature stress, in combination with the molecular cohesion induced by the high levels of cholesterol, poses an effective restriction to the insertion of external agents into the lipid bilayer surrounding the cells. Thus, after studying LOC behaviour in a monolayer system, giant unilamellar vesicles (GUVs) and supported planar bilayers (SPBs) provide bona fide starting models to directly visualise and analyse LOC interactions with membranes bearing a curvature stress and surface change comparable to those of the plasma membrane surrounding eukaryotic cells (van Meer, 2005; Mcintosh and Simon, 2007; Apellaniz *et al.*, 2010).

Also in line with that idea, it was taken into consideration in this study the fact that the plasma membrane presents an additional level of physicochemical complexity, which is directly related to the existence of laterally segregated lipid platforms or "rafts". Thus, we studied two different effects: i) possible LOC interaction with lipid bilayer model systems and, ii) LOC preferential interaction for specific domains using ternary ("raft-like") lipid mixtures. Depending on their lipophilic modification, LOCs could incorporate with preference either into liquid-ordered (L_o) or into liquid-disordered (L_d) domains, as shown for peptides, proteins and oligonucleotides bearing lipophilic moieties (Wang *et al.*, 2001; Baumgart *et al.*, 2007; Bunge *et al.*, 2007; Sengupta *et al.*, 2008; Bunge *et al.*, 2009; Loew *et al.*, 2010). L_o domains are rich in saturated phospholipids and cholesterol and show an increased acyl chain order. By contrast, in L_d domains, the lipid are loosely packed and enriched with phospholipids carrying unsaturated hydrocarbon chains (Bunge *et al.*, 2009).

In this work a ternary lipid mixture of DOPC, eSM and Chol was used for the formation of both GUVs and SPBs, roughly mimicking the chemical composition and the properties of the lipid rafts found in the exoplasmic leaflet of plasma membrane (Baumgart *et al.*, 2003; Garcia-Saez *et al.*, 2007). Therefore, in the next set of experiments we sought to analyse the effect of L_d and L_o lipid phase co-existence on LOC partitioning.

Specifically, these lipid bilayer systems were composed of DiO- or DiD-labelled DOPC/eSM/Chol (2:2:1). DiO (green) and DiD (red) lipophilic dyes specifically partitioned into L_d phase and L_o domains were seen as probe-depleted dark areas within the bilayers. To perform these experiments Alexa 488- or Cy5-labelled LOCs were used.

As previously described in the Experimental procedures section, Alexa 488 fluorescent tag was primarily selected to couple with the LOCs. Unfortunately, labelling with Alexa 488 presented some undesired problems with the oligonucleotides carrying lipid modification at the 3'-end of the DNA strand.

In the case of the LOC that contained $C_{12}NH_2$ modification at the 3'-termini, it was not possible to couple Alexa 488 dye specifically to the 5'-termini due to the presence of another reactive primary amine at the end of the lipophilic tail.

On the other hand, when bioconjugates carrying C_{14} or C_{18} alkyl modifications at the 3'-termini were coupled with Alexa 488 at the 5'-end of the DNA strand, low purity yields were obtained (50% and 30%, respectively). As a result, Cy5 dye was also selected to label the 5'-termini of the aforementioned LOCs.

GUVs

As mentioned above, GUVs were composed of DiO- or DiD-labelled DOPC/eSM/Chol (2:2:1), showing L_o/L_d phase coexistence and well defined domains at 22ºC.
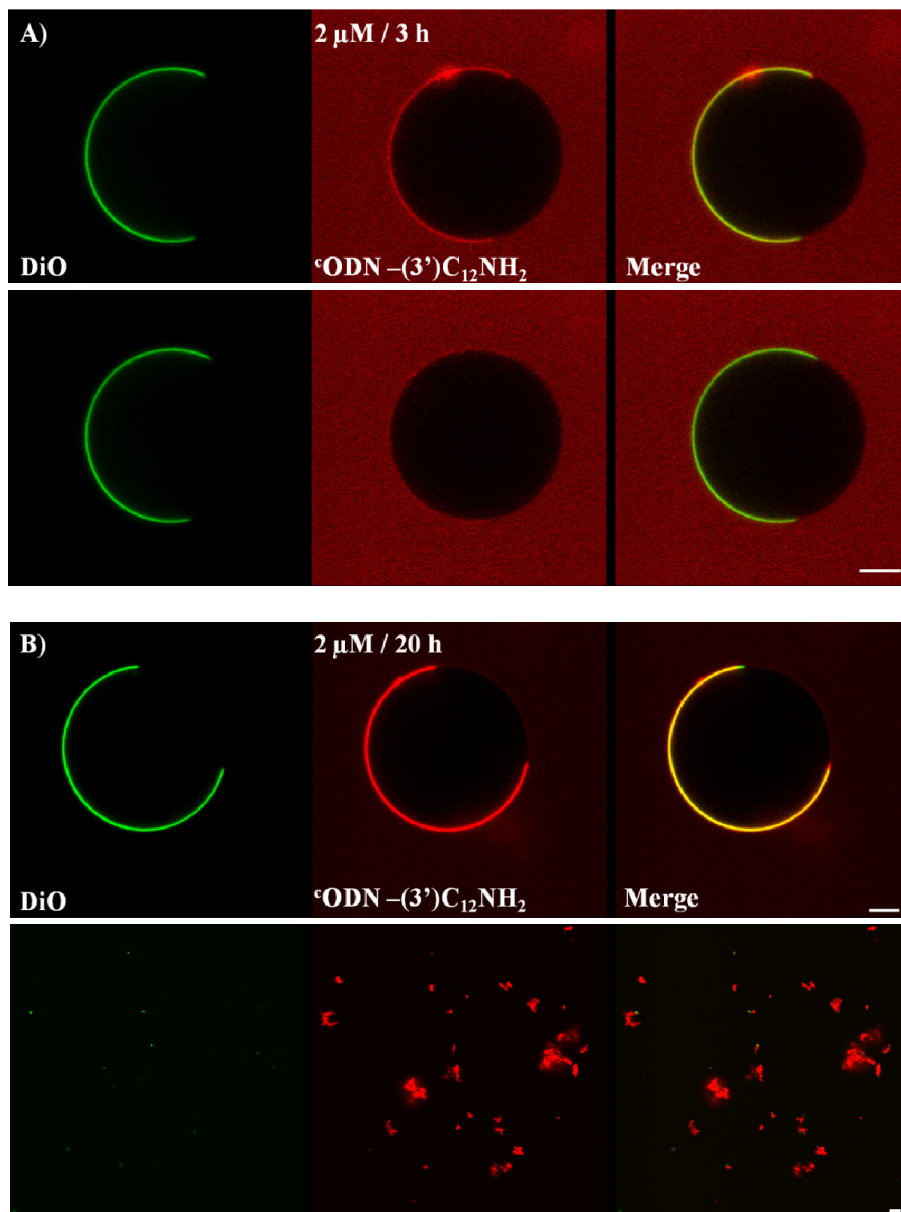
Figure 4.4 Imaging of Cy5-labelled ODN-(3')C$_{12}$NH$_2$ binding to GUVs. Confocal microscopy images of DiO-labelled DOPC/eSM/Chol (2:2:1) GUVs (equatorial sections) incubated with 2 μM of Cy5-labelled ODN-(3')C$_{12}$NH$_2$ for 3 h (A) or 20 h (B). ^{c}ODN stands for Cy5(5')-GEM91. Lipid (green) and LOC (red) staining are shown in the left and centre columns, respectively. The right column displays the merging of both detection channels. (A) Images from the bottom panels were acquired a few seconds after the first acquisition (upper panels). Images were taken at 22ºC. Scale bars represent 5 μm.

152

As observed in Figure 4.4, Cy5-labelled ODN-$C_{12}NH_2$ shows a very weak binding to GUVs, since the fluorescence signal coming from Cy5 fluorophore looses intensity and almost disappears when the sample is radiated again with the laser in order to acquire a second image (Figure 4.4A). After 20 h of incubation, a better Cy5 fluorescence signal is observed, which co-localises with DiO dye in the L_d phase of GUVs (upper panels of Figure 4.4B), as well as big red aggregates (bottom panels of Figure 4.4B).
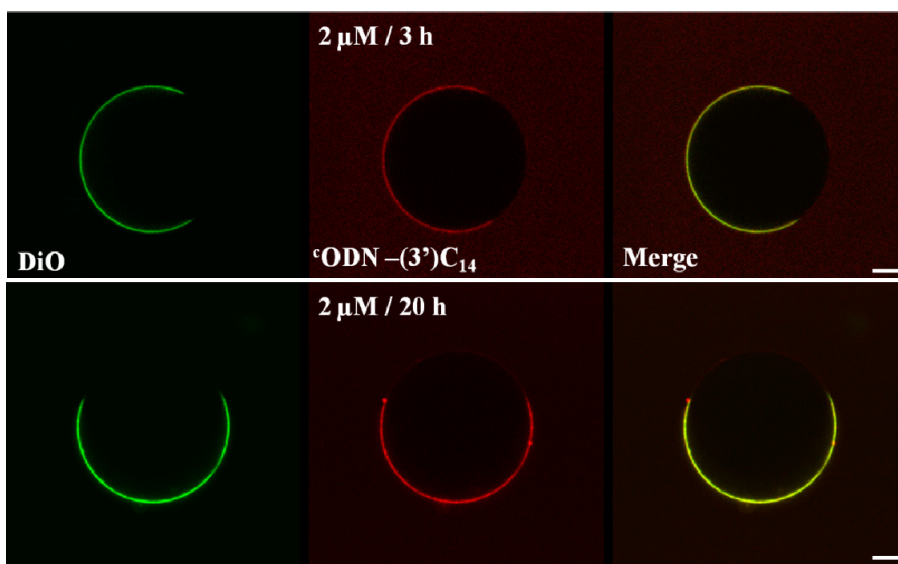
Figure 4.5 Imaging of Cy5-labelled ODN-(3')C_{14} binding to GUVs. Confocal microscopy images of DiO-labelled DOPC/eSM/Chol (2:2:1) GUVs (equatorial sections) incubated with 2 μM of Cy5-labelled ODN-(3')C_{14} for 3 h (upper panels) and 20 h (bottom panels). ᶜODN stands for Cy5(5')-GEM91. Lipid (green) and LOC (red) staining are shown in the left and centre columns, respectively. The right column displays the merging of both detection channels. Images were taken at 22ºC. Scale bars represent 5 μm.

The confocal micrographs displayed in Figure 4.5 showed that Cy5-labelled ODN-(3')C_{14} was efficiently detected in GUVs at the concentration tested (2 μM). This LOC was co-localised with DiO dye, suggesting its incorporation into the L_d phase of the GUVs.
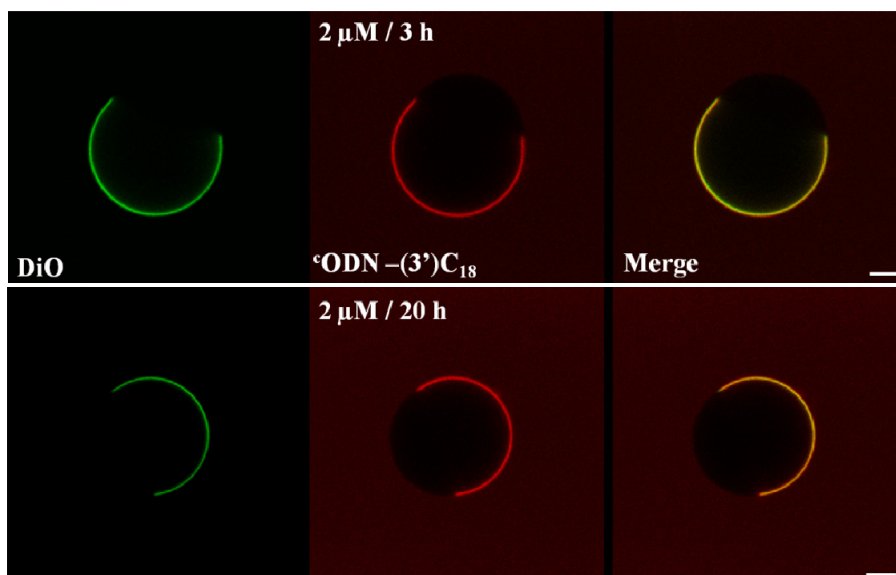
Figure 4.6 Imaging of Cy5-labelled ODN-(3')C$_{18}$ binding to GUVs. Confocal microscopy images of DiO-labelled DOPC/eSM/Chol (2:2:1) GUVs (equatorial sections) incubated with 2 μM of Cy5-labelled ODN-(3')C$_{18}$ for 3 h (upper panels) and 20 h (bottom panels). °ODN stands for Cy5(5')-GEM91. Lipid (green) and LOC (red) staining are shown in the left and centre columns, respectively. The right column displays the merging of both detection channels. Images were taken at 22ºC. Scale bars represent 5 μm.

Similar results were obtained for Cy5-labelled ODN-(3')C$_{18}$, which was also incorporated into GUVs at the concentration tested (2 μM) (Figure 4.6). As expected, this LOC was only detected in the L$_d$ phase of the GUVs and did not partition into L$_o$ phase, possibly due to its diunsaturated chain (Uline *et al.*, 2010).

To analyse the behaviour of Alexa 488-labelled LOCs in GUVs, DiD dye was used instead of DiO, which also partitioned into the L$_d$ phase in a specific manner.
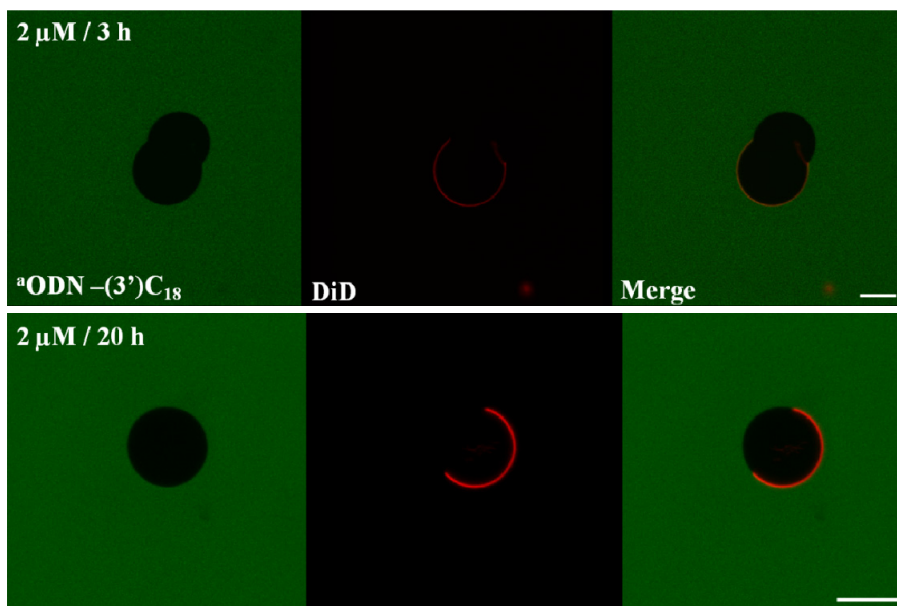
Figure 4.7 Imaging of Alexa 488-labelled ODN-(3')C$_{18}$ incubation with GUVs. Confocal microscopy images of DiD-labelled DOPC/eSM/Chol (2:2:1) GUVs (equatorial sections) incubated with 2 µM of Alexa 488-labelled ODN-(3')C$_{18}$ for 3 h (upper panels) and 20 h (bottom panels). [a]ODN stands for Alexa 488(5')-GEM91. LOC (green) and lipid (red) staining are shown in the left and centre columns, respectively. The right column displays the merging of both detection channels. Images were taken at 22ºC. Scale bars represent 5 µm.

As seen in Figure 4.7, Alexa 488-labelled ODN-(3')C$_{18}$ did not show any detectable interaction with the GUVs. This is opposite to the results obtained by Cy5-labelled ODN-(3')C$_{18}$, where a clear incorporation into the L$_d$ phase was observed. Since the labelling of ODN-(3')C$_{18}$ with Alexa 488 was not successful (only 30% of the compound was labelled), a 4% (w/v) agarose gel was performed in order to check the state of this LOC. Unfortunately, Alexa 488-labelled ODN-(3')C$_{18}$ did not run through the agarose gel and appeared at the top of the gel in the well where the sample was loaded (see Appendix, Figure A.2). This behaviour suggests that Alexa 488-labelled ODN-(3')C$_{18}$ was not as stable as Cy5-labelled ODN-(3')C$_{18}$ and was prone to form aggregates.

155
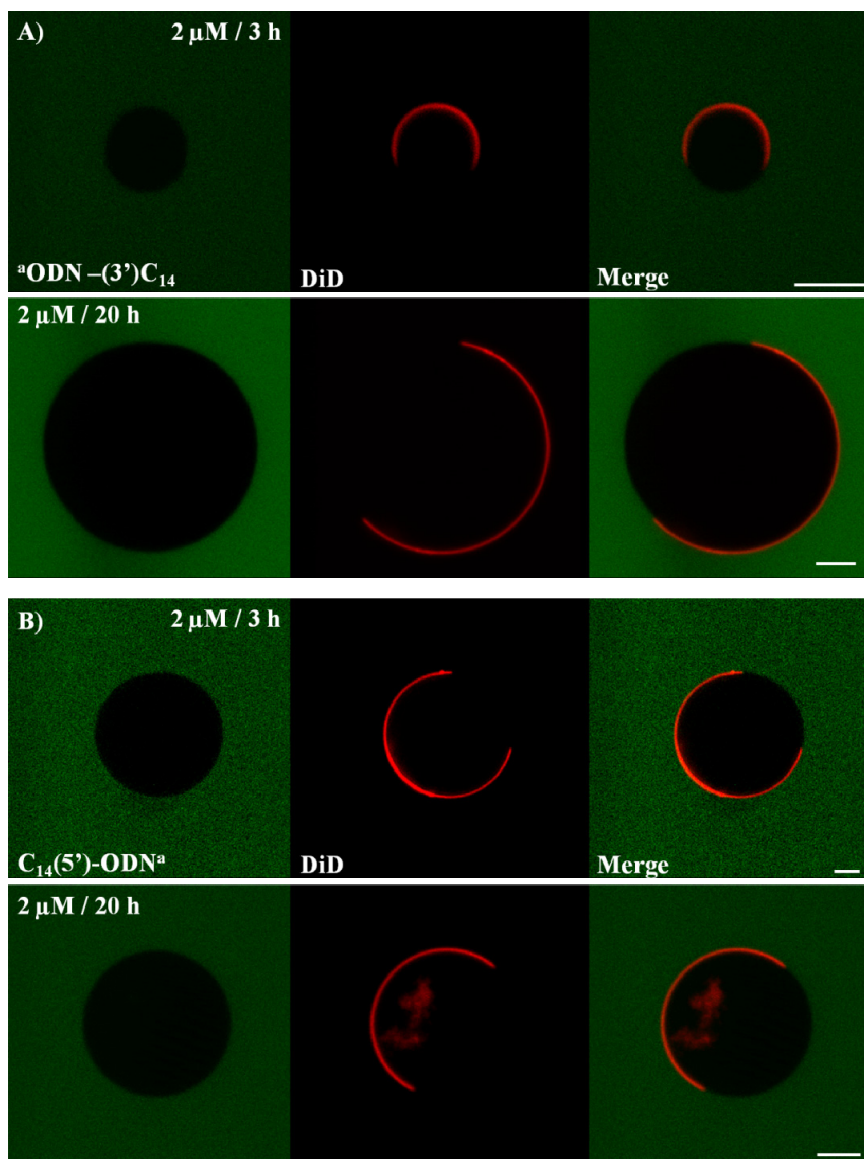
Figure 4.8 Imaging of Alexa 488-labelled ODN-(3')C$_{14}$ and Alexa 488-labelled C$_{14}$(5')-ODN incubation with GUVs. Confocal microscopy images of DiD-labelled DOPC/eSM/Chol (2:2:1) GUVs (equatorial sections) incubated with 2 μM of Alexa 488-labelled ODN-(3')C$_{14}$ (A) or C$_{14}$(5')-ODN (B) for 3 h and 20 h. [a]ODN and ODN[a] stand for Alexa 488(5')-GEM91 and GEM91-(3')Alexa 488, respectively. LOC (green) and lipid (red) staining are shown in the left and centre columns, respectively. The right column displays the merging of both detection channels. Images were taken at 22ºC. Scale bars represent 5 μm.

156

Both Alexa 488-labelled ODN-(3')C_{14} and C_{14}(5')-ODN conjugates did not show detectable binding to GUVs (Figure 4.8), unlike to what it was observed when GUVs were incubated with Cy5-labelled ODN-(3')C_{14}. The state of these LOCs was also checked by performing 4% (w/v) agarose gel and they run as monomers, obtaining similar running profiles compared to either the unlabelled or Cy5-labelled compounds (see Appendix, Figure A.2). These results suggest that the linker and/or fluorophore nature could somehow alter the binding properties of these LOCs.
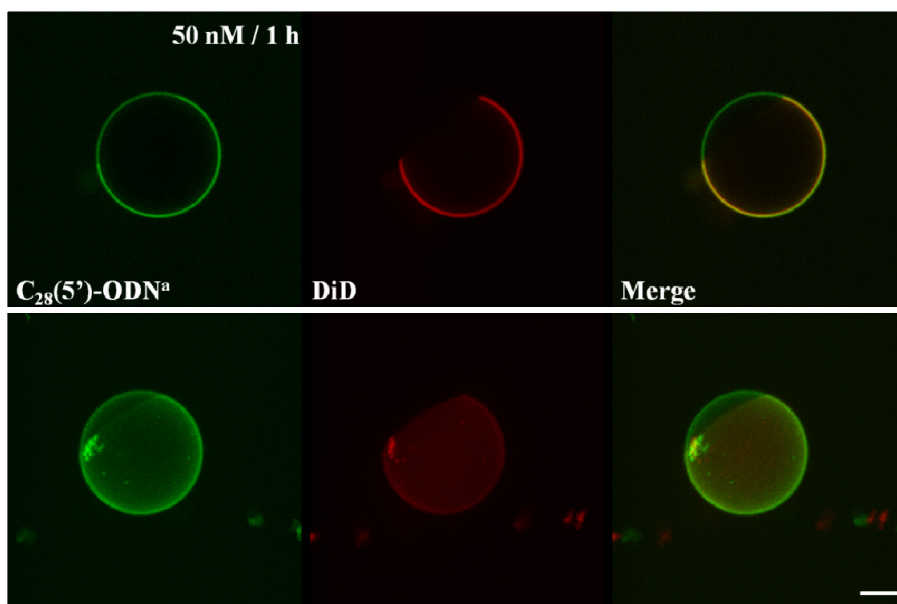
Figure 4.9 Imaging of Alexa 488-labelled C_{28}(5')-ODN binding to GUVs. Confocal microscopy images of DiD-labelled DOPC/eSM/Chol (2:2:1) GUVs [equatorial sections (upper panels); 3D reconstruction (bottom panels)] incubated with 50 nM of Alexa 488-labelled C_{28}(5')-ODN for 1 h. ODN[a] stands for GEM91-(3')Alexa 488. LOC (green) and lipid (red) staining are shown in the left and centre columns, respectively. The right column displays the merging of both detection channels. Images were taken at 22ºC. Scale bars represent 5 µm.

157
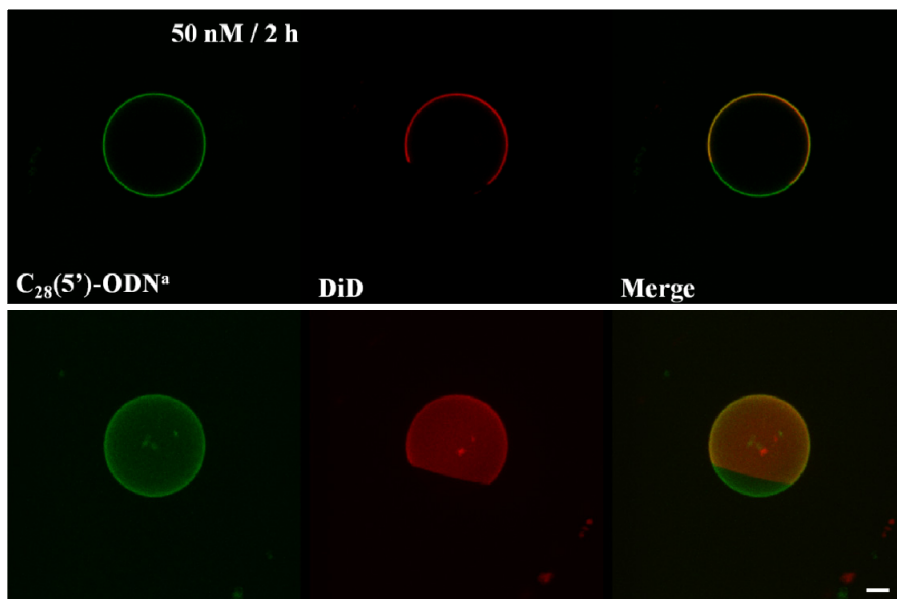
Figure 4.10 Imaging of Alexa 488-labelled C$_{28}$(5')-ODN binding to GUVs. Confocal microscopy images of DiD-labelled DOPC/eSM/Chol (2:2:1) GUVs [equatorial sections (upper panels); 3D reconstruction (bottom panels)] incubated with 50 nM of Alexa 488-labelled C$_{28}$(5')-ODN for 2 h. ODN[a] stands for GEM91-(3')Alexa 488. LOC (green) and lipid (red) staining are shown in the left and centre columns, respectively. The right column displays the merging of both detection channels. Images were taken at 22ºC. Scale bars represent 5 μm.

When GUVs were incubated with Alexa 488-labelled C$_{28}$(5')-ODN, a rapid and remarkable interaction was observed. This LOC showed special binding properties since it was able to insert either in the L$_d$ or L$_o$ phase. As seen in Figures 4.9 and 4.10, at first the interaction of this compound is more detectable in the L$_d$ phase, but it appears homogeneously distributed in both L$_d$ and L$_o$ phases after a certain incubation time.

158
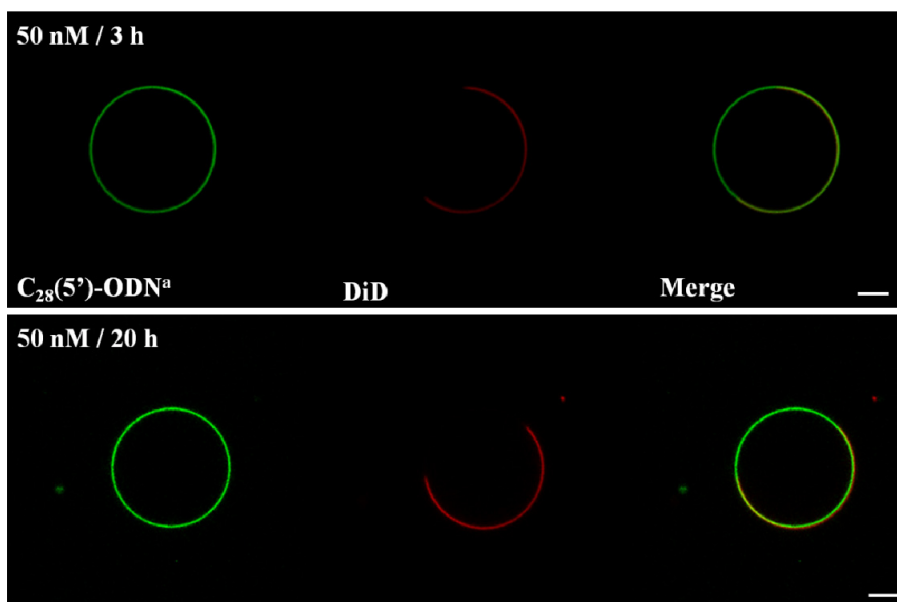
Figure 4.11 Imaging of Alexa 488-labelled C_{28}(5')-ODN binding to GUVs. Confocal microscopy images of DiD-labelled DOPC/eSM/Chol (2:2:1) GUVs (equatorial sections) incubated with 50 nM of Alexa 488-labelled C_{28}(5')-ODN for 3 h (upper panels) and 20 h (bottom panels). ODN[a] stands for GEM91-(3')Alexa 488. LOC (green) and lipid (red) staining are shown in the left and centre columns, respectively. The right column displays the merging of both detection channels. Images were taken at 22ºC. Scale bars represent 5 µm.

As observed in Figure 4.11, the incorporation of Alexa 488-labelled C_{28}(5')-ODN is stable during longer incubation time periods in both L_d and L_o phases. These observations point to a nonspecific phase partitioning of this LOC.

159

Table 4.1 sums up briefly the results obtained by the incubation of LOCs with GUVs.

LOC	Interaction preference
Cy5(5')-GEM91-C$_{12}$NH$_2$	L$_d$*
Cy5(5')-GEM91-C$_{14}$	L$_d$
Cy5(5')-GEM91-C$_{18}$	L$_d$
Alexa 488(5')-GEM91-C$_{18}$	n.d.i.
Alexa 488(5')-GEM91-C$_{14}$	n.d.i.
C$_{14}$(5')-GEM91-(3')Alexa 488	n.d.i.
C$_{28}$(5')-GEM91-(3')Alexa 488	L$_d$ + L$_o$

Table 4.1 Schematic table that summarises the results obtained by the incubation of LOCs with GUVs. The asterisk (*) corresponds to a very weak interaction observed by incubation of Cy5(5')-GEM91-C$_{12}$NH$_2$ with GUVs under these experimental conditions (see Figure 4.4); n.d.i. stands for no detectable interaction.

SPBs

Liquid domain co-existence and interacting LOCs can be also directly visualised by confocal microscopy of SPBs. As mentioned before, SPBs were composed of DiO- or DiD-labelled DOPC/eSM/Chol (2:2:1), showing L$_o$/L$_d$ phase coexistence and well defined domains at 22ºC. Initially, AFM measurements allowed us to check the presence of SPBs in mica supports and to measure the height difference of the domains present.
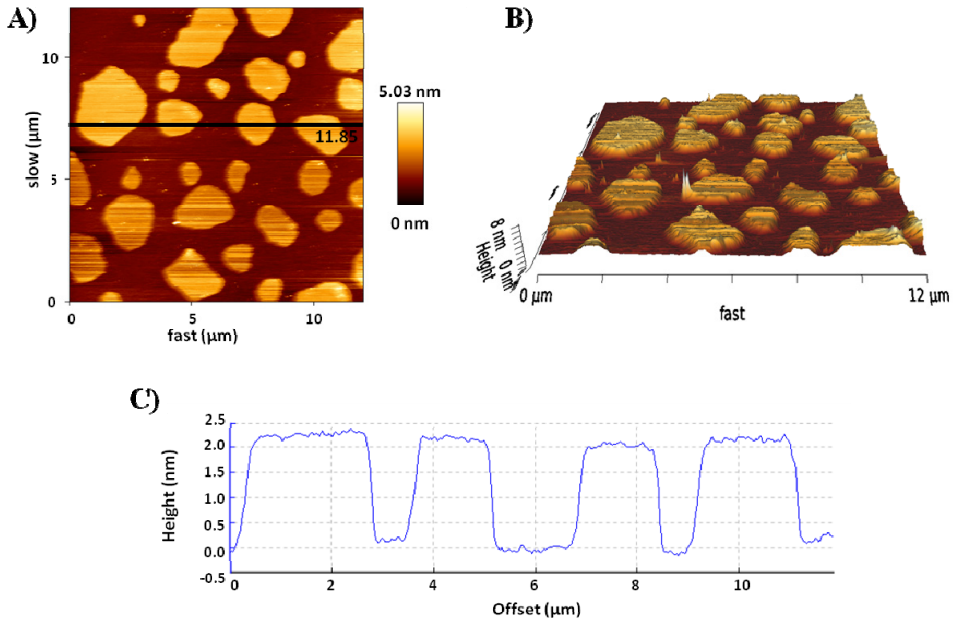
Figure 4.12 AFM images of DOPC/eSM/Chol (2:2:1) SPBs taken at 22ºC. (A) Height image. (B) 3D topography of Figure A. (C) Cross section (height profile) of black line in Figure A.

Thanks to AFM measurements interesting topographic information of the SPBs was obtained. Here, L_d an L_o domains were clearly differentiated, being L_o domains ~2 nm higher than the rest of the bilayer (Figure 4.12).
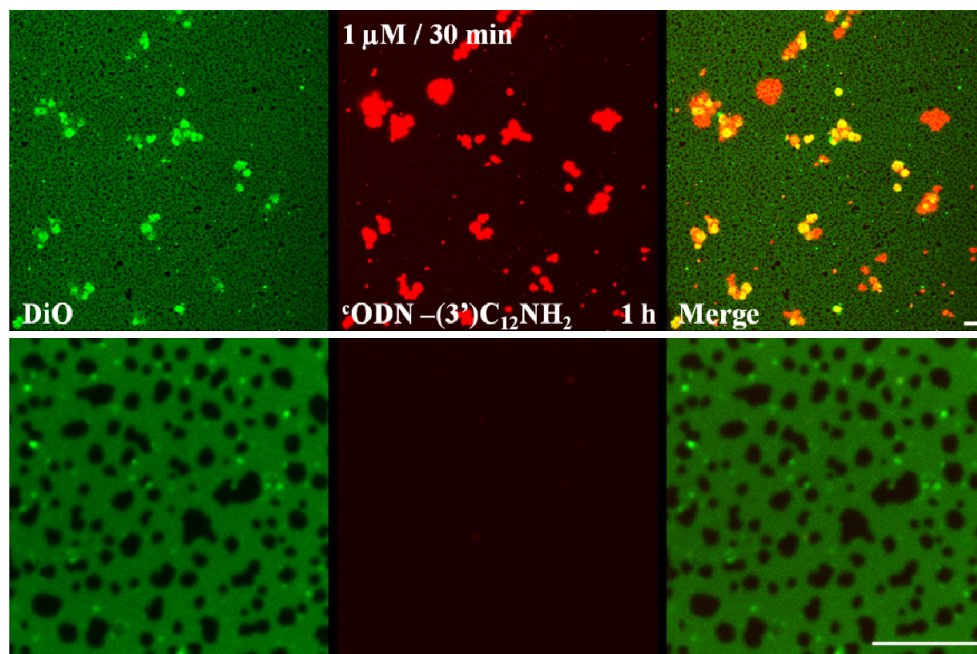
Figure 4.13 Imaging of Cy5-labelled ODN-(3')C$_{12}$NH$_2$ incubation with SPBs. Confocal microscopy images of DiO-labelled DOPC/eSM/Chol (2:2:1) SPBs incubated with Cy5-labelled ODN-(3')C$_{12}$NH$_2$. First, 500 nM Cy5-labelled ODN-(3')C$_{12}$NH$_2$ were added to the SPBs and incubated for 30 min. Then, additional 500 nM Cy5-labelled ODN-(3')C$_{12}$NH$_2$ were added to the sample and incubated for another 30 min. ^{c}ODN stands for Cy5(5')-GEM91. Lipid (green) and LOC (red) staining are shown in the left and centre columns, respectively. The right column displays the merging of both detection channels. Images were taken at 22ºC. Scale bars represent 10 μm.

As observed in Figure 4.13, Cy5-labelled ODN-C$_{12}$NH$_2$ did not show apparent binding to the SPB at the concentration tested during the incubation time specified in the figure legend. Again, LOC aggregates were observed, similar to those present in GUV experiments (see Figure 4.4).
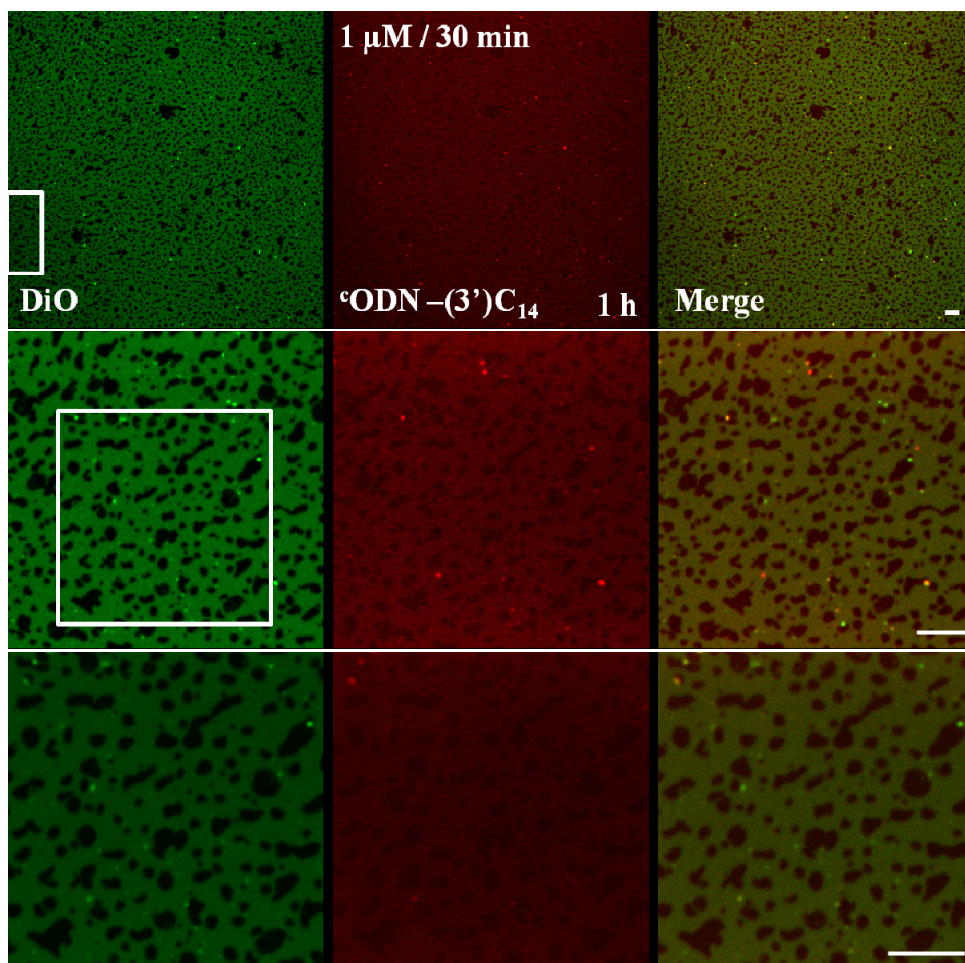
Figure 4.14 Imaging of Cy5-labelled ODN-(3')C₁₄ binding to SPBs. Confocal microscopy images of DiO-labelled DOPC/eSM/Chol (2:2:1) SPBs incubated with Cy5-labelled ODN-(3')C₁₄. First, 500 nM Cy5-labelled ODN-(3')C₁₄ were added to the SPBs and incubated for 30 min. Then, additional 500 nM Cy5-labelled ODN-(3')C₁₄ were added to the sample and incubated for another 30 min. °ODN stands for Cy5(5')-GEM91. White squares represent the zoom taken, corresponding to the images below. Lipid (green) and LOC (red) staining are shown in the left and centre columns, respectively. The right column displays the merging of both detection channels. Images were taken at 22ºC. Scale bars represent 10 μm.

Under these experimental conditions, Cy5-labelled ODN-(3')C₁₄ was efficiently detected in the SPB, co-localising with DiO dye (Figure 4.14).

163

Thus, these results suggest its incorporation into the L_d phase of SPBs, in agreement with the results obtained in GUV experiments (Figure 4.5).
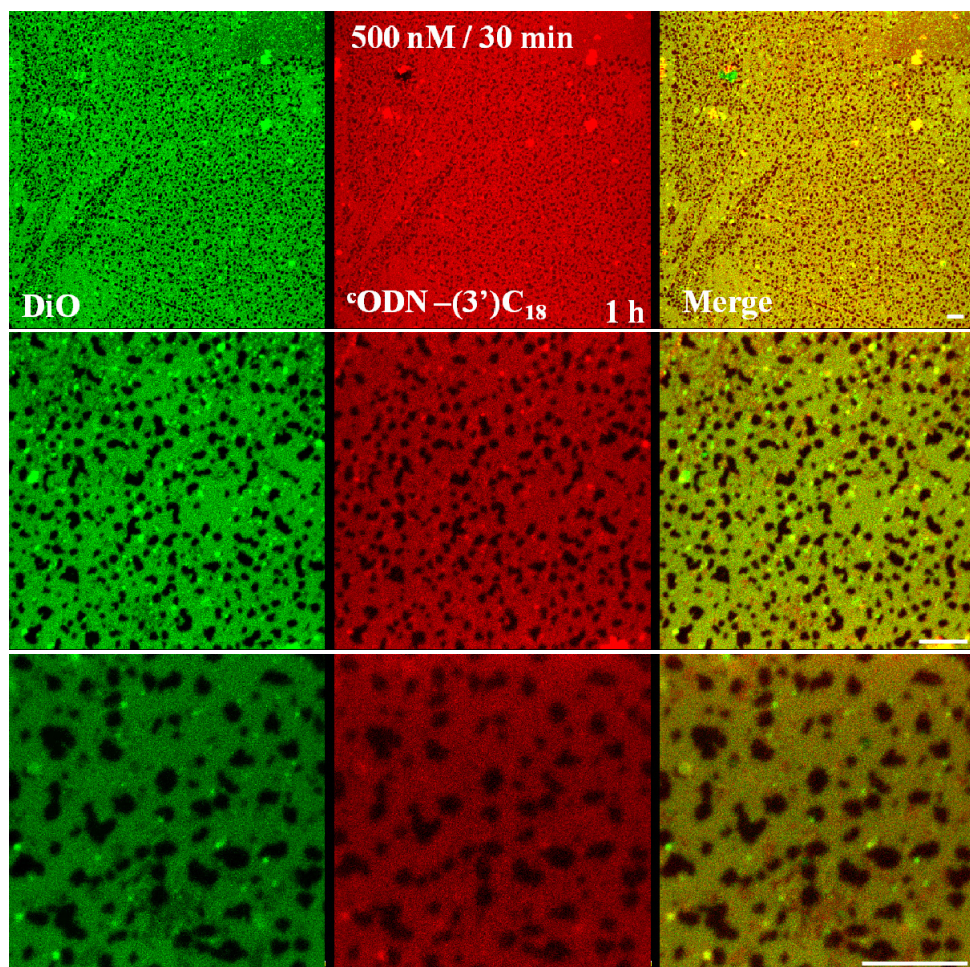
Figure 4.15 Imaging of Cy5-labelled ODN-(3')C$_{18}$ binding to SPBs. Confocal microscopy images of DiO-labelled DOPC/eSM/Chol (2:2:1) SPBs incubated with Cy5-labelled ODN-(3')C$_{18}$. First, 100 nM Cy5-labelled ODN-(3')C$_{18}$ were added to the SPBs and incubated for 30 min. Then, additional 400 nM Cy5-labelled ODN-(3')C$_{18}$ were added to the sample and incubated for another 30 min. ^{c}ODN stands for Cy5(5')-GEM91. Lipid (green) and LOC (red) staining are shown in the left and centre columns, respectively. The right column displays the merging of both detection channels. Images were taken at 22°C. Scale bars represent 10 μm.

Cy5-labelled ODN-(3)C_{18} was efficiently detected in the L_d phase of the SPB under these experimental conditions (Figuer 4.15). Likewise, these observations correlate with the results obtained by this LOC in GUV experiments (Figure 4.6).
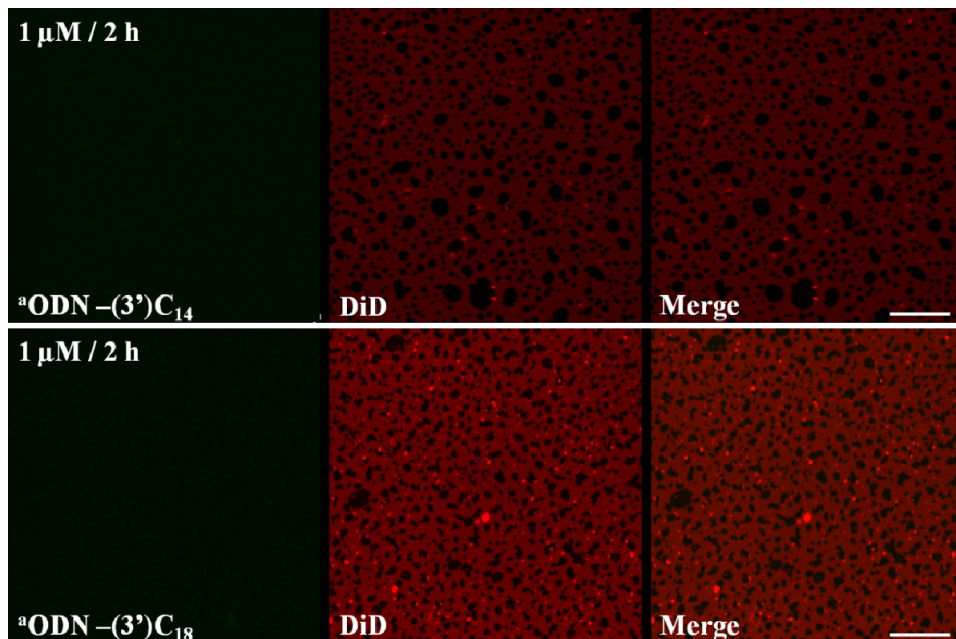
Figure 4.16 Imaging of Alexa 488-labelled ODN-(3')C_{14} and Alexa 488-labelled ODN-(3')C_{18} incubation with SPBs. Confocal microscopy images of DiD-labelled DOPC/eSM/Chol (2:2:1) SPBs incubated with 1 μM Alexa 488-labelled ODN-(3')C_{14} (upper panels) or Alexa 488-labelled ODN-(3')C_{18} (bottom panels) for 2 h. [a]ODN stands for Alexa 488(5')-GEM91. LOC (green) and lipid (red) staining are shown in the left and centre columns, respectively. The right column displays the merging of both detection channels. Images were taken at 22ºC. Scale bars represent 10 μm.

As seen in Figure 4.16, Alexa 488-labelled LOCs carrying C_{14} or C_{18} alkyl modifications at the 3'-termini of the DNA strand did not show any detectable interaction with the SPB membrane. These results are contradictory to those obtained when these LOCs were labelled with Cy5 fluorophore, where a clear incorporation into the L_d phase was observed.

As previously mentioned, since the labelling these LOCs with Alexa 488 was not successful (only 50% and 30% was labelled for ODN-(3')C_{14} and ODN-(3')C_{18}, respectively) a 4% (w/v) agarose gel was performed in order to check the state of these LOC. This assay underscored the poor stability of Alexa 488-labelled ODN-(3')C_{18}, which was prone to form aggregates, whereas Alexa 488-labelled ODN-(3')C_{14} behaved similarly to the unlabelled or Cy5-labelled compounds (see Appendix, Figure A.2).
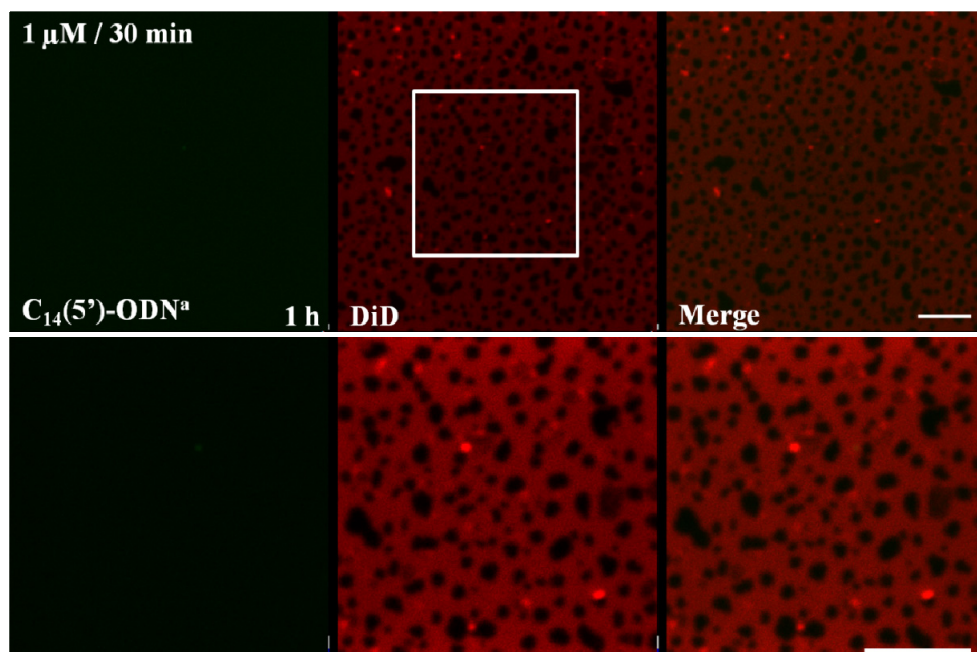
Figure 4.17 Imaging of Alexa 488-labelled $C_{14}(5')$-ODN incubation with SPBs. Confocal microscopy images of DiD-labelled DOPC/eSM/Chol (2:2:1) SPBs incubated with Alexa 488-labelled $C_{14}(5')$-ODN. First, 500 nM Alexa 488-labelled $C_{14}(5')$-ODN were added to the SPBs and incubated for 30 min. Then, additional 500 nM Alexa 488-labelled $C_{14}(5')$-ODN were added to the sample and incubated for another 30 min. ODN[a] stands for GEM91(3')-Alexa 488. The white square represents the zoom taken, corresponding to the images below. LOC (green) and lipid (red) staining are shown in the left and centre columns, respectively. The right column displays the merging of both detection channels. Images were taken at 22ºC. Scale bars represent 10 μm.

The results shown in Figure 4.17, in agreement with the results obtained in Figure 4.8B, point out that Alexa 488-labelled $C_{14}(5')$-ODN did not show any detectable binding to bilayer membranes in neither GUV nor SPB systems.
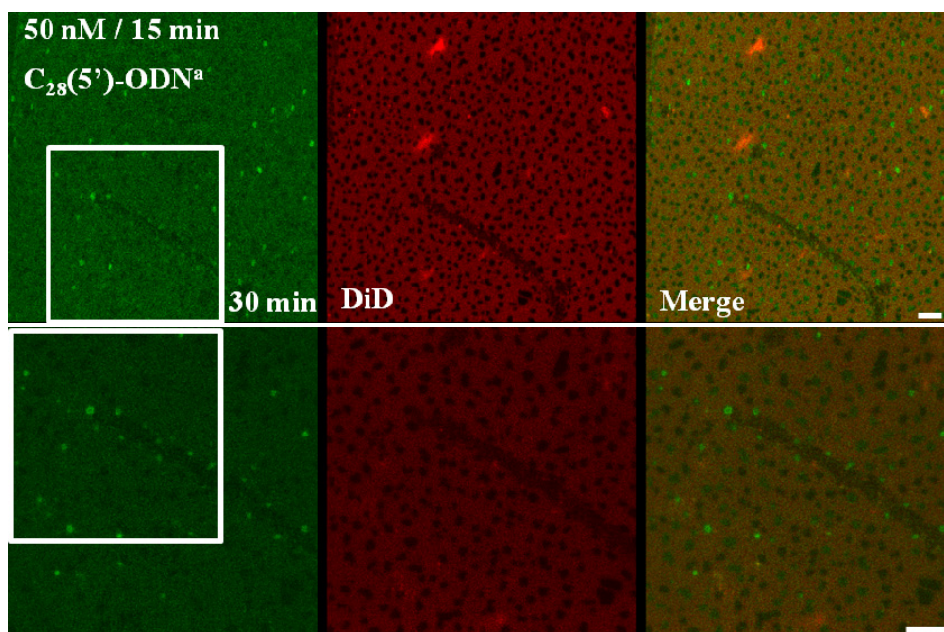
Figure 4.18 Imaging of Alexa 488-labelled $C_{28}(5')$-ODN binding to SPBs. Confocal microscopy images of DiD-labelled DOPC/eSM/Chol (2:2:1) SPBs incubated with Alexa 488-labelled $C_{28}(5')$-ODN. First, 25 nM Alexa 488-labelled $C_{28}(5')$-ODN were added to the SPBs and incubated for 15 min. Then, additional 25 nM Alexa 488-labelled $C_{28}(5')$-ODN were added to the sample and incubated for another 15 min. ODN[a] stands for GEM91(3')-Alexa 488. White squares represent the zoom taken, corresponding to the images below. LOC (green) and lipid (red) staining are shown in the left and centre columns, respectively. The right column displays the merging of both detection channels. Images were taken at 22ºC. Scale bars represent 10 μm.

Alexa 488-labelled $C_{28}(5')$-ODN showed a rapid and consistently detectable interaction with the SPB, even when only 25 nM LOC was incubated for 15 min (Figure 4.18).

Again, this LOC was incorporated into both L_d and L_o domains, in agreement with the results obtained in GUV experiments (Figures 4.9 and 4.10).
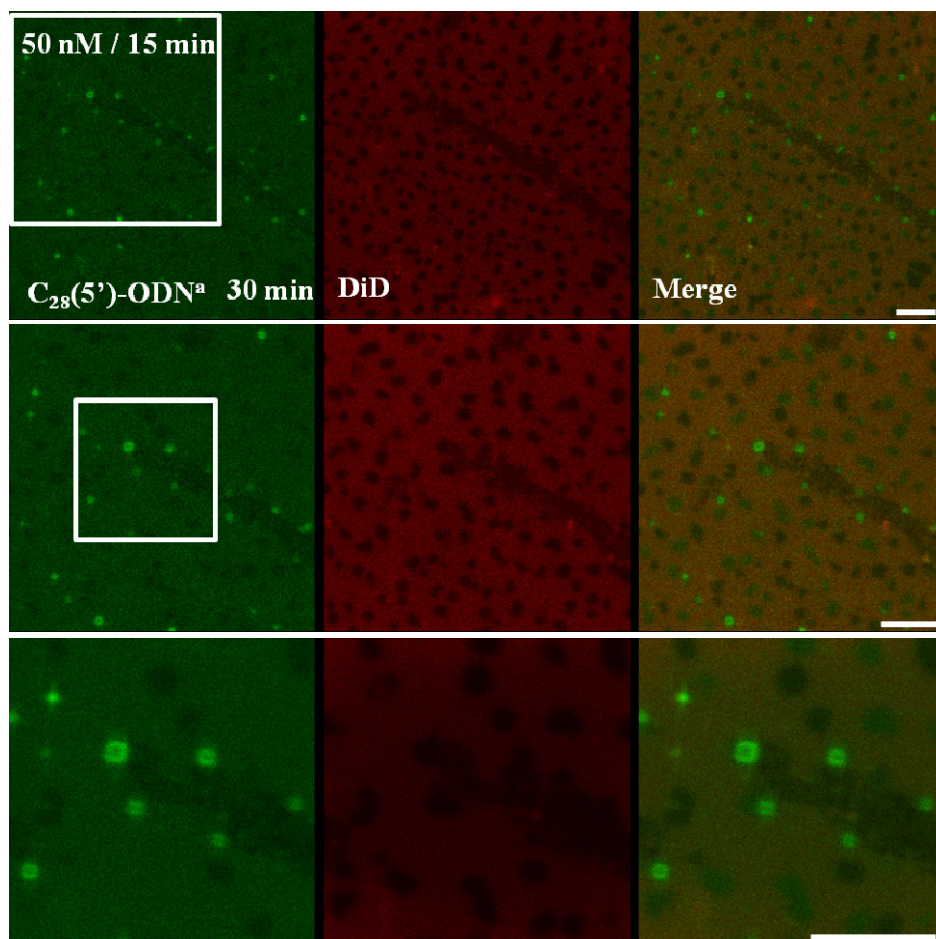
Figure 4.19 Imaging of Alexa 488-labelled C$_{28}$(5')-ODN binding to SPBs. Confocal microscopy images of DiD-labelled DOPC/eSM/Chol (2:2:1) SPBs incubated with Alexa 488-labelled C$_{28}$(5')-ODN. This figure is the continuation of the preceding figure (Figure. 4.18). Then, additional 25 nM Alexa 488-labelled C$_{28}$(5')-ODN were added to the sample and incubated for another 15 min. ODN[a] stands for GEM91(3')-Alexa 488. White squares represent the zoom taken, corresponding to the images below. LOC (green) and lipid (red) staining are shown in the left and centre columns, respectively. The right column displays the merging of both detection channels. Images were taken at 22ºC. Scale bars represent 10 μm.

168

Surprisingly, when increasing concentrations of this LOC were added to the SPB (*i.e.*, 50 nM), reproducible peculiar Alexa 488-enriched rounded structures were observed, as seen in Figure 4.19, suggesting that these structures were at least in part formed by this LOC. More detailed information of these structures is given in the next chapter (see Chapter 5).

Overall, it can be assumed that each LOC apparently showed similar behaviour in both GUV and SPB systems. Table 4.2 sums up briefly the results obtained by the incubation of LOCs with GUVs and SPBs.

LOC	Interaction preference (GUVs)	Interaction preference (SPBs)
Cy5(5')-GEM91-$C_{12}NH_2$	L_d*	n.d.i.
Cy5(5')-GEM91-C_{14}	L_d	L_d
Cy5(5')-GEM91-C_{18}	L_d	L_d
Alexa 488(5')-GEM91-C_{18}	n.d.i.	n.d.i.
Alexa 488(5')-GEM91-C_{14}	n.d.i.	n.d.i.
C_{14}(5')-GEM91-(3')Alexa 488	n.d.i.	n.d.i.
C_{28}(5')-GEM91-(3')Alexa 488	$L_d + L_o$	$L_d + L_o$

Table 4.2 Summary of the results obtained by the incubation of LOCs with GUVs and SPBs. The asterisk (*) corresponds to a very weak interaction observed by incubation of Cy5(5')-GEM91-$C_{12}NH_2$ with GUVs under these experimental conditions (see Figure 4.4); n.d.i. stands for no detectable interaction.

4.2.2 Cell system: HeLa cell line

Once it was analysed LOCs behaviour in membrane model systems, HeLa cell line was chosen for further experiments in order to examine the cellular uptake and subcellular localisation profiles of these LOCs, as HeLa cell line is commonly used to study cell biology of uptake mechanisms (Osaki *et al.*, 2004; Chithrani *et al.*, 2006; Dausend *et al.*, 2008; dos Santos *et al.*, 2011).

As described in Experimental procedures section and in Chapter 3, *Mycoplasma* free HeLa cultures were used in order to avoid *Mycoplasma* infection-induced enhanced oligonucleotide uptake. After verifying a good quality of the cell cultures, cytotoxicity studies were assayed to evaluate the possible toxic effects that these LOCs could trigger in HeLa cells.
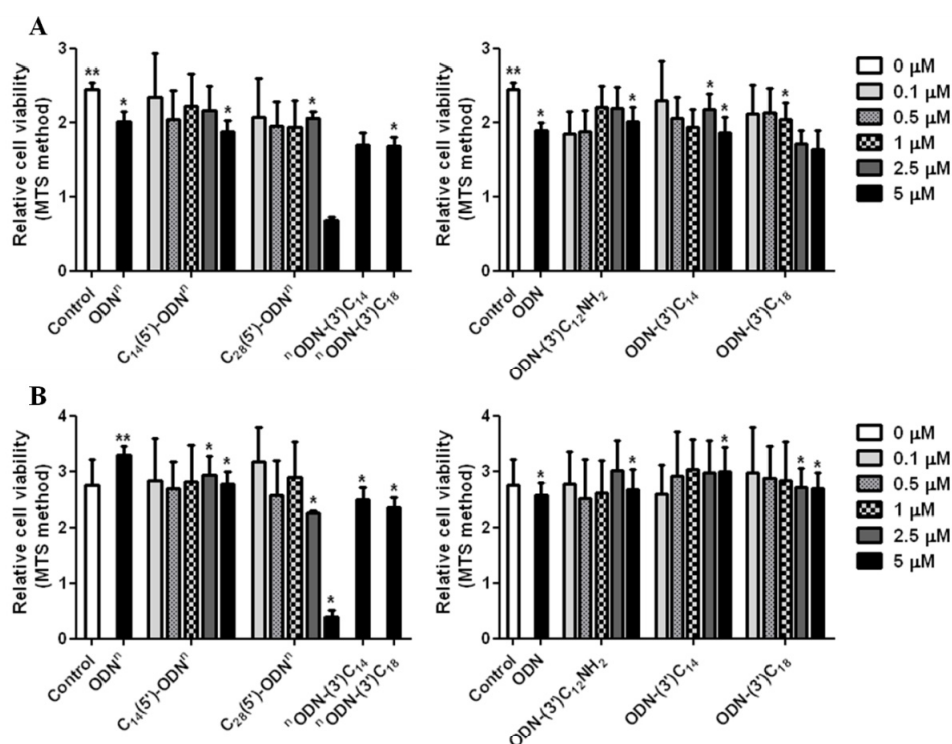
Figure 4.20 Cell cytotoxicity assay performed in HeLa cells in the presence of control-oligodeoxynucleotides and LOCs. Cells were seeded (2.5×10^3 cells/well) in 96 well plates and incubated overnight in appropriate growth medium. The next day cells were washed with DPBS and incubated in 100 μl OptiMEM in the absence or presence of the control-oligodeoxynucleotides (ODN^n or ODN) or LOC for 24 h (A) and 48 h (B) at 37ºC. Untreated cells were used as negative control (Control); ODN^n and ODN stand for GEM91-(3')NH$_2$ and GEM91, respectively. Data were normalised to the control value (untreated cells at 0 h of incubation) and are expressed as the mean ± SEM of 3 independent experiments performed in triplicate (*p<0.05; **p<0.01).

In Figure 4.20, it can be observed that all LOC, except C_{28}(5')-ODN-(3')NH$_2$, had neither cytotoxic nor antiproliferative effect in HeLa cells during both 24 h and 48 h of incubation, since 5 µM LOC treated cells presented similar growth compared to untreated cells, which were only incubated with OptiMEM. Unfortunately, when 5 µM C_{28}(5')-ODN-(3')NH$_2$ was used, cell viability was decreased by over 32% during the first 24 h of incubation and 60% during 48 h of incubation.

Then, LOC cellular uptake and subcellular localisation profiles were analysed by flow cytometry and confocal microscopy. To perform these experiments commercial Transfectin Lipid Reagent, a mixture of a proprietary cationic compound and DOPE co-lipid, was used as a complexation model. Thus, we could also compare conjugation and complexation patterns. Lipoplex formation and incubation parameters (4 h; 37ºC) were set depending on the maximum transfection yield described for Transfectin complexes, following manufacturer's instructions. All these experiments were performed using OptiMEM serum free medium owing to the fact that the transfection efficiency of several standard transfection reagents is reduced in the presence of serum (Lindner *et al.*, 2006).

When Cy5-labelled control-ODN and LOCs were incubated with HeLa cells, it was not possible to discriminate between extracellular and intracellular Cy5 fluorescence, since we did not find any suitable quencher. Therefore, only total fluorescence could be measured from Cy5-containing samples by flow cytometry.

The subsequent results showed a high interaction/incorporation of Cy5-labelled ODN-lipoplexes, ODN-(3')C_{14} and ODN-(3')C_{18} into HeLa cells compared to Cy5-labelled control-ODN (Figure 4.21). Instead, Cy5-labelled ODN-(3')$C_{12}NH_2$ showed only a slight increase in Cy5 fluorescence, similar to that obtained with Cy5-labelled control-ODN. Interestingly, these observations are consistent with the results achieved in lipid bilayer model systems (*i.e.*, GUVs, SPBs), where Cy5-labelled LOCs bearing C_{14} and C_{18} moieties at the 3'-termini of the DNA strand showed a notable binding to these model membranes.
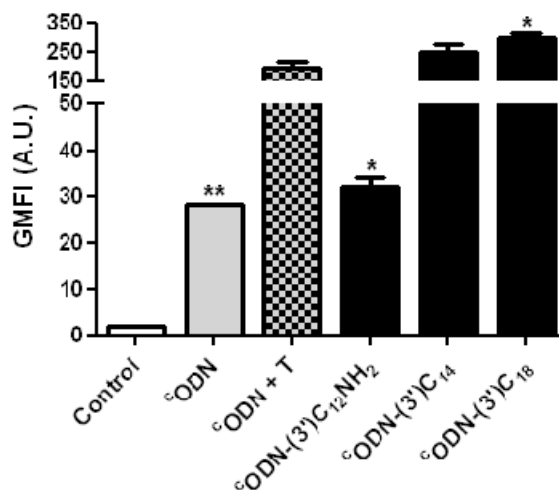
Figure 4.21 Total cellular fluorescence observed in HeLa cells after incubation with Cy5-labelled control-ODN and Cy5-labelled LOCs. Cells were seeded (1.25×10^5 cells/well) in 24 well plates and cultured overnight in appropriate growth medium. The next day cells were washed with DPBS and incubated with 500 nM bioconjugate for 4 h at 37ºC in OptiMEM. After incubation, cells were washed three times, resuspended in ice-cold PBS, and analysed by flow cytometry. Control stands for untreated cells, representing cell basal fluorescence intensity; ᶜODN stands for Cy5(5')-GEM91; T stands for treatment with cationic lipid agents; (ᶜODN + T) corresponds to lipoplexes formed with Cy5(5')-GEM91 and Transfectin reagent. GMFI corresponds to Geometric Mean of Fluorescence Intensity. Results are expressed as GMFI ± SD of 2 independent experiments performed in duplicate (*p<0.05; **p<0.01).

We next performed cellular uptake assays by incubating Alexa 488-labelled control-ODN and LOCs with HeLa cells. In this case, apart from measuring total Alexa 488 fluorescence, it was also possible to measure internalised Alexa 488 fluorescence by the use of Trypan blue as quencher.
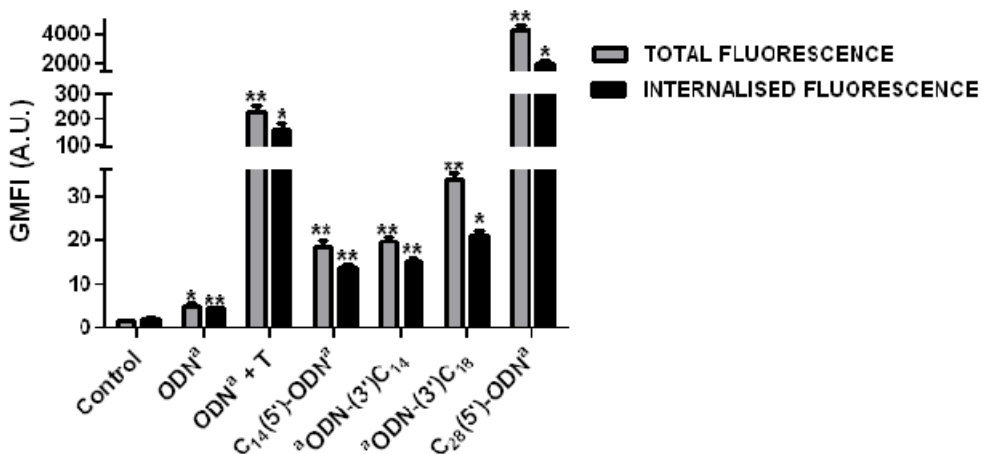
Figure 4.22 Cellular uptake of Alexa 488-labelled control-ODN and Alexa 488-labelled LOCs in HeLa cells. Cells were seeded (1.25×10^5 cells/well) in 24 well plates and cultured overnight in appropriate growth medium. The next day cells were washed with DPBS and incubated with 500 nM bioconjugate for 4 h at 37ºC in OptiMEM. After incubation, cells were washed three times, resuspended in ice-cold PBS, and analysed by flow cytometry. Control stands for untreated cells, representing cell basal fluorescence intensity; [a]ODN and ODN[a] stand for Alexa 488(5')-GEM91 and GEM91-(3')Alexa 488, respectively; T stands for treatment with cationic lipid agents; (ODN[a] + T) corresponds to lipoplexes formed by the complexation of GEM91-(3')Alexa 488 with Transfectin reagent. GMFI corresponds to Geometric Mean of Fluorescence Intensity. Results are expressed as GMFI ± SEM of 3 independent experiments performed in duplicate (*p<0.05; **p<0.01).

As observed in Figure 4.22, all Alexa 488-labelled ODN-lipoplexes and LOCs showed higher interaction and incorporation into HeLa cells, compared to Alexa 488-labelled control-ODN. More in detail, Alexa 488-labelled $C_{14}(5')$-ODN and ODN-$(3')C_{14}$ showed a similar binding and uptake profile, suggesting that this moiety apparently presents the same binding and uptake behaviour when conjugated to either 5' or 3' termini of the DNA strand. Furthermore, when a longer alkyl chain was conjugated to the ODN, as Alexa 488-labelled LOC bearing C_{18} moiety, higher total and internalised Alexa 488 fluorescence was observed in HeLa cells. Most interestingly, when two alkyl chains were conjugated to the ODN, as Alexa 488-labelled LOC bearing two C_{14} moieties (*i.e.*, C_{28} moiety), a dramatic increase in both total and internalised Alexa 488 fluorescence was observed, which was even higher than that of Alexa 488-labelled ODN-lipoplexes. The latter results point out that conjugation of C_{28} moiety seems better for ODN internalisation than complexation with cationic lipids in HeLa cells under these experimental conditions.

Finally, subcellular localisation assays were performed by confocal microscopy in order to analyse the intracellular destination of internalised LOCs. Again, Cy5- and Alexa 488-labelled ODN-lipoplexes were formed in order to compare conjugation and complexation patterns.
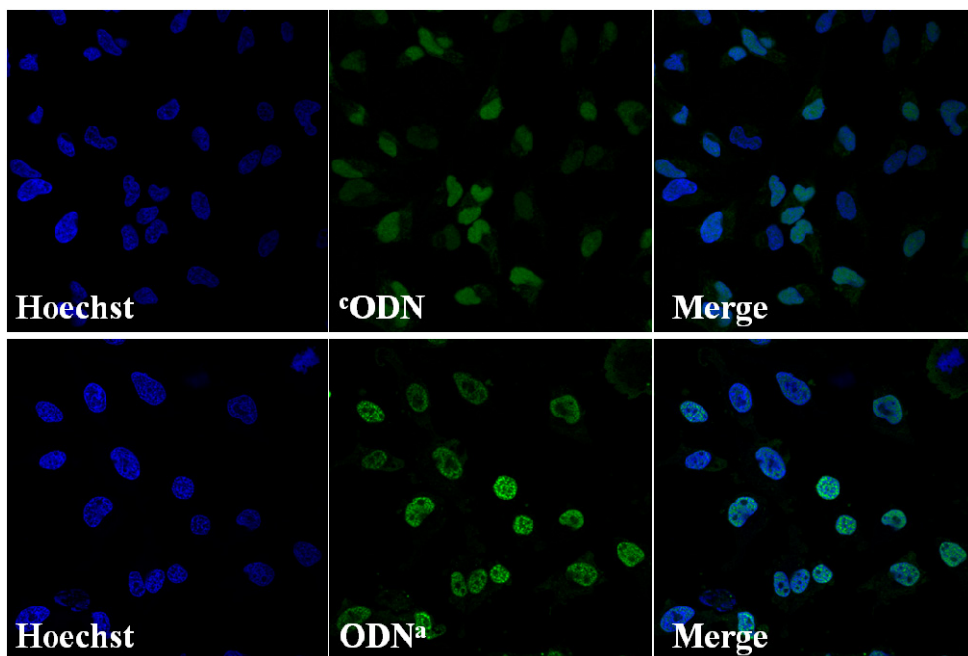
Figure 4.23 Cellular uptake and subcellular localisation of Cy5- and Alexa 488-labelled control-ODNs in HeLa cells. Cells were seeded (5×10^4 cells/well) in 8 well-Lab-Tek™ Chamber slides pretreated with Poly-L-lysine solution and cultured overnight in appropriate growth medium. The next day cells were washed with DPBS and incubated with 500 nM ODN for 4 h at 37ºC in OptiMEM. After incubation, cells were washed three times, fixed with 4% (w/v) PFA and treated with Hoechst for nucleus staining. ᶜODN and ODNᵃ stand for Cy5(5')-GEM91 and GEM91(3')-Alexa 488, respectively. Nucleus (blue) and ODN (green) staining are shown in the left and centre columns, respectively. The right column displays the merging of both detection channels.

Both Cy5- and Alexa 488-labelled control-ODNs showed a notable nuclear localisation as reported by other authors (Figure 4.23A) (Ohrt *et al.*, 2006). When complexation method was used, nuclear localisation of Cy5- and Alexa 488-labelled ODN was also detected, suggesting a good transfection profile (Figure 4.24).

In addition, intensely fluorescent spots were observed around or within HeLa cells when lipoplexes were used, which could be related to the formation/aggregation of these ODN-complexes (Figure 4.24). Indeed, these bright fluorescent spots are commonly observed in samples treated with ODN-complexes for nucleic acid based transfection (Felgner *et al.*, 1987; Zelphati and Szoka, 1996a; Lindner *et al.*, 2006; Resina *et al.*, 2009).
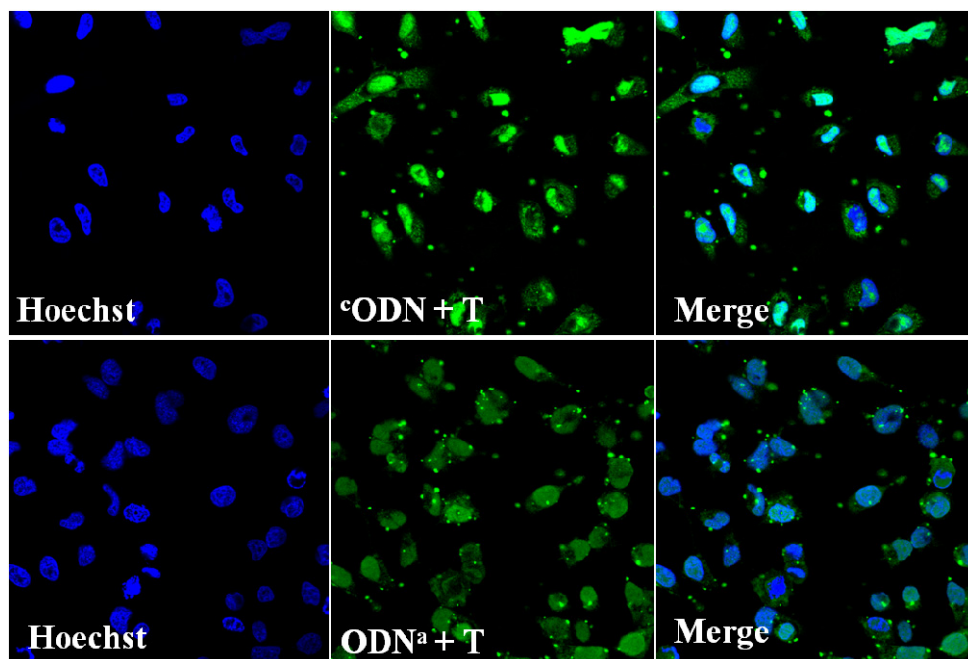
Figure 4.24 Cellular uptake and subcellular localisation of Cy5- and Alexa 488-labelled ODN-lipoplexes in HeLa cells. Cells were seeded (5×10^4 cells/well) in 8 well-Lab-Tek™ Chamber slides pretreated with Poly-L-lysine solution and cultured overnight in appropriate growth medium. The next day cells were washed with DPBS and incubated with 500 nM ODN-containing lipoplexes for 4 h at 37ºC in OptiMEM. After incubation, cells were washed three times, fixed with 4% (w/v) PFA and treated with Hoechst for nucleus staining. (ᶜODN + T) and (ODNª + T) correspond to lipoplexes formed by the complexation of Cy5(5')-GEM91 or Alexa 488(5')-GEM91 with Transfectin reagent, respectively. Nucleus (blue) and ODN (green) staining are shown in the left and centre columns, respectively. The right column displays the merging of both detection channels.
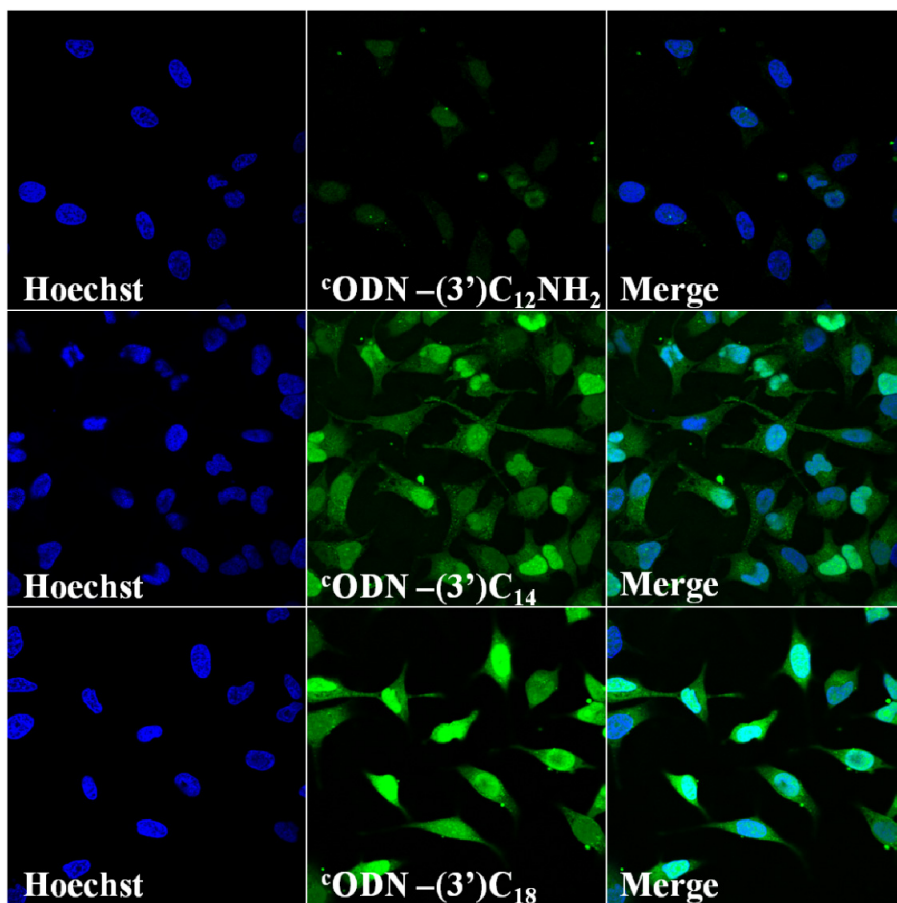
Figure 4.25 Cellular uptake and subcellular localisation of Cy5-labelled LOCs in HeLa cells. Cells were seeded (5×10^4 cells/well) in 8 well-Lab-Tek™ Chamber slides pretreated with Poly-L-lysine solution and cultured overnight in appropriate growth medium. The next day cells were washed with DPBS and incubated with 500 nM LOC for 4 h at 37ºC in OptiMEM. After incubation, cells were washed three times, fixed with 4% (w/v) PFA and treated with Hoechst for nucleus staining. ^{c}ODN stands for Cy5(5')-GEM91. Nucleus (blue) and LOC (green) staining are shown in the left and centre columns, respectively. The right column displays the merging of both detection channels.

Cy5-labelled LOCs were detected in the nucleus of HeLa cells, as control-ODN (upper panels in Figure 4.23).

In addition, LOCs bearing C_{14} and C_{18} moieties were also detected in membrane-like regions, suggesting that their cellular uptake is presumably mediated through their incorporation into plasma membrane (Figure 4.25). This observation is consistent with the results obtained in bilayer membrane model systems, where they were inserted into the L_d phase of the membrane.
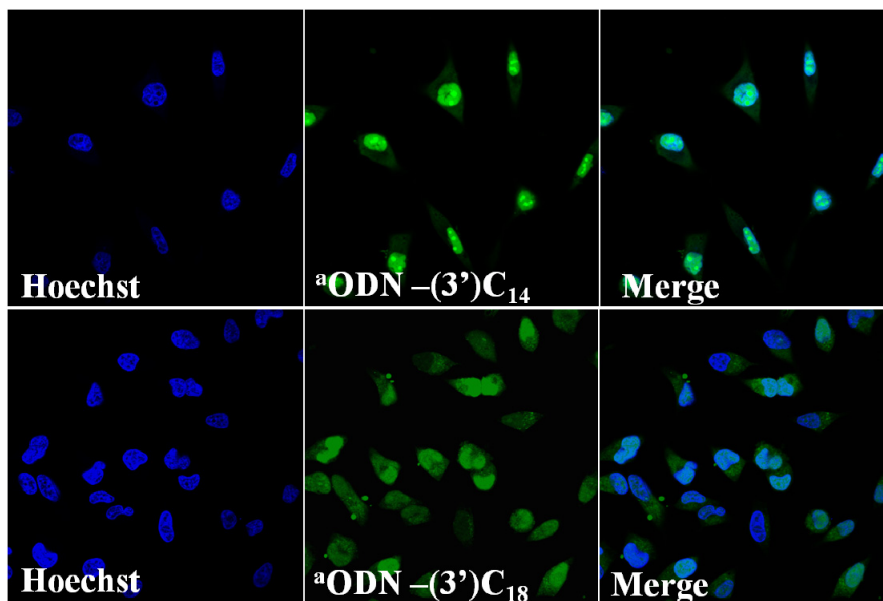
Figure 4.26 Cellular uptake and subcellular localisation of Alexa 488-labelled ODN-(3')C_{14} and Alexa 488-labelled ODN-(3')C_{18} in HeLa cells. Cells were seeded (5×10^4 cells/well) in 8 well-Lab-Tek™ Chamber slides pretreated with Poly-L-lysine solution and cultured overnight in appropriate growth medium. The next day cells were washed with DPBS and incubated with 500 nM LOC for 4 h at 37ºC in OptiMEM. After incubation, cells were washed three times, fixed with 4% (w/v) PFA and treated with Hoechst for nucleus staining. ªODN stands for Alexa 488(5')-GEM91. Nucleus (blue) and LOC (green) staining are shown in the left and centre columns, respectively. The right column displays the merging of both detection channels.

When Alexa 488-labelled LOCs bearing C_{14} or C_{18} moiety at the 3' of the DNA strand were analysed, both LOCs were clearly localised in the nucleus (Figure 4.26), as control-ODN (bottom panels in Figure 4.23).

178

Part of the LOC was also detected outside the nucleus, in the cytoplasm. But in this case this small fraction was not related to membrane-like regions, as observed in Cy5-labelled ODN-(3')C_{14} or ODN-(3')C_{18} containing samples (Figure 4.25). Again, these observations are in accordance with the results obtained in bilayer membrane model systems, where these two Alexa 488-labelled LOCs did not show any interaction with the membrane.
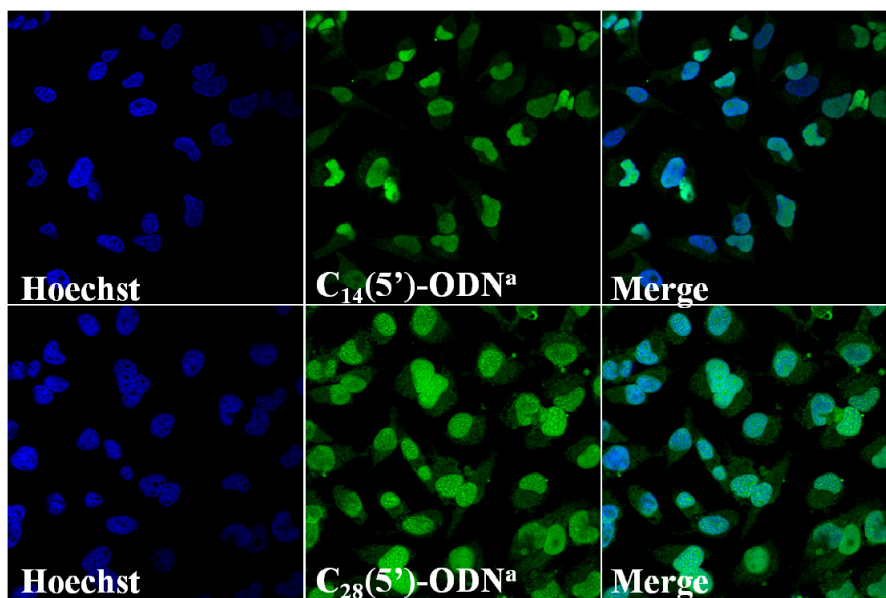
Figure 4.27 Cellular uptake and subcellular localisation of Alexa 488-labelled C_{14}(5')-ODN and Alexa 488-labelled C_{28}(5')-ODN in HeLa cells. Cells were seeded (5×10^4 cells/well) in 8 well-Lab-Tek™ Chamber slides pretreated with Poly-L-lysine solution and cultured overnight in appropriate growth medium. The next day cells were washed with DPBS and incubated with 500 nM LOC for 4 h at 37ºC in OptiMEM. After incubation, cells were washed three times, fixed with 4% (w/v) PFA and treated with Hoechst for nucleus staining. ODN[a] stands for GEM91-(3')Alexa 488. Nucleus (blue) and LOC (green) staining are shown in the left and centre columns, respectively. The right column displays the merging of both detection channels.

179

Also, Alexa 488-labelled LOC containing C_{14} at the 5'-termini of the DNA strand was mostly detected in the nucleus of HeLa cells, co-localising with the nuclear staining, whereas a very small fraction was also observed in the cytoplasm (upper panels in Figure 4.27). These results are very similar to those observed in Alexa 488-labelled ODN-(3')-C_{14} (upper panels in Figure 4.26), suggesting that C_{14} moiety presents similar uptake and subcellular localisation when conjugated to either 5'- or 3'-termini of the ODN.

The LOC that showed the best cellular uptake profile, Alexa 488-labelled C_{28}(5')-ODN, was mainly localised in the nucleus of HeLa cells (bottom panels in Figure 4.27), as Alexa 488-labelled control-ODN (bottom panels in Figure 4.23). A small part of this compound was also detected in membrane-like regions, which implies that its cellular uptake is probably achieved through its incorporation into the plasma membrane. In addition, small discrete and intense fluorescent spots within the nucleus were observed, suggesting a massive cellular uptake of this LOC which is presumably saturating the nucleus under these experimental conditions (500 nM).

Furthermore, we incubated HeLa cells with 50 nM Alexa 488-labelled C_{28}(5')-ODN for 30 min and 4 h, in order to examine the cellular localisation profile and uptake dynamics of this compound under non saturating conditions (Figure 4.28).

Remarkably, Alexa 488-labelled C_{28}(3')-ODN was localised within the nucleus of HeLa cells when very low concentration of LOC (50 nM) and short periods of incubation time (30 min) were used (upper panels of Figure 4.28). By contrast, when longer periods of time were used (4 h), a redistribution of this LOC was observed, an ODN efflux from the nucleus to the cytoplasmic membrane-bound compartments and membrane-like regions (Forsha *et al.*, 2010).
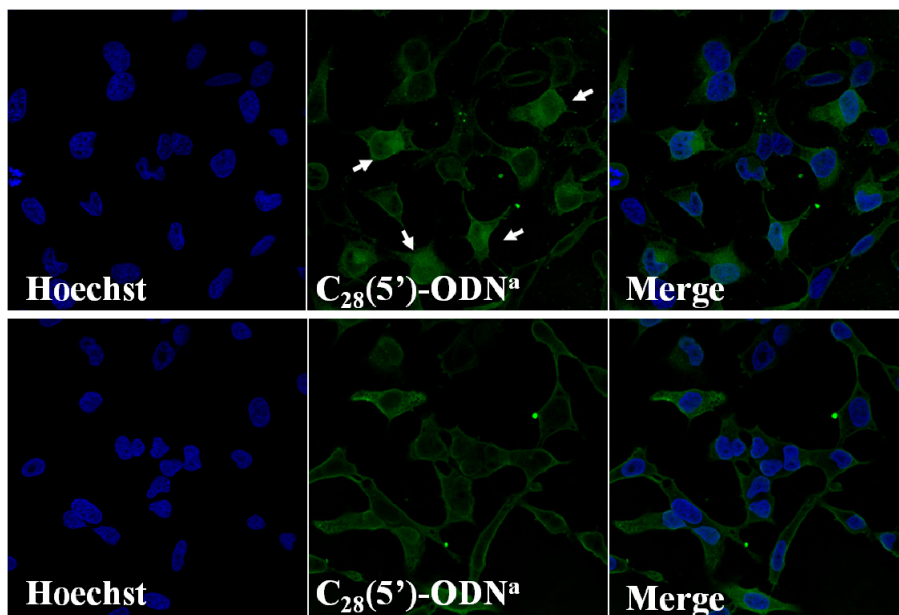
Figure 4.28 Cellular uptake and subcellular localisation of 50 nM Alexa 488-labelled C$_{28}$(5')-ODN in HeLa cells. Cells were seeded (5×10^4 cells/well) in 8 well-Lab-Tek™ Chamber slides pretreated with Poly-L-lysine solution and cultured overnight in appropriate growth medium. The next day cells were washed with DPBS and incubated with 50 nM Alexa 488-labelled C$_{28}$(5')-ODN for 30 min (upper panels) and 4 h (bottom panels) at 37ºC in OptiMEM. After incubation, cells were washed three times, fixed with 4% (w/v) PFA and treated with Hoechst for nucleus staining. ODN[a] stands for GEM91-(3')Alexa 488. White arrows indicate nuclear localisation of this LOC. Nucleus (blue) and LOC (green) staining are shown in the left and centre columns, respectively. The right column displays the merging of both detection channels. White arrows indicate noticeable nuclear localisation of Alexa 488-labelled C$_{28}$(5')-ODN.

These observations point to a rapid and successful cellular uptake of Alexa 488-labelled C$_{28}$(5')-ODN, even at low concentrations of this compound, indicating that C$_{28}$ moiety may function as an effective cellular enhancer without interfering in ODN destinations, which are the nucleus and the cytoplasm (Lemaitre *et al.*, 1987; Alahari *et al.*, 1998).

181

4.3 Discussion

Efficient incorporation into cells is a prerequisite for oligonucleotides to exert their blocking function. Unfortunately, the plasma membrane is the first biological barrier encountered by oligonucleotides on their way into the cell cytoplasm. Conjugation of lipophilic molecules to these oligonucleotides can endow them with new interesting properties, leading to enhanced cellular uptake through their interaction with the lipid bilayer of the cell membrane, lipoprotein particles, lipoprotein receptors and transmembrane proteins (Wolfrum *et al.*, 2007).

Our work was based on the investigation of potential lipid anchor candidates for improving cellular uptake of oligonucleotides, thereby examining LOCs differing in length, saturation level and number of alkyl chains (Grijalvo *et al.*, 2010, 2011). Particularly, using the Langmuir monolayer technique to mimic half a lipid bilayer may be advantageous because properties such as composition, lateral pressure, surface elasticity and surface density are easily controlled (Caseli *et al.*, 2010; Montanha *et al.*, 2010). Thus, this emphasises the interest of physicochemical surface studies in elucidating the nature of the ODN conjugate/lipid interactions at the molecular level. Since electrically neutral phospholipids are generally assumed to be the major components of the external leaflet of the plasma membrane, we examined the incorporation of LOCs using preformed DOPC monolayers, thereby avoiding any electrostatic interaction between the LOCs and the zwitterionic lipid (van Meer, 2005), instead of selecting cationic lipid based monolayers, which are mainly used to study ODN/lipid complexation processes (Texeira *et al.*, 2001). In particular, we observed that LOCs surface activity in both lipid-free and/or DOPC monolayers increased in the following order: ODN-(3')$C_{12}NH_2$ < C_{14}(5')-ODN / ODN-(3')C_{14} < ODN-(3')C_{18} < C_{28}(5')-ODN. Most importantly, only C_{28}(5')-ODN could be inserted into DOPC monolayers at initial lateral pressures above those assumed for cell membranes (around 30 mN/m), implying that this compound may be easily incorporated into the external leaflet of the cell membrane (Marsh, 1996; Busto *et al.*, 2007).

Second, we investigated the spontaneous incorporation of LOCs into membranes bearing a curvature stress and surface change comparable to those of the plasma membrane surrounding eukaryotic cells by the use of GUVs and SPBs (van Meer, 2005; Mcintosh and Simon, 2007; Apellaniz *et al.*, 2010). These lipid bilayer systems were composed of DiO or DiD-labelled DOPC/eSM/Chol (2:2:1) in order to analyse the effect of L_d and L_o lipid phase co-existence on LOC partitioning. Here, each LOC apparently showed similar behaviour in both GUV and SPB systems.

Previous reports underscored that binding of oligonucleotides with only one lipid anchor to lipid membranes could be apparently too weak (Pfeiffer and Höök, 2004; Bunge *et al.*, 2009). In this regard, Cy5-labelled ODN-(3')$C_{12}NH_2$ showed very weak fluorescence in the L_d phase of the GUVs that was subsequently disappeared when the sample was again radiated. Moreover, this compound tended to form big LOC aggregates which were clearly visualised by confocal microscopy. A possible explanation for the loss of fluorescence could be a consequence of a very few amount of LOC inserted into the GUV at short incubation times, resulting in a rapid Cy5 bleaching when the laser radiated again the sample. On the other hand, the second phenomenon could be related to the presence of the reactive primary amine at the end of the alkyl tail, which could appear protonated under these experimental conditions [physiological pH (pH 7.4)] and bind to the negatively charged backbone of the oligonucleotide via electrostatic interactions, leading to big LOC aggregates (van Duijvenbode *et al.*, 1998; Maiti *et al.*, 2005). Moreover, in the complexation approach the formation of ODN-complexes/aggregates is based on the electrostatic interactions between reactive amines of the cationic agents and the negatively charged phosphate backbone of the oligonucleotides (Meidan *et al.*, 2000; Weisman *et al.*, 2004; Gordon *et al.*, 2005).

Of note, under long incubation times (*i.e.*, 20 h), a very stable interaction between this LOC and the L_d phase of GUVs was detected. The latter result could be considered to a great extent an artefact since under those experimental conditions precipitation could enhance the association of the LOC with the GUV (Xu and Anchordoquy, 2011).

ODN-(3')C_{14} and ODN-(3')C_{18} compounds behave differently when conjugated to Cy5 or Alexa 488 fluorophores. More in detail, Cy5-labelled C_{14} and C_{18} containing LOCs were notably visualised in the L_d phase co-localising with DiO dye, but when conjugated to Alexa 488 they did not show any remarkable interaction or insertion into the lipid bilayer, neither did Alexa 488-labelled $C_{14}(5')$-ODN. This discrepancy may simply be due to the presence of the linker in combination with the size and hydrophobicity differences between the conjugated fluorophores, which could be incorporated with different efficiencies and/or interfere in the stability and/or properties of LOCs. Indeed, Cy5 is more hydrophobic than Alexa 488 fluorophore (Glen Research, Invitrogen). Similarly, other authors also reported that assessment of uptake by fluorescein-labelled ODN-conjugates could be altered due to the lipophilic nature of this fluorophore (Manoharan, 2002).

Essentially, it could be reasonably expected that Alexa 488-labelled $C_{28}(5')$-ODN would also spontaneously incorporate into L_o domains since it is long known that dual lipid modification appears to facilitate association with lipid rafts (Zacharias *et al.*, 2002). However, this LOC showed a remarkable and rapid incorporation into lipid bilayer systems, being equally distributed between L_d and L_o domains after equilibration. Similar observations have been reported by other authors who used a single cholesterol moiety or two cholesteryl-TEG moieties containing double stranded DNA structures, which did not exclusively partition into the L_o phase (Beales and Vanderlick, 2009; Bunge *et al.*, 2009).

This could be due to the fact that probes designed as cholesterol mimics usually do not satisfactorily reproduce the properties of pure cholesterol (Beales and Vanderlick, 2009; Bunge *et al.*, 2009). On the other hand, the presence of two ether bonds in the structure of this LOC could be related to its homogeneous distribution in lipid membrane model systems, since it is long assumed that ether linked glycerophospholipids appear more loosely packed in membranes, thereby increasing their fluidity (Boggs, 1980; Taguchi and Armarego, 1998).

By contrast, the fact that Alexa 488-labelled $C_{28}(5')$-ODN compound, possessing two neighbouring alkyl chains, could be associated with model membranes is opposite to what it was observed by other authors who reported that a lipid-anchored oligonucleotide with two neighbouring alkyl chains may tend to form stable supramolecular structures in an aqueous environment, making it difficult to insert into preformed membranes (Gosse *et al.*, 2004). In this case the oligonucleotide was conjugated to a chalcone moiety bearing longer alkyl chains ($2 \times C_{16}$) than those of $C_{28}(5')$-ODN compound ($2 \times C_{14}$), leading to an structural difference between the lipid anchor used by these authors and that used in this work. Our interpretation for this different behaviour presumably relies on the higher pronounced hydrophobicity of the chalcone moiety with regard to the lipid anchor used in our work.

Importantly, the homogeneous distribution of Alexa 488-labelled $C_{28}(5')$-ODN in liquid domain co-existing bilayers may provide several advantages in cell systems in terms of alternative internalisation routes. Thus, once this LOC is inserted into the lipid bilayer, it could interact with a number of transmembrane proteins involved in distinct uptake pathways, thereby inducing its internalisation through different routes.

The biological relevance was also studied by examining the uptake and subcellular localisation of LOCs in HeLa cell system. Cytotoxicity assay revealed that these LOCs were neither cytotoxic nor antiproliferative at 5 µM, except the LOC bearing C_{28} moiety at the 5'-termini of the ODN, which decreased cell viability by over 32% and 60% during 24 and 48 h of incubation, respectively. This undesired result achieved by this LOC is probably related to its high and rapid incorporation into membranes as well as to the presence of two ether bonds in this LOC, being more difficult to be degraded compared to ester lipids, thereby being more toxic (Leventis and Silvius, 1990; Lindner *et al.*, 2006).

The observations of binding/uptake experiments carried out with Cy5-labelled LOCs were consistent with those observed in lipid membrane model systems, showing LOCs bearing C_{14} and C_{18} moieties at the 3'-end of the ODN a remarkable binding/incorporation into both lipid membrane model and HeLa cell systems. Instead, Cy5-labelled ODN-(3')$C_{12}NH_2$ showed only a slight increase in Cy5 fluorescence, similar to that obtained with Cy5-labelled control-ODN. Similar results were observed by Love and co-workers, who reported that an optimised combination of amine group and tail length is necessary to impart delivery activity since not all tested siRNA conjugates carrying a C_{12}-amine part moiety but differing in the amine presentation were successful for siRNA silencing, though these siRNA conjugates were formulated in combination with cholesterol, distearoyl phosphatidylcholine and mPEG-DMG (Love *et al.*, 2010).

In addition to Cy5-labelled compounds, when HeLa cells were incubated with Alexa 488-labelled LOCs, they showed higher cellular uptake compared to Alexa 488-labelled control-ODN. In this regard, the following internalisation behaviour was observed (from the lowest to the highest uptake profile): $C_{14}(5')$-ODN / ODN-(3')C_{14} < ODN-(3')C_{18} < $C_{28}(5')$-ODN. These results point to a better incorporation behaviour when longer and dual alkyl chains are conjugated with the ODN (*i.e.*, higher hydrophobicity).

However, the latter observation is not fully in agreement with the results obtained in GUVs and SPBs by the Alexa 488-labelled LOCs bearing C_{14} or C_{18} moiety at the 3'or 5'-termini since these LOCs did not show any noticeable incorporation into those membrane model systems. Presumably, the experimental conditions chosen in uptake assays could not be ideal since under these conditions (4 h of incubation) precipitation may enhance the association of the LOCs with the cell surface, which could artifactually elevate transfection rates of the LOCs that apparently do not insert into model membranes (Xu and Anchordoquy, 2011). Similarly, these results are in agreement with the values obtained by Kubo and co-workers, who reported that palmitic acid (C_{16})-conjugated 21 nucleotide siRNA showed very weak fluorescence and insufficient RNAi effect in the absence of a transfecting agent termed Lipofectamine 2000 (Kubo *et al.*, 2011).

A further aspect that deserves some comment is that Alexa 488-labelled C_{28}(5')-ODN showed higher internalisation efficiency than that of Alexa 488-labelled ODN-lipoplexes. The latter result underscores the observations reported by Grijalvo and co-workers, where the siRNA carrying the C_{28} moiety at the 5'-end of the passenger strand showed the best inhibitory effects in the absence of a transfecting agent termed oligofectamine. Unfortunately, this compound was the less active siRNA conjugate when combined with the transfecting agent (Grijalvo *et al.*, 2011). Also, Lindner and co-workers convincingly demonstrated that myristoyl chains seem to play an important role in cationic liposome mediated ODN delivery, as in a functional assay with ODN, dimyristoyl analogs were the best cationic lipids for ODN transfection even in the absence of the helper lipid DOPE (Lindner *et al.*, 2006).

Finally, subcellular localisation assays revealed that all LOCs, as well as control-ODNs either in the absence or presence of a transfecting agent termed Transfectin, were visualised in the nucleus of HeLa cells, indicating that these lipid moieties attached to ODN do not interfere in the ODN destination.

In the case of the LOC containing C_{28} moiety, this compound show very high fluorescence localised in the nucleus of HeLa cells, with small intense fluorescent spots within it, suggesting that the concentration used (500 nM) in this assay could be saturating due to its high and rapid incorporation into cells. Strikingly, when a lower concentration of this LOC was tested (50 nM), this compound was still capable of reaching the nucleus even at 30 min of incubation. The latter observation underscores the fact that the C_{28} lipid modification seems to be a promising anchor for small nucleic acid based delivery since it does not interfere in the ODN destination or disrupt RNAi machinery when conjugated to siRNA (Grijalvo *et al.*, 2011).

Taken together, these data indicate that lipid modifications containing longer or double-tailed anchors showed better incorporation into both membrane lipid model and cell systems, being the dual saturated lipid neighbouring modification (C_{28}) at the 5'-termini of the ODN the best lipid anchor tested. This promising lipid modification was further examined for a deeper characterisation.

Chapter 5:

Characterisation of
lipophilic C_{28}(5')-ODN conjugate

Chapter 5: Characterisation of lipophilic C$_{28}$(5')-ODN conjugate

5.1 Introduction

A deep analysis of small nucleic acid based delivery systems is still a complex challenge. For instance, although extensive research has been focused on the characterisation of these delivery systems, only a few studies have investigated biophysical and biochemical properties of them and their interactions with cellular components (Zelphati and Szoka, 1996b; Jääskeläinen *et al*., 1998; Meidan *et al.*, 2000; Teixeira *et al.*, 2001; Weisman *et al*., 2004; Gordon *et al.*, 2005; Beales and Vanderlick, 2007, 2009; Bunge *et al.*, 2007, 2009). As accurate manipulation of plasma membranes in intact cells is difficult to achieve, monolayers at an air/water interface, giant unilamellar vesicles (GUVs) and supported planar bilayers (SPBs) seem to be good models to mimic cellular membranes (Gordon *et al.*, 2005).

On the other hand, an ability to characterise the mechanism of uptake and intracellular traffic of macromolecular entities designed for this kind of delivery through endocytic pathways is fundamental to the realisation of their true potential as candidate therapies (Jones *et al.*, 2003; Watson *et al.*, 2005; Fretz *et al.*, 2006).

In particular, if endocytosis is to be used as a gateway for this kind of delivery, a number of features concerning the delivery system must be resolved including the interaction of the compound with the plasma membrane, the mechanism by which it is internalised into the cells and its final destination within the cell (Watson *et al.*, 2005).

In general there are five major pathways of energy dependent cellular uptake. These pathways include phagocytosis (mainly performed by specialised cells), clathrin-mediated endocytosis (leading to the degradation of the material in the lysosome), caveolae-mediated endocytosis, macropinocytosis and clathrin- and

caveolae-independent endocytosis (Conner and Schmid, 2003; Khalil *et al.*, 2006; Gould and Lippincott-Schwartz, 2009).

These endocytic routes vary in the composition of the membrane coat, the size of the transporting vesicles, and the fate of the internalised materials. Thus, a good selection of the uptake pathways becomes a key requirement for a successful internalisation, intracellular trafficking and silencing efficiency of small nucleic acids.

Among all the LOCs tested in Chapter 4, the LOC bearing a C$_{28}$ anchor at the 5'-end of the DNA strand showed the best interaction with the membrane lipid model systems as well as the best cellular uptake profiles. Therefore, C$_{28}$(5')-ODN molecule showed promising results to warrant further investigations on assessing its physicochemical properties in membrane lipid model systems, cellular uptake in different cell lines and the mechanisms behind it.

5.2 Results

5.2.1 Membrane lipid model systems

5.2.1.1 Lipid monolayers

As previously mentioned in Chapter 4, we investigated the interfacial behaviour of this LOC at the free air-water interface in a Langmuir balance. C$_{28}$(5')-GEM91-(3')NH$_2$ suspended in 1X PBS was injected into the subphase, and the change in surface pressure (π) was recorded during 2,000 s and 4,000 s. C$_{28}$(5')-GEM91-(3')NH$_2$ showed an important surface activity, causing a dose-dependent increase in surface pressure at the air-buffer interface. Surprisingly, two different behaviours were observed: i) a linear concentration-dependent rapid surface pressure increase in the 0-0.5 µM range and, ii) a much slower π increase at higher LOC concentrations (0.5-15 µM) probably due to the formation of LOC-monolayers in non-equilibrium conditions, with a constant slow LOC migration

into the interface causing the observed concentration-related minor surface pressure increases (Figure 5.1).
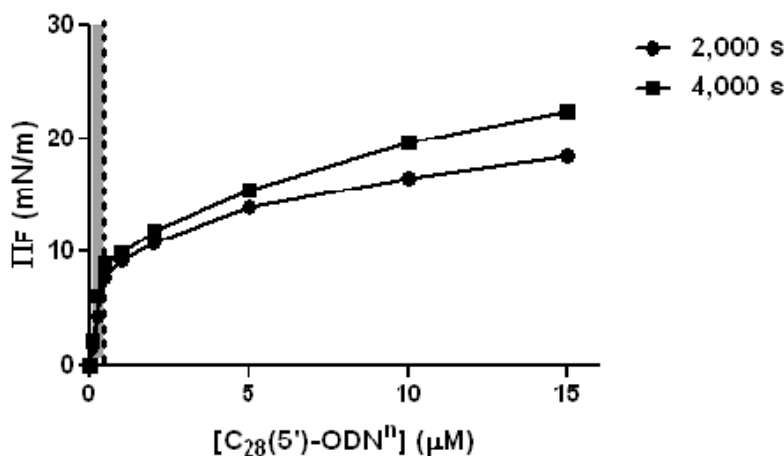
Figure 5.1 Comparison of changes in surface pressure at the air-buffer interface induced by $C_{28}(5')$-GEM91-(3')NH$_2$ at different incubation time periods. The π values obtained at 2,000 s (black circles) and 4,000 s (black squares) of incubation are shown. ODN^n stands for GEM91-(3')NH$_2$. A dotted line was used to separate the two different behaviours mentioned above (0-0.5 µM in grey; 0.5-15 µM in white). Average values ± SD (n=2). Subphase composition was 1X PBS. The LOC was injected into the subphase with constant stirring.

Then, we examined its insertion into phospholipid monolayers using again the Langmuir balance. Monolayers composed of pure DOPC or DOPC/eSM/Chol (2:2:1) ternary mixtures at the air-buffer interface were prepared, and subsequently $C_{28}(5')$-GEM91-(3')NH$_2$ injected into the subphase. The effect of 0.5 µM $C_{28}(5')$-GEM91-(3')NH$_2$ was studied, concentration rendering maximum surface-activity in the low LOC-concentration linear trend above detailed, to test LOC insertion into DOPC and DOPC/eSM/Chol (2:2:1) monolayers at varying initial π values (Figure 5.2).

193
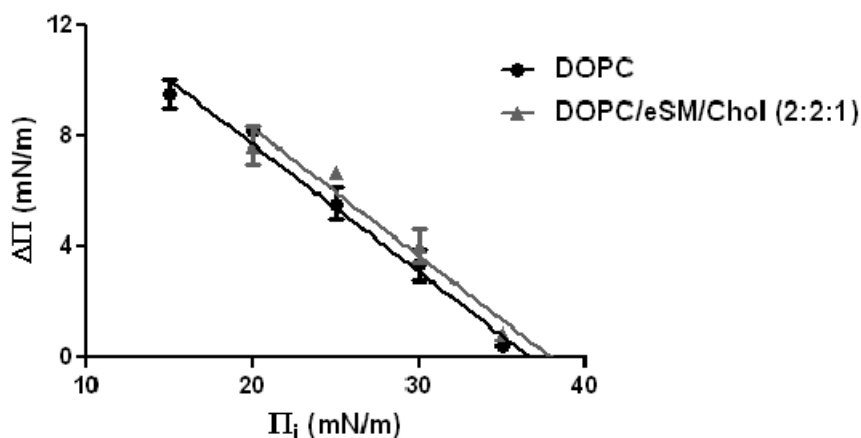
Figure 5.2 Changes in surface pressure of pure DOPC and DOPC/eSM/Chol monolayers oriented at the air-buffer interface as a result of C$_{28}$(5')-GEM91-(3')NH$_2$ insertion, at varying initial pressures. Pure DOPC (black circles) and DOPC/eSM/Chol (2:2:1) (grey triangles) monolayers were formed at the air-buffer interface at increasing initial pressures. The plateau values of surface pressure increase ($\Delta\pi$) after LOC insertion are plotted as a function of initial π value (π_i), and line fitted. Average values $\pm$ SD (n=2). Subphase composition was 1X PBS. LOCs were injected into the subphase with constant stirring.

LOC insertion-derived increases in surface pressures of DOPC and DOPC/eSM/Chol (2:2:1) monolayers strongly depended on the initial π value (π_i). The data were fitted to a straight line, whose extrapolation to $\Delta\pi$=0 gives an idea of the maximum monolayer surface pressure allowing LOC insertion. As seen in Figure 5.2, C$_{28}$(5')-GEM91-(3')NH$_2$ could become inserted into both monolayers at initial π above 35 mN/m. Although a similar behaviour was observed in both lipid monolayers, presumably implying a positive LOC insertion into pure DOPC and both DOPC-rich and SM/Chol-rich phases in the ternary mixture, results cannot be directly compared as molecular packing in the two monolayers at equal surface pressures has not been determined.

194

A different packing would be expected for the two systems, thus possibly affecting LOC insertion and making hardly-comparable both insertion patterns. However, these results point to a positive LOC-insertion into both lipid monolayers, and are in agreement with what was observed in GUVs and SPBs composed of the same ternary mixture [DOPC/eSM/Chol (2:2:1)], where the insertion of this LOC was not restricted to L_d phase, but showed a homogeneous incorporation into both L_d and L_o domains. Thus, it is expected to observe an easy and efficient incorporation of this LOC into different domains of cell membranes since biological membranes are considered to support a lateral pressure $\pi \approx 30$ mN/m, albeit the large fluctuations around this average value (Marsh, 1996; Busto *et al.*, 2007).

5.2.1.2 Lipid bilayers

In this chapter, deeper analysis of the interaction between C_{28}(5')-GEM91 and lipid model systems (*i.e.*, GUVs and SPBs) differing in lipid composition was performed by fluorescence confocal microscopy. With this aim, GUVs and SPBs based on a ternary DOPC/eSM/Chol mixture were used. As previously mentioned in Chapter 4, these are commonly used as minimal model systems for heterogeneities in natural biomembranes often referred to as raft-containing bilayers, presenting a DOPC-enriched fluid L_d phase and an eSM/Chol-enriched L_o phase, roughly mimicking the chemical composition and the properties of the lipid rafts supposed to be found in the exoplasmic leaflet of plasma membrane (Baumgart *et al.*, 2003; Garcia-Saez *et al.*, 2007). Thus, we studied the incorporation behaviour of this LOC in GUVs and SPBs presenting these phases. Independently, GUVs and SPBs in pure L_d (DOPC) and L_o [eSM/Chol (2:1)] phase states were also analysed in order to study LOC insertion into both pure phases and to analyse the possible dependence of the L_o-L_d interface on the insertion.

Specifically, these lipid bilayer systems were composed of DiD-labelled pure DOPC, DOPC/eSM/Chol (2:2:1) and eSM/Chol (2:1). In DOPC/eSM/Chol (2:2:1) system, DiD lipophilic dye specifically partitioned into L$_d$ phase and L$_o$ domains were seen as probe-depleted dark areas within the bilayers. To perform these experiments Alexa 488-labelled C$_{28}$(5')-GEM91 was used.

GUVs
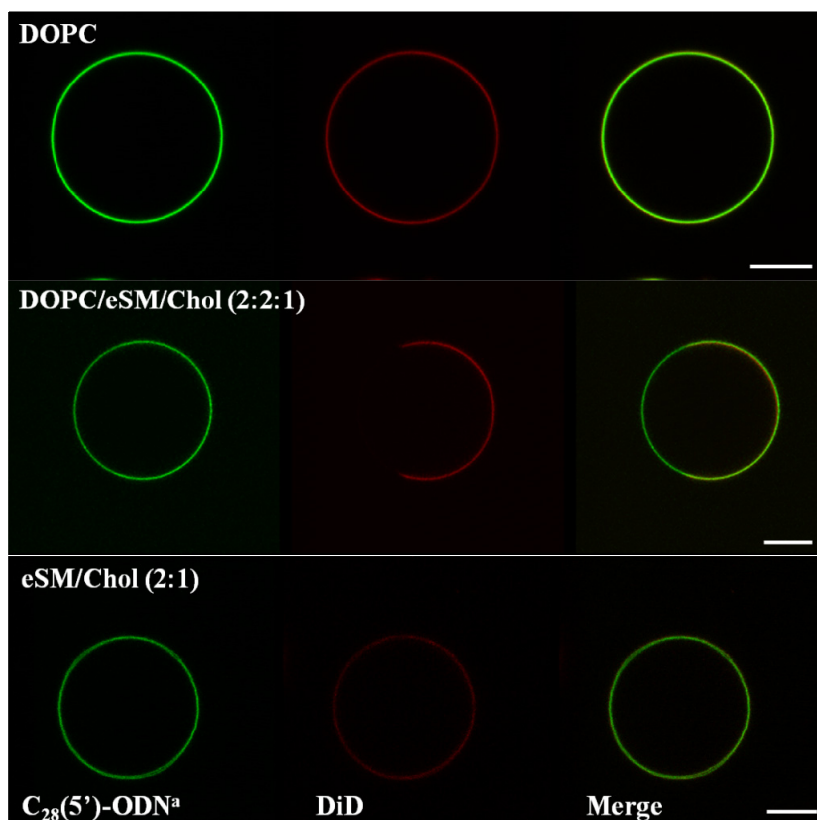
Figure 5.3 Imaging of Alexa 488-labelled C$_{28}$(5')-ODN binding to GUVs. Confocal microscopy images (equatorial sections) of DiD-labelled pure DOPC (upper panels), DOPC/eSM/Chol (2:2:1) (middle panels) and eSM/Chol (2:1) (bottom panels) GUVs incubated with 50 nM of Alexa 488-labelled C$_{28}$(5')-ODN for 2 h. ODN[a] stands for GEM91-(3')Alexa 488. LOC (green) and lipid (red) staining are shown in the left and centre columns, respectively. The right column displays the merging of both detection channels. Images were taken at 22ºC. Scale bars represent 10 μm.

196

When GUVs were incubated with Alexa 488-labelled C$_{28}$(5')-ODN, a rapid and remarkable interaction was observed, independently of the lipid composition. This LOC showed special binding properties since it was able to insert either into the L$_d$ or L$_o$ phase (middle panels), and even into GUVs in pure liquid-disordered (upper panels) and liquid-ordered (bottom panels) phase states (Figure 5.3).

According to the results obtained in Chapter 4, when DiD-labelled DOPC/eSM/Chol (2:2:1) GUVs were incubated with this LOC the interaction of this compound was at first more detectable in the L$_d$ phase, but it appeared homogeneously distributed in both L$_d$ and L$_o$ phases after a certain incubation time, possibly due to a slower incorporation into the L$_o$ phase. Thus, these observations point to a nonspecific phase partitioning of this LOC.

SPBs

First we examined the incorporation behaviour and kinetics of this LOC in SPBs composed of DiD-labelled pure DOPC.

Alexa 488-labelled C$_{28}$(5')-ODN was efficiently detected at very short incubation periods in DOPC SPBs which represent a pure L$_d$ state, even when only 15 nM LOC was incubated for 15 min (Figure 5.4, upper panels). These observations correlate with the results obtained by this LOC in GUV experiments (Figure 5.3, upper panels). As seen in Figure 5.4, with increasing concentrations of this compound, a number of Alexa 488-enriched bright spots were observed which were redistributed to the boundary between the SPB containing and not-containing (mica defects shown as dark areas) areas. In the present experiment, a lower lipid vesicle amount was initially incubated with the mica support in order for bilayer-depleted areas to appear, which helped for a better sample focusing and confocal imaging. Then, these Alexa 488-enriched spots were further examined.
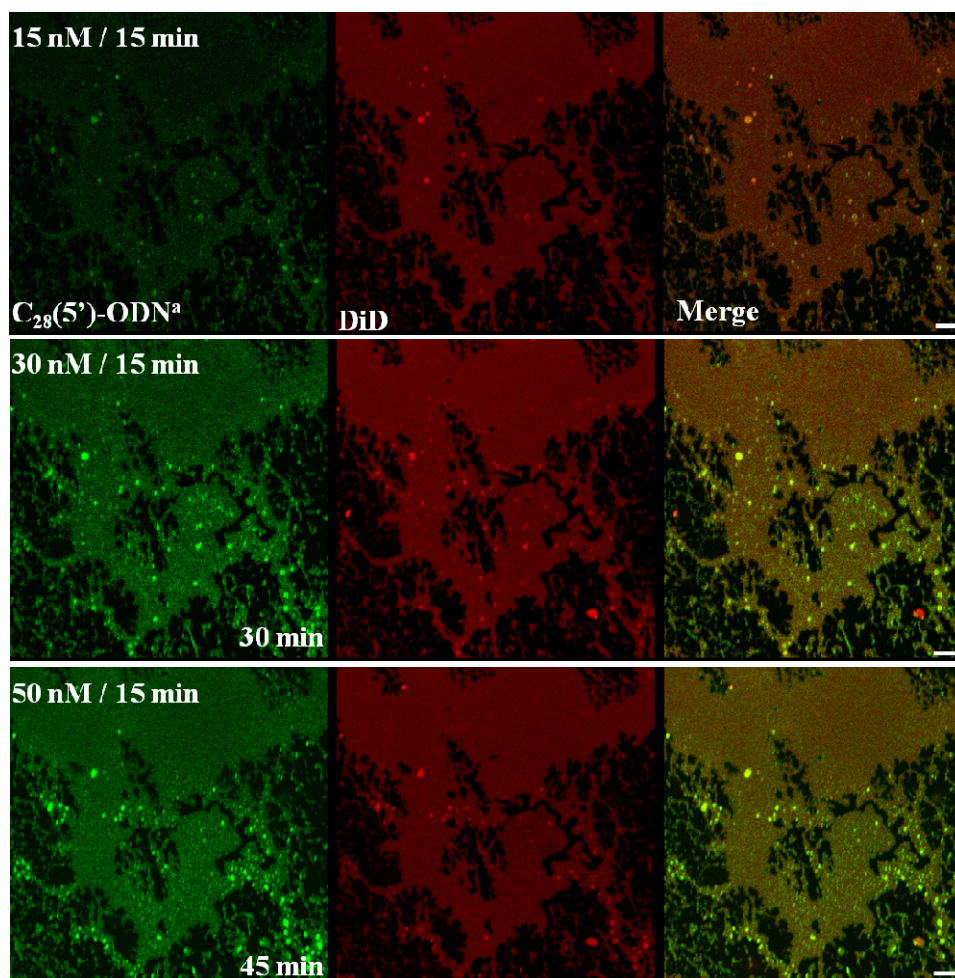
Figure 5.4 Incorporation kinetics of Alexa 488-labelled C$_{28}$(5')-ODN into DiD-labelled DOPC SPBs. Confocal microscopy images of SPBs incubated with Alexa 488-labelled C$_{28}$(5')-ODN. Increasing concentrations of Alexa 488-labelled C$_{28}$(5')-ODN were added to the SPBs and incubated for a determined time (see figure). ODN[a] stands for GEM91(3')-Alexa 488. LOC (green) and lipid (red) staining are shown in the left and centre columns, respectively. The right column displays the merging of both detection channels. Images were taken at 22ºC. Scale bars represent 10 μm.
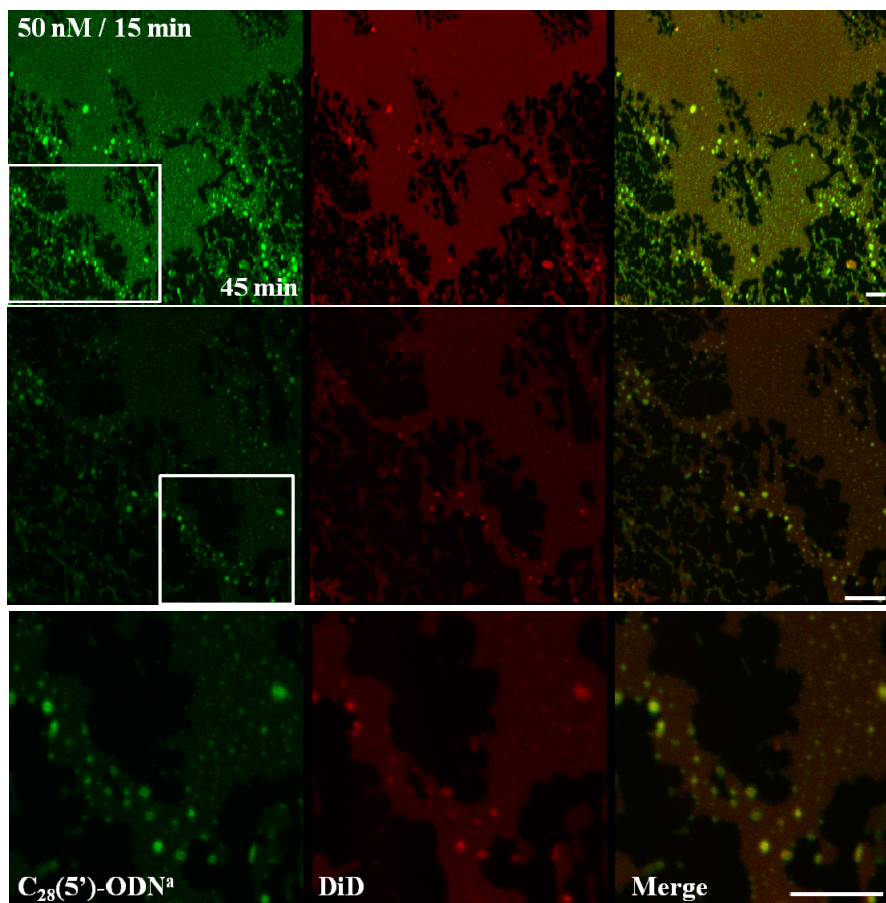
Figure 5.5 Imaging of Alexa 488-labelled C$_{28}$(5')-ODN binding to DiD-labelled DOPC SPBs. Confocal microscopy images of SPBs incubated with Alexa 488-labelled C$_{28}$(5')-ODN. Here, different zooms were taken to visualise the structures formed by this LOC. ODN[a] stands for GEM91(3')-Alexa 488. White squares represent the zoom taken, corresponding to the images below. LOC (green) and lipid (red) staining are shown in the left and centre columns, respectively. The right column displays the merging of both detection channels. Images were taken at 22ºC. Scale bars represent 10 μm.

As shown in Figure 5.5, reproducible peculiar Alexa 488-enriched rounded structures were observed near the boundary between SPB and mica defects (darks areas lacking DiD and Alexa 488 fluorescence), most of them being as well DiD-enriched.

199

These results suggest the structures to be LOC-lipid based, and might point to possible instability at SPB-mica boundaries to favour structure generation. Figure 5.6 shows a better example of these peculiar rounded structures prone to be localised and concentrated at the boundary between SPB and dark mica areas.
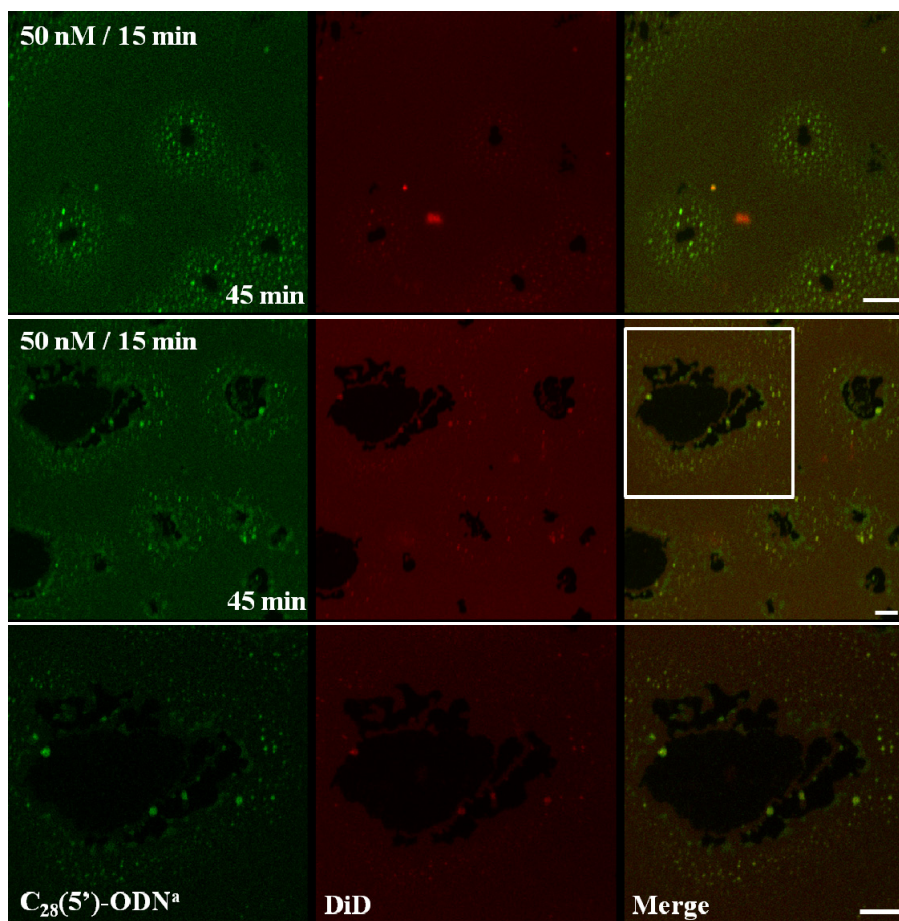
Figure 5.6 Imaging of Alexa 488-labelled C$_{28}$(5')-ODN binding to DiD-labelled DOPC SPBs. Confocal microscopy images of SPBs incubated with Alexa 488-labelled C$_{28}$(5')-ODN. Here, different zones of the SPB were visualised. ODN[a] stands for GEM91(3')-Alexa 488. White squares represent the zoom taken, corresponding to the images below. LOC (green) and lipid (red) staining are shown in the left and centre columns, respectively. The right column displays the merging of both detection channels. Images were taken at 22ºC. Scale bars represent 10 µm.

Then, we analysed the incorporation behaviour and kinetics of this LOC in SPBs composed of DiD-labelled DOPC/eSM/Chol (2:2:1).
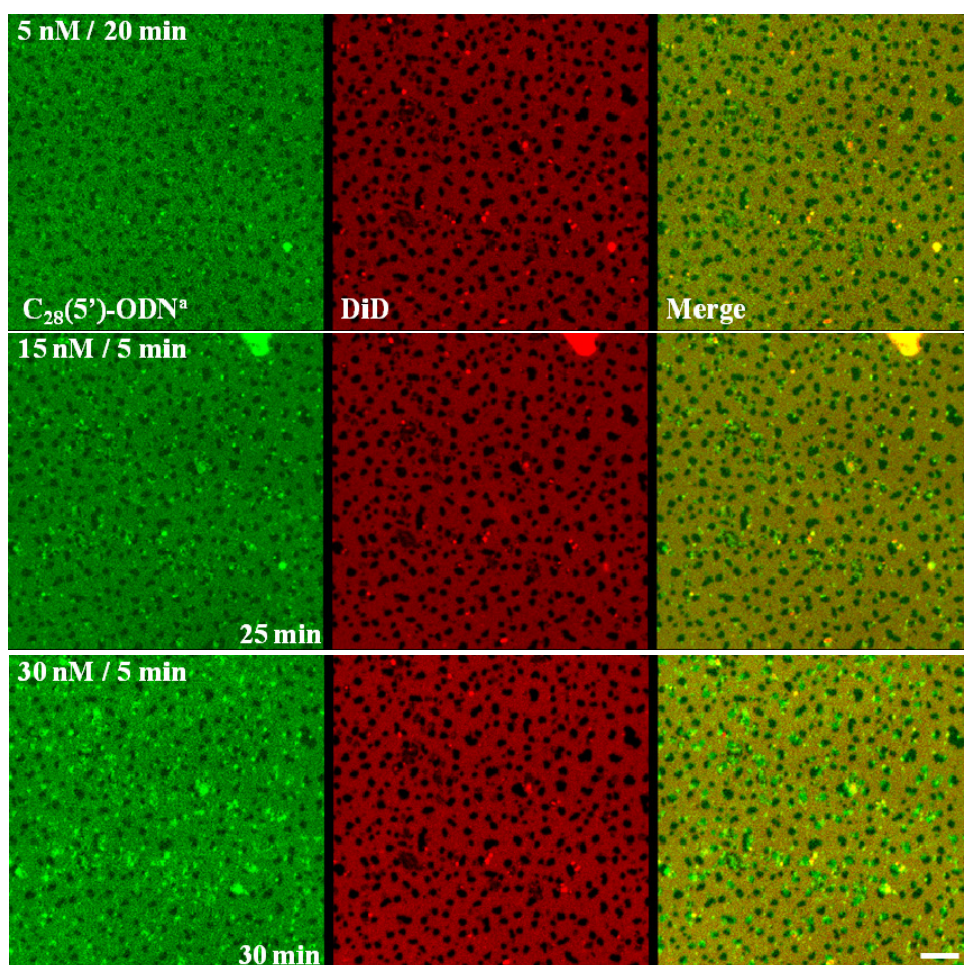
Figure 5.7 Incorporation kinetics of Alexa 488-labelled C$_{28}$(5')-ODN into DiD-labelled DOPC/eSM/Chol (2:2:1) SPBs. Confocal microscopy images of SPBs incubated with Alexa 488-labelled C$_{28}$(5')-ODN. Increasing concentrations of Alexa 488-labelled C$_{28}$(5')-ODN were added to the SPBs and incubated for a determined time (see figure). ODN[a] stands for GEM91(3')-Alexa 488. LOC (green) and lipid (red) staining are shown in the left and centre columns, respectively. The right column displays the merging of both detection channels. Images were taken at 22ºC. Scale bars represent 10 µm.
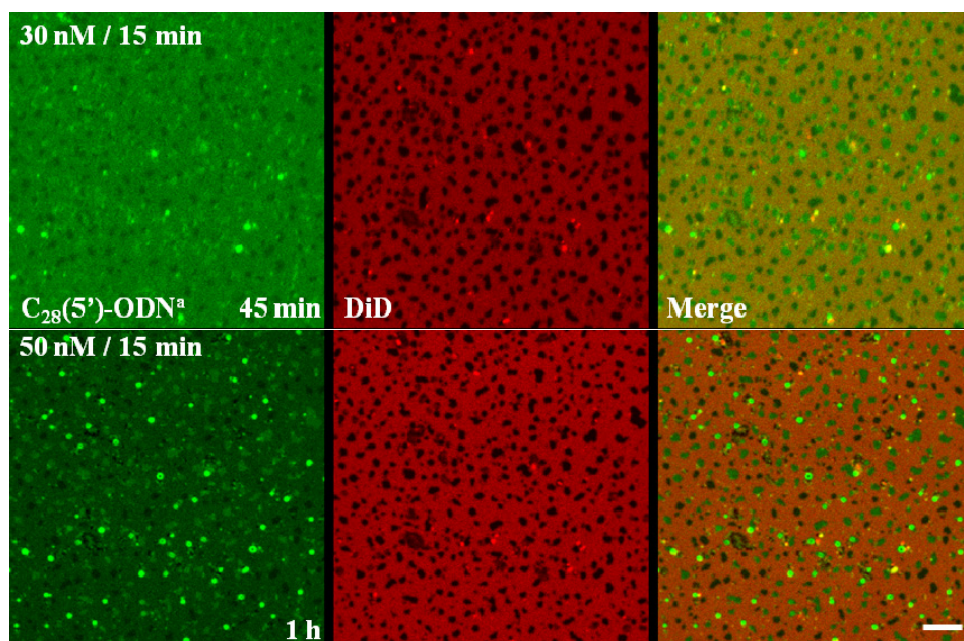
Figure 5.8 Incorporation kinetics of Alexa 488-labelled C$_{28}$(5')-ODN into DiD-labelled DOPC/eSM/Chol (2:2:1) SPBs. Confocal microscopy images of SPBs incubated with Alexa 488-labelled C$_{28}$(5')-ODN. This figure is the continuation of the previous figure (Figure 5.7). Increasing concentrations of Alexa 488-labelled C$_{28}$(5')-ODN were added to the SPBs and incubated for a determined time (see figure). ODN[a] stands for GEM91(3')-Alexa 488. LOC (green) and lipid (red) staining are shown in the left and centre columns, respectively. The right column displays the merging of both detection channels. Images were taken at 22ºC. Scale bars represent 10 μm.

Alexa 488-labelled C$_{28}$(5')-ODN showed a rapid and consistently detectable interaction with the L$_d$ phase of the SPB when 5 nM LOC was incubated for 20 min (Figure 5.7, upper panels). As seen in Figures 5.7 and 5.8, when higher concentrations of this LOC were used a number of Alexa 488-enriched bright spots were observed in the boundary between the L$_d$ and L$_o$ domains, followed by the incorporation of this LOC to L$_o$ domains. Similarly, this LOC was incorporated into both L$_d$ and L$_o$ domains, in agreement with the results obtained in GUV experiments (see Figure 5.3).

In accordance to what it was observed in SPBs composed of pure DOPC (Figure 5.4), when concentrations up to 50 nM of this LOC were added to SPBs composed of DOPC/eSM/Chol (2:2:1), again reproducible peculiar rounded structures were detected. In this case, the structures were only Alexa 488-enriched but detected on top of L$_o$ domains, suggesting their enrichment in pure LOC and/or in LOC and lipid from the L$_o$ phase (Figure 5.8, bottom panels).
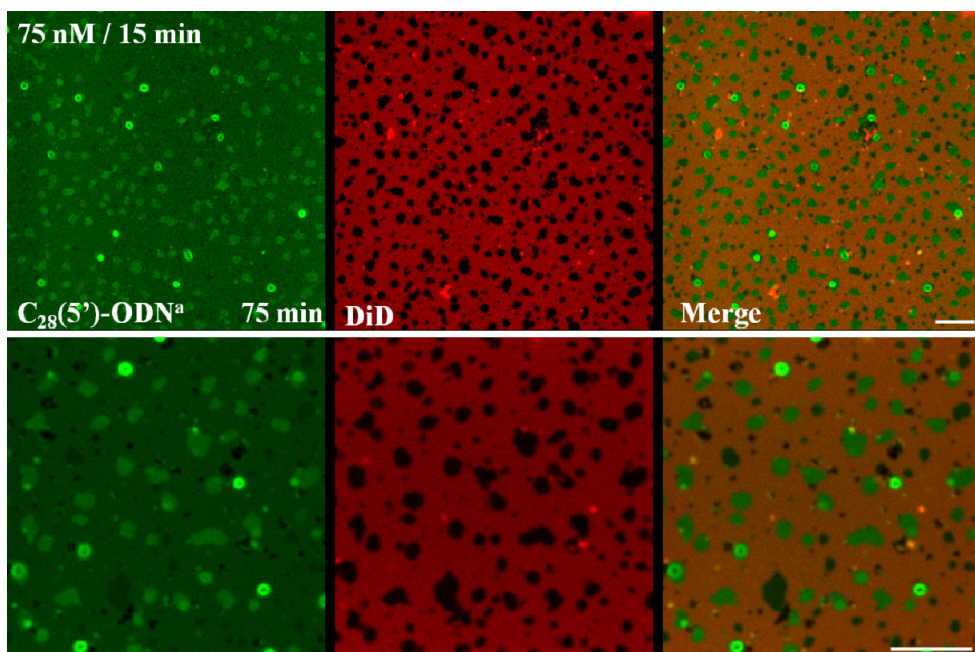
Figure 5.9 Imaging of Alexa 488-labelled C$_{28}$(5')-ODN binding to DiD-labelled DOPC/eSM/Chol (2:2:1) SPBs. Confocal microscopy images of SPBs incubated with Alexa 488-labelled C$_{28}$(5')-ODN. Here, additional 25 nM Alexa 488-labelled C$_{28}$(5')-ODN (75 nM) were added to the sample shown in the previous figure (Figure 5.7) and incubated for another 15 min. ODN[a] stands for GEM91(3')-Alexa 488. LOC (green) and lipid (red) staining are shown in the left and centre columns, respectively. The right column displays the merging of both detection channels. Images were taken at 22ºC. Scale bars represent 10 μm.

As it can be clearly observed in Figure 5.9, LOC-rich rounded structures were also observed near DiD-depleted areas. At the present we cannot confirm that these areas correspond to mica defects or to L$_o$ phases to which LOC did not partition. However, the observation that in pure DOPC bilayers the structures mostly contained both probes while in the present case were only Alexa 488-enriched, could point dark DiD-depleted areas to be L$_o$ phase where LOC did not yet partition at the time the image was taken. In spite of all, all of the results are of importance since the structures arise near boundaries where higher instability could be assumed, namely L$_d$-L$_o$ phase and/or lipid-mica boundaries.

Finally, we studied the incorporation behaviour and kinetics of this LOC in SPBs composed of DiD-labelled eSM/Chol (2:1). In this case, the formation of the SPB was not very successful since only small patches of DiD-labelled eSM/Chol (2:1) SPBs were observed by fluorescence confocal microscopy. This issue could be related to the higher rigidity of eSM/Chol vesicles and to a lower extension within the mica support during SPB preparation (Figure 5.10).

Under these experimental conditions, Alexa 488-labelled C$_{28}$(5')-ODN was efficiently detected in SPBs containing eSM/Chol (2:1), co-localising with DiD dye (Figure 5.10). Thus, these results suggest its rapid incorporation into the L$_o$ phase state, in agreement with the results obtained in GUV experiments.
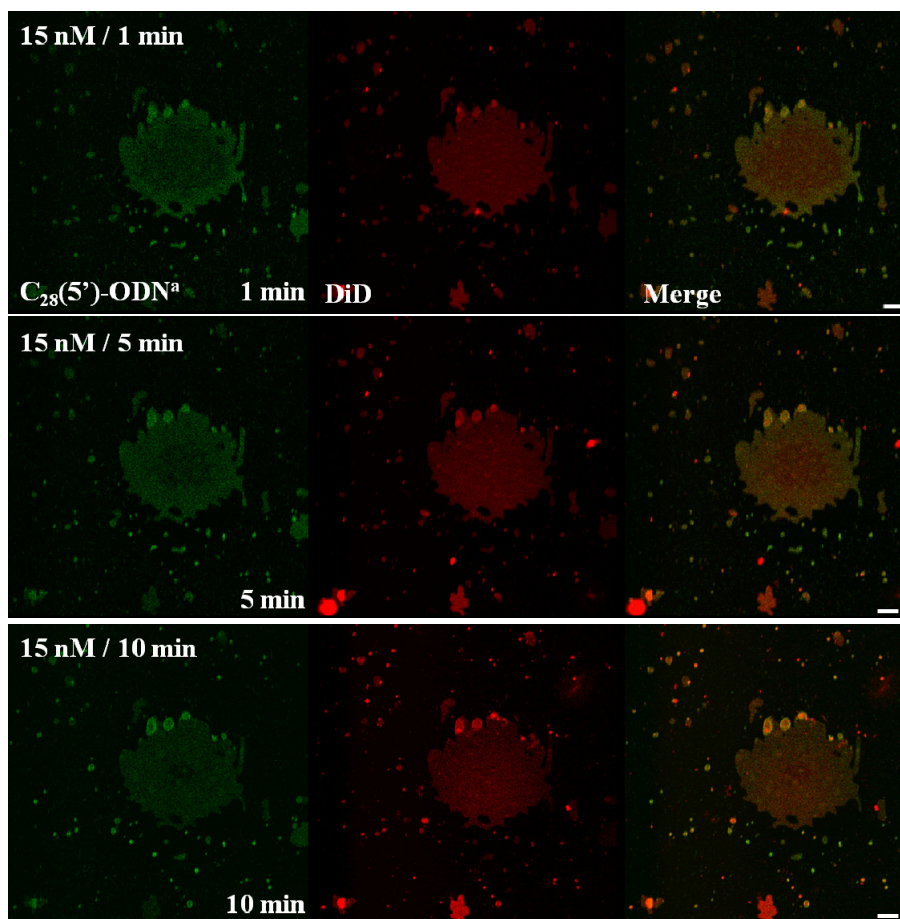
Figure 5.10 Incorporation kinetics of Alexa 488-labelled C$_{28}$(5')-ODN into DiD-labelled eSM/Chol (2:1) SPBs. Confocal microscopy images of SPBs incubated with Alexa 488-labelled C$_{28}$(5')-ODN. Initial 15 nM Alexa 488-labelled C$_{28}$(5')-ODN were added to the SPBs the incorporation of this LOC was recorded in short time periods (see figure). ODN[a] stands for GEM91(3')-Alexa 488. LOC (green) and lipid (red) staining are shown in the left and centre columns, respectively. The right column displays the merging of both detection channels. Images were taken at 22ºC. Scale bars represent 10 µm.
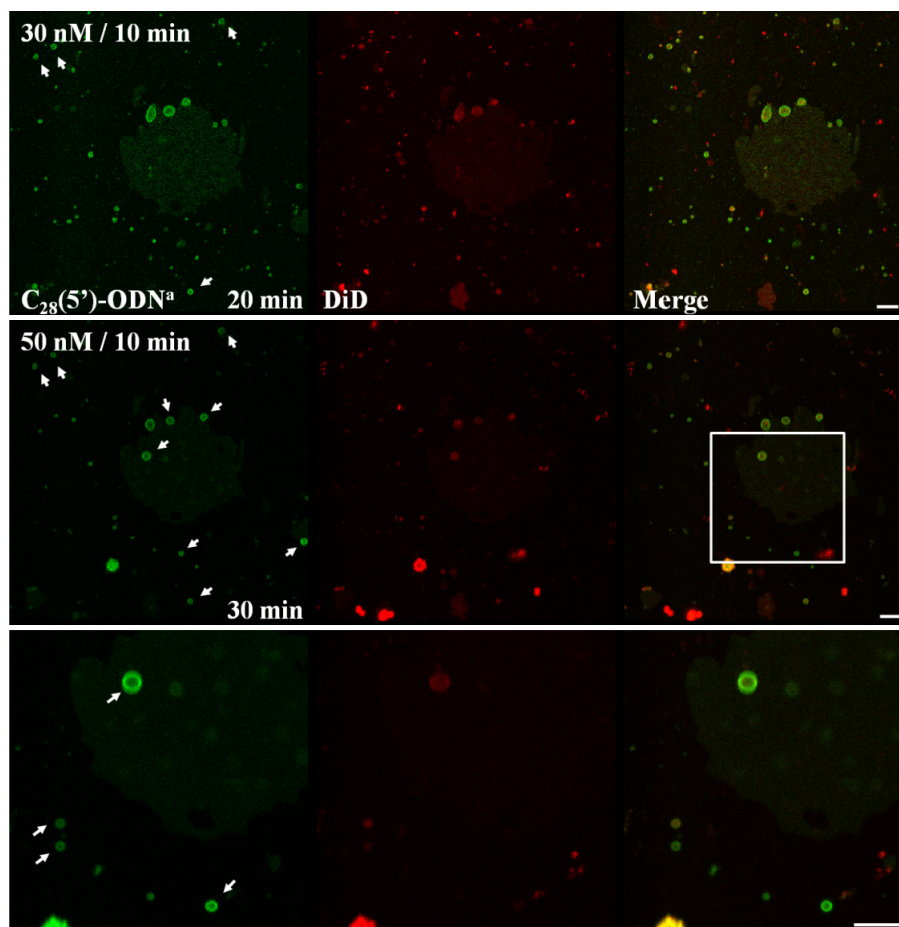
Figure 5.11 Imaging of Alexa 488-labelled C$_{28}$(5')-ODN binding to DiD-labelled eSM/Chol (2:1) SPBs. Confocal microscopy images of SPBs incubated with Alexa 488-labelled C$_{28}$(5')-ODN. Here, additional 15 nM Alexa 488-labelled C$_{28}$(5')-ODN (30 nM) were added to the previous sample (Figure 5.9) and incubated for 10 min (20 min). Then, 20 nM Alexa 488-labelled C$_{28}$(5')-ODN (50 nM) were added and incubated for another 10 min (30 min). ODN[a] stands for GEM91(3')-Alexa 488. White squares represent the zoom taken, corresponding to the images below. White arrows indicate Alexa 488-enriched structures. LOC (green) and lipid (red) staining are shown in the left and centre columns, respectively. The right column displays the merging of both detection channels. Images were taken at 22ºC. Scale bars represent 10 μm.

As seen in Figure 5.11 and in agreement with the results obtained in SPBs composed of DOPC and DOPC/eSM/Chol (2:2:1), Alexa 488-enriched rounded

structures were also observed in SPBs composed of eSM/Chol (2:1). These structures were in this case also DiD-enriched, supporting their possible LOC-lipid origin.
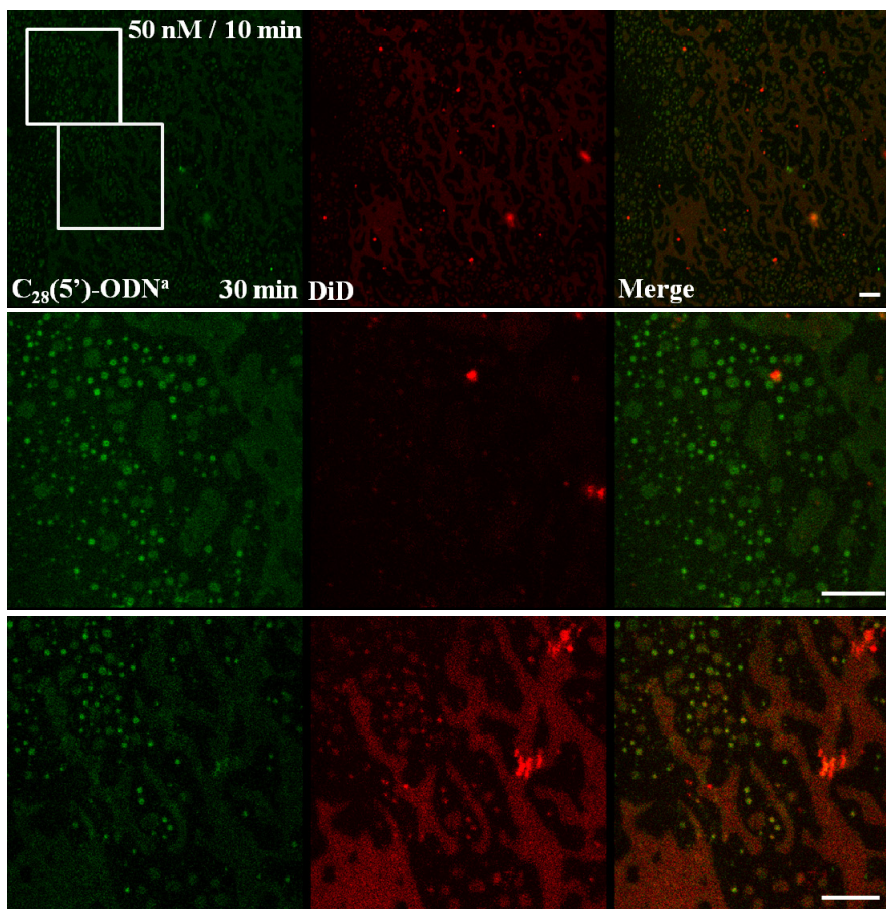
Figure 5.12 Imaging of Alexa 488-labelled C$_{28}$(5')-ODN binding to DiD-labelled eSM/Chol (2:1) SPBs. Confocal microscopy images of SPBs incubated with Alexa 488-labelled C$_{28}$(5')-ODN. Here, another zone of the mica was visualised. ODN[a] stands for GEM91(3')-Alexa 488. White squares represent the zoom taken, corresponding to the images below. LOC (green) and lipid (red) staining are shown in the left and centre columns, respectively. The right column displays the merging of both detection channels. Images were taken at 22ºC. Scale bars represent 10 μm.
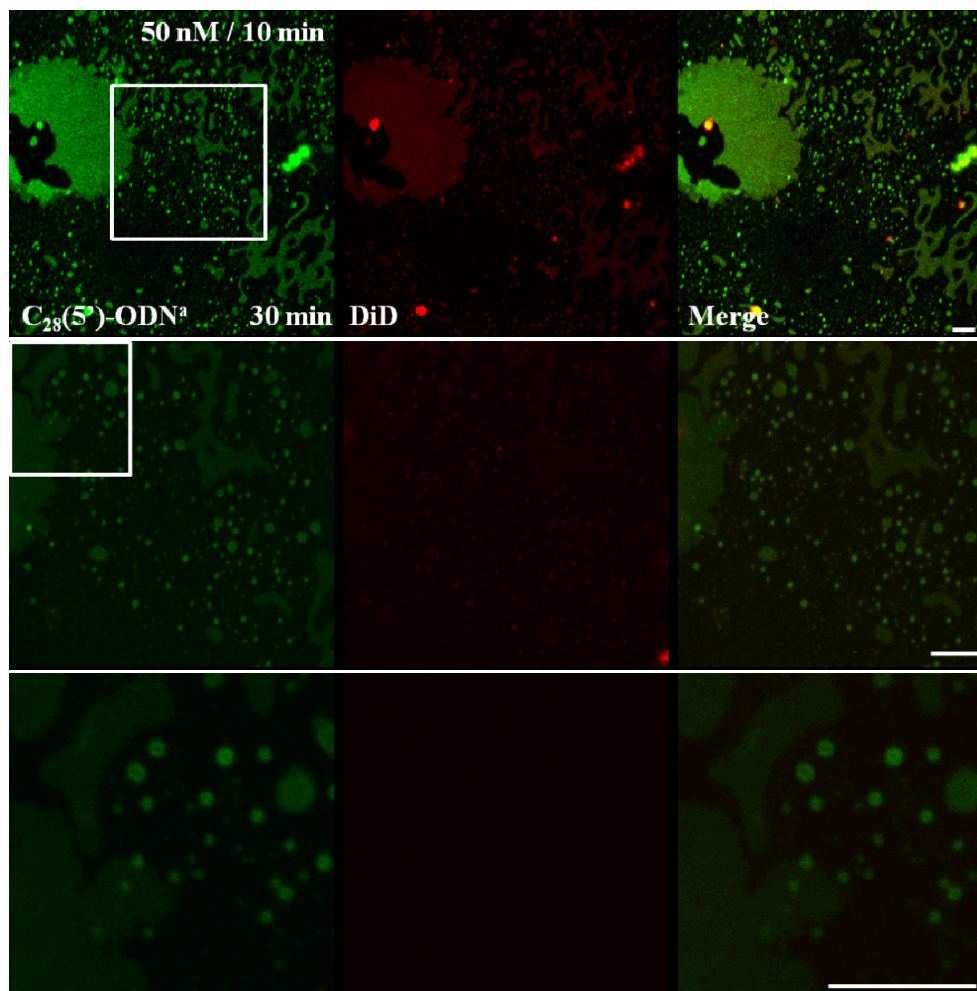
Figure 5.13 Imaging of Alexa 488-labelled C$_{28}$(5')-ODN binding to DiD-labelled eSM/Chol (2:1) SPBs. Confocal microscopy images of SPBs incubated with Alexa 488-labelled C$_{28}$(5')-ODN. Here, another zone of the mica was visualised. ODN[a] stands for GEM91(3')-Alexa 488. White squares represent the zoom taken, corresponding to the images below. LOC (green) and lipid (red) staining are shown in the left and centre columns, respectively. The right column displays the merging of both detection channels. Images were taken at 22ºC. Scale bars represent 10 μm.

Figures 5.12 and 5.13 show different zones of the mica, where the formation of the SPB composed of eSM/Chol (2:1) was also irregular.

However, in these zones Alexa 488- and DiD-enriched structures were also detected. On the other hand, it can be appreciated that DiD lipophilic dye was rapidly bleached in this system when the sample was radiated several times (see Figure 5.13 bottom-centred image).

Taken together, it can be assumed that $C_{28}(5')$-ODN apparently showed similar behaviour in both GUV and SPB systems. Indeed, $C_{28}(5')$-ODN was able to incorporate into bilayers in pure L_d and L_o phase states and also into both phases of L_d/L_o containing lipid systems.

Specially, in DiD-labelled SPBs composed of DOPC/eSM/Chol (2:2:1) this LOC was preferentially incorporated into the L_d phase. At increasing concentrations of this LOC its incorporation into the L_o phase was also observed. These observations are of importance since they discard a possible influence of domain boundaries on LOC insertion, since it is incorporated even in bilayers showing no lateral segregation. Moreover, the reproducible Alexa 488-enriched rounded structures were visualised in all the SPBs tested [DOPC, DOPC/eSM/Chol (2:2:1) and eSM/Chol (2:1)].

From these results we can support the pure LOC and/or LOC-lipid nature of the structures and their generation through bilayer areas with higher instability. As could be think off, a high LOC concentration near one of the above-explained boundaries could favour its generation due to an increased LOC preference for highly curved structures. Indeed, their highly curved nature is supported by the observance that the rounded structures appeared anchored to the membrane, as extensive washing did not remove them. Furthermore, we can also point out that from these studies the rounded structures generated in the ternary phases could be enriched in lipids from the L_o phase (*i.e.*, eSM and/or Chol). The actual relevance of these structures, if any, is yet unknown but it could be important on LOC internalisation in more complex vesicle and/or cell experiments.

209

Binding properties of double stranded C$_{28}$(5')-ODN in lipid bilayers

Here, we investigated whether C$_{28}$ anchor maintain similar binding properties when hybridised with the antisense strand, thereby forming a DNA duplex based conjugate. These studies were carried out using again membrane lipid model systems (*i.e.*, GUVs and SPBs).

As described in the Experimental procedures section, C$_{28}$(5')-ODN was hybridised with its complementary strand (AntiGEM91) in order to form double stranded compounds, presenting Alexa 488 fluorophore in the 5'-end of the AntiGEM91 strand or in the 3'-end of the C$_{28}$(5')-ODN strand.

Different migrating rates were observed when these compounds were loaded into non-denaturing 15% polyacrylamide gels (left panels) and 4% agarose gels (right panels) compared to the DNA ladder (Figure 5.14), which could be possibly attributed more to the limitations of polyacrylamide gel technology than to a problem with the ladder composition, as previously mentioned in the Experimental procedures section.

As observed in Figure 5.14, Alexa 488 fluorophore did not alter the migration behaviour of the compounds since each unlabelled and Alexa 488-labelled ODNs showed very similar migration rates (Figure 5.14). In addition, two bands were observed in the lanes of unlabelled and Alexa-488 labelled AntiGEM91 when migrated in 4% agarose gels. This phenomenon could be due to the G-rich sequence on AntiGEM91 strand, which could form a specific structure such as a bimolecular quadruplex, although it failed to form any G-quadruplex structure when predicted with QGRS Mapper (Kikin *et al.*, 2006).

Interestingly, C$_{28}$ lipid anchor did not apparently interfere in the formation of the double stranded ODN. This result is similar to those achieved by Iglina and co-workers who reported that the introduction of a lipophilic group into the 5'-end

of sense strand of siRNA did not lead to noticeable stabilisation or destabilisation of their duplexes with antisense strand (Iglina *et al.*, 2009).
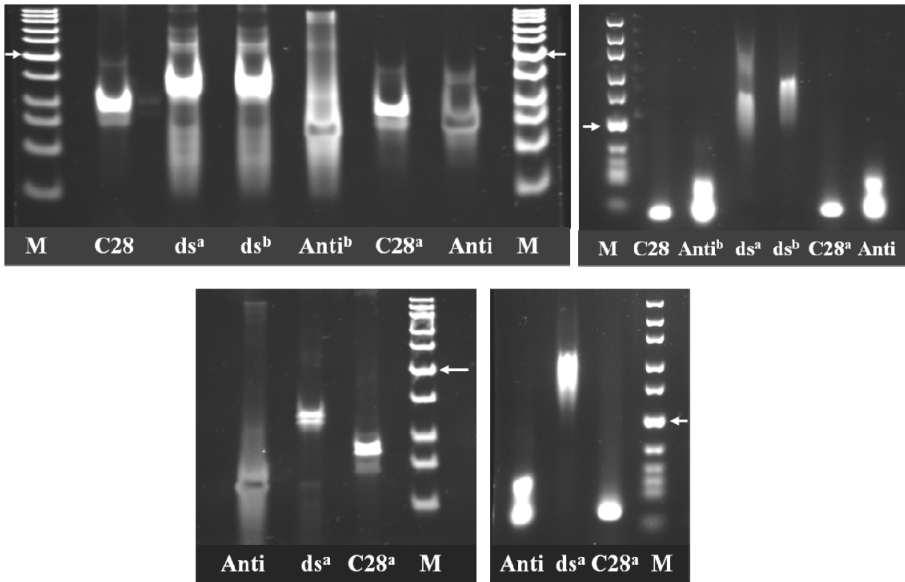
Figure 5.14 Characterisation of double stranded C$_{28}$(5')-ODN by SDS-PAGE and agarose gels. Non-denaturing 15% polyacrylamide gels (left panels) and 4% agarose gels (right panels) were performed to visualise by SIBR Gold staining the corresponding bands of unlabelled and Alexa 488-labelled AntiODN and single and double stranded C$_{28}$(5')-ODNs. From single stranded ODN stock solutions (200 µM) 1 µl unlabelled and 0.5 µl Alexa 488-labelled ODNs were mixed with the loading buffer. From double stranded ODN stock solutions (50 µM) 0.5 µl Alexa 488-labelled ODNs were added to the loading buffer. 3 µl DNA ladder were used for each M termed well. C28 and C28[a] stand for unlabelled and Alexa 488-labelled single stranded C$_{28}$(5')-GEM91, respectively. Anti and Anti[b] stand for unlabelled and Alexa 488-labelled single stranded AntiGEM91, respectively. Double stranded C$_{28}$(5')-GEM91 are represented as ds[a] (presenting Alexa 488 at the 3'-end of C$_{28}$(5')-GEM91) and ds[b] (presenting Alexa 488 at the 5'-end of AntiGEM91). M: DNA ladder (10, 15, 25, 35, 50, 75, 100, 150, 200, 300 bp). White arrows indicate the 50 bp fragment of the DNA ladder.

Once it was checked the formation of double stranded C$_{28}$(5')-ODNs, we first analysed their interaction behaviour when incubated with GUVs.

GUVs

A control experiment was initially performed in order to confirm that neither GEM91 nor AntiGEM91 were able to interact with GUVs presenting L$_d$ and L$_o$ phases, even at long incubation periods (*i.e.*, 20 h) (Figure 5.15).
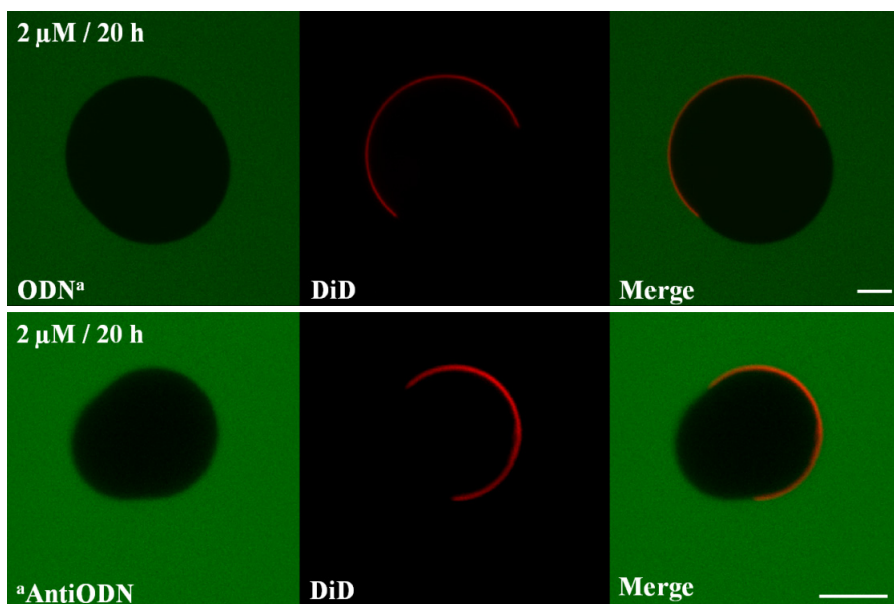
Figure 5.15 Imaging of Alexa 488-labelled ODN and AntiODN incubation with GUVs. Confocal microscopy images of DiD-labelled DOPC/eSM/Chol (2:2:1) GUVs (equatorial sections) incubated with 2 µM of Alexa 488-labelled acyl chain-free control-oligonucleotide (upper panels) and its complementary oligonucleotide (bottom panels) for 20 h. ODN[a] and [a]AntiODN stand for GEM91-(3')Alexa 488 and Alexa 488(5')-AntiGEM91, respectively. LOC (green) and lipid (red) staining are shown in the left and centre columns, respectively. The right column displays the merging of both detection channels. Images were taken at 22ºC. Scale bars represent 5 µm.

As observed in Figure 5.16, both double stranded C$_{28}$(5')-ODNs were incorporated into GUVs composed of DOPC, similarly to single stranded C$_{28}$(5')-ODN, suggesting that this compound is able to insert into a pure liquid-disordered phase state being either in single or double stranded ODN form.
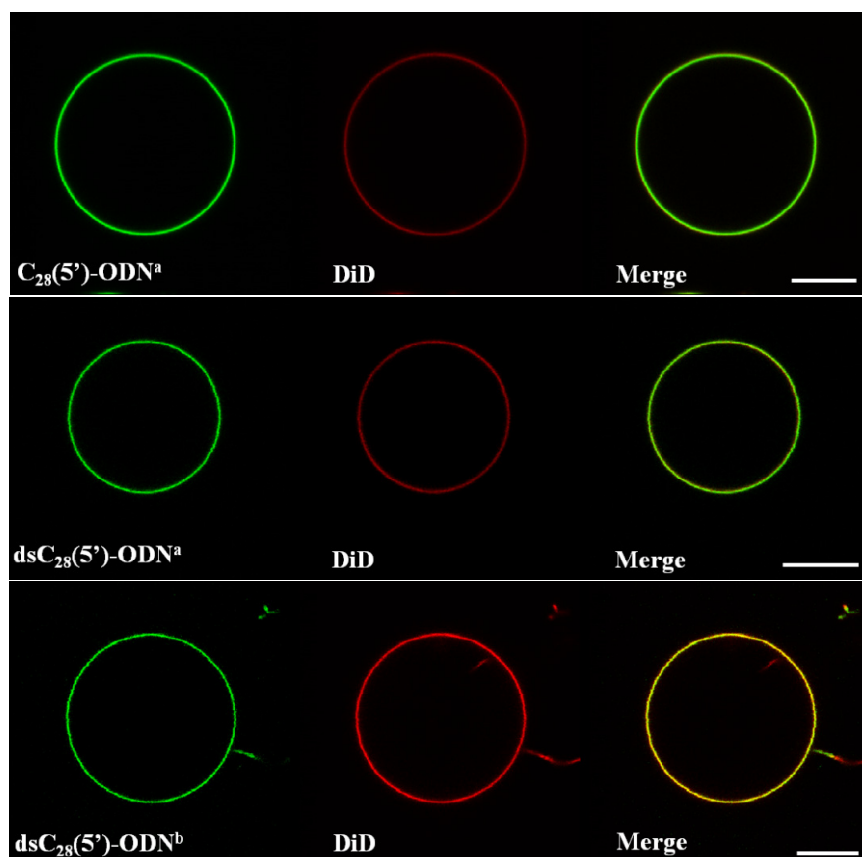
Figure 5.16 Imaging of Alexa 488-labelled single and double-stranded C$_{28}$(5')-ODN binding to DiD-labelled DOPC GUVs. Confocal microscopy images of GUVs (equatorial sections) incubated for 2 h with 50 nM of Alexa 488-labelled single-stranded C$_{28}$(5')-ODN (upper panels) and 100 nM (50 nM Alexa 488-labelled) double-stranded C$_{28}$(5')-ODN, carrying Alexa 488 fluorophore bound to the 3'-end of the C$_{28}$(5')-ODN strand (middle panels) or to the 5'-end of the AntiODN strand (bottom panels). ODN[a] and ODN[b] stand for GEM91-(3')Alexa 488 and Alexa 488(5')-AntiGEM91, respectively. LOC (green) and lipid (red) staining are shown in the left and centre columns, respectively. The right column displays the merging of both detection channels. Images were taken at 22ºC. Scale bars represent 10 μm.

213

As previously mentioned in Chapter 4, single stranded C$_{28}$(5')-ODN showed special binding properties since it was able to insert either in the L$_d$ or L$_o$ phase.
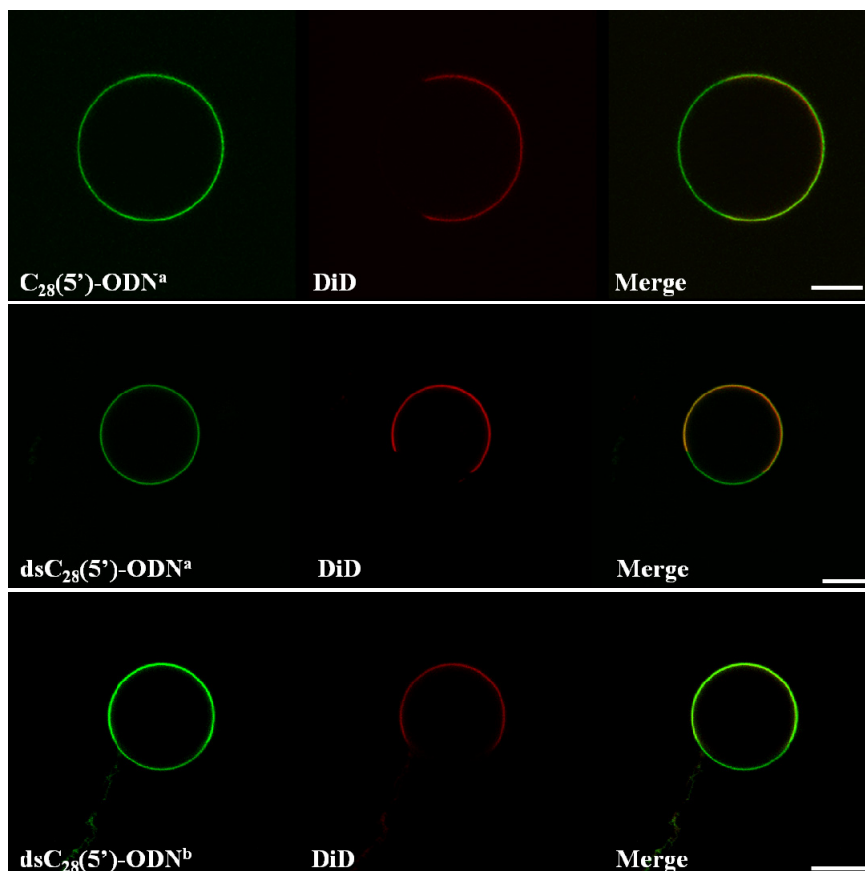
Figure 5.17 Imaging of Alexa 488-labelled single and double-stranded C$_{28}$(5')-ODN binding to DiD-labelled DOPC/eSM/Chol (2:2:1) GUVs. Confocal microscopy images of GUVs (equatorial sections) incubated for 2 h with 50 nM of Alexa 488-labelled single-stranded C$_{28}$(5')-ODN (upper panels) and 100 nM (50 nM Alexa 488-labelled) double-stranded C$_{28}$(5')-ODN, carrying Alexa 488 fluorophore bound to the 3'-end of the C$_{28}$(5')-ODN strand (middle panels) or to the 5'-end of the AntiODN strand (bottom panels). ODN[a] and ODN[b] stand for GEM91-(3')Alexa 488 and Alexa 488(5')-AntiGEM91, respectively. LOC (green) and lipid (red) staining are shown in the left and centre columns, respectively. The right column displays the merging of both detection channels. Images were taken at 22ºC. Scale bars represent 10 µm.

214

Interestingly, both double stranded compounds were also detected in L$_d$ and L$_o$ phases (Figure 5.17). These observations point to a nonspecific phase partitioning of this LOC being either in single or double stranded ODN form.
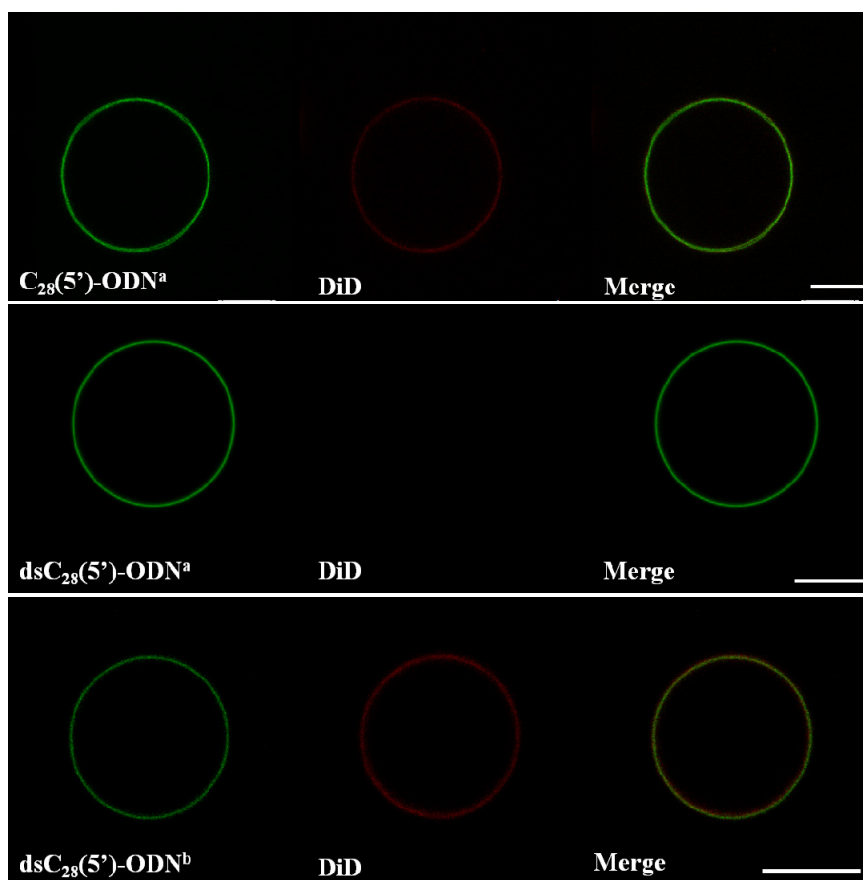
Figure 5.18 Imaging of Alexa 488-labelled single and double-stranded C$_{28}$(5')-ODN binding to DiD-labelled eSM/Chol (2:1) GUVs. Confocal microscopy images of GUVs (equatorial sections) incubated for 2 h with 50 nM of Alexa 488-labelled single-stranded C$_{28}$(5')-ODN (upper panels) and 100 nM (50 nM Alexa 488-labelled) double-stranded C$_{28}$(5')-ODN, carrying Alexa 488 fluorophore bound to the 3'-end of the C$_{28}$(5')-ODN strand (middle panels) or to the 5'-end of the AntiODN strand (bottom panels). ODN[a] and ODN[b] stand for GEM91-(3')Alexa 488 and Alexa 488(5')-AntiGEM91, respectively. LOC (green) and lipid (red) staining are shown in the left and centre columns, respectively. The

right column displays the merging of both detection channels. Images were taken at 22ºC. Scale bars represent 10 μm.

In GUVs composed of eSM/Chol (2:1), DiD lipophilic dye was not efficiently incorporated in all the vesicles formed, as observed in the middle panels of the Figure 5.18. However, when both single and double stranded C$_{28}$(5')-ODNs were incubated with these GUVs, a remarkable interaction was observed, suggesting that this compound is able to insert into a pure liquid-ordered phase state being either in single or double stranded ODN form.

Overall, it can be assumed that C$_{28}$ anchor acts similarly when conjugated to either single or double stranded ODNs, being capable of inserting into both L$_d$ and L$_o$ domains of GUVs composed of DOPC, DOPC/eSM/Chol (2:2:1) and eSM/Chol (2:1).

SPBs

Thereafter, we analysed the incorporation behaviour and kinetics of double stranded C$_{28}$(5')-ODNs when incubated with SPBs composed of DOPC/eSM/Chol (2:2:1).

Initially, Alexa 488-labelled double stranded C$_{28}$(5')-ODN (labelled at the 3'-termini of the C$_{28}$(5')-ODN strand) showed a consistently detectable interaction with the L$_d$ phase of the SPB (Figure 5.19). This is in agreement with the results achieved by incubation of Alexa 488-labelled single stranded C$_{28}$(5')-ODN with SPBs composed of DOPC/eSM/Chol (2:2:1) (Figure 5.7).
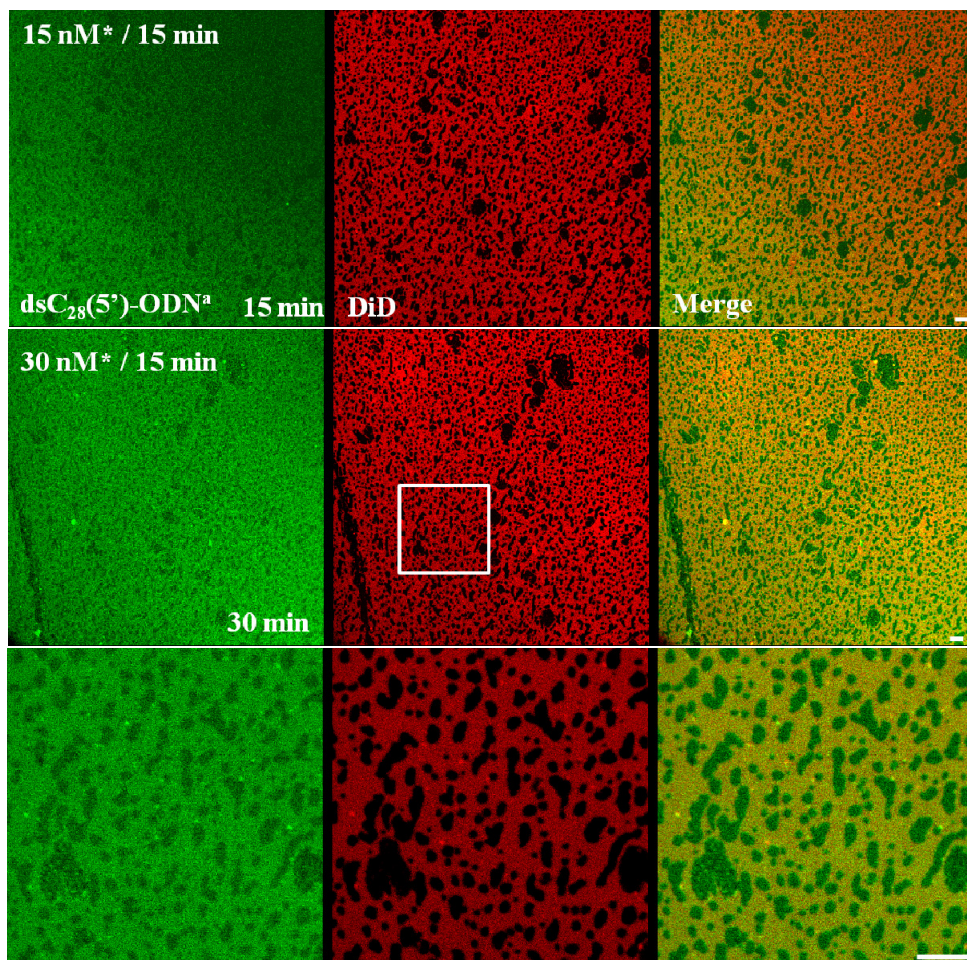
Figure 5.19 Incorporation kinetics of Alexa 488-labelled double-stranded C$_{28}$(5')-ODN into DiD-labelled DOPC/eSM/Chol (2:2:1) SPBs. Confocal microscopy images of SPBs incubated with Alexa 488-labelled double-stranded C$_{28}$(5')-ODN. Increasing concentrations of Alexa 488-labelled C$_{28}$(5')-ODN were added to the SPBs and incubated for a determined time (see figure). dsC$_{28}$(5')-ODN[a] stands for double-stranded C$_{28}$(5')-GEM91, carrying Alexa 488 fluorophore bound to the 3'-end of the C$_{28}$(5')-ODN strand. The concentration with an asterisk corresponds to the concentration of Alexa 488-labelled strand. White square represents the zoom taken, corresponding to the images below. LOC (green) and lipid (red) staining are shown in the left and centre columns, respectively. The right column displays the merging of both detection channels. Images were taken at 22ºC. Scale bars represent 10 µm.

217

Figure 5.20 Incorporation kinetics of Alexa 488-labelled double-stranded C$_{28}$(5')-ODN into DiD-labelled DOPC/eSM/Chol (2:2:1) SPBs. Confocal microscopy images of SPBs incubated with Alexa 488-labelled double-stranded C$_{28}$(5')-ODN. This figure is the continuation of the previous figure (Figure 5.19). Increasing concentrations of Alexa 488-labelled C$_{28}$(5')-ODN were added to the SPBs and incubated for a determined time (see figure). dsC$_{28}$(5')-ODN[a] stands for double-stranded C$_{28}$(5')-GEM91, carrying Alexa 488 fluorophore bound to the 3'-end of the C$_{28}$(5')-ODN strand. The concentration with an asterisk corresponds to the concentration of Alexa 488-labelled strand. LOC (green) and lipid (red) staining are shown in the left and centre columns, respectively. The right column displays the merging of both detection channels. Images were taken at 22ºC. Scale bars represent 10 μm.

When increasing concentrations of this LOC were used, its incorporation into L$_o$ domains was observed, followed by the detection of reproducible Alexa 488-enriched rounded structures, suggesting that these structures were at least in part formed by this LOC, and presumably LOC/L$_o$ phase lipids-enriched (Figure 5.20).
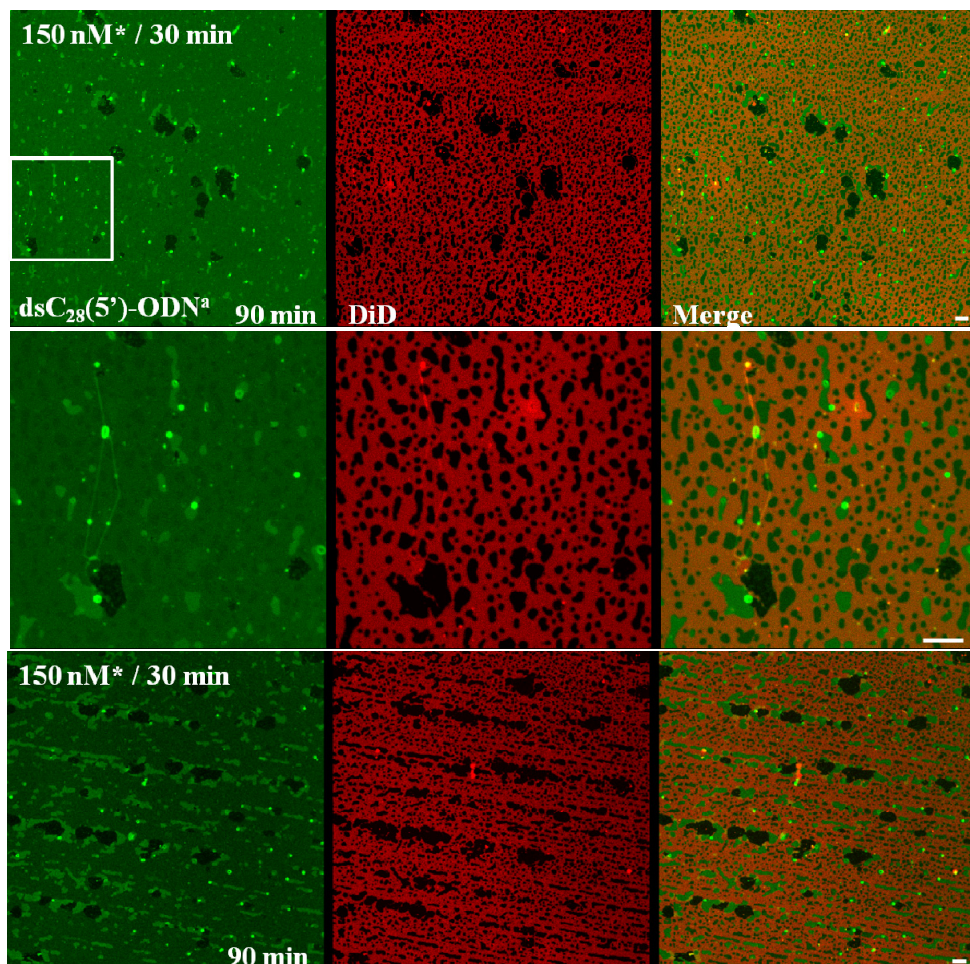
Figure 5.21 Imaging of Alexa 488-labelled double-stranded C$_{28}$(5')-ODN binding to DiD-labelled DOPC/eSM/Chol (2:2:1) SPBs. Confocal microscopy images of SPBs incubated with Alexa 488-labelled double-stranded C$_{28}$(5')-ODN. Here, additional concentration of Alexa 488-labelled double stranded C$_{28}$(5')-ODN were added to the sample shown in the previous figure (Figure 5.20) and incubated for another 30 min. dsC$_{28}$(5')-ODN[a] stands for double-stranded C$_{28}$(5')-GEM91, carrying Alexa 488 fluorophore bound to the 3'-end of the C$_{28}$(5')-ODN strand. The concentration with an asterisk corresponds to the concentration of Alexa 488-labelled strand. White square represents the zoom taken, corresponding to the images below. Bottom panels correspond to a different area of the SPB. LOC (green) and lipid (red) staining are shown in the left and centre columns, respectively. The right column displays the merging of both detection channels. Images were taken at 22ºC. Scale bars represent 10 µm.

219

In particular and as previously observed, these Alexa 488-enriched spots were localised at the boundaries between L$_d$ and L$_o$ domains or between L$_d$ domains and possible defects in the mica [darks areas lacking DiD and Alexa 488 fluorescence (Figure 5.21)].

A deeper analysis of these Alexa 488-enriched rounded structures was performed by varying the zeta plane of the fluorescence confocal microscope (Figures 5.22 and 5.23).

As seen in Figure 5.22, some of these Alexa 488-enriched structures were partially static in time (white arrows) whereas other dynamic structures were in continuous motion (white circles). In addition, the dynamic structures seem to be more tubular-like shaped than rounded-like shaped (see bottom panels of Figure 5.22), and they remained anchored to the bilayer along the time of the experiment.

When a single Alexa 488-enriched rounded structure was deeper analysed, it was confirmed that this particular structure was localised at the boundary between L$_d$ and L$_o$ phases (Figure 5.23). Interestingly, when some of the static rounded structures were highly zoomed and laser-radiated, they became tubular-shaped and dynamic, possible due to a structure destabilisation.
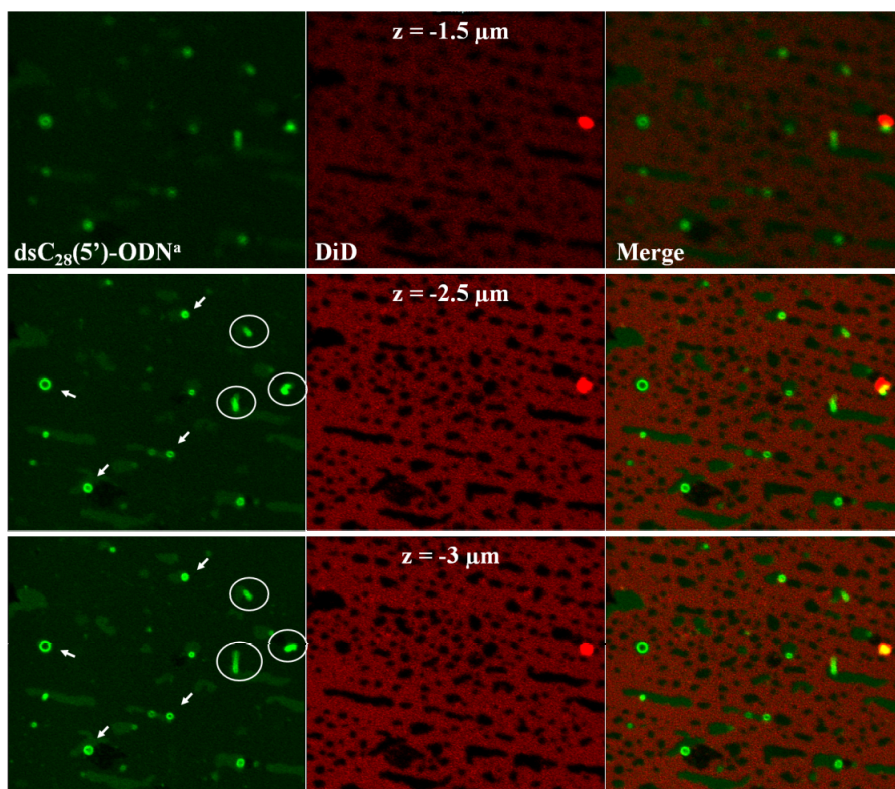
Figure 5.22 Imaging of specific Alexa 488-labelled double-stranded C$_{28}$(5')-ODN structures in DiD-labelled DOPC/eSM/Chol (2:2:1) SPBs. Confocal microscopy images of the structures formed by Alexa 488-labelled double-stranded C$_{28}$(5')-ODN when incubated in SPBs. This is a deeper analysis from the previous figure (Figure 5.21). Different z planes were taken from a single SPB zone. dsC$_{28}$(5')-ODN[a] stands for double-stranded C$_{28}$(5')-GEM91, carrying Alexa 488 fluorophore bound to the 3'-end of the C$_{28}$(5')-ODN strand. White arrows and circles stand for static and dynamic stable Alexa 488-enriched structures in time, respectively. LOC (green) and lipid (red) staining are shown in the left and centre columns, respectively. The right column displays the merging of both detection channels. Images were taken at 22ºC. Scale bars represent 10 µm.
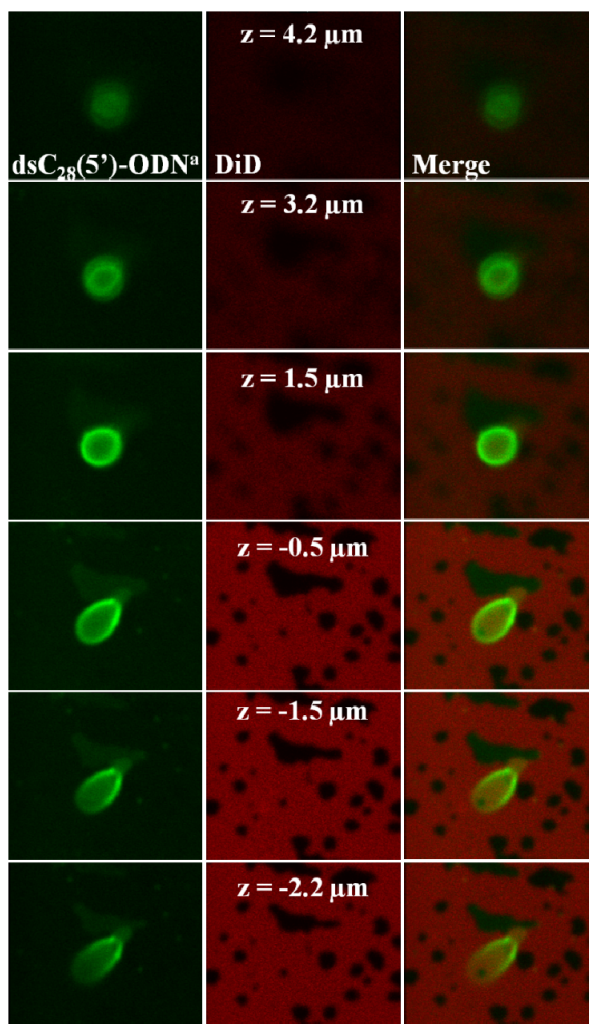
Figure 5.23 Imaging of a peculiar Alexa 488-labelled double-stranded C$_{28}$(5')-ODN structure in DiD-labelled DOPC/eSM/Chol (2:2:1) SPBs. Confocal microscopy images of one of the structures formed by Alexa 488-labelled double-stranded C$_{28}$(5')-ODN when incubated in SPBs. This is a deeper analysis from the previous figure (Figure 5.20). Different z planes were taken from a single SPB zone. dsC$_{28}$(5')-ODN[a] stands for double-stranded C$_{28}$(5')-GEM91, carrying Alexa 488 fluorophore bound to the 3'-end of the C$_{28}$(5')-ODN strand. LOC (green) and lipid (red) staining are shown in the left and centre columns, respectively. The right column displays the merging of both detection channels. Images were taken at 22ºC. Scale bars represent 10 µm.

Finally, the incorporation behaviour and kinetics of Alexa 488-labelled double stranded C_{28}(5')-ODN (labelled at the 5'-termini of the AntiGEM91 strand) were examined when incubated with SPBs composed of DOPC/eSM/Chol (2:2:1).
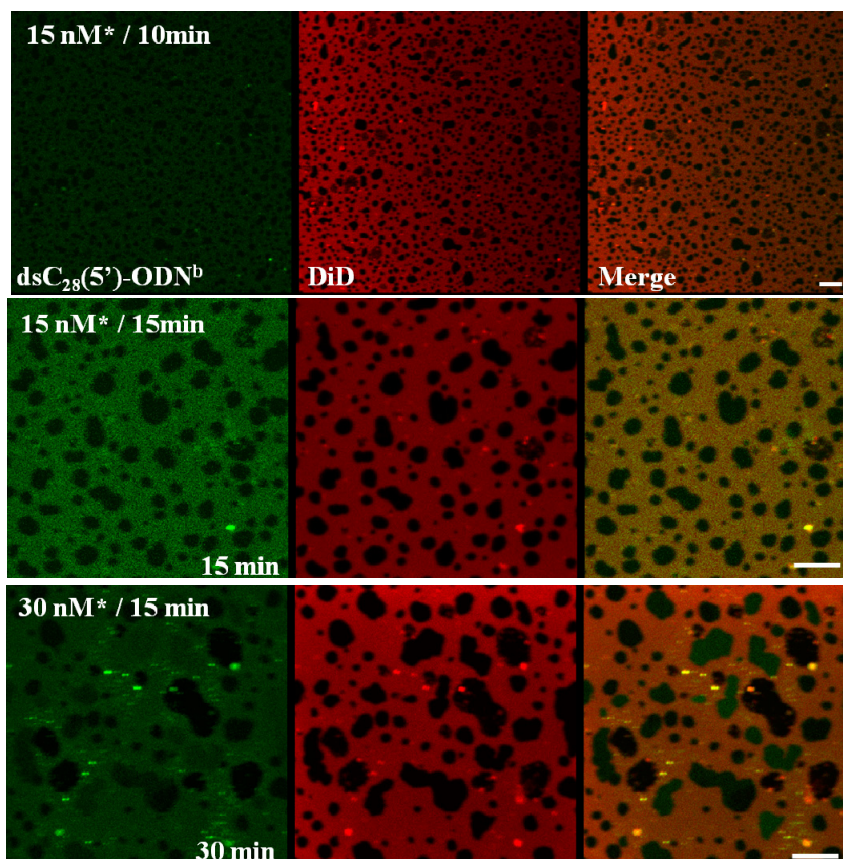
Figure 5.24 Incorporation kinetics of Alexa 488-labelled double-stranded C_{28}(5')-ODN into DiD-labelled DOPC/eSM/Chol (2:2:1) SPBs. Confocal microscopy images of SPBs incubated with Alexa 488-labelled double-stranded C_{28}(5')-ODN. Increasing concentrations of Alexa 488-labelled C_{28}(5')-ODN were added to the SPBs and incubated for a determined time. dsC_{28}(5')-ODN[b] stands for double-stranded C_{28}(5')-GEM91, carrying Alexa 488 fluorophore bound to the 5'-end of the AntiODN strand. The concentration with an asterisk corresponds to the concentration of Alexa 488-labelled strand. LOC (green) and lipid (red) staining are shown in the left and centre columns, respectively. The right column displays the merging of both detection channels. Images were taken at 22ºC. Scale bars represent 10 µm.

Alexa 488-labelled double stranded C$_{28}$(5')-ODN (labelled at the 5'-termini of the AntiGEM91 strand) showed initially a detectable interaction with the L$_d$ phase of the SPB (Figure 5.24, upper and middle panels). When increasing concentrations of this LOC were used, its incorporation into L$_o$ domains was also observed, followed by the detection of Alexa 488-enriched intense spots.
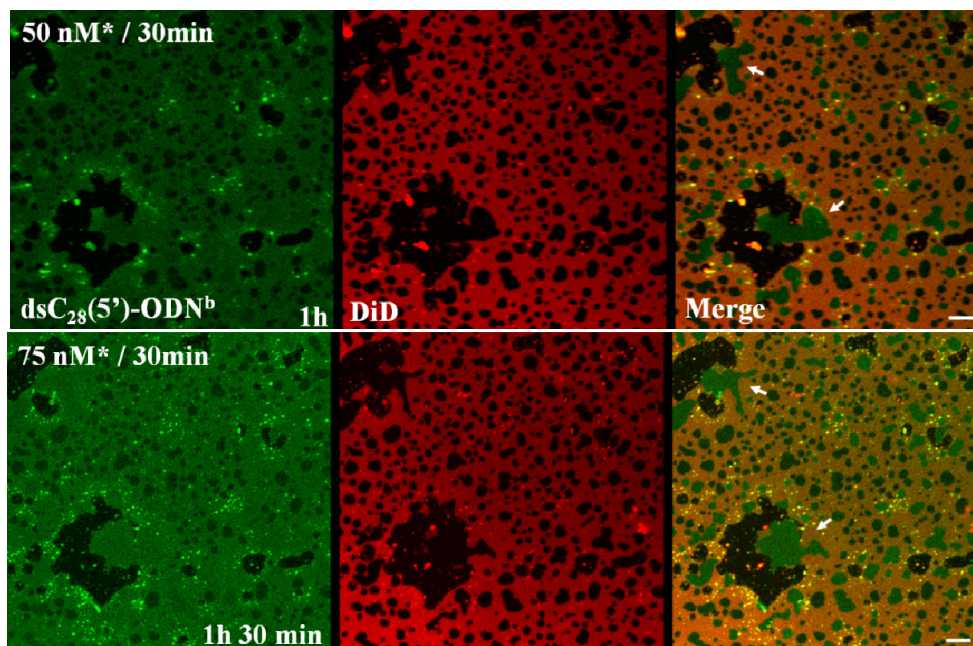
Figure 5.25 Imaging of Alexa 488-labelled double-stranded C$_{28}$(5')-ODN binding to DiD-labelled DOPC/eSM/Chol (2:2:1) SPBs. Confocal microscopy images of SPBs incubated with Alexa 488-labelled double-stranded C$_{28}$(5')-ODN. Here, additional concentrations of Alexa 488-labelled double stranded C$_{28}$(5')-ODN were added to the sample shown in the previous figure (Figure 5.22) and incubated for a determined time. dsC$_{28}$(5')-ODN[b] stands for double-stranded C$_{28}$(5')-GEM91, carrying Alexa 488 fluorophore bound to the 5'-end of the AntiODN strand. The concentration with an asterisk corresponds to the concentration of Alexa 488-labelled strand. White arrows indicate L$_o$ domain morphological rearrangement when increasing LOC concentrations were added. LOC (green) and lipid (red) staining are shown in the left and centre columns, respectively. The right column displays the merging of both detection channels. Images were taken at 22ºC. Scale bars represent 10 µm.
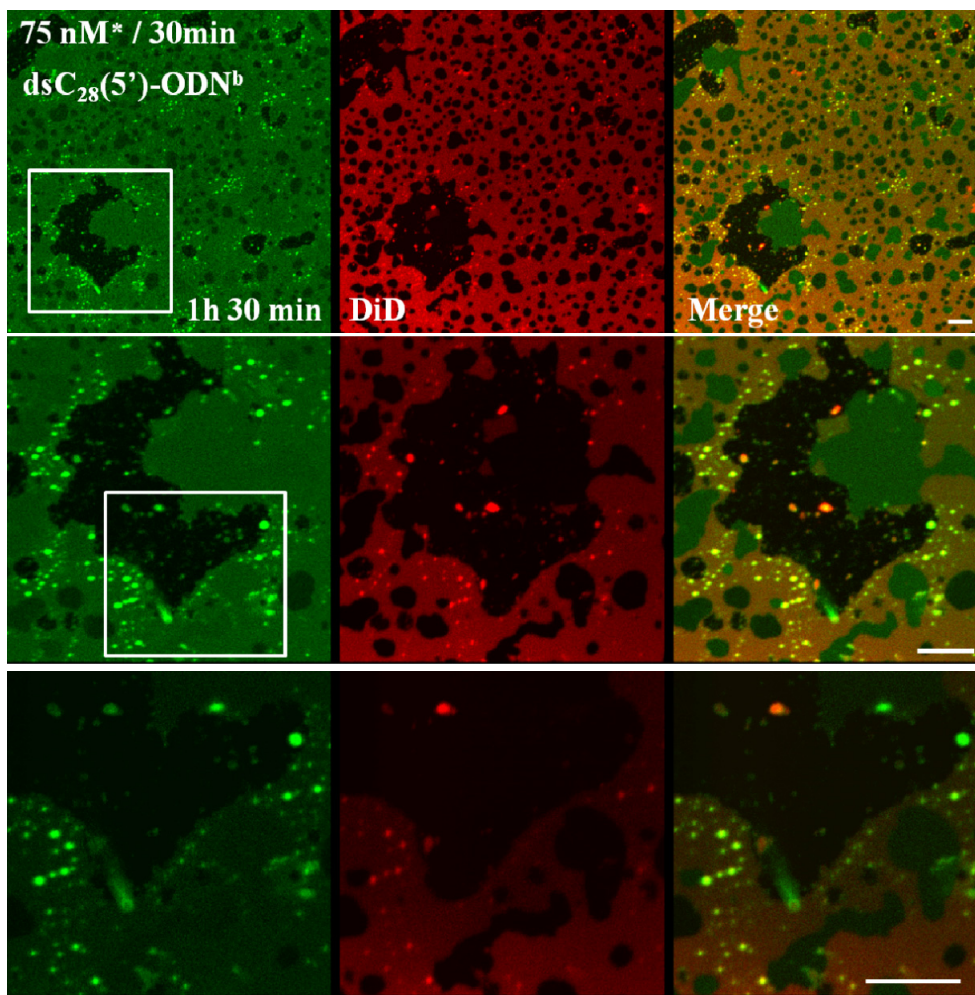
Figure 5.26 Imaging of Alexa 488-labelled double-stranded C$_{28}$(5')-ODN binding to DiD-labelled DOPC/eSM/Chol (2:2:1) SPBs. Confocal microscopy images of SPBs incubated with Alexa 488-labelled double-stranded C$_{28}$(5')-ODN. This is the continuation the previous figure (Figure 5.25). dsC$_{28}$(5')-ODN[b] stands for double-stranded C$_{28}$(5')-GEM91, carrying Alexa 488 fluorophore bound to the 5'-end of the AntiODN strand. The concentration with an asterisk corresponds to the concentration of Alexa 488-labelled strand. White squares represent the zoom taken, corresponding to the images below. LOC (green) and lipid (red) staining are shown in the left and centre columns, respectively. The right column displays the merging of both detection channels. Images were taken at 22ºC. Scale bars represent 10 µm.

As seen in Figure 5.26, reproducible Alexa 488-enriched rounded structures were again detected, suggesting that these structures were at least in part formed by this LOC. In the present case, these structures mostly contained both fluorescent probes (*i.e.*, DiD and Alexa 488). Indeed, some of them were close to L_o phases and bilayer defects or mica holes suggesting their generation at those boundaries. It must be said that at the present we cannot exclude the structures to be as well generated at bilayer areas with no boundaries due to the localisation of high LOC concentrations at a certain spots. This observation is partly in agreement with the results achieved by incubation of SPBs composed of DOPC/eSM/Chol (2:2:1) with either single stranded and double stranded $C_{28}(5')$-ODNs labelled with Alexa 488 in the 3'-termini of the $C_{28}(5')$-ODN strand (Figures 5.7-5.9 and 5.19-5.23, respectively). The structures were as well observed in this case but their origin and nature may vary with regard to the others.

Another important aspect to be mentioned is the fact that in this experiment, a morphological rearrangement of the L_o domain was observed from irregular to more rounded shapes (Figure 5.25). This phenomenon was also observed by single stranded $C_{28}(5')$-ODN when higher concentrations (*i.e.*, 50 nM) were used from the beginning of the experiment, resulting in circle-shaped L_o domains. This could be a result of a massive LOC incorporation into the bilayer, and possibly into the L_o phase resulting in important changes on domains' line tension leading to the corresponding morphological rearrangement.

In accordance with the results obtained in GUVs and SPBs, it can be assumed that C_{28} anchor acts similarly when conjugated to either single or double stranded ODNs, being capable of inserting into both L_d and L_o domains of GUVs composed of DOPC, DOPC/eSM/Chol (2:2:1) and eSM/Chol (2:1) and SPBs composed of DOPC/eSM/Chol (2:2:1) and generating reproducible Alexa 488-enriched rounded structures in all the SPBs tested. These structures arise near boundaries where higher instability could be assumed, namely L_d-L_o phase and/or lipid-mica boundaries.

226

5.2.2 Cell systems

5.2.2.1 Study of the internalisation routes of C$_{28}$(5')-ODN in HeLa cell line

By using flow cytometry and confocal microscopy we studied the internalisation process of C$_{28}$(5')-ODN in HeLa cells by analysing the uptake inhibition after treating cells at low temperature, with several active molecules that selectively block the different endocytic pathways or silencing clathrin- and caveolae-dependent pathways by appropriate siRNA molecules. HeLa cell line was chosen to perform this set of experiments owing to the fact that it is widely used for the characterisation of cell entry (Bayer *et al.*, 1998).

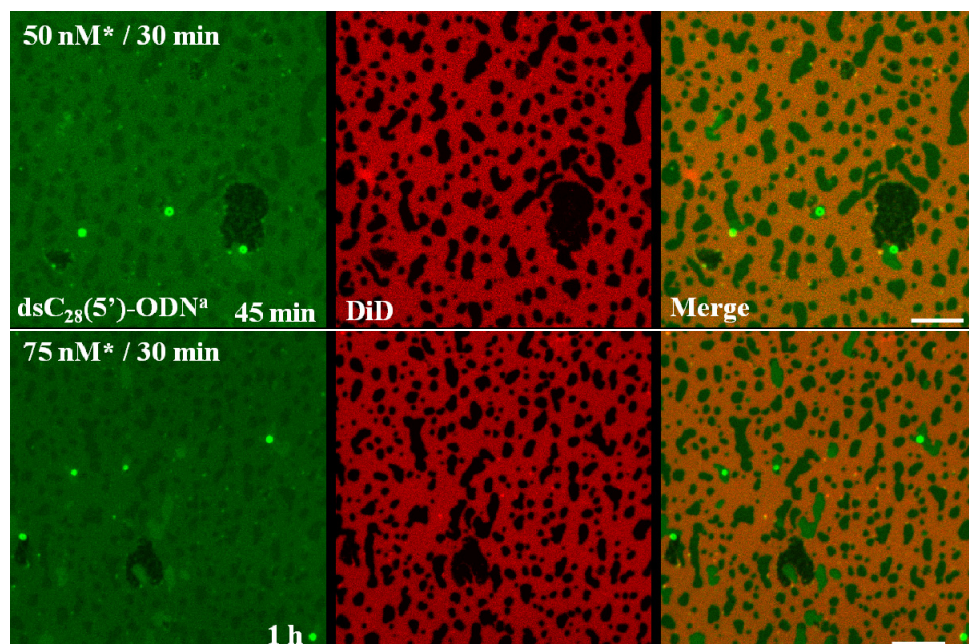Since C$_{28}$(5')-ODN is considered to be naturally cell membrane permeable, as previously observed in both membrane lipid model systems and HeLa cells, we first carried out cellular uptake experiments at different temperatures (37ºC and 4ºC) in these cells to elucidate whether enhanced cellular uptake of this compound was energy-dependent.
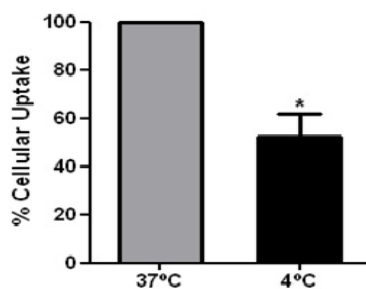
Figure 5.27 Cellular uptake of Alexa 488-labelled C28(5')-GEM91 is temperature dependent in HeLa cells. Cells were seeded (1.25×10^5 cells/well) in 24 well plates and cultured overnight in appropriate growth medium. The next day cells were washed with DPBS and incubated with 500 nM Alexa 488-labelled C$_{28}$(5')-GEM91 for 2 h at 37ºC or 4ºC. After incubation, cells were washed three times, resuspended in ice-cold PBS, and analysed by flow cytometry. Cellular uptake achieved at 37ºC was considered as the maximum internalisation (100%). Results are expressed as percentage of cellular uptake ± SEM of 5 independent experiments performed in duplicate (*p<0.05).

As shown in Figure 5.27, the C$_{28}$(5')-ODN internalisation was significantly decreased at 4ºC in comparison with that at 37ºC. Hence, this observation suggests that the C$_{28}$(5')-ODN uptake is most likely through energy-dependent endocytic pathways.

In order to investigate the role of a possible endocytosis mechanism, HeLa cells were treated with several inhibitors prior to incubation with Alexa 488-labelled C$_{28}$(5')-ODN. Thus, seven endocytic inhibitors were used to determine which endocytic pathway may be involved in the uptake process with C$_{28}$(5')-ODN (Table 5.1). In the following table the inhibitory pathways and concentrations used by these inhibitors are listed. The concentrations of inhibitors employed were based on other's work reported in the literature (Bayer *et al.*, 1998; Rejman *et al.*, 2005; Zaro *et al.*, 2005; Zhang *et al.*, 2009; Bawa *et al.*, 2011).

Endocytic pathway	Inhibitors	Concentration
Clathrin-dependent endocytosis	Hypertonic sucrose medium	0.3 M
	Chlorpromazine (CPZ)	10 µg/ml
Caveolae-dependent endocytosis	Filipin	5 µg/ml
	Genistein	200 µM
Macropinocytosis	5-(N,N-dimethyl)amiloride (DMA)	100 µM
	Cytochalasin D (Cyt D)	10 µg/ml
Microtubule-mediated endocytosis	Nocodazole	20 µM

Table 5.1 List of endocytic inhibitors used in this study, specifying the concentration tested and the internalisation route blocked.

To rule out that the treatment of cells with inhibitors influences the cellular uptake efficiency of C$_{28}$(5')-ODN, we first investigated the viability of HeLa cells after treatment with endocytic inhibitors by MTS assay, as described in the Experimental procedures section.
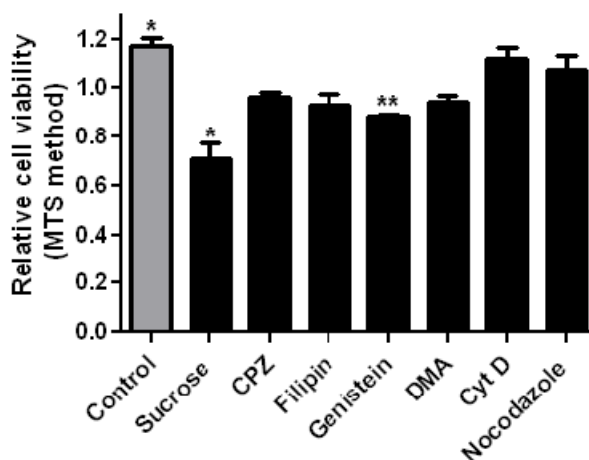
Figure 5.28 Cell cytotoxicity assay performed in HeLa cells in the presence of endocytic inhibitors. Cells were seeded (5×10^3 cells/well) in 96 well plates and incubated overnight in appropriate growth medium. The next day cells were washed with DPBS and incubated in 100 µl OptiMEM in the absence or presence of the endocytic inhibitors for 2 h and 30 min at 37ºC. Selected inhibitors: 0.3 M sucrose, 10 µg/ml chlorpromazine (CPZ), 5 µg/ml filipin, 200 µM genistein, 100 µM 5-(N,N-dimethyl)amiloride (DMA), 10 µg/ml cytochalasin D (Cyt D), 20 µM nocodazole. Untreated cells were used as negative control (Control). Data were normalized to the control value (untreated cells at 0 h of incubation) and are expressed as the mean ± SEM of 3 independent experiments performed in triplicate (*p<0.05; **p<0.01).

Apparently, none of the inhibitors was cytotoxic under these experimental conditions, except for sucrose solution (Figure 5.28). Nevertheless, ~70% of the HeLa cell population still survived at 0.3 M sucrose concentration. Thus, these findings suggest that cytotoxicity can be ruled out as an explanation of the effects of the endocytic inhibitors tested.

229

As a control experiment, FITC-labelled transferrin was used as a marker of clathrin-dependent pathway to probe the effectiveness of the inhibitors selected to block this route (*i.e.*, CPZ and sucrose).
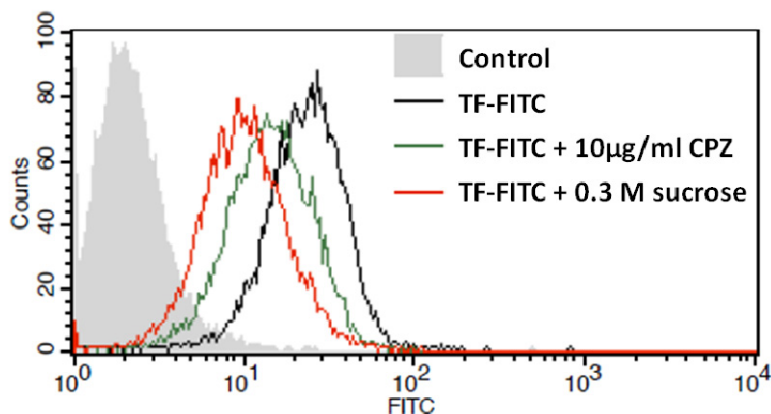
Figure 5.29 Effects of chlorpromazine (CPZ) and sucrose inhibitors on the cellular uptake of human transferrin-FITC in HeLa cells. Cells were seeded (1.25×10^5 cells/well) in 24 well plates and cultured overnight in appropriate growth medium. The next day cells were washed with DPBS and pretreated in the presence of 10 µg/mL CPZ or 0.3 M sucrose for 30 min at 37ºC in OptiMEM. Then, cells were incubated with 100 µg/ml transferrin-FITC (TF-FITC) for 2 h at 37ºC. After incubation, cells were washed three times, resuspended in ice-cold PBS, and analysed by flow cytometry. This is a representative histogram showing the inhibition mediated by CPZ (42.61%) and sucrose (62.12%) on the cellular uptake of TF-FITC. Control stands for untreated cells, representing cell basal fluorescence intensity.

As expected, CPZ and hypertonic sucrose solution were able to block the internalisation of clathrin-dependent FITC-labelled transferrin by 42.61% and 62.12%, respectively (Figure 5.29).
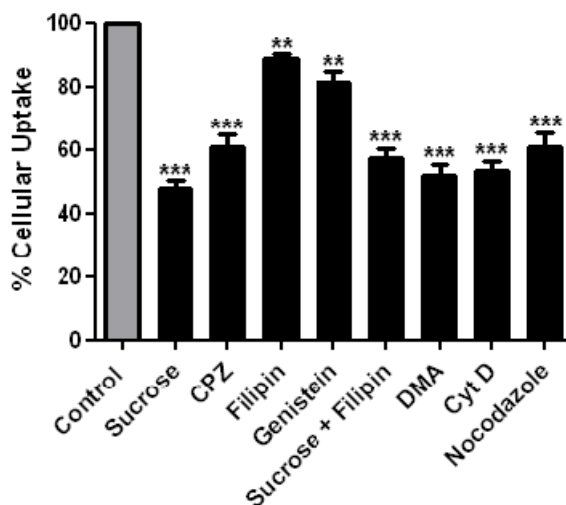
Figure 5.30 Effects of inhibitors on the cellular uptake of Alexa 488-labelled C$_{28}$(5')-GEM91 in HeLa cells. Cells were seeded (1.25 × 10^5 cells/well) in 24 well plates and cultured overnight in appropriate growth medium. The next day cells were washed with DPBS and pretreated in the presence of the appropriate endocytic inhibitor for 30 min at 37ºC in OptiMEM. Then, cells were incubated with 500 nM Alexa 488-labelled C$_{28}$(5')-GEM91 for 2 h at 37ºC. After incubation, cells were washed three times, resuspended in ice-cold PBS, and analysed by flow cytometry. Selected inhibitors: 0.3 M sucrose, 10 µg/ml chlorpromazine (CPZ), 5 µg/ml filipin, 200 µM genistein, 100 µM 5-(N,N-dimethyl)amiloride (DMA), 10 µg/ml cytochalasin D (Cyt D), 20 µM nocodazole. Cellular uptake achieved in the absence of endocytic inhibitors was considered as the maximum internalisation (100%), specified as Control in the figure. Results are expressed as percentage of cellular uptake ± SEM of 5 independent experiments performed in duplicate (**p<0.01; ***p<0.001).

As depicted in Figure 5.30, pre-treatment of HeLa cells with filipin or genistein, both reported to block caveolae-mediated uptake processes (Schnitzer *et al.*, 1994; Orlandi and Fishman, 1998), prior to incubation with the LOC had no remarkable effect in its uptake.

By contrast, cells pretreated with CPZ and sucrose, which are known to perturb clathrin-mediated endocytosis (Wang *et al.*, 1993; Zhang *et al.*, 2009), showed a more noticeable decreased LOC internalisation, suggesting that this entry route may be involved in the LOC uptake. The combination of sucrose and filipin did not cause any further decrease in LOC uptake, suggesting that this inhibition could only be attributable to the effect of sucrose.

Nocodazole was used to disrupt microtubules which are known to play an important role in the regulation of cargo trafficking within endosomal compartments, interfering with the later phase of endocytosis from early to late endosomes (Zelphati and Szoka, 1996a; Vasquez *et al.*, 1997; Huang *et al.*, 2011). As seen in Figure 5.29, this inhibitor showed similar results to those obtained by CPZ pretreatment, reinforcing the view that microtubules could be in part involved in the internalisation of this LOC.

To inhibit macropinocytosis, a process of bulk fluid-phase endocytosis, cytochalasin D and DMA were used. Several studies demonstrated that cytochalasin, leading to disassembly of actin filaments, completely inhibits both macropinocytosis and micropinocytosis (Valberg *et al.*, 1981; Gottlieb *et al.*, 1993; Jackman *et al.*, 1994). On the other hand, DMA is an inhibitor of sodium/proton exchange which decreases cytosolic pH and thereby inhibits the activation of specific GTPases in submembraneous zones (Kälin *et al.*, 2010; Koivusalo *et al.*, 2010). The pretreatment with cytochalasin D and DMA markedly diminished C$_{28}$(5')-ODN uptake, implying that macropinocytosis may be also involved in the internalisation of this LOC.

Specific siRNAs to clathrin (heavy chain) HC and caveolin-1 proteins were also used to silence these two proteins in HeLa cells, prior to incubation with the LOC. These proteins are considered as key molecules in clathrin- and caveolae-dependent pathways, respectively.

A)
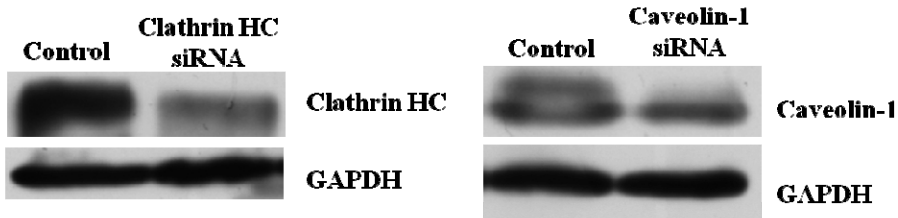
B)
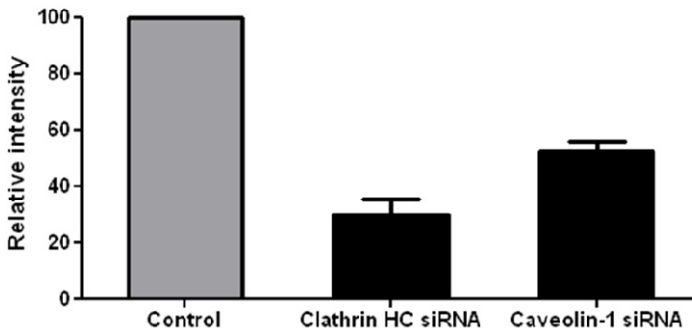
C)
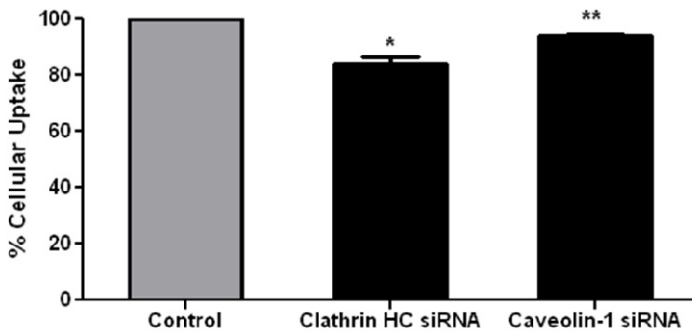
Figure 5.31 Role of clathrin and caveolae-dependent pathways in the cellular uptake of Alexa 488-labelled C$_{28}$(5')-GEM91 in HeLa cells. (A) Western blotting assay of clathrin heavy chain (HC) and caveolin-1 protein expression in HeLa cells after treatment with the appropriate siRNA molecule. The procedure was performed as described in Experimental procedures section. The presence of clathrin HC (left) and caveolin-1 (right) was analysed using an antibody specific to clathrin HC and caveolin-1 proteins, respectively. Equal loading of protein was monitored using a specific antibody to GAPDH

protein. Results are representative of one experiment and were confirmed in an additional experiment. (B) Results of scanning densitometry of the exposed films. Data are expressed as arbitrary units of intensity relative to control value (Control) which stands for untreated sample and results are the mean ± SD of 2 independent experiments. (C) Cellular uptake of Alexa 488-labelled C28(5')-GEM91 in HeLa cells pretreated with clathrin HC and caveolin-1 siRNAs. After siRNA treatment, cells were seeded (1.25×10^5 cells/well) in 24 well plates and cultured overnight in appropriate growth medium. The next day cells were washed with DPBS and incubated in OptiMEM with 500 nM Alexa 488-labelled C$_{28}$(5')-GEM91 for 2 h at 37ºC. After incubation, cells were washed three times, resuspended in ice-cold PBS, and analysed by flow cytometry. Clathrin HC siRNA and caveolin-1 siRNA stand for HeLa cells pretreated with clathrin HC siRNA and caveolin-1 siRNA, respectively. Cellular uptake achieved in siRNA untreated cells (Control) was considered as the maximum internalisation (100%). Results are expressed as percentage of cellular uptake ± SEM of 3 independent experiments performed in duplicate (*$p<0.05$; **$p<0.01$).

As shown in Figure 5.31, siRNA treatment efficiently silenced the expression of clathrin HC and caveolin-1 proteins. However, no remarkable decrease on LOC internalisation was observed under these experimental conditions.

In order to validate aforementioned findings obtained in the presence of endocytic blockers, the cellular uptake and intracellular trafficking of C$_{28}$(5')-ODN were studied by fluorescence confocal microscopy, which could reveal the co-localisation of several fluorescently-labelled cellular markers (Figure 5.32).

DMA-pretreated cells were incubated with Alexa 488-labelled C$_{28}$(5')-ODN, followed by cell fixation and incubation with Alexa Fluor 546-Phalloidin for actin staining. As seen in Figure 5.32A, LOC was mainly visualised at the plasma membrane, co-localising with actin filaments (shown as yellow zones in the merge image).
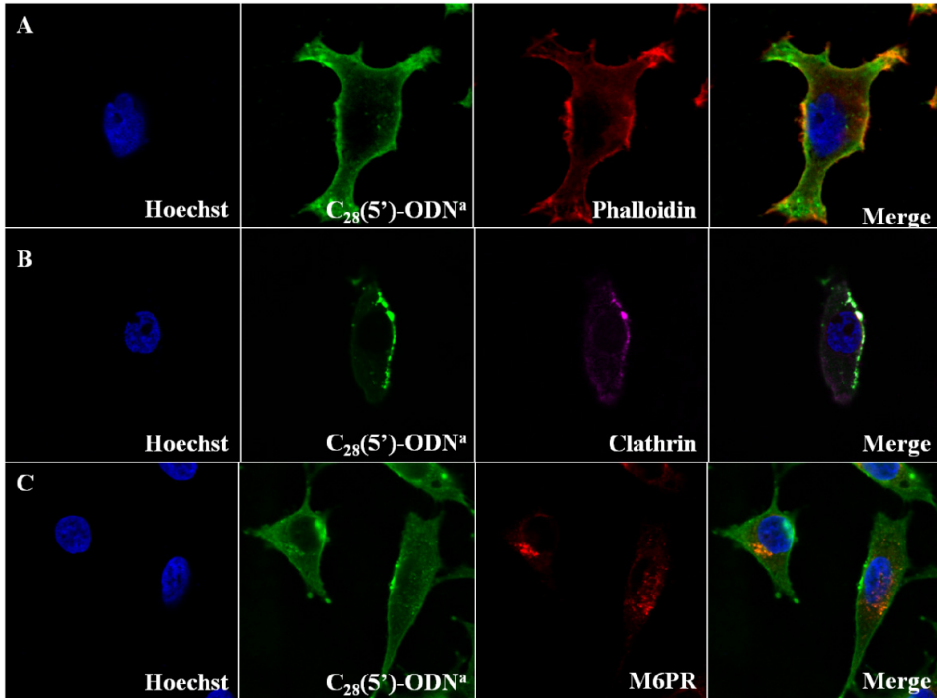
Figure 5.32 Co-localisation assay of 100 nM Alexa 488-labelled C_{28}(5')-ODN cellular uptake with endocytic markers in HeLa cells in the presence of endocytic inhibitors. Cells were seeded (5×10^4 cells/well) in 8 well-Lab-Tek™ Chamber slides pretreated with Poly-L-lysine solution and cultured overnight in appropriate growth medium. The next day cells were washed with DPBS and pretreated in OptiMEM in the presence of the appropriate endocytic inhibitor for 30 min at 37ºC. Then, cells were incubated with 100 nM Alexa 488-labelled C_{28}(5')-GEM91 for 2 h at 37ºC. After incubation, cells were washed three times, fixed with 4% (w/v) PFA and immunostained with an endocytic marker followed by Hoechst treatment for nucleus staining. ODN[a] stands for GEM91-(3')Alexa 488. (A) HeLa cells pretreated with 100 μM DMA. Alexa Fluor 546-Phalloidin was used for actin staining (red). (B) HeLa cells pretreated with 0.3 M sucrose. Primary antibody to Clathrin HC and Alexa Fluor 633 secondary antibody were used for clathrin staining (magenta). (C) HeLa cells pretreated with 5 μg/ml filipin. Primary antibody to mannose 6 phosphate receptor (M6PR) and Alexa Fluor 546 secondary antibody were used for late endosome staining (red). Nucleus (blue) and LOC (green) staining are shown in the left and centre columns, respectively. The right column displays the merging of middle detection channels, showing co-localisation in yellow (upper and bottom panels) or white (middle panel).

235

HeLa cells were also incubated with Alexa 488-labelled C$_{28}$(5')-ODN in the presence of hypertonic sucrose medium. In this case, clathrin HC was used as a marker of clathrin-dependent pathway. As shown in Figure 5.32B, poor LOC internalisation was also observed. In addition, a remarkable co-localisation of the LOC and clathrin HC was achieved near the plasma membrane (shown as white spots in the merge image).

Finally, filipin-pretreated cells were incubated with Alexa 488-labelled LOC followed by cell fixation and M6PR staining. The M6PR is responsible for the trafficking of acid hydrolases from the Trans-Golgi network to the endosome. Once in the endosome, the M6PR and its ligand travel to the lysosomal compartment, where acidic pH results in the dissociation of ligand from the receptor, at which time the M6PR resides back to the TGN (Ghosh *et al.*, 2003; Goldenberg *et al.*, 2007). Thus, it is commonly used as a marker of late endosomes. Under these experimental conditions, intracellular LOC fluorescence was easily visualised, with a slight M6PR co-localisation (shown as yellow spots in the merge image of Figure 5.32C).

Taking into account all these results, it can be assumed that energy-dependent C$_{28}$(5')-ODN internalisation is mainly mediated by macropinocytosis and to a lesser extent by clathrin-mediated endocytosis, where microtubules may also be involved.

5.2.2.2 Cellular uptake behaviour of C$_{28}$(5')-ODN in different cell lines

In order to demonstrate whether the results obtained by C$_{28}$(5')-ODN in HeLa cells were more generally applicable, eight more cell lines were examined. Hence, the first step was to set up a rutine procedure to check whether these cell cultures were contaminated or not by *Mycoplasma*. To study this issue, Venor®GeM *Mycoplasma* Detection Kit was applied regularly in order to ensure the reliability of our results (Figure 5.33).
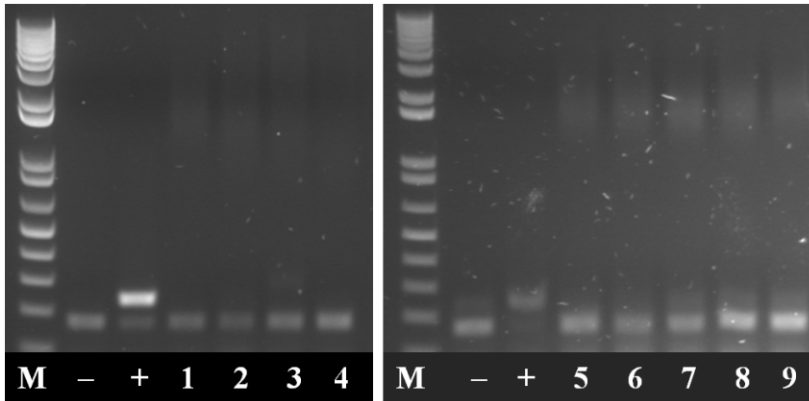
Figure 5.33 PCR products obtained from Mycoplasma detection kit. Cell culture samples tested: (1) HeLa, (2) PANC-1, (3) C2C12, (4) U87.CD4.CXCR4, (5) CHO K1, (6) CHO CR3+, (7) J774A.1 CR3-, (8) J774A.1, (9) RAW 264.7; (-) negative control, (+) positive control; M: 1 Kb Plus DNA Ladder.

Once we tested that the cell cultures were not contaminated by *Mycoplasma*, we then examined whether C$_{28}$(5')-ODN and control-ODN were cytotoxic in these cell lines.
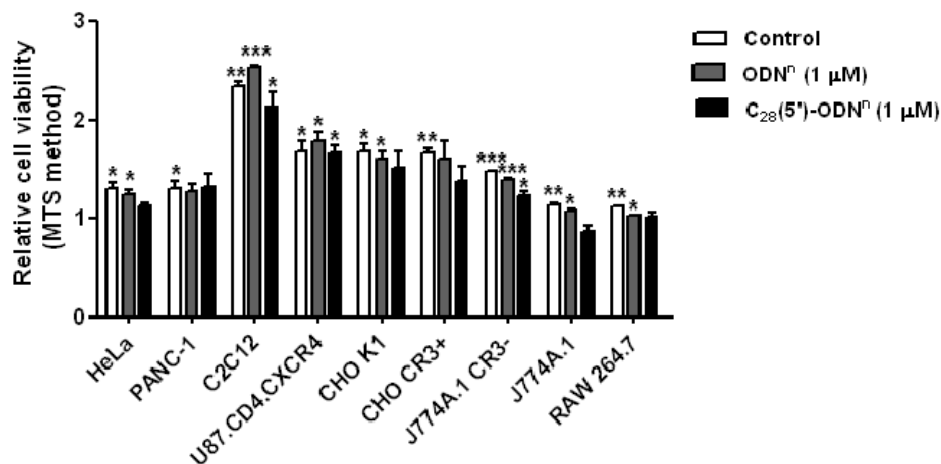
Figure 5.34 Cell cytotoxicity assay performed in the presence of control-ODN and C$_{28}$(5')-ODN in different cell lines. Cells were seeded (5×10^3 cells/well) in 96 well plates and incubated overnight in appropriate growth medium. The next day cells were washed with DPBS and incubated in 100 µl OptiMEM in the absence or presence of the control-ODN or C$_{28}$(5')-ODN (1 µM) for 24 h at 37ºC. Untreated cells were used as negative control (Control); ODN^n stands for GEM91-(3')NH$_2$. Data were normalised to the control value (untreated cells at 0 h of incubation) and are expressed as the mean ± SEM of 3 independent experiments performed in triplicate (*p<0.05; **p<0.01; *** p<0.001).

As observed in Figure 5.34, the LOC concentration (1 µM) had neither cytotoxic nor antiproliferative effect in all cell lines tested during 24 h of incubation. Nevertheless, in J774A.1 and RAW 264.7 cells cell growth was not notably detected compared to the control cells. However, LOC cytotoxicity was only observed in J774A.1 cells, being very low (~80% of the J774A.1 cell population still survived under these conditions).

Thereafter, C$_{28}$(5')-ODN cellular uptake and subcellular localisation profiles were analysed in these cell lines by flow cytometry and confocal microscopy.
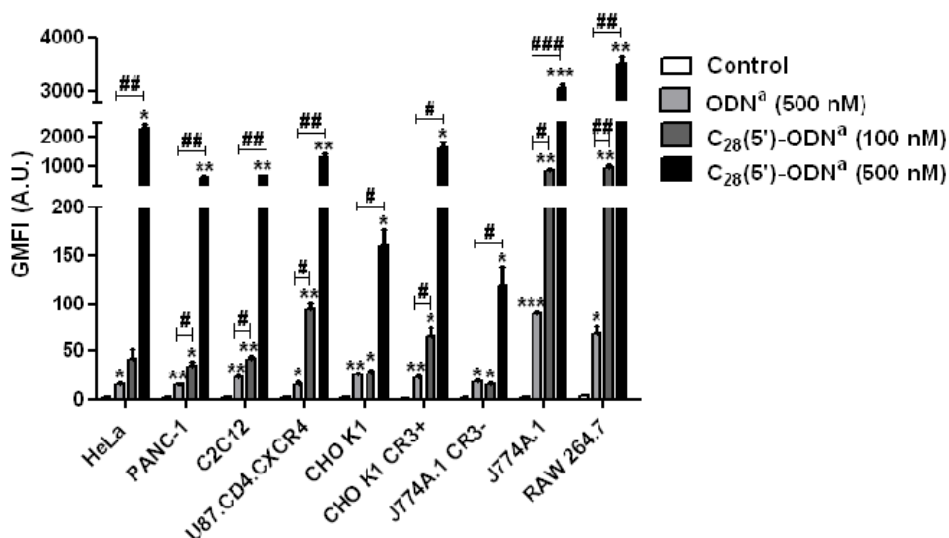
Figure 5.35 Cellular uptake of Alexa 488-labelled control-ODN and C$_{28}$(5')-ODN in different cell lines. Cells were seeded (1.25×10^5 cells/well) in 24 well plates and cultured overnight in appropriate growth medium. The next day cells were washed with DPBS and incubated with 500 nM control-ODN or 100 and 500 nM C$_{28}$(5')-ODN for 4 h at 37ºC in OptiMEM. After incubation, cells were washed three times, resuspended in ice-cold PBS, and analysed by flow cytometry. Control stands for untreated cells, representing cell basal fluorescence intensity; ODN[a] stands for GEM91-(3')Alexa 488. GMFI corresponds to Geometric Mean of Fluorescence Intensity. Results are expressed as GMFI ± SEM of 3 independent experiments performed in duplicate (*p<0.05, **p<0.01 and *** p<0.001 *vs* the control value; #p<0.05, ##p<0.01 and ###p<0.001 *vs* ODN[a] value).

As depicted in Figure 5.35, C$_{28}$(5')-ODN was better internalised in all cell lines tested compared to control-ODN. In particular, U87.CD4.CXCR4, CHO CR3+, J774A.1 and RAW 264.7 cells showed higher internalisation profiles even at 100 nM LOC. Indeed, J774A.1 and RAW 264.7 cell lines showed the highest uptake behaviour for both control-ODN and C$_{28}$(5')-ODN. The latter result is in agreement with previous reports that suggested an enhanced ODN internalisation mediated by β$_2$ integrins (Benimetskaya *et al.*, 1997).
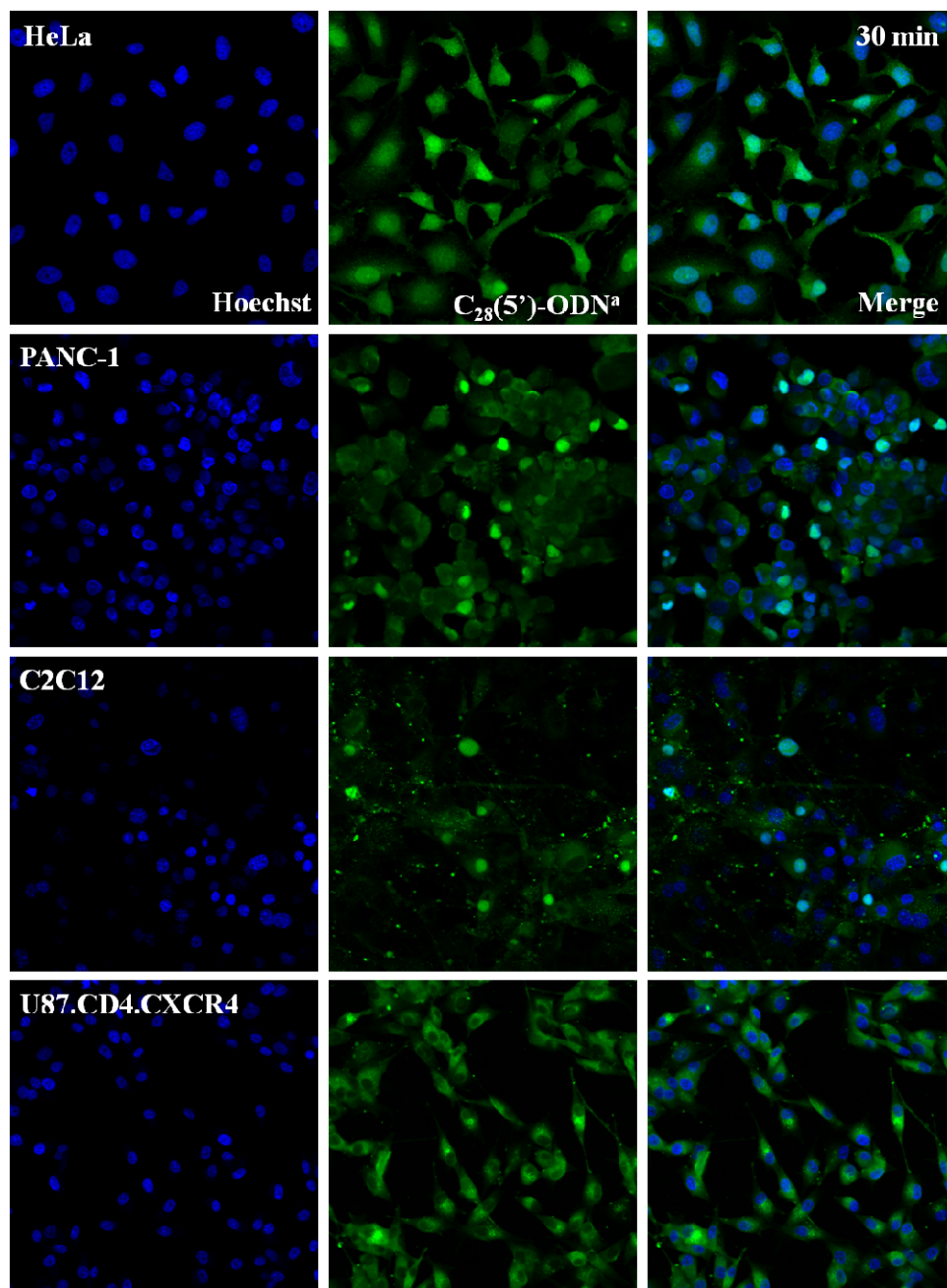
Figure 5.36 Cellular uptake and subcellular localisation of 100 nM Alexa 488-labelled C$_{28}$(5')-ODN in HeLa, PANC-1, C2C12 and U87.CD4.CXCR4 cells after 30 min incubation time. Cells were seeded (2 × 10^4 cells/well) in 96 well-BD Falcon™ Tissue Culture Treated Imaging plates and cultured overnight in appropriate growth medium. The

next day cells were washed with DPBS and incubated with 100 nM Alexa 488-labelled C$_{28}$(5')-ODN for 30 min at 37ºC in OptiMEM. After incubation, cells were washed three times, fixed with 4% (w/v) PFA and treated with Hoechst for nucleus staining. ODN[a] stands for GEM91-(3')Alexa 488. Nucleus (blue) and C$_{28}$ moiety bearing LOC (green) staining are shown in the left and centre columns, respectively. The right column displays the merging of both detection channels. Images were acquired with a 20X objective and zoom factor of 2X.

As seen in Figures 5.36 and 5.37, HeLa, PANC-1 and C2C12 cells first showed a nuclear LOC localisation (at 30 min of incubation) that was further redistributed into the cell cytoplasm after longer time periods (4 h of incubation). By contrast, a weak fluorescence was observed in the nucleus of U87.CD4.CXCR4 cells, being LOC localisation in this cell line more cytoplasmic at short incubation times (30 min). Similarly, at 4 h of incubation this LOC also showed a cytoplasmic distribution (around the nucleus) in this cell line.
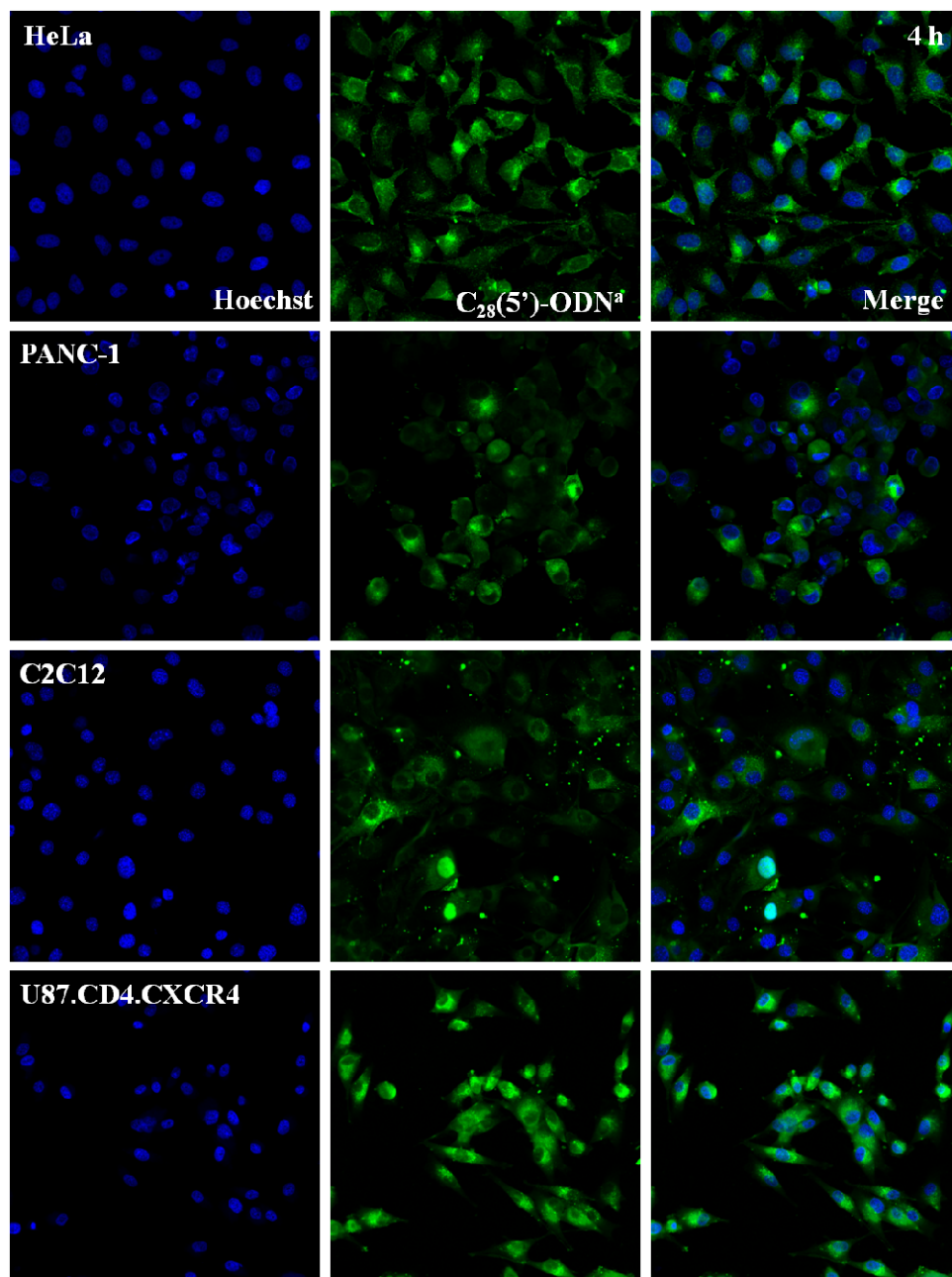
Figure 5.37 Cellular uptake and subcellular localisation of 100 nM Alexa 488-labelled C$_{28}$(5')-ODN in HeLa, PANC-1, C2C12 and U87.CD4.CXCR4 cells after 4 h incubation time. Cells were seeded (2×10^4 cells/well) in 96 well-BD Falcon™ Tissue Culture Treated Imaging plates and cultured overnight in appropriate growth medium. The next day cells were washed with DPBS and incubated with 100 nM Alexa 488-labelled

C$_{28}$(5')-ODN for 4 h at 37ºC in OptiMEM. After incubation, cells were washed three times, fixed with 4% (w/v) PFA and treated with Hoechst for nucleus staining. ODN[a] stands for GEM91-(3')Alexa 488. Nucleus (blue) and C$_{28}$ moiety bearing LOC (green) staining are shown in the left and centre columns, respectively. The right column displays the merging of both detection channels. Images were acquired with a 20X objective and zoom factor of 2X.

CHO K1

Hoechst   C$_{28}$(5')-ODN^a 30 min   Merge

CHO CR3+

J774A.1 CR3-

J774A.1

RAW 264.7

Figure 5.38 Cellular uptake and subcellular localisation of 100 nM Alexa 488-labelled C$_{28}$(5')-ODN in CHO K1, CHO CR3+, J774A.1 CR3-, J774A.1 and RAW 264.7 cells after 30 min incubation time. Cells were seeded (2×10^4 cells/well) in 96 well-BD Falcon™ Tissue Culture Treated Imaging plates and cultured overnight in appropriate growth medium. The next day cells were washed with DPBS and incubated with 100 nM Alexa 488-labelled C$_{28}$(5')-ODN for 30 min at 37ºC in OptiMEM. After incubation, cells were washed three times, fixed with 4% (w/v) PFA and treated with Hoechst for nucleus staining. ODN[a] stands for GEM91-(3')Alexa 488. Nucleus (blue) and C$_{28}$ moiety bearing LOC (green) staining are shown in the left and centre columns, respectively. The right column displays the merging of both detection channels. Images were acquired with a 20X objective and zoom factor of 2X.

CHO K1 — 4 h

Hoechst — $C_{28}(5')$-ODN[a] — Merge

CHO CR3+

J774A.1 CR3-

J774A.1

RAW 264.7

Figure 5.39 Cellular uptake and subcellular localisation of 100 nM Alexa 488-labelled C$_{28}$(5')-ODN in CHO K1, CHO CR3+, J774A.1 CR3-, J774A.1 and RAW 264.7 cells after 4 h incubation time. Cells were seeded (2×10^4 cells/well) in 96 well-BD Falcon™ Tissue Culture Treated Imaging plates and cultured overnight in appropriate growth medium. The next day cells were washed with DPBS and incubated with 100 nM Alexa 488-labelled C$_{28}$(5')-ODN for 4 h at 37ºC in OptiMEM. After incubation, cells were washed three times, fixed with 4% (w/v) PFA and treated with Hoechst for nucleus staining. ODN[a] stands for GEM91-(3')Alexa 488. Nucleus (blue) and C$_{28}$ moiety bearing LOC (green) staining are shown in the left and centre columns, respectively. The right column displays the merging of both detection channels. Images were acquired with a 20X objective and zoom factor of 2X.

CHO K1 and J774A.1 CR3- cell lines showed very weak fluorescence at either 30 min or 4 h incubation times, suggesting an inefficient LOC uptake by these cells (Figures 5.38 and 5.39). This observation is consistent with the results obtained by flow cytometry where these two cell lines showed the worst LOC cellular uptake behaviours.

Similarly to what it was observed in U87.CD4.CXCR4 cells, very weak LOC fluorescence was observed in the nucleus of CHO CR3+, J774A.1 and RAW 264.7 cell lines under these experimental conditions, being more noticeable at the cell cytoplasm (Figures 5.38 and 5.39).

As seen in Figure 5.35, $\alpha_M\beta_2$ integrin presenting cells (*i.e.*, CHO CR3+, J774A.1 and RAW 264.7 cells) showed higher C$_{28}$(5')-ODN uptake than cells lacking this integrin (*i.e.*, CHO K1 and J774A.1 CR3- cells). Related to this fact, previous investigations established an important role of β_2 integrins in the enhancement of ODN internalisation, thereby promoting a receptor-mediated endocytosis (Benimetskaya *et al.*, 1997). Thus, we examined whether this enhanced LOC internalisation was mediated by β_2 integrins.

First, cell surface CD11b expression was analysed by flow cytometry. CD11b (α_M) is a component of the CR3 (CD11b/CD18, also known as $\alpha_M\beta_2$) integrin.

CHO K1 and J774A.1 CR3- cell lines were used as negative controls for cell surface CD11b staining. As observed in Figure 5.40, CHO CR3+ cell population showed a wide FITC peak, implying a heterogeneous cell surface CD11b expression. This result could be related to the fact that in stably transfected cells the expression of the desired protein (*e.g.*, CR3 integrin) is induced by an exogenous agent (*e.g.*, hygromycin B). This phenomenon was not observed in J774A.1 and RAW 264.7 cells, which constitutively express CR3 integrin, leading to an apparently narrow FITC peak.
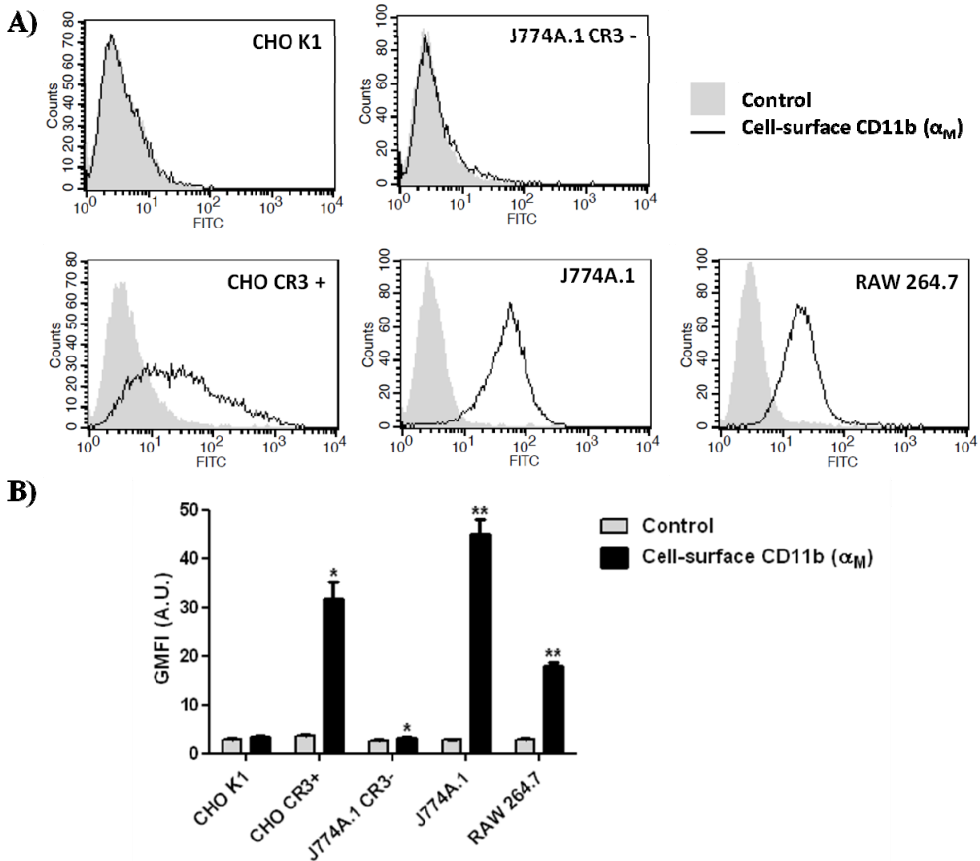
Figure 5.40 Cell-surface CD11b (αM) expression in CHO K1, CHO CR3+, J774A.1 CR3-, J774A.1 and RAW264.7 cells. Cells were seeded (1.25×10^5 cells/well) in 24 well plates and cultured overnight in appropriate growth medium. The next day cells were washed with 0.1% (w/v) BSA dissolved in 1X PBS and scrapped followed by cell-surface CD11b staining by the use of anti-CD11b FITC conjugated antibody, as described in Experimental procedures section. After staining, samples were analysed by flow cytometry. Control stands for untreated cells, representing cell basal fluorescence intensity. (A) Representative histograms of cell-surface CD11b staining corresponding to each cell line tested. Similar results were obtained in 3 independent experiments. (B) GMFI corresponds to Geometric Mean of Fluorescence Intensity. Results are expressed as GMFI ± SEM of 3 independent experiments performed in duplicate (*p<0.05; **p<0.01).

To perform a deeper analysis of the involvement of $\alpha_M\beta_2$ integrins in the LOC uptake, we used soluble fibrinogen, a natural ligand for this integrin, in order to compete with the LOC for the binding sites of this receptor, thereby blocking LOC internalisation, as previously reported by other authors (Zhou *et al.*, 1994; Benimetskaya *et al.*, 1997; Kirsch *et al.*, 2002; Lishko *et al.*, 2004).

In this experiment, again CHO K1 and J774A.1 CR3- cell lines were used as negative controls for β_2-mediated LOC internalisation, which did not vary in the presence of soluble fibrinogen. However, in the presence of soluble fibrinogen the cellular uptake of Alexa 488-labelled C$_{28}$(5')-ODN was significantly blocked in cell-surface $\alpha_M\beta_2$ presenting cells (*i.e.*, CHO CR3+, J774A.1 and RAW 264.7 cells), as depicted in Figure 5.41. These observations suggest that $\alpha_M\beta_2$ integrin is involved in the enhanced internalisation of C$_{28}$(5')-ODN.

B)
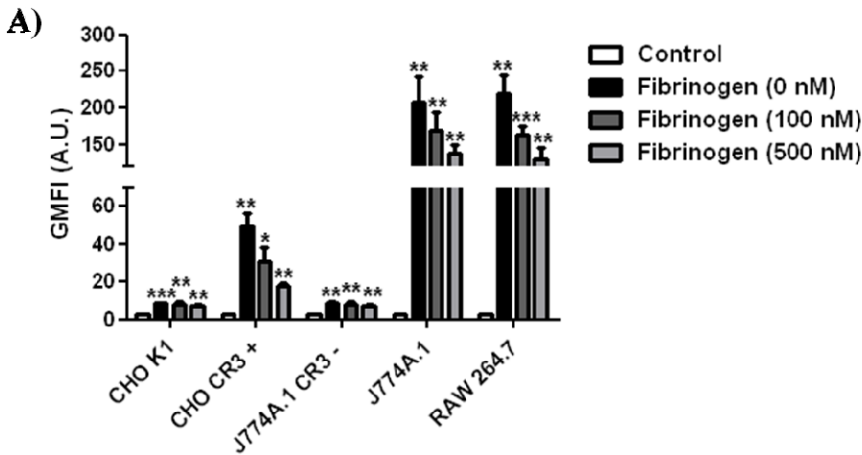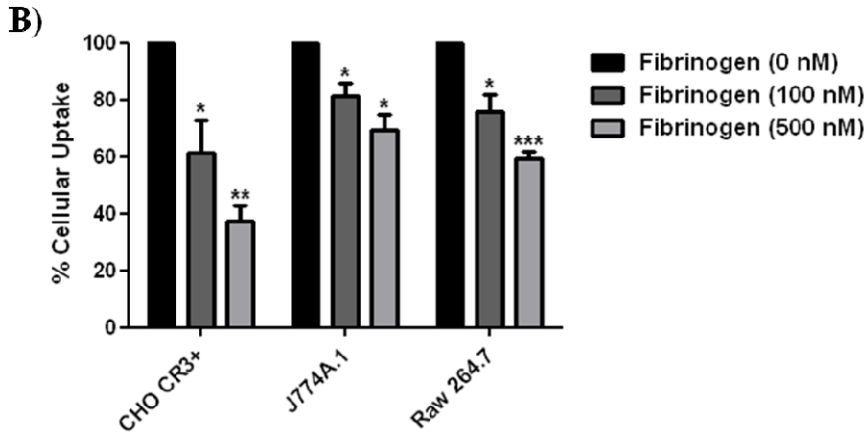
Figure 5.41 Effects of the soluble fibrinogen on cellular uptake of Alexa 488-labelled C$_{28}$(5')-GEM91 in CHO K1, CHO CR3+, J774A.1 CR3-, J774A.1 and RAW264.7 cells. Cells were seeded (1.25×10^5 cells/well) in 24 well plates and cultured overnight in appropriate growth medium. The next day cells were washed with DPBS and pretreated in the presence of 100 nM or 500 nM soluble fibrinogen for 30 min at 37°C in OptiMEM. Then, cells were incubated with 100 nM Alexa 488-labelled C$_{28}$(5')-GEM91 for 30 min at 37°C. After incubation, cells were washed three times, resuspended in ice-cold PBS, and analysed by flow cytometry. (A) Control stands for untreated cells, representing cell basal fluorescence intensity. GMFI corresponds to Geometric Mean of Fluorescence Intensity. Results are expressed as GMFI ± SEM of 4 independent experiments performed in duplicate (*$p<0.05$; **$p<0.01$; ***$p<0.001$). (B) Cellular uptake achieved in the absence of soluble fibrinogen was considered as the maximum internalisation (100%). Results are expressed as percentage of cellular uptake ± SEM of 4 independent experiments performed in duplicate (*$p<0.05$; **$p<0.01$; ***$p<0.001$).

5.3 Discussion

Lipid-anchored RNA and DNA oligonucleotides have emerged as attractive chimeric molecules for various applications in nanobiotechnology, in cell biology, and for the development of therapeutic strategies in medicine (Kurz *et al.*, 2006). Therefore, there is a need of performing a deep analysis of them in order to understand the mechanisms by which these molecules enter the cell, with the aim of reaching their target and exerting their function.

Clearly, the use of model membranes does not include the complex cellular environment, yet it allows for probing certain biophysical aspects of ODN delivery under controlled experimental conditions and well-defined lipid compositions (Gordon *et al.*, 2005).

Taking into account the results obtained in membrane lipid model systems, it can be assumed that C$_{28}$ anchor acts similarly when conjugated to either single or double stranded ODNs, being capable of inserting into both L$_d$ and L$_o$ domains of GUVs composed of DOPC, DOPC/eSM/Chol (2:2:1) and eSM/Chol (2:1) and SPBs composed of DOPC/eSM/Chol (2:2:1). Moreover, it seems to insert initially into the L$_d$ phase of membrane models presenting L$_d$ and L$_o$ phase coexistence, but it is also capable of incorporating into membrane models in pure L$_o$ [eSM/Chol (2:1)] phase states. As previously discussed in Chapter 4, the conjugation of ODN molecules with two alkyl chains endows them with entirely new properties, leading to their interaction with different lipid membrane domains which may provide several advantages in cell systems in terms of alternative internalisation routes. In this regard, once this LOC is inserted into the lipid bilayer, it could interact with a number of transmembrane proteins involved in distinct uptake pathways, thereby inducing its internalisation through different routes.

Moreover, the increase in the hydrophilicity of the LOC by hybridisation of the antisense ODN strand (*i.e.*, GEM91) with its complementary strand (*i.e.*, AntiGEM91), did not seem to alter the binding properties of C_{28} moiety. Hence, this lipid moiety could be considered a promising conjugation anchor to be analysed in a wide range of nucleic acid-based molecules being either single or double stranded compounds.

Interestingly, reproducible Alexa 488-enriched rounded structures were visualised in all the SPB systems tested after their incubation with either single or double stranded LOC, suggesting that these structures were at least in part formed by this LOC. These observations could be related to the bilayer-couple hypothesis, initially popularised by Sheetz and Singer in 1974, which postulates that the two halves of a closed lipid bilayer, by virtue of asymmetries between the bilayer leaflets, could have differential responses to various perturbations (Sheetz and Singer, 1974; Sheetz *et al.*, 1976). Thus, a relative increase in surface area of one leaflet of a closed bilayer (*e.g.*, by the insertion of this LOC to the outer leaflet) is predicted to increase spontaneous curvature of the bilayer. To minimise its energy state and maintain hydrophobic and van der Waals interactions between the leaflets, an unopposed bilayer will conform to its spontaneous curvature (Nossal and Zimmerberg, 2002). Specifically, the leaflet to which additional surface area is added will be the side to which the bilayer will deform in compensation (Farsad and De Camilli, 2003). In this regard, the bilayer-coupled theory could explain the mechanism through which this LOC affect morphological changes in planar membranes (*e.g.*, SPBs). By physically inserting into the outer face of the bilayer, the LOC could cause membrane deformation to the exterior due to the big hydrophilic part of the LOC.

These particular structures were bigger than 1 µm in diameter and arose near boundaries where higher instability could be assumed, namely L_d-L_o phase and/or lipid-mica boundaries.

253

Indeed, it is long known that the boundary between domains of different composition provides an energy source for both membrane budding and fission (Lipowsky, 1992). As for any phase boundary, the membrane domain boundary presents the excess energy associated with the "unhappiness" of the lipid molecules that are surrounded only partially by their preferred companions (*e.g.*, by those having similar lipophilic tails) (Kuzmin *et al.*, 2005). The associated stress is characterised by the line tension, the energy required to create the unit length of the boundary (Lipowsky, 1992). The line tension tends to minimise the boundary length, leading to the budding of the lipid domain and formation of a thin neck (Schmid and Frolov, 2011). Related to this fact, in SPBs composed of DOPC/eSM/Chol (2:2:1), cholesterol could also favour the budding process of LOC containing structures localised at the boundary between L_d and L_o domains since cholesterol could influence on membrane structure through differential partitioning, probably minimising the energy needed for budding by both decreasing local membrane stiffness and by preserving hydrophobic and van der Waals forces between the leaflets as the bilayer deforms (Baba *et al.*, 2001; Brown *et al.*, 2001, 2002).

In addition, some of these Alexa 488-enriched structures were partially static in time whereas other dynamic structures were in continuous motion showing more tubular-like shape than rounded-like shape. A possible explanation for this observation is that there is a force determined by the aforementioned line tension, which is inevitably associated with the edge of the morphological domain (MOD) formed by this LOC, and intrinsically linked to the fact that molecules localised on the edge want to be inside the MOD (Lipowsky, 1992; Koyhama *et al.*, 2003). This edge energy can be minimised by decreasing the size of the edge through transformation of a planar or slightly curved domain with a large edge into a spherical bud with a small edge (Lipowsky *et al.*, 1992). Thus, line tension stimulates MOD maturation and generally imposes spherical morphology, similarly to that observed in partially static LOC-containing MODs generated in our work.

Also, the morphological reproducibility of these LOC-containing MODs could be related to the Brownian ratcheting principle as follows: a MOD's growth is driven by random thermal fluctuations in its shape, and the template (the molecule, usually a protein, with a role in stabilising the domain shapes) catches and stabilises only those shapes that match the template geometry (Shnyrova *et al.*, 2009). According to the latter event, in this work the LOC itself could play the template role.

Moreover, LOC-driven generation of such structures might as well reinforce LOC preference for highly curved membranes connected with various internalisation routes.

On the other hand, in order to study the biological relevance of C$_{28}$(5')-ODN, we first analysed the internalisation pathways involved in the cellular uptake of this LOC in HeLa cells. Experiments performed at 37ºC and 4ºC demonstrated profound temperature dependence in the cellular internalisation of this compound, suggesting that its uptake is most likely through energy-dependent endocytic pathways. Similar results were obtained by Nelson and co-workers who reported a temperature dependent cellular uptake of myristoilated cargos (Nelson *et al.*, 2007).

Understanding the entry mechanism of a molecule is still a challenge in part due to a lack of pharmacological inhibitors that specifically inhibit a single pathway leaving delivery through other avenues unperturbed. It suggests that these agents, directly or indirectly, could be altering a multitude of endocytic processes (Fretz *et al.*, 2006). Furthermore, complete inhibition is not often observed, implying that different pathways may be operating simultaneously or may take over if one pathway is blocked (Hoekstra *et al.*, 2007).

Taking into account the results obtained in the presence of endocytic inhibitors and with fluorescently-labelled cellular markers, it can be assumed that C$_{28}$(5')-ODN enters the cell mainly via macropinocytosis and in part through clathrin-dependent endocytosis in HeLa cells although complete inhibition was not achieved by these agents. However, siRNA treatment performed to silence specifically clathrin HC protein showed no remarkable dependence on clathrin pathway. A possible explanation for this result could be the compensation of the uptake process by other pathways such as macropinocytosis due to the inhibition of clathrin-mediated endocytosis. Similarly, the effect achieved by sucrose inhibitor was non-specific since it not only blocks clathrin-dependent endocytosis but also fluid-phase endocytosis, thereby affecting other endocytic pathways, such as macropinocytosis (Bradley *et al.*, 1993; Synens *et al.*, 1999; Ivanov, 2008). Nevertheless, the incorporation of this LOC into both L$_d$ and L$_o$ domains, could probably lead to an indirect and little internalisation of the LOC by other entry pathways owing to its presence at the plasma membrane.

Macropinocytosis is a term commonly used to describe a receptor-independent form of endocytosis that occurs via the formation of actin-driven membrane protusions resulting in extended external domains of the plasma membrane that engulf large volumes of extracellular fluid (Maniak, 2001; Amyere *et al.*, 2002). Material ingested by macropinocytosis is eventually invaginated as macropinosomes. In addition, this process is usually used by cells to internalise relatively large particles (*i.e.*, 1-5 µm in diameter) (Swanson and Watts, 1995; Conner and Schmid, 2003; Patel *et al.*, 2007). This description could be also related to the specific LOC-containing MODs visualised in SPBs, since they were bigger than 1 µm in diameter and could be internalised by this non-receptor mediated endocytosis if generated in cells.

Unlike endosomes generated by clathrin- and caveolar-mediated endocytosis, macropinosomes were thought to be inherently leaky vesicles, if compared with other types of endosomes (Norbury *et al.*, 1995; Meier *et al.*, 2002).

Notably, although the pH of the macropinosomes decreases, in some cell types the fluid content of the macropinosomes do not tend to merge with the degradative pathway, preventing fusion with lysosomes and further degradation by lysosomal enzymes (Hewlett *et al.*, 1994; Hamasaki *et al.*, 2004; Wadia *et al.*, 2004; Holzer and Howell, 2006; Ruozi *et al.*, 2009). Hence, by selecting this entry pathway the C_{28}(5')-ODN molecule could efficiently reach the nucleus and cytoplasm, avoiding the destabilising lysosomal environment. These observations are consistent with our results because this LOC was capable of reaching the nucleus of HeLa cells in an efficient manner, suggesting that the selected entry pathway provided a successful intracellular fate (*i.e.*, the nucleus).

Although the universality in membrane traffic, each cell type shows major unique features which obviously may influence intracellular delivery and traffic of the compound to be internalised (Watson *et al.*, 2005). Thus, it can be assumed that a particular cell type may select a specific uptake pathway for the internalisation of a delivery system leading to an uptake efficiency, which may largely differ from those achieved by other cell types selecting different internalisation routes. Related to this assumption, the results obtained in the cellular uptake and subcellular localisation assays imply that C_{28}(5')-ODN can be localised mostly in the nucleus of several but not all the cell lines tested under these experimental conditions, and be further redistributed to the cytoplasm, around the nucleus space. Likewise, the transport of ODNs first to and then out of the nucleus was previously reported by other authors (Forsha *et al.*, 2010). These observations are also in agreement with the results achieved by Petrova and co-workers who reported that the efficiency of cellular accumulation of lipophilic siRNAs was dependent upon the type of cell line tested (Petrova *et al.*, 2012).

A further aspect that deserves some comment is the enhanced cellular uptake of ODN and C_{28}(5')-ODN by $\alpha_M\beta_2$ integrin presenting cells compared to those lacking the expression of this receptor.

In addition, the subcellular distribution of this LOC in $\alpha_M\beta_2$ integrin presenting cells was similar to that observed in U87.CD4.CXCR4 cells. This is in agreement with previous investigations that established an important role of β_2 integrins in the enhancement of ODN internalisation, thereby promoting a receptor-mediated endocytosis (Benimetskaya *et al.*, 1997). Moreover, C$_{28}$(5')-ODN uptake in U87.CD4.CXCR4 cells could be also triggered by CD4 receptor-mediated endocytosis as it has been reported that recombinant soluble CD4 can bind to alkylating phosphodiester ODNs (Benimetskaya *et al.*, 1995), although deeper analysis should be done to confirm this hypothesis.

CD11b (α_M) staining used in this work only corresponds to the whole cell-surface CD11b expression, without providing information about the larger quantity that exists as a cytoplasmic pool, which is inserted into the plasma membrane in response to the treatment of the cells with specific molecules such as cytokines and lipids (Benimetskaya *et al.*, 1997). Moreover, not all the $\alpha_M\beta_2$ integrins present on the cell surface are available since they need to be activated to acquire their ligand-binding capacity. Integrin activation involves both a conformational change in the $\alpha\beta$ heterodimer and the clustering in the plasma membrane of laterally diffusing integrins. The latter effect, which increases the valency (avidity) of integrins *vs* their substrate, has sometimes been proposed as the essential event regulating integrin activation (Stewart *et al.*, 1998; van Kooyk and Figdor, 2000; Bouaouina *et al.*, 2004). Therefore, this experiment only reinforced the view that these three cell lines express CD11b (α_M) in the cell-surface, which could interact, if activated, with the LOC at the plasma membrane, leading to its enhanced internalisation. Indeed, the use of soluble fibrinogen to examine the role of $\alpha_M\beta_2$ integrin in this cell-entry process confirmed that C$_{28}$(5')-ODN uptake was significantly blocked in cell-surface $\alpha_M\beta_2$ presenting cells, suggesting the direct involvement of this receptor in LOC internalisation.

Hence, C$_{28}$ lipid moiety provides better cellular incorporation by macropinocytosis without causing cytotoxicity in cells or altering the binding properties of the ODN itself, thereby enabling binding to different molecules, such as receptors present on the cell-surface, intracellular proteins involved in the intracellular ODN transport, complementary strands and target mRNA molecules. All these features make C$_{28}$ lipid modification a good conjugation candidate for improving ODN delivery.

Chapter 6:

Conclusions

Chapter 6: Conclusions

1. Carbohydrate-oligonucleotide conjugates (COCs) presenting a certain distance (15 to 18 atoms) between DNA and sugar modification showed the best incorporation pattern into the target cell. Thus, it seems to be a necessary requirement to pinpoint a defined distance (15 to 18 atoms) between the DNA molecule and the sugar moiety for further promising COC design.

2. Lipid-oligonucleotide conjugates (LOCs) presenting longer or double-tailed lipid modifications (*i.e.*, with higher hydrophobicity) showed the best incorporation behaviour into both membrane lipid model and cell systems. The dual saturated lipid neighbouring moiety (C_{28}) at the 5'-termini of the ODN turn out to be the most powerful lipophilic anchor, being capable of inserting into both L_d and L_o domains.

3. C_{28} lipid moiety provides efficient cellular incorporation by macropinocytosis without causing cytotoxicity in cells or altering the binding properties of the ODN itself. All these features make C_{28} lipid modification a good conjugation candidate to be analysed in a wide range of nucleic acid-based molecules for improving ODN delivery.

Euskaraz landutako

atalburua

Euskaraz landutako atalburua

Laburpena

Aspaldi jakina da, oligonukleotidoek funtzio interesgarriak bete ditzaketela, esaterako, gene adierazpenaren modulazioa, miRNAren eta proteina espezifikoen funtzioen blokeoa eta immunoestimulazioa (Praseuth *et al.*, 1999; Famulok *et al.*, 2000; Krieg, 2002; Opalinska and Gewirtz, 2002; Tomita *et al.*, 2003; Leuschner *et al.*, 2006; Juliano *et al.*, 2008).

Molekula txiki hauek bete ditzaketen funtzio desberdinen gainean sekulako interesa sortu da, ikerketa-tresna eta agente terapeutikotzat erabiliak izateko (Takeshita and Ochiya, 2006; Elsabahy *et al.*, 2011). Zoritxarrez, oligonukleotidoen ezartze biologikoak itzelezko bi muga aurkezten ditu: molekularen egonkortasun eskasa eta zelula-barneratze murritza.

Hainbat eraldaketa kimikori esker molekulen egonkortasuna hobetu daiteke, nukleasekiko erresistentzia handiagoko konposatuak sortuz (Kurreck, 2003). Zelula-sarrerak eragindako arazoa, aldiz, babesik gabeko oligonukleotidoek duten erabateko barneratze eskasarekin erlazionatuta dago, haien izaera polianionikotik eratorritako karga aldarapen handiek barneratzea oztopatzen baitute. Oligonukleotidoen barneratze egokia funtsezko pausua dela uste da, ekintza zuzena bermatu ahal izateko, hots, nukleora edo zitoplasmara heldu eta bertako itu-molekulei lotzeko (Lemaitre *et al.*, 1987; Alahari *et al.*, 1998). Mintz plasmatikoa zeharkatzeak erabateko zailtasuna suposatzen duenez, zelula-sarrera eraginkorra lortu nahian garraio-sistema egokiren bat garatzea sekulako desafio bihurtu da. Gaur egun, hainbat garraio-sistema garatu dira, zelulek molekula desberdinak barneratzeko erabiltzen dituzten berezko estrategietan oinarritzen direnak. Oro har, garraio-sistema artifizialek hiru ikuspegi desberdinetan oinarri daitezke: kapsulatzea (*i.e.*, liposomak), konplexu-eraketa (*i.e.*, elkarrekintza elektrostatikoen bidezko lipoplexo eta poliplexoen eraketa) eta elkartze edo

konjokatzea (*i.e.*, azido nukleiko zatiari molekula zehatz bat erantsiz, molekula konjokatuak eratzea).

DNA/RNA zati txikiak lotura hauskor edo hauskaitzen bidez molekula aproposekin konjokatzeak zenbait abantaila izan ditzake egitura-aldaketekin alderatuz. Konjokatzeak itu-lekura heltzeko espezifikotasuna igo ez ezik, haien ezaugarri farmakozinetikoak eta zelula-sarreraren eraginkortasuna ere hobetzen ditu, sortu berriak diren DNA/RNA-konjokatuek ezaugarri berri eta hobeak azalduz (Jeong *et al.*, 2009; Singh *et al.*, 2010).

Doktorego-tesi honetan garatu den lan zientifikoa konjokatze ikuspegiaren ikerketan oinarritu da, hots, oligodeoxinukleotido (ODN)-konjokatu desberdinen analisian. Estrategia honek izan ditzakeen aplikazio biak aztertu ditugu: itu-tokira zuzendutako garraio espezifikoa eta zelula-iragazkortasunaren handipena.

Azido nukleikoen garraio zuzenduan, karbohidratoen erabilerak abantaila terapeutiko garrantzitsuak aurkez ditzake, hartzaile espezifikoen estekatzaile gisa erabiliz (Yan and Tram, 2007; Zhang *et al.*, 2010). Horrez gain, GLUT hartzailearen 1, 3 eta 5 isoformak minbizian eta odoletik garunerako bidean zeharkatu beharreko hesi hematoentzefalikoan itu-molekula potentzialak izan daitezkeela uste da, bertako zelulen gainazalean gainadierazita baitaude. Hala, ODNei konjokatutako glukosa zatiak GLUT hartzaileen estekatzaile espezifiko gisa har daitezke, haiei lotuz eta hartzaile-bidezko barneratzea bultzatuz (Medina and Owen, 2002; Guo *et al.*, 2005; Watanabe *et al.*, 2010). Tesi-lan honetako lehen helburua 5 karbohidrato-oligonukleotido konjokaturen (COC) zelula-gainazaleko adsortzio eta zelula-sarreraren analisian oinarritu zen, zelula-gainazaleko GLUT hartzaileak adierazten dituzten HeLa eta U87.CD4.CXCR4 zelula-lerroak erabiliz. Karbohidrato aurkezpen aniztasuna ikertu nahian bi bereizgailu desberdin (*i.e.*, C2 eta PEG4) eta dendroi-aldamio bat (*i.e.*, DB) aukeratu ziren, glukosa eta glukosa-sakaridoak ODNari konjokatzeko (3.1 irudia). ODN-kontrol eta COCei Alexa 488 etiketa fluoreszentea ere erantsi zitzaien, zelula-gainazaleko adsortzioan eta zelula-

sarreran oinarritutako analisiak fluxu-zitometria bidez burutzeko (Ugarte-Uribe *et al.*, 2010).

Western blotting teknikaz baliatuz, bi zelula-lerroetan gainadierazitako isoformarik nabarmenena GLUT3 zela baieztatu genuen (3.4-3.7 irudiak). Izan ere, GLUT3 proteina, forma handiagoko isorforma bezala agertu zen (~70 kDa), GLUT garraiatzailearen masa molekularrarekin alderatuz (50-55 kDa); agian, N-glikosilazioan jazotako aldaketen ondorioz. Gainera, glukosarik gabeko baldintzetan isoforma honen adierazpena eta gainazalerako garraioa induzigarriak zirela ikusi genuen (Suzuki *et al.*, 1999).

Zelula-gainazaleko adsortzio eta zelula-sarrera saiakuntzetan emaitza berdintsuak lortu ziren, azterturiko bi zelula-lerroak COCekin inkubatu zirenean; oro har, COC desberdinen emaitzen artean desberdintasun gutxi behatuz, eta emaitza nabarmenenak glukosarik gabeko baldintzetan lortuz (3.8-3.11 irudiak). Glukosa-multibalentziak COCaren zelula-sarrera oztopa dezakeela ondorioztatu genuen, seguruenik ODN konjokatuak erakusten duen eragozpen esterikoa dela eta. Glukosa unitateen eta ODN zatiaren artean, PEG4 bereizgailu luzea (maltosa-PEG4) edo dendrimero simetriko bikoiztua [(glukosa-C2)$_2$-DB] aurkezten zuten COCek [*i.e.*, maltosa-PEG4(5')-ODN eta (glukosa-C2)$_2$-DB(5')-ODN konjokatuak], adsorztio eta barneratze altuenak adierazi zituzten, bi zelula-lerroetan egindako saiakuntzetan, bestelako COCekin edo ODN-kontrolarekin alderatuz. Beraz, emaitza hauek guztiak kontutan hartuz, hurrengo ondorioa atera daiteke: DNA zatiaren eta azukre-aldaketaren artean distantzia zehatza (15-18 arteko atomo kopurua) mantentzea garrantzitsua izan daitekeela, itu-zeluletan ODN-konjokatuaren zelula-barneratze hobea lortu ahal izateko. Horregatik, distantzia jakin hau mantentzea komenigarria izan daiteke etorkizun handiko COC diseinuetarako.

Bestalde, ezaguna da azido nukleiko zati txikiek konposatu lipofilikoekin konjokatzean izaera hidrofobikoagoa lortzen dutela (Singh *et al.*, 2010). Ondorioz,

sortu berria den molekulak zelula-sarrera handitu dezake mintz-iragazkortasunaren handipenaren eraginez, mintzarekin izan ditzaken elkarrekintzak edo/eta txertaketa faboratuz (Bunge *et al.*, 2007; Ye *et al.*, 2007). Ikerkuntza-lan honetan, zazpi lipido-oligonukleotido konjokatu (LOC) aztertu ziren. LOC hauek ODNaren konjokatze tokian, alkilo zatian edota aukeratutako etiketa fluoreszentean (*i.e.*, Cy5 eta Alexa 488) desberdintasunak aurkezten zituzten (4.1 eta A.1-A-3 irudiak). LOCen eta lipidoen arteko elkarrekintzak eta LOCen zelula-sarrera eta kokapen-portaerak aztertu ziren, lipidoz osaturiko hiru modelo-mintz [*i.e.*, monogeruzak, GUVak (*giant unilamellar vesicles*), SPBak (*supported planar bilayers*)] eta zelula-sistema bat (*i.e.*, HeLa zelula-lerroa) erabiliz.

Lipido gabeko eta DOPCez osatutako monogeruzen interfasean, LOCen albo-presioaren igoera, alkilo-ainguraketak aurkezten zuen hidrofobizitatearen araberakoa zela behatu genuen (4.2 eta 4.3 irudiak). LOC desberdinen artean, bi kate lipidikoz eratutako LOCak [C_{28}(5')-ODN] soilik 30 mN/m-ko hasierako albo-presioa zuten monogeruzetan txertatzeko gaitasuna aurkeztu zuen, zelula-mintzetan onartuta dagoen albo-presioari dagokiona hain zuzen ere (~30 mN/m) (Marsh, 1996; Busto *et al.*, 2007). Horrez gain, LOC bakoitzak portaera berdintsua adierazi zuen L_o/L_d (likido-ordenatu/likido-desordenatu) faseen baterako existentzia zeukaten GUV eta SPBetan (4.4-4.19 irudiak). Cy5(5')-ODN-(3')$C_{12}NH_2$ konposatuak GUVen L_d faseari loturiko fluoreszentzia eskasa eta LOC agregatu erraldoiak sortzeko erraztasuna aurkeztu zuen. Agregatu hauen eraketaren azalpen posible bat honakoa da: baldintza esperimental zehatz hauetan (pH 7.4), alkilo zatiaren ondoko lehen mailako amina erreaktiboa protonatuta ager daitekeela; karga negatiboa duen ODNko fosfato-estrukturarekin elkarrekintza elektrostatikoak faboratuz eta LOC-agregatuak sortuz (van Duijvenbode *et al.*, 1998; Maiti *et al.*, 2005). Cy5 fluoroforoa zuten ODN-(3')C_{14} eta ODN-(3')C_{18} konposatuak GUVen eta SPBen L_d fasean txertatzen zirela argi ikusi zen; Alexa 488 fluoroforoa zeukatenean, berriz, ez zen elkarrekintza edo txertaketa nabarmenik behatu, ezta C_{14}(5')-ODN-(3')-Alexa 488 konposatua aztertu zenean ere. LOC hauek

azaldutako portaera desberdina LOC-eraketan erabilitako lokailuak eta konjokatutako fluoroforoek duten tamainaren eta hidrofobizitatearen eraginez sortua izan daiteke. Honela, fluoroforoek konjokatze-efikazia desberdinak aurkez ditzakete edo/eta LOCen ezaugarriak eta egonkortasuna eragotzi. Bereziki, C_{28}(5')-ODN-(3')Alexa 488 konjokatuak mintz-sistema lipidikoetan aparteko txertaketa arina adierazi zuen, orekara heltzean L_d eta L_o domeinuen artean berdinki banatuz.

Sistema lipidikoekin lortutako emaitzen antzera, HeLa zelulekin burututako entseguetan, Cy5 eta Alexa 488 fluoroforoez etiketaturiko LOCek hidrofobizitatearen menpeko zelula-lotura/barneratze adierazi zuten. Zelula-lotura/barneratze portaera hau ODN-kontrolarekin lortutakoa baino hobea suertatu zen (4.21-4.22 irudiak). Izan ere, C_{28}(5')-ODN-(3')Alexa 488 konposatuak zelula-sarreran efikaziarik hoberena adierazi zuen; hain zuzen ere, Alexa 488 fluoroforoaz etiketaturiko ODN-lipoplexoek baino hobea izanik. Horrez gain, HeLa zelulekin egindako kokapen-saiakuntzetan, LOC guztiek banaketa nuklear garbia adierazi zuten (4.25-4.27 irudiak). Azken emaitza honek aditzera ematen du aztertutako lipido aldaketa hauek ez dutela ODN zatia helmugara iristea eragozten.

Arestian aipatutako behaketak kontuan hartuz, hurrengoa ondorioztatu daiteke: lipido-aldaketa luzeagoak edo bikoitzak (*i.e.*, bi lipido-kate) aurkezten zituzten LOCek txertaketa eta zelula-sarrera hobea adierazi zuten aztertutako bi sistemetan (*i.e.*, mintz-modelo lipidikoetan eta HeLa zelula-lerroan), bestelako LOCekin edo ODN-kontrolarekin alderatuz. Gainera, ODNaren 5'-muturrean lipido-kate bikoitza (C_{28}) zeukan LOCak emaitza onenak eman zituenez, aldaketa lipidiko honen karakterizazio sakonago bat burutzea erabaki genuen.

Konposaketa lipidiko desberdinez osaturiko mintz-modelo sistemetan lortutako emaitzek honakoa aditzera ematen dute: C_{28} lipido-aldaketak antzerako portaera adierazten duela, kate bakarreko ODNari zein kate osagarriarekin hibridatzean sorturiko bi kateko ODNari konjokatuta agertzean (5.3-5.26 irudiak). Hasierako inkubazio-uneetan L_d eta L_o faseen baterako existentzia zuten mintz-

modeloetan, C_{28} aldaketaz osatutako konjokatu hauek guztiak L_d fasean txertatzeko lehentasuna erakutsi arren, L_o fase-egoeran zeuden mintz-modeloetan ere txertatzeko gaitasuna adierazi zuten.

Alexa 488-an aberatsak ziren egitura biribildu birproduzigarriak behatu genituen aztertutako SPB guztietan, kate bakarreko zein bi kateko $C_{28}(5')$-ODN konposatua erabili zenean. Beraz, LOCak estruktura berri hauen eraketan parte hartzen zuela ondoriozta dezakegu (5.4-5.13 eta 5.19-5.26 irudiak). Estruktura hauek 1 µm baino gehiagoko diametroa zeukaten eta aldakortasun handiko mugetatik gertu (*i.e.*, L_d-L_o faseen edo lipido-mikaren arteko mugetan) agertu ziren. Hortaz, azken datu honek berebiziko garrantzia du, LOCak barneratze-bidezidorrekin lotuta egon daitezken kurbadura handiko mintzekiko duen lehentasuna indartzen baitu.

HeLa zelula-lerroan kate bakarreko LOCaren zelula-sarrera sakonago aztertu genuen, barneratze-bidezidor desberdinak aztertuz. LOC honen barneratzea tenperaturaren menpekoa zela behatu genuen; hain zuzen ere, energiaren menpeko endozitosi-prozesuren bat gutxienez barneratze honen partaidetzat hartuz (5.27 irudia). Endozitosi-inhibitzaileen eta zelula-markatzaile fluoreszenteen presentzian egindako zelula-sarrera saiakuntzetan argi ikusi zen konposatu honen barneratzea bereziki makropinozitosi bidezkoa eta apur bat klatrinaren menpeko endozitosiaren bidezkoa zela, nahiz eta klatrinaren kate astunaren kontrako siRNA-tratamenduak klatrinaren eginkizun aipagarririk ez adierazi LOC honen barneratzean (5.30-5.32 irudiak). Azken fenomenoari dagokion azalpen posible bat honakoa da: klatrinaren menpeko bidezidorraren falta konpentsatuta egon daitekeela, LOCaren barneratzean parte hartzen duten bestelako bidezidorren parte-hartzeagatik edo/eta bidezidor batzuen bidezko LOC-barneratzea (klatrinaren bidezko bidezidorra barne) zeharkako prozesu bat izan daitekeelako, LOCak mintz plasmatikoan sortarazten duen txertaketa eraginkorraren eraginez sortua, alegia.

Ondoren, zelula lerro desberdinak erabili genituen LOCaren zelula-sarrera eta zelula barneko kokapena aztertzeko. Inkubazioaren hasierako uneetan (*i.e.*, 30 min), LOCaren kokapena nukleoan behatu genuen zenbait zelula-lerroetan (baina ez guztietan); eta inkubazio denbora luzeetara (*i.e.*, 4 h), LOCaren kokapen-berrantolaketa bat behatu genuen, nukleotik zitoplasmara igaroz, nukleoaren ondoko guneetara, hain zuzen ere (5.37-5.39 irudiak). Bestalde, $\alpha_M\beta_2$ hartzailea zelularen gainazalean aurkezten zuten zelula-lerroek (*i.e.*, CHO CR3+, J774A.1 eta RAW 264.7 zelulek) $C_{28}(5')$-ODN konjokatuaren barneratze hobea azaldu zuten, hartzaile honen gabezia zeukaten zelula-lerroekin alderatuz (*i.e.*, CHO K1 eta J774A.1 CR3- zelulek). Honenbestez, $\alpha_M\beta_2$ hartzailearen estekatzaile natural ezaguna den fibrinogeno molekula LOCaren lehiakide gisa erabili genuen, LOCaren barneratzean hartzaile honek bete dezakeen eginkizuna aztertzeko. Entsegu honetan LOC-barneratzearen inhibizioa gertatu zenez, prozesu honetan $\alpha_M\beta_2$ hartzailearen parte-hartze zuzena iradoki zen (5.41 irudiak).

Laburbilduz, hurrengo kontzeptuak ondorioozta ditzakegu: C_{28} lipido-aldaketak ez duela zeluletan zitotoxikotasunik eragiten, ezta ODN zatiak berak dituen lotura-ezaugarriak aldatzen ere. Hala bada, ODN zatia hainbat molekulari lotu dakioke (*i.e.*, zelula-gainazaleko hartzaile zehatzei, zelula barneko ODN-garraioan parte hartzen duten proteinei, bere harizpi osagarriari eta mRNA itu-molekulei). Ezaugarri bikain hauek guztiak, C_{28} lipido-aldaketa aparteko hautagai bihurtzen dute ODN-garraioaren hobekuntzan, ODNari erantsita, ODN-konjokatu bezala erabilia izan dadin.

Eztabaida

Karbohidrato-oligonukleotido konjokatuen erabilera azido nukleikoen garraio zuzenduan

Oligonukleotidoetan oinarritutako terapiak garatzea arazo larria suertatzen zaigu, oraindik oligonukleotidoen garraio sistema eraginkor eta segururik ez baita diseinatu. Izan ere, molekula desegonkor hauek zelula barrura sartzeko espezifikotasun urria aurkezten dute. Glikokonjokatze-estrategiak azken arazo honi aurre egin diezaioke, karbohidratoek betetzen dituzten zenbait funtziotaz baliatuz, adibidez, seinalizazio-prozesuetan eta ehun espezifikotasunean betetzen dituzten funtzio garrantzitsuak kontuan hartuz (Ikeda *et al.*, 2010).

Gaur egun hainbat metodo berri garatzen ari dira, non karbohidratodun molekulak erabiltzen diren (*i.e.*, glikosilaturiko poliaminak eta estreptabidina) (Lemarchand *et al.*, 2004). Elkarrekintza ez-kobalenteen bidez eratutako azido nukleiko-konplexu hauek karakterizazio zaila eta toxikotasuna (*i.e.*, 100 µM gorako kontzentrazioetan) aurkezten dute. Lotura kobalenteen bidez eratutako karbohidrato-oligonukleotido konjokatuek (COCek), aldiz, zenbait abantaila aurkezten dituzte aurreko sistemekin alderatuz, hots, karbohidratoz osotutako konjokatuek toxikotasun urria eta egitura-homogeneotasuna adierazten dute, konjokatua osatzen duten konposatu bakoitzaren ehuneko erlatiboak era zehatzean mantenduz (Zatsepin and Oretskaya, 2004). Izan ere, jakina da lotura kobalentea duten COCek elkarrekintza ez-kobalenteen bidez eratutako konplexuek baino ekintza biologiko nabarmenagoa adierazten dutela (Maier *et al.*, 2003).

Zitotoxikotasun saiakuntzetan lortutako emaitzek aditzera ematen dute aztertutako COCek edo oligonukleotido (ODN)-kontrolak ez dutela zitotoxikotasunik eragiten, 5 µM-eko kontzentrazioa erabiltzean. Esperotako emaitza lortu genuela esan dezakegu, oro har karbohidrato gehienak (*i.e.*, glukosa

eta glukosa deribatuak) neutroak (kargari dagokionez) eta arruntak baitira edozein sistema bizidunetan.

Tumore-zelula mota desberdinetan glukosa sarrera areagotuta dago, maiz GLUT1 eta GLUT3 isoformen gainadierazpenaren ondorioz sortua dena (Watanabe *et al.*, 2010). Bi isoforma hauek egitura eta funtzio oso antzekoak dituzte. Amino-sekuentziaren %65a berdin-berdina bada ere, desberdintasun batzuk aurkezten dituzte C-muturreko domeinuetan eta zelula kanpoko loop egituretan. Horrez gain, bi isoformek D-glukosarekiko afinitate altua dute zelula-gainazalean adierazita daudenean (Sakyo *et al.*, 2007). Ezaugarri hauek guztiak direla eta, karbohidrato deribatuekin eratutako oligonukleotido konjokatuek garrantzia izan dezakete, tumore-zelulei zuzendutako garraio estrategietan erabiliak izateko. Beraz, glukosa molekulekin eratutako konjokatuak garraio sistema zuzendu gisa erabili daitezke tumore-zelulen gainazalean gainadierazita dauden GLUT1 eta GLUT3 isoformei eskuarki lotuz eta haien barneratzea bultzatuz (Rodríguez-Enríquez *et al.*, 2009).

Western blotting teknikaz baliatuz, GLUT1 eta GLUT3 hartzaileen adierazpen-maila aztertu genuen. Teknika honekin lortutako emaitzei esker, HeLa eta U87.CD4.CXCR4 zelula-lerroetan gainadierazitako isoformarik nabarmenena GLUT3 zela baieztatu genuen (3.4-3.7 irudiak). Izan ere, GLUT3 proteina, bai mintz-frakzioan zein frakzio zitoplasmatikoan, forma handiagoko isoforma bezala agertu zen (~70 kDa), GLUT garraiatzailearen masa molekular teorikoarekin alderatuz (50-55 kDa). Agian, forma handiagotze hau N-glikosilazioan jazotako aldaketen ondorioz sortua da. Gainera, glukosarik gabeko baldintzetan, isoforma honen adierazpena eta gainazalerako garraioa induzigarriak zirela ikusi genuen (Suzuki *et al.*, 1999). Egindako zatikapen prozesuarekin erretikulu endoplasmatiko (ER)/Golgi eta mintz-plasmatiko frakzioen arteko banaketa ez genuen lortu, frakzio biak batera agertuz. Frakzio horretan behatutako GLUT3 isoformaren N-glikosilazioak aditzera ematen digu proteinak ER/Golgi-tik igaro eta aurreragoko pausu batean aurkitzen dela (Suzuki *et al.*, 1999). Frakzio zitoplasmatikoko

GLUT3 isoformak ere N-glikozilazio prozesua jasan zuela antzeman genuen, behatutako proteina-banda, masa molekular handiagoko isoformari zegokiolako. Emaitza hauek guztiak kontuan hartuz honakoa postula dezakegu: GLUT3 isoformaren adierazpena induzitu daitekela, zelula barruko besikuletan proteina hau pilatuta mantenduz estimulu egokia heldu arte. Momentu aproposa heltzean besikuletako GLUT3 edukia zelula-gainazalera translokatuko da, zelula kanpoko gunean topa ditzaken glukosa eta glukosa deribatuei lotzeko (Hiraki *et al.*, 1988; Heijnen *et al.*, 1997; Thoidis *et al.*, 1999; Watanabe *et al.*, 2010; Iwabuchi and Kawahara, 2011).

COCekin egindako zelula-gainazaleko adsortzio eta zelula-sarrera saiakuntzetan, emaitza berdintsuak lortu genituen, azterturiko bi zelula-lerroetan; oro har, COC desberdinen emaitzen artean desberdintasun gutxi behatuz (3.8-3.11 irudiak). Glukosarik gabeko baldintzetan COC guztiek zelula-gainazaleko itzelezko adsortzioa adierazi zuten, baita ODN-kontrolak ere. Aipatu beharra dago emaitza hau inkubazio baldintzen eraginez azaldutakoa izan daitekeela, zelulek inkubazio epe luzean zehar (*i.e.*, 48 ordu) glukosarekiko "gose" larria jasan izanagatik, alegia.

U87.CD4.CXCR4 zeluletan glukosa-tetrabalentedun COCak [(glucose-C2)$_4$-DB-DB] ODN-kontrolak baino adsortzio hobea erakutsi zuen. HeLa zeluletan, aldiz, konposatu honek adsortzio eskasena aurkeztu zuen. Gainera, bi zelula-lerroetan lortutako barneratze murritzetik hurrengoa ondoriozta daiteke: glukosa-multibalentziak COCaren zelula-sarrera oztopa dezakela, seguruenik ODN-konjokatuak erakusten duen eragozpen esterikoaren ondorioz. Azken azalpen honek erlazio zuzena du Aviñó-ren ikerketa taldeak behatutakoarekin, non estekatzaile-adarkatzeak siRNAren ezaugarri inhibitzaileak murrizten zituen HeLa zeluletan (Aviñó *et al.*, 2011). Hala ere, azalpen hau beste ikerketa talde batzuek argitara eman dutenaren kontrakoa da. Artikulu hauetan karbohidrato multzo zatiez eratutako konjokatuak zelula-gainazaleko lektinei (*i.e.*, karbohidrato hartzaileei) hobeago lotu ziren (Sliedregt *et al.*, 1999; Maier *et al.*, 2003). Beraz, karbohidrato

multzo hauek lektinen estekatzaile eraginkorrak direla egiaztatu zuten, eragindako prozesua taldekatze efektu modura izendatuz.

Bi zelula-lerroetan burututako saiakuntzetan, maltosa-PEG4(5')-ODN eta (glukosa-C2)$_2$-DB(5')-ODN konposatuak, adsortzio eta barneratze hoberenak adierazi zituzten ODN-konjokatuak izan ziren, bestelako COCekin edo ODN-kontrolarekin alderatuz. Aipatu beharra dago COC hauek PEG4 bereizgailu luzea (maltosa-PEG4) edo dendrimero simetriko bikoiztua [(glukosa-C2)$_2$-DB] aurkezten zutela glukosa unitateen eta ODN zatiaren artean. Fluxu-zitometria teknikaz baliatuz, fluoreszentzia diferentzia gutxi behatu genuen glukosaren presentzian egindako zelula-sarrera entseguetan, agian, glukosa askea eta konjokatuen kontzentrazioen artean alde handia zegoelako (*i.e.*, 5.5 mM glukosa askea eta 2 µM COC). Emaitza arrakastatsu hauek glukosarik gabeko baldintzetan nabarmenagoak izan ziren; beraz, medioko glukosa molekula askeek COCen lehiakide gisa joka lezaketela suposa daiteke, GLUT proteinek dituzten lotura-guneetako COCen atxikimendua oztopatuz.

Orokorki, emaitza hauek guztiak kontuan hartuz, hurrengo ondorioa atera daiteke: DNA zatiaren eta azukre-aldaketaren artean distantzia zehatza (15-18 arteko atomo kopurua) mantentzea garrantzitsua izan daitekela, itu-zeluletan ODN-konjokatuaren barneratze hobea lortu ahal izateko. Izan ere, ikerketa talde batzuek ere lektinei dagokien antzerako azalpena ondorioztatu dute, hurrengoa argituz: 4-20 Åetako bereizgailuen erabilerak, estekatzaile eta lektinen arteko loturan eragin zuzena duela, haien arteko lotura estutuz. Hori dela eta, distantzia jakin hau mantentzea komenigarria izan daiteke etorkizun handiko COC diseinuetarako.

Lipido-oligonukleotido konjokatuen azterketa, mintz-modelo lipidikoak eta HeLa zelulak erabiliz

Ezaguna da oligonukleotidoek zelula-barneratze egokia behar dutela haien funtzioa bete ahal izateko. Hala ere, zelularen zitoplasmara heldu baino lehen mintz plasmatikoa zeharkatu behar dute, barneratze prozesuan aurkitutako lehen oztopo larria suposatuz. Azido nukleiko txiki hauek ezaugarri bereziak irabaz ditzakete molekula lipidikoei konjokatzean, hots, izaera hidrofobikoagoa irabazi. Hala, sortu berria den molekulak zelula-barneratzea handitu dezake mintz-iragazkortasunaren handipenaren eraginez; mintzarekin izan ditzaken elkarrekintzak edo/eta txertaketa faboratu ez ezik, serumeko lipoproteinei, zelula-gainazaleko lipoproteinen hartzaileei eta transmitz proteinei ere atxiki dakiekeelako (Wolfrum *et al.,* 2007).

Ikerkuntza-lan honetan, zazpi lipido-oligonukleotido konjokatu (LOC) aztertu ziren, oligonukleotidoen zelula-sarrera hobetu lezaken lipido aldaketa eraginkorren bat aurkitu nahian. LOC hauek ODNaren konjokatze tokian, alkilo zatian (*i.e.*, lipido zatiaren luzeeran, saturazio mailan eta alkilo kate kopuruan) edota aukeratutako etiketa fluoreszentean (*i.e.*, Cy5 eta Alexa 488) zenbait desberdintasun aurkezten zituzten (4.1 eta A.1-A.3 irudiak) (Grijalvo *et al.*, 2010, 2011).

Langmuir teknikaren bidez, LOC hauen portaera monogeruzetan aztertu genuen, mintz lipidiko erdia antzeratuz. Teknika honen erabilerak abantaila interesgarriak eskaini ditzake, ezaugarri asko erraz kontrola daitezkeelako; adibidez, mitz-konposaketa, albo-presioa, azalera-elastikotasuna eta dentsitatea (Caseli *et al.*, 2010; Montanha *et al.*, 2010). Beraz, ezaugarri hauek guztiek azalerako azterketa fisiko-kimikoen interesa indartzen dute, ODN-konjokatuaren eta lipidoen arteko elkarrrekintzen izaera, maila molekularrean argitu ahal izateko. Bestalde, jakina da mintz plasmatikoan kanpoaldera orientatuta dagoen bigeruzaren zatia karga elektriko neutroa duten fosfolipidoz osatuta dagoela. Beraz, DOPC

lipidoak karga neutroa duenez, DOPC monogeruzak erabili genituen LOC bakoitzaren txertaketa posiblea aztertzeko, LOCen eta lipidoaren arteko elkarrekintza elektrostatikoak ekidinez (van Meer, 2005). Aldiz, konplexuen eraketarako, ODNaren fosfato-egituraren eta eragile kationikoen arteko elkarrekintza elektrostatikoak beharrezkoak direnez, lipido kationikoz osatutako monogeruzak erabilgarriak izan daitezke, Langmuir teknikaren bidez konplexu eraketan eman daitezken elkarrekintza posibleak aztertzeko (Texeira *et al.*, 2001). Lipidorik gabeko edo DOPC monogeruzen interfasean, LOCen albo-presioaren igoera hidrofobizitaren menpekoa zela behatu genuen, hurrengo patroia lortuz: ODN-(3')C$_{12}$NH$_2$ < C$_{14}$(5')-ODN / ODN-(3')C$_{14}$ < ODN-(3')C$_{18}$ < C$_{28}$(5')-ODN. Horrez gain, LOC guztien artetik C$_{28}$(5')-ODN konposatuak soilik 30 mN/m baino altuagoko hasierako albo-presioa zuten monogeruzetan txertatzeko gaitasuna adierazi zuen. Beraz, LOC honek zelula-mintzaren kanpoaldeko bigeruzaren aldean (*i.e.*, kanpoaldeko monogeruzan) erraz txerta daitekela iradoki dezakegu, ezaguna baita zelula-mintzak 30 mN/m inguruko albo-presioak izaten dituela (Marsh, 1996; Busto *et al.*, 2007).

Bestalde, bigeruza lipidikoz osotutako bi modelo-sistema erabili genituen LOCen txertaketa posiblea ikertzeko: GUVak (ingelesetik, *Giant Unilamellar Vesicles*) eta SPBak (ingelesetik, *Supported Planar Bilayers*). Bi modelo-mintz hauek bereziki aukeratu ziren, zelulen mintz plasmatikoan aurki ditzakegun antzerako estres-kurbatura eta azalera-aldaketa dituzteelako (van Meer, 2005; McIntosh and Simon, 2007; Apellaniz *et al.*, 2010). Horrez gain, GUVak eta SPBak, DOPC/eSM/Chol (DOPC/esfingomielina/kolesterola) (2:2:1) lipido-nahasketaz sortu genituen, L$_d$ (likido-desordenatua) eta L$_o$ (likido-ordenatua) fase lipidikoen baterako existentziaren efektua, LOCen banaketan analizatzeko. Modelo-mintz hauen behaketarako DiO edo DiD zunda lipofiliko eta fluoreszenteak ere erabili genituen, mikroskopio konfokalaren bidez egitura hauek behatu ahal izateko. LOC bakoitzak antzerako portaera erakutsi zuen GUV eta SPB sistemekin burututako esperimentuetan.

Ikerketa-artikulu batzuen iritziz, lipido kate bakarrari konjokatutako oligonukleotidoek mintzari lotzeko gaitasun urria erakutsi dezakete (Pfeiffer and Höök, 2004; Bunge *et al.*, 2009). Honekin bat dator, Cy5(5')-ODN-(3')C$_{12}$NH$_2$ konposatuarekin lortutako emaitzak, GUVaren L$_d$ faseari loturiko fluoreszentzia murritza erakutsi baitzuen. Fluoreszentzia hau berehala galtzen genuen lagina laserrarekin berriro erradiatzean. Emaitza arraro honen azalpen posible bat honakoa da: laserrak Cy5 zunda koloregabetu zuela lagina berriro erradiatzean; agian, GUVaren L$_d$ fasean LOC kopuru gutxiegi txertatu izanagatik. Lagin berberan konjokatuaren agregatu erraldoiak ere behatu genituen, konjokatu honek agregatuak eratzeko duen erraztasuna adieraziz. Azken honi dagokionez, litekeena da baldintza esperimental zehatz hauetan (pH 7,4), alkilo zatiaren ondoko lehen mailako amina erreaktiboa protonatuta agertzea. Beraz, positiboki kargatutako amina honen eta karga negatiboa duen ODNko fosfato-egituraren arteko lotura eman daiteke, elkarrekintza elektrostatikoen bidez, LOC-agregatuen eraketa faboratuz (van Duijvenbode *et al.*, 1998; Maiti *et al.*, 2005). Izan ere, konplexu-eraketan oinarritutako estrategian ODN-konplexu/agregatuak elkarrekintza elektrostatikoen bidez eratzen dira, eragile kationikoan dauden amina erreaktiboen eta ODNak duen fosfato-egitura anionikoaren artean, hain zuzen ere (Meidan *et al.*, 2000; Weisman *et al.*, 2004; Gordon *et al.,* 2005). Aipatu beharra dago LOC honek GUVen L$_d$ fasearekin elkarrekintza egonkorra adierazi zuela inkubazio-denbora luzeetara buruturako entseguetan (*i.e.*, 20 ordu). Azken emaitza hau, baldintza hauetan sortutako artefaktua izan daiteke, inkubazio-denbora luzeetan LOCaren hauspeatzea gerta daitekeelako, GUVekin izan dezaken atxikimendua bultzatuz (Xu and Anchordoquy, 2011).

Cy5 fluoroforoa zuten ODN-(3')C$_{14}$ eta ODN-(3')C$_{18}$ konposatuak, GUVen eta SPBen L$_d$ fasean txertatzen zirela argi ikusi zen; Alexa 488 fluoroforoa zeukatenean, berriz, ez zen elkarrekintza edo txertaketa nabarmenik behatu, ezta C$_{14}$(5')-ODN-(3')-Alexa 488 konposatua aztertu zenean ere. Litekeena da, LOC-eraketan erabilitako lokailuak eta konjokatutako fluoroforoen tamaina eta

hidrofobizitate desberdintasunak, emaitza desberdin hauen arduradunak izatea. Honela, fluoroforoek konjokatze-eraginkortasun desberdinak aurkez ditzakete edo/eta LOCen ezaugarriak eta egonkortasuna eragotzi (Glen Research, Invitrogen). Antzerako azalpen bat aurki dezakegu Manoharanek argitaratutako artikulu batean, non fluoreszeina zundaz etiketaturiko ODN-konjokatuen ezaugarriak eraldatuak izan daitezkela aipatzen den, fluorofoaren izaera lipofilikoak eraginda, alegia (Manoharan, 2002).

Ikertzaile batzuen ustez, bi lipido-kateko aldaketak dituzten molekula eraldatuek, L_o egoerako baltsa lipidikoetan (ingelesez, *lipid rafts*) batez ere txertatzeko erraztasuna adieraz dezaketela espero daiteke (Zacharias *et al.,* 2002). Hala ere, $C_{28}(5')$-ODN-$(3')$Alexa 488 konjokatuak mintz-sistema lipidikoetan aparteko txertaketa arina adierazi zuen, orekara heltzean L_d eta L_o domeinuen artean berdinki banatuz. Beste ikerketa talde batzuk ere antzerako emaitzak lortu zituzten, DNAri kolesterol zati bat edo bi kolesteril-TEG zati konjokatzean, konposatu hauek ez baitziren L_o fasean bakarrik txertatu (Beales and Vanderlick, 2009; Bunge *et al.*, 2009). Litekeena da, kolesterolaren ezaugarriak imitatzeko diseinatutako konjokatuek, sarritan, ez dutela kolesterolak berak dituen ezaugarri berdinak erakusten (Beales and Vanderlick, 2009; Bunge *et al.*, 2009). Bestalde, LOC honek dituen bi eter loturek, mintz-modeloetan behatutako banaketa homogeneoan eragin zuzena izan dezakete. Izan ere, aspalditik jakina da eter lotura duten glizerofosfolipidoak ez direla horren zurrun topatzen mintzetan, bertako jariakortasuna handiagotuz (Boggs, 1980; Taguchi and Armarego, 1998).

Hala ere, aurreko emaitza hauek ez datoz bat beste ikertzaile batzuk esandakoarekin, haien ustez aldameneko bi alkilo katez eratutako konjokatuek, egitura supramolekular egonkorrak sortarazteko joera erakutsi dezaketelako, mintz-modeloetan txertaketa zailduz (Gosse *et al.*, 2004). Desadostasun honen jatorria ODN-konjokatuen egitura desberdintasunean egon daiteke. Ikertzaile hauek aukeratutako lipido ainguraketak kate luzeagoak ($2 \times C_{16}$) zituen, gure LOCaren lipido aldaketarekin alderatuz ($2 \times C_{14}$). Beraz, lipido ainguraketan kate luzeagoak

aurkezteak LOCaren hidrofobizitatea handitu dezake, egitura supramolekularren eraketa faboratuz.

Horrez gain, L_d/L_o domeinuen baterako existentzia zeukaten bigeruza artifizialetan, $C_{28}(5')$-ODN konjokatuak adierazitako banaketa homogeneoak zenbait abantaila sor ditzake, zeluletan barneratze bide desberdinen bidez sar litekeelako. Izan ere, behin LOC hau zelula-mintzean txertatzean, bertan topa ditzaken transmintz proteinekin elkarrekintzak eragin ditzake, proteina hauek parte hartzen dituzten sarrera bide desberdinen bidezko LOCaren barneratzea bultzatuz.

LOC guztien garrantzi biologikoa ere aztertu genuen HeLa zelula-lerroan, haien barneratzea eta zelula barruko lokalizazioa analizatuz. LOC hauek guztiak ez zuten zitotoxikotasunean ezta proliferazioan efektu negatiborik eragin. Hala ere, C_{28} aldaketa zuen LOCak, zelula-heriotza sortarazi zuen (*i.e.*, %32 eta %60ko heriotz zelularra, 24 eta 48 orduz inkubatu genuenean) kontzentrazio altuetan (*i.e.*, 5 µM). Agian, emaitza desatsegin hau, LOC honek zeluletan erakutsitako txertaketa/sarrera azkar eta masiboarekin erlaziona dezakegu, edo LOCan aurki ditzakegun eter loturek sortua izana; jakina baita zeluletan eter loturek ester loturek baino degradazio zailagoa dutela, zitotoxikotasuna faboratuz (Leventis and Silvius, 1990; Linder *et al.*, 2006).

Sistema lipidikoekin lortutako emaitzen antzera, HeLa zelulekin burututako entseguetan, Cy5 fluoroforoaz etiketaturiko LOCen artean, C_{14} eta C_{18} lipido aldaketak zituzten LOCek zelula-atxikidura/barneratze hobea adierazi zuten. Aldiz, $C_{12}NH_2$ aldaketa zuen LOCak Cy5 fluoreszentzia eskasa aurkeztu zuen, ODN-kontrolaren portaera oso antzekoa izanik. Beste ikerketa-talde batek ere emaitza berdintsuak lortu zituzten, hainbat aminadun lipido-kate siRNA-konjokatuak aztertzean. Ikertzaile hauen iritziz, amina taldearen eta lipido-katearen luzeeraren arteko konbinazio aproposa beharrezkoa da garraio eraginkorra lortzeko. Izan ere, C_{12} lipido-kate berbera baina amina talde desberdinak zituzten konjokatu guztiek ez zuten ekintza egokia eragin, nahiz eta bestelako lipido

laguntzaileekin (*i.e.*, kolesterola, diestearoil fosfatidilkolina eta mPEG-DMG) konplexuak eratu, haien barneratzea errazteko (Love *et al*., 2010).

Alexa 488 fluoroforoaz etiketaturiko LOC guztiek, ODN-kontrolak baino zelula-atxikidura/barneratze hobea adierazi zuten, hurrengo barneratze patroia behatuz (barneratze eskasenetik handienera): $C_{14}(5')$-ODN / ODN-$(3')C_{14}$ < ODN-$(3')C_{18}$ < $C_{28}(5')$-ODN. Azken emaitza kontuan hartuz, LOCek hidrofobizitatearen menpeko zelula-atxikidura/barneratze eragin zutela ondoriozta dezakegu. Hala ere, C_{14} eta C_{18} lipido aldaketak ODNaren 3' muturrean zituzten Alexa 488-dun LOCen kasuan, zelula-sarrera entseguetan lortutako emaitzak ez datoz guztiz bat GUVekin eta SPBekin lortutako emaitzekin; modelo-mintz saiakuntzetan ez baitzen mintzaren eta LOC hauen arteko elkarrekintzarik behatu. Agian, aukeratutako baldintza esperimentalak ez ziren egokienak suertatu, inkubazio-baldintza hauetan (4 ordu) LOCen hauspeatzea gerta baitaiteke, zelulen gainazalerarekin elkarrekintzak areagotuz. Ondorioz, hasiera batean mintz modeloetan txertaketa erakutsi ez zuten LOCen transfekzio-abiadura igo liteke, benetako barneratze egokia ez izanik (Xu and Anchordoquy, 2011). Antzerako emaitzak lortu zituzten Kuboren ikerketa-taldeak, azido palmitikoa (C_{16}) siRNAri (ingelesez, *small interfering RNA*) konjokatzean. siRNA-konjokatu hauek zelulari lotutako fluoreszentzia urria erakutsi zuten, RNAi (ingelesez, *RNA interference*) efektu murritzarekin batera, Lipofectamine 2000 izeneko transfekzio-eragilerik gabe formulatu zirenean (Kubo *et al.*, 2011).

Aipatu beharra dago, $C_{28}(5')$-ODN-$(3')$Alexa 488 konposatuak zelula-sarreran eraginkortasun hoberena adierazi zuela; Alexa 488 fluoroforoaz etiketaturiko ODN-lipoplexoak (*i.e.*, Transfectin izeneko transfekzio-eragilearekin eratutako ODN-konplexuak) baino hobea izanik. Emaitza interesgarri hauek, Grijalvoren ikerketa taldeak argitaratutako emaitzekin erlaziona ditzakegu. Kasu honetan, C_{28} lipido-aldaketa, siRNA molekularen harizpi bidaiariari (ingelesez, *passenger strand*) lotu zitzaion eta siRNAren efektu inhibitzaileak aztertu zituzten, Oligofectamine izeneko transfekzio-eragilearekin edo gabe formulatuz. C_{28}-dun

283

konjokatuak efektu inhibitzailerik bortitzena adierazi zuen Oligofectamine eragilerik gabe formulatzean, azterturiko bestelako siRNA-konjokatu lipofilikoekin alderatuz. Alderantziz, C_{28}dun siRNA-konjokatuak efektu inhibitzaile txarragoa adierazi zuen oligofektaminarekin formulatzean (Grijalvo *et al.*, 2011). Honekin batera, beste ikerketa-talde batek honakoa frogatu zuten: miristoil-kateek liposoma kationikoen bidezko ODN garraioan funtzio garrantzitsua bete dezaketela, bi miristoil-katez osatutako lipido kationikoek ODN-transfekzio hoberena adierazi baitzuten, nahiz eta DOPE lipido laguntzailerik gabe formulatua izan (Lindner *et al.*, 2006).

Horrez gain, HeLa zelulekin egindako kokapen-saikuntzetan, LOC guztiek banaketa nuklear garbia adierazi zuten. Azken emaitza honek aditzera ematen du, aztertutako lipido aldaketa hauek ez dutela ODN zatia helmugara iristea eragozten. Bereziki, C_{28}dun ODN-konjokatuak itzelezko fluoreszentzia erakutsi zuen zelulen nukleoan, non fluoreszentzia handiko orban txikiak ere behatu genituen. Litekeena da, erabilitako LOC kontzentrazioa (500 nM) gehiegizkoa izatea kasu honetan; LOC honen barneratze arina eta handiaren ondorioz, zelula guztiz asetuz. LOC hau nukleoan ere kokatu zen kontzentrazio baxuagoak (50 nM) erabili genituenean, inkubazio-denbora laburra (30 min) erabili genuen arren. Beraz, C_{28} lipido-aldaketa azido nukleiko zati txikiei konjokatzeko molekula oso egokia dela dirudi, ODNari konjokatuta agertzean ez baitu ODN zaita helmugara iristea eragozten, ezta siRNAri lotuta agertzean RNAi makineria oztopatzen ere (Grijalvo *et al.*, 2011).

Arestian aipatutako behaketa guztiak kontuan hartuz hurrengoa ondorioztka daiteke: lipido-aldaketa luzeagoak edo bikoitzak (*i.e.*, bi lipido-kate) aurkezten zituzten LOCek txertaketa eta zelula-sarrera hobea adierazi zutela aztertutako bi sistemetan (*i.e.*, mintz-modelo lipidikoetan eta HeLa zelula-lerroan), bestelako LOCekin edo ODN-kontrolarekin alderatuz. Gainera, ODNaren 5'-muturrean lipido-kate bikoitza (C_{28}) zeukan LOCak emaitza onenak eman zituen. Horregatik, aldaketa lipidiko honen karakterizazio sakonago bat burutzea erabaki genuen.

C$_{28}$(5')-ODN konjokatuaren karakterizazioa

Ezaguna da, lipido-ainguraketak aurkezten dituzten RNA eta DNA zati txikiak, molekula kimeriko interesgarriak izan daitezkela zenbait aplikazioetan, adibidez, nanobioteknologian, biologian zelularrean eta medikuntzan erabilgarriak izan daitezkeen estrategia terapeutikoen garapenean (Kurz *et al.*, 2006). Hori dela eta, beharrezkoa zaigu molekula hauen analisi sakonagoa burutzea, haien zelula-sarreran parte hartzen duten mekanismoak aztertuz, konposatu hauek itu-molekularekin lotzeko eta funtzio egokia bete ahal izateko beharrezkoak direnak, hain zuzen ere.

Nahiz eta mintz-modeloen erabilerak zelula-ingurune konplexua guztiz ez kopiatu, ODN garraioaren zenbait ezaugarri biofisiko ikertzea baimentzen digute, kontrola daitezken baldintza esperimentalak eta lipido-konposaketa zehatzak erabiliz (Gordon *et al.*, 2005).

Konposaketa lipidiko desberdinez osaturiko mintz-modelo sistemetan lortutako emaitzek honakoa aditzera ematen dute: C$_{28}$ lipido-aldaketak antzerako portaera adierazten duela, kate bakarreko ODNari zein kate osagarriarekin hibridatzean sorturiko bi kateko ODNari konjokatuta agertzean. Izan ere, aztertu genituen bi kateko ODN-konjokatu biek DOPC, DOPC/eSM/Chol (2:2:1) eta eSM/Chol (2:1) lipido-nahasketaz sortutako GUVen L$_d$ eta L$_o$ domeinuetara txertatzeko gaitasuna mantendu zuten (5.3-5.23 irudiak). C$_{28}$ aldaketaz osatutako konjokatu hauek guztiek L$_d$ fasean txertatzeko lehentasuna erakutsi zuten hasierako inkubazio-uneetan L$_d$ eta L$_o$ faseen baterako existentzia zuten mintz-modeloetan. Hala ere, L$_o$ fase-egoeran [eSM/Chol (2:1)] zeuden mintz-modeloetan ere txertatzeko gaitasuna adierazi zuten.

Arestian esan bezala, lipido-kate bikoitzeko aldaketari konjokatutako ODN zatiak hainbat ezaugarri berri eta berezi irabazten ditu; lipido domeinu desberdinetan txertatzeko gaitasuna, besteak beste. Azken ezaugarri honek

abantaila interesgarri bat suposa dezake, zeluletan sarrera-bide desberdinen bidez sartzeko. Izan ere, behin LOC hau zelula-mintzean txertatzean, bertako transmintz proteinekin elkarrekintzak eragin ditzakete, proteina hauek parte hartzen duten sarrera-bideen bidezko LOCaren barneratzea bultzatuz.

Nahiz eta hibridazio prozesuaren ondorioz, hots, LOCaren ODN katea bere osagarriarekin hibridatzean bi kateko LOC berria sortzearen ondorioz, LOCean hidrofilizitatea igo, C_{28} lipido-aldaketak txertaketa ezaugarri berdintsuak izaten jarraitu zuen. Beraz, lipido-aldaketa hau, kate bakarreko zein bi kateko azido nukleiko zati txikiei konjokatzeko baliagarria izan daitekela ondoriozta dezakegu.

Alexa 488an aberatsak ziren egitura biribildu birproduzigarriak behatu genituen aztertutako SPB guztietan, kate bakarreko zein bi kateko $C_{28}(5')$-ODN konposatua erabili zenean. Beraz, LOCek egitura berri hauen eraketan parte hartzen zutela ondoriozta dezakegu (5.4-5.12 eta 5.18-5.23 irudiak). Emaitza hau Sheetz eta Singer zientzialariek proposatutako bigeruza lipidikoaren hipotesiarekin erlazionatuta egon daiteke. Hipotesi hau hurrengoan datza: hemigeruzen arteko asimetria duen bigeruza lipidiko itxi batean, hemigeruza bakoitzak era desberdinetan erantzun lezakela zenbait asalduren aurrean (Sheetz and Singer, 1974; Sheetz *et al.,* 1996). Hori horrela izanik, bigeruza horren hemigeruza batek azalera handitzean (*e.g.*, LOCa kanpoaldeko hemigeruzean txertatzean), bigeruzaren berezko kurbatura igotzea espero dezakegu. Beraz, bigeruzaren energia egoera gutxitzeko eta hemigeruzen arteko van der Waals elkarrekintzak eta elkarrekintza hidrofobikoak mantentzeko, aurkakotasun-bigeruza kurbatura espontaneoari egokituko zaio (Nossal and Zimmerberg, 2002). Beraz, bigeruza, azalera handituta duen hemigeruza aldera deformatuko da, sistema osoa orekatzeko (Farsad and De Camili, 2003). Azalpen hau kontuan hartuz, bigeruza lipidikoaren teoriaren bidez, mintz lauetan (*i.e.*, SPBetan) LOCak eragindako aldaketa morfologikoak azaldu dezakegu. Beste era batera esanda, bigeruza lauaren kanpoaldeko hemigeruzean gertaturiko LOCaren txertaketak, bigeruzaren

deformazioa kanpoalderantz eragingo luke, LOCak duen zati hidrofiliko handiaren eraginez, alegia.

Egitura berezi hauek 1 µm baino gehiagoko diametroa zeukaten eta aldakortasun handiko mugetatik gertu (*i.e.*, L_d-L_o faseen edo lipido-mikaren arteko mugetan) agertu ziren. Izan ere, aspaldi jakina da konposaketa desberdina duten domeinuen arteko mugak, mintz-kimaketa eta fisio prozesuetarako beharrezkoa den energia eman dezakeela (Lipowsky, 1992). Edozein fase-mugetan, mintz-domeinuen mugak gehiegizko energia aurkezten du, zenbait lipido molekulen "dohakabetasunarekin" erlazionatuta dagoena, alegia. Dohakabetasuna aurkezten duten lipidoak, antzerako lipido kateak dituzten lipidoez hein batean inguratuta dauden lipidoak dira (Kuzmin *et al.*, 2005). Prozesu honi loturiko estresak tentsio-lerroa du ezaugarri, hots, mugaren eremu unitatea sortzeko beharrezkoa den energia (Lipowsky, 1992). Tentsio-lerroak mugaren eremua gutxitzeko joera izango du, lepo estu batez lotutako lipido-domeinuaren kimu bat sortaraziz (Schmid and Frolov, 2011). Azalpen honek erlazio zuzena izan dezake, DOPC/eSM/Chol (2:2:1) lipido-nahasketaz sortutako SPBetan, L_d-L_o faseen arteko mugetan behatutako LOC-egiturekin. Gainera, kolesterolak LOC-egitura hauen kimaketa prozesuan lagundu lezake; kolesterolak aurkezten duen banaketa desberdinari esker, mintzaren egituran zuzenean eragiten baitu. Bereziki, kimuaren eraketarako beharrezkoa den energia gutxituko luke, bertako mintz-zurruntasuna txikiagotuz, eta hemigeruzen arteko van der Waals indarrak eta indar hidrofobikoak mantenduz, behin bigeruza deformatzen hastean (Baba *et al.*, 2001; Brown *et al.*, 2001, 2002).

Horrez gain, LOC-egitura batzuk hein batean estatiko agertzen ziren bitartean, beste batzuk, aldiz, etengabe mugitzen ari ziren. Egitura dinamiko hauek ek ez zuten forma-biribildurik, hodi-itxurako forma baizik. Emaitza honen azalpen posible bat hurrengoa da: arestian aipatutako tentsio-lerroak indar bat zehaztuko du. Indar hau, LOCak eratutako domeinu morfologikoaren [ingelesez, *morphological domain* (MOD)] ertzari lotuta egongo da, eta bide batez, ertzean

dauden molekulek MODaren barruan egon nahi duten gertaerari ere (Lipowsky, 1992; Koyhama *et al.*, 2003). Ertz-energia hau, ertzaren tamaina txikituz gutxitu daiteke; ertz luzea duen kurbatura gutxiko doimeinutik edo domeinu lauetik, ertz laburra duen kimu esferikora igaroz (Lipowsky *et al.*, 1992). Beraz, tentsio-lerroak MODaren garapena bizkortu dezake, oro har morfologia esferikoa ezarriz. Azken azalpen hau lagungarria egiten zaigu, ikerketa-lan honetan behatutako LOC-MOD estatikoen egitura ulertzeko.

Gainera, LOC-MOD hauen erreproduzigarritasun morfologikoa, "*Brownian ratcheting*" izeneko printzipioarekin erlaziona dezakegu. Printzipio hau honakoan datza: MODaren forman emandako zenbait aldaketa termikok, MOD beraren garapena bideratzen dute; eta moldeak (domeinuen formak egonkortzen dituen molekulak, maiz proteina bat dena) moldearen geometriarekin bat datozen formak soilik hartu eta egonkortuko ditu (Shnyrova *et al.*, 2009). Azken hau kontuan hartuz, guk behatutako LOC-MODetan, LOCak berak moldearen funtzioa bete dezakela pentsa dezakegu.

Hortaz, azken datu honek berebiziko garrantzia du, LOCak kurbatura handiko mintzetan txertatzeko lehentasuna erakutsi dezakeelako, bertan egitura berezi hauen garapena bideratuz eta mintzaren gune hauei lotuta egon daitezkeen barneratze-bidezidorrekin elkarrekintzak bultzatuz.

LOCaren garrantzi biologikoa ere aztertu genuen, HeLa zeluletan erabilitako barneratze-bidezidorrak aztertuz. Tenperatura desberdinetan (*i.e.*, 4ºC eta 37ºC) burututako esperimentuetan, LOCaren barneratzea tenperaturaren menpekoa zela behatu zuen, energiaren menpeko endozitosi-prozesuren bat gutxienez, barneratze honen partaidetzat hartuz. Emaitza hau beste ikerketa-talde batek esandakoarekin bat dator, miristoilatutako molekulen barneratze zelularra tenperaturaren menpekoa zela adierazi baitzuen (Nelson e*t al.*, 2007).

Oraindik, molekula baten sarrera-mekanismoak sakonki aztertzea zaila da, inhibitzaile farmakologikoek desiratutako bidezidor zehatz bat blokeatu ez ezik, bestelako sarrera-bideetan ere zeharkako efektuak eragin ditzaketeelako. Beraz, inhibitzaileek zenbait prozesu endozitikoetan aldi berean eragin dezakete, era zuzen edota zeharkako era batean (Fretz *et al.*, 2006). Horrez gain, sarritan ez dugu barneratzearen erabateko inhibizioa lortzen. Azken honek aditzera ematen du, molekularen barneratzean bidezidor desberdinak batera parte har dezaketeela, edota bidezidor bat blokeatzean, beste bidezidorren bat molekularen barneratzeaz ardura daitekeela (Hoekstra *et al.*, 2007).

Endozitosi-inhibitzaileen eta zelula-markatzaile fluoreszenteen presentzian egindako zelula-sarrera saiakuntzetan, konposatu honen barneratze zelularra, bereziki makropinozitosi bidezkoa eta apur bat klatrinaren menpeko endozitosiaren bidezkoa zela argi ikusi zen, endozitosi-inhibitzaileen bidezko erabateko inhibizioa lortu ez arren. Hala ere, klatrinaren kate astunaren kontrako siRNA-tratamenduak, ez zuen klatrinaren eginkizun aipagarririk adierazi LOCaren barneratze prozesuan. Azken fenomenoari dagokion azalpen posible bat honakoa da: klatrinaren menpeko bidezidorrak utzitako hutsunea beste bidezidor batekin konpentsatuta egon daitekela, adibidez makropinozitosiarekin. Gainera, jakina da sakarosaren efektu inhibitzailea ez dela guztiz espezifikoa izaten, klatrinaren menpeko endozitosia blokeatu ez ezik, fase-urtsuko endozitosia ere inhibitu dezakeelako; esaterako, makropinozitosiaren bidezidorra (Bradley *et al.*, 1993; Synens *et al.*, 1999; Ivanov, 2008). Hala eta guztiz ere, LOCa L_d eta L_o domeinuetan txertatzeko gai denez, mintzean dauden zenbait bidezidorren bidez LOCaren barneratzea zeharkako era batean gerta daiteke.

Oro har, makropinozitosi prozesuan hartzailerik gabeko barneratzea gertatzen da, non aktinak mintz plasmatikoan tolesturak edo uhindurak eragiten dituen, kanpoalderantz domeinu luzapenak sortuz eta kanpo-medioko likido bolumen handia barneratuz (Maniak, 2001; Amyere *et al.*, 2002). Endozitosi prozesu honen bidez barneratutako besikulei makropinosomak deritze eta

normalean partikula handiak (*i.e.*, 1-5 μm diametroko partikulak) barneratzeko erabilia den endozitosi mota da (Swanson and Watts, 1995; Conner and Schmid, 2003; Patel *et al.*, 2007). Azken deskribapen hau, SPBetan behatutako LOC-MODekin ere erlaziona dezakegu, 1 μm diametro baino gehiagoko egitura berezi hauek zeluletan sortaraziko balira, hartzailerik gabeko endozitosi hau piztu lezaketelako, haien barneratze zelularra bultzatuz.

Barneratze prozesu desberdinetan sorturiko endosomek desberdintasunak erakusten dituzte. Badirudi makropinosometako materialak zitoplasmara ihes egin dezakeela, besikula hauek eskuarki aurkeztu ditzaketen zulo eta pitzaduretatik zehar askatuz (Norbury *et al*., 1995; Meier *et al.*, 2002). Nahiz eta makropinosometan pH jaitsiera bat izan, zenbait zelula-motetan besikula hauen garraio intrazelularra ez dago lisosometara bideratua. Beraz, makropinosomak ez dira lisosomekin fusionatzen eta barneratutako materialak ez du lisosometako entzimen bidezko degradazioa jasan behar (Hewlett *et al.*, 1994; Hamasaki *et al.*, 2004; Wadia *et al.*, 2004; Holzer and Howell, 2006; Ruozi *et al.*, 2009). Aurreko azalpen hau kontuan hartuz, barneratze-bide hau eraginkorra izan daiteke, $C_{28}(5')$-ODN konposatua nukleora eta zitoplasmara hel dadin eta lisosometan jasan dezaken degradazioa ekidin dezan. Gainera, azalpen hau HeLa zeluletan behatutako emaitzekin bat dator, LOC honek nukleora heltzeko gaitasuna erakutsi baitzuen, bere barneratzea bidezidor eraginkor baten bidez bideratua zela adieraziz.

Zelula-mota bakoitzak adierazten dituen ezaugarri bereziek, barneratu beharreko zenbait molekulen garraioan eta zelula-sarbideetan eragin zuzena dituzte (Watson *et al.*, 2005). Hori dela eta, zelula-mota guztiek ez dute barneratze-bidezidor berbera aukeratzen molekula zehatz baten barneratzea burutzeko. Zelula-lerro desberdinekin lortutako emaitzei dagokienez, $C_{28}(5')$-ODN konposatua zelula-lerro askoren, baina ez guztien, nukleoan behatu genuen. Ondoren, LOC hau nukleotik zitoplasmara igaro zen, nukleoaren ondoko guneetan kokatuz. Izan ere, behatutako LOCaren kokapen-berrantolaketa berezi hau, beste ikertzaile talde batzuk ere aztertu dute, ODNaren nukleotik zitoplasmarako garraio bat dagoela

azpimarratuz (Forsha *et al.*, 2010). Gainera, zelula-lerro desberdinetan lortutako emaitzak Petrovaren ikerketa lan taldeak argitaratu zutenarekin bat datoz, siRNA lipofilikoen barneratzearen eraginkortasuna, zelula-lerro motaren menpekoa zela ondorioztatuz (Petrova *et al.*, 2012).

Aipatu beharra dago, $\alpha_M\beta_2$ hartzailea zelula-gainazalean aurkezten zuten zelula-lerroek $C_{28}(5')$-ODN konjokatuaren barneraketa hobea azaldu zutela, hartzaile honen gabezia zeukaten zelula-lerroekin alderatuz. Horrez gain, U87.CD4.CXCR4 zelulek eta $\alpha_M\beta_2$ hartzailea zuten zelula-lerroek antzerako LOCaren banaketa intrazelularra erakutsi zuten. Emaitza hauek aspaldian argitaratutako artikulu batean esandakoarekin erlaziona ditzakegu, bertan β_2 integrinek ODNen barneratzea handitzen baitzuten, hartzaile bidezko endozitosia bultzatuz (Benimetskaya *et al.*, 1997). U87.CD4.CXCR4 zeluletan hartzaile bidezko LOCaren barneratzea ere gerta daiteke, CD4 hartzailearen bidezkoa, alegia. Izan ere, CD4 proteina errekonbinante solugarriak alkilodun ODN bati lotzeko gaitasuna duela ezaguna da (Benimetskaya *et al.*, 1995). Hala ere, azken hipotesi hau onartzeko azterketa sakonago bat egin beharko genuke.

Tesi-lan honetan erabili dugun CD11b (α_M) tindaketak zelula-gainazaleko CD11b adierazpena aztertzeko balio du soilik, ez baitu zitoplasman egon daiteken CD11b adierazpena ikertzeko balio. Zitoplasman dagoen CD11b proteina edukia gainazalera igarotzeko estimulu berezi bat behar du, behin estimulua jazotzean, gainazalean txertatuz. Estimulu hau molekula espezifikoen bidez lor dezakegu, adibidez zitokinen edo zenbait lipidoen bidez (Benimetskaya *et al.*, 1997). Horrez gain, zelula-gainazalean topa daitezken $\alpha_M\beta_2$ integrina guztiak ez daude modu aktiboan, hots, denak ez dira gai estekatzailearekin lotzeko. Beraz, integrinen aktibaziorako beharrezkoa da $\alpha\beta$ heterodimeroan egitura-aldaketa bat egotea eta integrinen taldekatzea gertatzea. Integrinen taldekatze hau, mintzeko integrinen albo-difusioari esker sortua da. Azken efektu honek, integrinek substratuenganako duten balentzia handitzen duela eta integrinen aktibazioa erregulatzen duela proposatu dute zenbait ikertzailek (Stewart *et al.*, 1998; van Kooyk and Figdor,

2000; Bouaouina *et al.*, 2004). Beraz, CD11b tindaketa metodo honekin lortutako emaitzak ikusita honakoa ondoriozta dezakegu: CHO CR3+, J774A.1 eta RAW 264.7 zelula-lerroek zelula-gainazaleko CD11b (α_M) adierazpena erakusten dutela, eta hartzaile hauek aktibatuta egotekotan, mintzean txertatutako LOCarekin elkarrekintzak izan ditzaketela, LOCaren barneratzea bultzatuz eta barneratze handiagoa lortuz, alegia. Honenbestez, $\alpha_M\beta_2$ hartzailearen estekatzaile natural ezaguna den fibrinogeno molekula, LOCaren lehiakide gisa erabili genuen, hartzaile honek LOCaren barneratzean bete dezaken eginkizuna aztertzeko. Entsegu honetan LOC-barneratzearen inhibizioa gertatu zenez, prozesu honetan $\alpha_M\beta_2$ hartzailearen parte-hartze zuzena iradoki zen.

Laburbilduz, hurrengo kontzeptuak ondoriozta ditzakegu: C_{28} lipido-aldaketak makropinozitosi bidezko barneratze eraginkorra aurkezten duela, zeluletan zitotoxikotasuna eragin gabe eta ODN zatiak berak dituen lotura-ezaugarriak aldatu gabe. Hala bada, ODN zatia hainbat molekulei lotu dakieke (*i.e.*, zelula-gainazaleko hartzaile zehatzei, zelula barneko ODN-garraioan parte hartzen duten proteinei, bere harizpi osagarriari eta mRNA itu-molekulei). Ezaugarri bikain hauek guztiek, C_{28} lipido-aldaketa ODN-garraioaren hobekuntzan aparteko hautagai bihurtzen dute, mota desberdinetako azido nukleiko zati txikiei lotuta, konjokatu bezala erabilia izan dadin.

Ondorioak

1. DNA zatiaren eta azukre-aldaketaren artean 15-18 atomo tarteko distantzia zeukaten karbohidrato-oligonukleotido konjokatuek (COCek), zelula-barneratze hoberena erakutsi zuten aztertutako itu-zeluletan (*i.e.*, HeLa eta U87.CD4.CXCR4 zelula-lerroetan), bestelako COCekin edo ODN-kontrolarekin alderatuz. Hori dela eta, distantzia zehatz hau (15-18 arteko atomo kopurua) mantentzea komenigarria izan daiteke etorkizun handiko COC diseinuetarako.

2. Lipido-aldaketa luzeagoak edo bikoitzak (*i.e.*, bi lipido-kate) aurkezten zituzten lipido-oligonukleotido konjokatuek (LOCek), txertaketa eta zelula-sarrera hobea adierazi zuten aztertutako bi sistemetan (*i.e.*, mintz-modelo lipidikoetan eta HeLa zelula-lerroan), bestelako LOCekin edo ODN-kontrolarekin alderatuz. ODNaren 5'-muturrean lipido-kate bikoitza (C_{28}) zeukan LOCak emaitza onenak eman zituen, domeinu likido-desordenatuan (L_d) zein likido-ordenatuan (L_o) txertatzeko gaitasuna erakutsiz.

3. C_{28} lipido-aldaketak makropinozitosi bidezko barneratze eraginkorra sortarazten du, zeluletan zitotoxikotasuna eragin gabe eta ODN zatiak berak dituen lotura-ezaugarriak aldatu gabe. Ezaugarri bikain hauek guztiek, C_{28} lipido-aldaketa ODN-garraioaren hobekuntzan aparteko hautagai bihurtzen dute, mota desberdinetako azido nukleiko zati txikiei lotuta, konjokatu bezala erabilia izan dadin.

Appendix
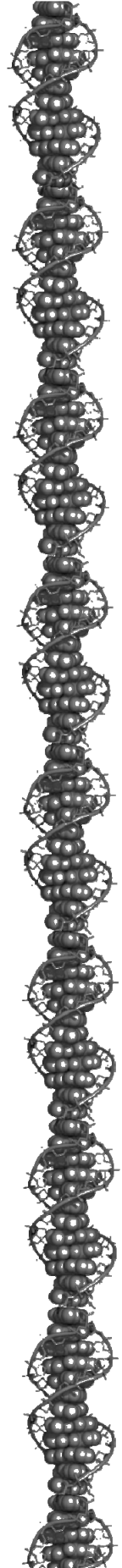
Appendix
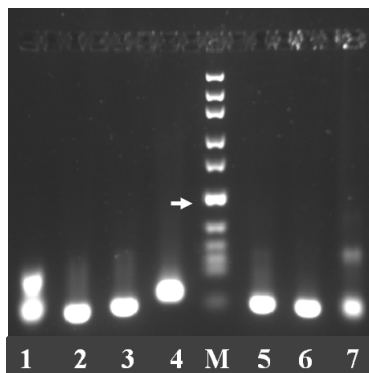
Figure A.1 Characterisation of unlabelled control-ODNs and LOCs by agarose gels.
4% agarose gels were performed to visualise by SIBR Gold staining the corresponding
bands of unlabelled control-ODNs and LOCs. 1 µl unlabelled control-ODN and LOC stock
solutions (200 µM) were mixed with the loading buffer. 3 µl DNA ladder were used for
each M termed well. Figure legend: (1) $NH_2(5')$-AntiGEM91; (2) GEM91-$(3')$-NH_2; (3)
$C_{14}(5')$-GEM91-$(3')NH_2$; (4) $C_{28}(5')$-GEM91-$(3')NH_2$; (5) GEM91-$(3')C_{12}NH_2$; (6)
GEM91-$(3')C_{14}$; (7) GEM91-$(3')C_{18}$. M: DNA ladder (10, 15, 25, 35, 50, 75, 100, 150, 200,
300 bp). White arrow indicates the 50 bp fragment of the DNA ladder.
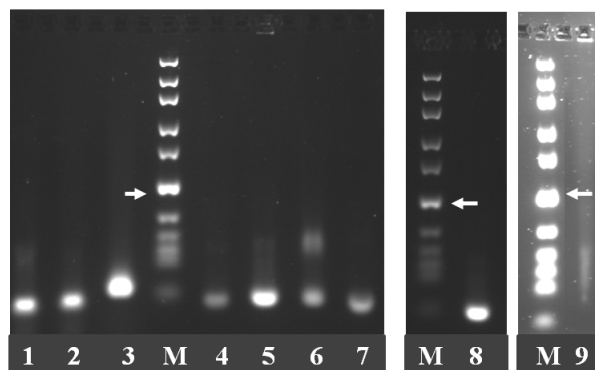
Figure A.2 Characterisation of Cy5- and Alexa 488-labelled control-ODNs and LOCs by agarose gels. 4% agarose gels were performed to visualise by SIBR Gold staining the corresponding bands of unlabelled control-ODNs and LOCs. 0.5 µl Cy5- or Alexa 488-labelled control-ODN and LOC stock solutions (200 µM) were mixed with the loading buffer, except for compound number 5, where 1 µl Cy5(5')-GEM91-(3')$C_{12}NH_2$ stock solution (200 µM) was used. 3 µl DNA ladder were used for each M termed well. Figure legend: (1) GEM91-(3')-Alexa 488; (2) C_{14}(5')-GEM91-(3')Alexa 488; (3) C_{28}(5')-GEM91-(3')Alexa 488; (4) Cy5(5')-GEM91; (5) Cy5(5')-GEM91-(3')$C_{12}NH_2$; (6) Cy5(5')-GEM91-(3')C_{14}; (7) Cy5(5')-GEM91-(3')C_{18}; (8) Alexa 488(5')-GEM91-(3')C_{14}; (9) Alexa 488(5')-GEM91-(3')C_{18}. M: DNA ladder (10, 15, 25, 35, 50, 75, 100, 150, 200, 300 bp). White arrows indicate the 50 bp fragment of the DNA ladder.

Compound No.	Control oligonucleotides	Structure
1	GEM91-(3')NH₂	
8	GEM91-(3')Alexa 488	
15	GEM91	
16	Cy5(5')-GEM91	
17	NH₂(5')-AntiGEM91	
18	Alexa 488(5')-GEM91	

Table A.1 Structures of unlabelled and Cy5- and Alexa 488-labelled control-ODNs and complementary strands used in this study.
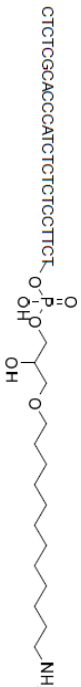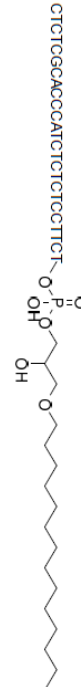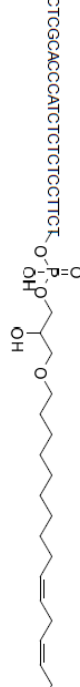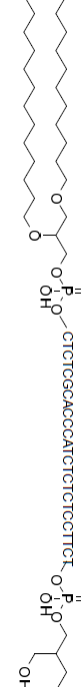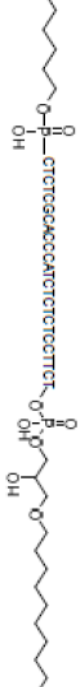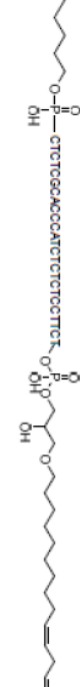
Compound No.	Unlabelled LOCs	Structure
19	GEM91-(3')C$_{12}$NH$_2$	
20	GEM91-(3')C$_{14}$	
21	GEM91-(3')C$_{18}$	
22	C$_{14}$(5')-GEM91-(3')NH$_2$	
23	C$_{28}$(5')-GEM91-(3')NH$_2$	
24	NH$_2$(5')-GEM91-(3')C$_{14}$	
25	NH$_2$(5')-GEM91-(3')C$_{18}$	

Table A.2 Structures of unlabelled LOCs used in this study.

Compound No.	Cy5- and Alexa 488-labelled LOCs	Structure
26	Cy5(5')–GEM91-(3')C$_{12}$NH$_2$	
27	Cy5(5')–GEM91-(3')C$_{14}$	
28	Cy5(5')–GEM91-(3')C$_{18}$	
29	C$_{14}$(5')–GEM91-(3')Alexa 488	
30	C$_{28}$(5')–GEM91-(3')Alexa 488	
31	Alexa 488(5')–GEM91-(3')C$_{14}$	
32	Alexa 488(5')–GEM91-(3')C$_{18}$	

Table A.3 Structures of Cy5- and Alexa 488-labelled LOCs used in this study.

References

References

1.   Agrawal, S. and Zhao, Q. (1998) Mixed backbone oligonucleotides: improvement in oligonucleotide-induced toxicity *in vivo*. *Antisense & Nucleic Acid Drug Development*, **8**, 135-139.

2.   Akhtar, S. and Benter, I.F. (2007) Nonviral delivery of synthetic siRNAs *in vivo*. *The Journal of Clinical Investigation*, **117**, 3623-3632.

3.   Akhtar, S. and Juliano, R.L. (1992) Cellular uptake and intracellular fate of antisense oligonucleotides. *Trends in Cell Biology*, **2**, 139-144.

4.   Akhtar, S., Kole, R. and Juliano, R.L. (1991) Stability of antisense DNA oligodeoxynucleotide analogs in cellular extracts and sera. *Life Sciences*, **49**, 1793-1801.

5.   Akinc, A., Thomas, M., Klibanov, A.M. and Langer, R. (2005) Exploring polyethylenimine-mediated DNA transfection and the proton sponge hypothesis. *The Journal of Gene Medicine*, **7**, 657-663.

6.   Alahari, S.K., Dean, N.M., Fisher, M.H., Delong, R., Manoharan, M., Tivel, K.L. and Juliano, R.L. (1996) Inhibition of expression of the multidrug resistance-associated P-glycoprotein of by phosphorothioate and 5' cholesterol-conjugated phosphorothioate antisense oligonucleotides. *Molecular Pharmacology*, **50**, 808-819.

7.   Alahari, S.K., DeLong, R., Fisher, M.H., Dean, N.M., Viliet, P. and Juliano, R.L. (1998) Novel chemically modified oligonucleotides provide potent inhibition of P-glycoprotein expression. *The Journal of Pharmacology and Experimental Therapeutics*, **286**, 419-428.

8.   Allen, C, Dos Santos, N., Gallagher, R., Chiu, G.N., Shu, Y., Li, W.M., Johnstone, S.A., Janoff, A.S., Mayer, L.D., Webb, M.S. *et al.* (2002) Controlling the physical behavior and biological performance of liposome formulations through use of surface grafted poly(ethylene glycol). *Bioscience Reports*, **22**, 225-250.

9.   Allen, T.M. and Cullis, P.R. (2004) Drug delivery systems: entering the mainstream. *Science*, **303**, 1818-1822.

10. Allinquant, B., Hantraye, P., Mailleux, P., Moya, K., Bouillot, C. and Prochiantz, A. (1995) Downregulation of amyloid precursor protein inhibits neurite outgrowth *in vitro*. *The Journal of Cell Biology*, **128**, 919-927.

11. Amarzguioui, M., Holen, T., Babaie, E. and Prydz, H. (2003) Tolerance for mutations and chemical modifications in a siRNA. *Nucleic Acids Research*, **31**, 589-595.

12. Amyere, M., Mettlen, M., Van Der Smissen, P., Platek, A., Payrastre, B., Veithen, A. and Courtoy, P.J. (2002) Origin, originality, functions, subversions and molecular signalling of macropinocytosis. *International Journal of Medical Microbiology*, **291**, 487-494.

13. Angelova, M.I. and Dimitrov, D.S. (1986) Liposome electroformation. *Faraday Discussions of Chemical Society*, **81**, 303-311.

14. Angelova, M.I., Soleau, S., Meleard, P., Faucon, J.F. and Bothorel, P. (1992) Preparation of giant vesicles by external AC electric fields. Kinetics and applications. *Progress in Colloid and Polymer Science*, **89**, 127-131.

15. Apellaniz, B., Garcia-Saez, A.J., Huarte, N., Kunert, R., Vorauer-Uhl, K., Katinger, H., Schwille, P. and Nieva, J.L. (2010) Confocal microscopy of giant vesicles supports the absence of HIV-1 neutralizing 2F5 antibody reactivity to plasma membrane phospholipids. *FEBS Letters*, **584**, 1591-1596.

16. Astriab-Fisher, A., Sergueev, D., Fisher, M., Shaw, B.R. and Juliano, R.L. (2002) Conjugates of antisense oligonucleotides with the Tat and antennapedia cell-penetrating peptides: effects on cellular uptake, binding to target sequences, and biologic actions. *Pharmaceutical Research*, **19**, 744-754.

17. Augustine, K. (1997) Antisense approaches for investigating mechanisms of abnormal development. *Mutation Research*, **396**, 175-193.

18. Avino, A., Ocampo, S.M., Lucas, R., Reina, J.J., Morales, J.C., Perales, J.C. and Eritja, R. (2011) Synthesis and *in vitro* inhibition properties of siRNA conjugates carrying glucose and galactose with different presentations. *Molecular Diversity*, **15**, 751-757.

19. Baba, T., Rauch, C., Xue, M., Terada, N., Fujii, Y., Ueda, H., Takayama, I., Ohno, S., Farge, E. and Sato, S.B. (2001) Clathrin-dependent and clathrin-independent endocytosis are differentially sensitive to insertion of poly (ethylene glycol)-derivatized cholesterol in the plasma membrane. *Traffic*, **2**, 501-512.

20. Baek, D., Villen, J., Shin, C., Camargo, F.D., Gygi, S.P. and Bartel, D.P. (2008) The impact of microRNAs on protein output. *Nature*, **455**, 64-71.

21. Bagatolli, L.A. (2003) Thermotropic behavior of lipid mixtures studied at the level of single vesicles: giant unilamellar vesicles and two-photon excitation fluorescence microscopy. *Methods in Enzymology*, **367**, 233-253.

22. Bagatolli, L.A. (2006) To see or not to see: lateral organization of biological membranes and fluorescence microscopy. *Biochimica et Biophysica Acta*, **1758**, 1541-1556.

23. Baker, B.F., Lot, S.S., Condon, T.P., Cheng-Flournoy, S., Lesnik, E.A., Sasmor, H.M. and Bennett, C.F. (1997) 2'-O-(2-Methoxy)ethyl-modified anti-intercellular adhesion molecule 1 (ICAM-1) oligonucleotides selectively increase the ICAM-1 mRNA level and inhibit formation of the ICAM-1 translation initiation complex in human umbilical vein endothelial cells. *The Journal of Biological Chemistry*, **272**, 11994-12000.

24. Bally, M.B., Harvie, P., Wong, F.M., Kong, S., Wasan, E.K. and Reimer, D.L. (1999) Biological barriers to cellular delivery of lipid-based DNA carriers. *Advanced Drug Delivery Reviews*, **38**, 291-315.

25. Bartel, D.P. (2004) MicroRNAs: genomics, biogenesis, mechanism, and function. *Cell*, **116**, 281-297.

26. Bartlett, D.W. and Davis, M.E. (2007) Physicochemical and biological characterization of targeted, nucleic acid-containing nanoparticles. *Bioconjugate Chemistry*, **18**, 456-468.

27. Bauer, S. and Wagner, H. (2002) Bacterial CpG-DNA licenses TLR9. *Current Topics in Microbiology and Immunology*, **270**, 145-154.

28. Baumgart, T., Hammond, A.T., Sengupta, P., Hess, S.T., Holowka, D.A., Baird, B.A. and Webb, W.W. (2007) Large-scale fluid/fluid phase separation of proteins

and lipids in giant plasma membrane vesicles. *Proceedings of the National Academy of Sciences USA*, **104**, 3165-3170.

29.   Baumgart, T., Hess, S.T. and Webb, W.W. (2003) Imaging coexisting fluid domains in biomembrane models coupling curvature and line tension. *Nature*, **425**, 821-824.

30.   Bawa, R., Fung, S.Y., Shiozaki, A., Yang, H., Zheng, G., Keshavjee, S. and Liu, M. (2011) Self-assembling peptide-based nanoparticles enhance cellular delivery of the hydrophobic anticancer drug ellipticine through caveolae-dependent endocytosis. *Nanomedicine: Nanotechnology, Biology, and Medicine*. (in press).

31.   Bayer, N., Schober, D., Prchla, E., Murphy, R.F., Blaas, D. and Fuchs, R. (1998) Effect of bafilomycin A1 and nocodazole on endocytic transport in HeLa cells: implications for viral uncoating and infection. *Journal of Virology*, **72**, 9645-9655.

32.   Beales, P.A. and Vanderlick, T.K. (2007) Specific binding of different vesicle populations by the hybridization of membrane-anchored DNA. *The Journal of Physical Chemistry. A*, **111**, 12372-12380.

33.   Beales, P.A. and Vanderlick, T.K. (2009) Partitioning of membrane-anchored DNA between coexisting lipid phases. *The Journal of Physical Chemistry. B*, **113**, 13678-13686.

34.   Beljaars, L., Molema, G., Weert, B., Bonnema, H., Olinga, P., Groothuis, G.M., Meijer, D.K. and Poelstra, K. (1999) Albumin modified with mannose 6-phosphate: A potential carrier for selective delivery of antifibrotic drugs to rat and human hepatic stellate cells. *Hepatology*, **29**, 1486-1493.

35.   Bene, A., Kurten, R.C. and Chambers, T.C. (2004) Subcellular localization as a limiting factor for utilization of decoy oligonucleotides. *Nucleic Acids Research*, **32**, e142.

36.   Benimetskaya, L., Loike, J.D., Khaled, Z., Loike, G., Silverstein, S.C., Cao, L., el Khoury, J., Cai, T.Q. and Stein, C.A. (1997) Mac-1 (CD11b/CD18) is an oligodeoxynucleotide-binding protein. *Nature Medicine*, **3**, 414-420.

37.   Benimetskaya, L., Tonkinson, J.L., Koziolkiewicz, M., Karwowski, B., Guga, P., Zeltser, R., Stec, W. and Stein, C.A. (1995) Binding of phosphorothioate oligonucleotides to basic fibroblast growth factor, recombinant soluble CD4,

laminin and fibronectin is P-chirality independent. *Nucleic Acids Research*, **23**, 4239-4245.

38. Bennett, C.F., Chiang, M.Y., Chan, H., Shoemaker, J.E. and Mirabelli, C.K. (1992) Cationic lipids enhance cellular uptake and activity of phosphorothioate antisense oligonucleotides. *Molecular Pharmacology*, **41**, 1023-1033.

39. Bernstein, E., Caudy, A.A., Hammond, S.M. and Hannon, G.J. (2001) Role for a bidentate ribonuclease in the initiation step of RNA interference. *Nature*, **409**, 363-366.

40. Bijsterbosch, M.K., Manoharan, M., Dorland, R., Waarlo, I.H., Biessen, E.A. and van Berkel, T.J. (2001) Delivery of cholesteryl-conjugated phosphorothioate oligodeoxynucleotides to Kupffer cells by lactosylated low-density lipoprotein. *Biochemical Pharmacology*, **62**, 627-633.

41. Bijsterbosch, M.K., Rump, E.T., De Vrueh, R.L., Dorland, R., van Veghel, R., Tivel, K.L., Biessen, E.A., van Berkel, T.J. and Manoharan, M. (2000) Modulation of plasma protein binding and *in vivo* liver cell uptake of phosphorothioate oligodeoxynucleotides by cholesterol conjugation. *Nucleic Acids Research*, **28**, 2717-2725.

42. Binnig, G., Quate, C.F. and Gerber, C. (1986) Atomic force microscope. *Physical Review Letters*, **56**, 930-933.

43. Blake, K.R., Murakami, A., Spitz, S.A., Glave, S.A., Reddy, M.P., Ts'o, P.O. and Miller, P.S. (1985) Hybridization arrest of globin synthesis in rabbit reticulocyte lysates and cells by oligodeoxyribonucleoside methylphosphonates. *Biochemistry*, **24**, 6139-6145.

44. Boggs, J.M. (1980) Intermolecular hydrogen bonding between lipids: influence on organization and function of lipids in membranes. *Canadian Journal of Biochemistry*, **58**, 755-770.

45. Bondensgaard, K., Petersen, M., Singh, S.K., Rajwanshi, V.K., Kumar, R., Wengel, J. and Jacobsen, J.P. (2000) Structural studies of LNA:RNA duplexes by NMR: conformations and implications for RNase H activity. *Chemistry*, **6**, 2687-2695.

46.   Bouaouina, M., Blouin, E., Halbwachs-Mecarelli, L., Lesavre, P. and Rieu, P. (2004) TNF-induced beta2 integrin activation involves Src kinases and a redox-regulated activation of p38 MAPK. *The Journal of Immunology*, **173**, 1313-1320.

47.   Boutorin, A.S., Gus'kova, L.V., Ivanova, E.M., Kobetz, N.D., Zarytova, V.F., Ryte, A.S., Yurchenko, L.V. and Vlassov, V.V. (1989) Synthesis of alkylating oligonucleotide derivatives containing cholesterol or phenazinium residues at their 3'-terminus and their interaction with DNA within mammalian cells. *FEBS Letters*, **254**, 129-132.

48.   Bouxsein, N.F., McAllister, C.S., Ewert, K.K., Samuel, C.E. and Safinya, C.R. (2007) Structure and gene silencing activities of monovalent and pentavalent cationic lipid vectors complexed with siRNA. *Biochemistry*, **46**, 4785-4792.

49.   Braasch, D.A. and Corey, D.R. (2001) Locked nucleic acid (LNA): fine-tuning the recognition of DNA and RNA. *Chemistry & Biology*, **8**, 1-7.

50.   Braasch, D.A. and Corey, D.R. (2002) Lipid-mediated introduction of peptide nucleic acids into cells. *Methods in Molecular Biology*, **208**, 211-223.

51.   Braasch, D.A., Jensen, S., Liu, Y., Kaur, K., Arar, K., White, M.A. and Corey, D.R. (2003) RNA interference in mammalian cells by chemically-modified RNA. *Biochemistry*, **42**, 7967-7975.

52.   Bradley, J.R., Johnson, D.R. and Pober, J.S. (1993) Four different classes of inhibitors of receptor-mediated endocytosis decrease tumor necrosis factor-induced gene expression in human endothelial cells. *The Journal of Immunology*, **150**, 5544-5555.

53.   Breaker, R.R. and Joyce, G.F. (1994) A DNA enzyme that cleaves RNA. *Chemistry & Biology*, **1**, 223-229.

54.   Brown, D.A., Kang, S.H., Gryaznov, S.M., DeDionisio, L., Heidenreich, O., Sullivan, S., Xu, X. and Nerenberg, M.I. (1994) Effect of phosphorothioate modification of oligodeoxynucleotides on specific protein binding. *The Journal of Biological Chemistry*, **269**, 26801-26805.

55. Brown, M.F., Thurmond, R.L., Dodd, S.W., Otten, D. and Beyer, K. (2001) Composite membrane deformation on the mesoscopic length scale. *Physical Review. E, Statistical, Nonlinear, and Soft Matter Physics*, **64**, 010901-010904.

56. Brown, M.F., Thurmond, R.L., Dodd, S.W., Otten, D. and Beyer, K. (2002) Elastic deformation of membrane bilayers probed by deuterium NMR relaxation. *Journal of the American Chemical Society*, **124**, 8471-8484.

57. Bunge, A., Kurz, A., Windeck, A.K., Korte, T., Flasche, W., Liebscher, J., Herrmann, A. and Huster, D. (2007) Lipophilic oligonucleotides spontaneously insert into lipid membranes, bind complementary DNA strands, and sequester into lipid-disordered domains. *Langmuir: the ACS Journal of Surfaces and Colloids*, **23**, 4455-4464.

58. Bunge, A., Loew, M., Pescador, P., Arbuzova, A., Brodersen, N., Kang, J., Dahne, L., Liebscher, J., Herrmann, A., Stengel, G. *et al.* (2009) Lipid membranes carrying lipophilic cholesterol-based oligonucleotides--characterization and application on layer-by-layer coated particles. *The Journal of Physical Chemistry. B*, **113**, 16425-16434.

59. Burch, R.M. and Mahan, L.C. (1991) Oligonucleotides antisense to the interleukin 1 receptor mRNA block the effects of interleukin 1 in cultured murine and human fibroblasts and in mice. *The Journal of Clinical Investigation*, **88**, 1190-1196.

60. Busto, J.V., Sot, J., Goni, F.M., Mollinedo, F. and Alonso, A. (2007) Surface-active properties of the antitumour ether lipid 1-O-octadecyl-2-O-methyl-rac-glycero-3-phosphocholine (edelfosine). *Biochimica et Biophysica Acta*, **1768**, 1855-1860.

61. Busto, J.V., Sot, J., Requejo-Isidro, J., Goni, F.M. and Alonso, A. (2010) Cholesterol displaces palmitoylceramide from its tight packing with palmitoylsphingomyelin in the absence of a liquid-disordered phase. *Biophysical Journal*, **99**, 1119-1128.

62. Caseli, L., Pascholati, C.P., Teixeira, F., Jr., Nosov, S., Vebert, C., Mueller, A.H. and Oliveira, O.N., Jr. (2010) Interaction of oligonucleotide-based amphiphilic block copolymers with cell membrane models. *Journal of Colloid and Interface Science*, **347**, 56-61.

63. Cech, T.R., Zaug, A.J. and Grabowski, P.J. (1981) *In vitro* splicing of the ribosomal RNA precursor of Tetrahymena: involvement of a guanosine nucleotide in the excision of the intervening sequence. *Cell*, **27**, 487-496.

64. Chan, Y.H., van Lengerich, B. and Boxer, S.G. (2009) Effects of linker sequences on vesicle fusion mediated by lipid-anchored DNA oligonucleotides. *Proceedings of the National Academy of Sciences USA*, **106**, 979-984.

65. Chekulaeva, M. and Filipowicz, W. (2009) Mechanisms of miRNA-mediated post-transcriptional regulation in animal cells. *Current Opinion in Cell Biology*, **21**, 452-460.

66. Chelobanov, B.P., Laktionov, P.P. and Vlasov, V.V. (2006) Proteins involved in binding and cellular uptake of nucleic acids. *Biochemistry (Moscow)*, **71**, 583-596.

67. Chen, P.Y., Weinmann, L., Gaidatzis, D., Pei, Y., Zavolan, M., Tuschl, T. and Meister, G. (2008) Strand-specific 5'-O-methylation of siRNA duplexes controls guide strand selection and targeting specificity. *RNA*, **14**, 263-274.

68. Chen, X., Dudgeon, N., Shen, L. and Wang, J.H. (2005) Chemical modification of gene silencing oligonucleotides for drug discovery and development. *Drug Discovery Today*, **10**, 587-593.

69. Cheng, K., Ye, Z., Guntaka, R.V. and Mahato, R.I. (2006) Enhanced hepatic uptake and bioactivity of type alpha1(I) collagen gene promoter-specific triplex-forming oligonucleotides after conjugation with cholesterol. *The Journal of Pharmacology and Experimental Therapeutics*, **317**, 797-805.

70. Chin, D.J., Green, G.A., Zon, G., Szoka, F.C., Jr. and Straubinger, R.M. (1990) Rapid nuclear accumulation of injected oligodeoxyribonucleotides. *The New Biologist*, **2**, 1091-1100.

71. Chithrani, B.D., Ghazani, A.A. and Chan, W.C. (2006) Determining the size and shape dependence of gold nanoparticle uptake into mammalian cells. *Nano Letters*, **6**, 662-668.

72. Chiu, Y.L., Ali, A., Chu, C.Y., Cao, H. and Rana, T.M. (2004) Visualizing a correlation between siRNA localization, cellular uptake, and RNAi in living cells. *Chemistry & Biology*, **11**, 1165-1175.

73. Chiu, Y.L. and Rana, T.M. (2003) siRNA function in RNAi: a chemical modification analysis. *RNA*, **9**, 1034-1048.

74. Cho, C.S., Kobayashi, A., Takei, R., Ishihara, T., Maruyama, A. and Akaike, T. (2001) Receptor-mediated cell modulator delivery to hepatocyte using nanoparticles coated with carbohydrate-carrying polymers. *Biomaterials*, **22**, 45-51.

75. Choi, Y., Thomas, T., Kotlyar, A., Islam, M.T. and Baker, J.R., Jr. (2005) Synthesis and functional evaluation of DNA-assembled polyamidoamine dendrimer clusters for cancer cell-specific targeting. *Chemistry & Biology*, **12**, 35-43.

76. Chu, R.S., Targoni, O.S., Krieg, A.M., Lehmann, P.V. and Harding, C.V. (1997) CpG oligodeoxynucleotides act as adjuvants that switch on T helper 1 (Th1) immunity. *The Journal of Experimental Medicine*, **186**, 1623-1631.

77. Chu, T.C., Twu, K.Y., Ellington, A.D. and Levy, M. (2006) Aptamer mediated siRNA delivery. *Nucleic Acids Research*, **34**, e73.

78. Chung, H.J., Hong, C.A., Lee, S.H., Jo, S.D. and Park, T.G. (2011) Reducible siRNA dimeric conjugates for efficient cellular uptake and gene silencing. *Bioconjugate Chemistry*, **22**, 299-306.

79. Clarenc, J.P., Degols, G., Leonetti, J.P., Milhaud, P. and Lebleu, B. (1993) Delivery of antisense oligonucleotides by poly(L-lysine) conjugation and liposome encapsulation. *Anti-Cancer Drug Design*, **8**, 81-94.

80. Connell, S.D. and Smith, D.A. (2006) The atomic force microscope as a tool for studying phase separation in lipid membranes. *Molecular Membrane Biology*, **23**, 17-28.

81. Conner, S.D. and Schmid, S.L. (2003) Regulated portals of entry into the cell. *Nature*, **422**, 37-44.

82. Cooney, M., Czernuszewicz, G., Postel, E.H., Flint, S.J. and Hogan, M.E. (1988) Site-specific oligonucleotide binding represses transcription of the human c-myc gene *in vitro*. *Science*, **241**, 456-459.

83. Coppelli, F.M. and Grandis, J.R. (2005) Oligonucleotides as anticancer agents: from the benchside to the clinic and beyond. *Current Pharmaceutical Design*, **11**, 2825-2840.

84. Crooke, S.T. (2000) Progress in antisense technology: the end of the beginning. *Methods in Enzymology*, **313**, 3-45.

85. Crooke, S.T. (2004) Progress in antisense technology. *Annual Review of Medicine*, **55**, 61-95.

86. Crooke, S.T., Graham, M.J., Zuckerman, J.E., Brooks, D., Conklin, B.S., Cummins, L.L., Greig, M.J., Guinosso, C.J., Kornbrust, D., Manoharan, M. *et al.* (1996) Pharmacokinetic properties of several novel oligonucleotide analogs in mice. *The Journal of Pharmacology and Experimental Therapeutics*, **277**, 923-937.

87. Crooke, S.T., Lemonidis, K.M., Neilson, L., Griffey, R., Lesnik, E.A. and Monia, B.P. (1995) Kinetic characteristics of Escherichia coli RNase H1: cleavage of various antisense oligonucleotide-RNA duplexes. *The Biochemical Journal*, **312**, 599-608.

88. Czech, M.P. (2006) MicroRNAs as therapeutic targets. *The New England Journal of Medicine*, **354**, 1194-1195.

89. Dalpke, A.H., Zimmermann, S., Albrecht, I. and Heeg, K. (2002) Phosphodiester CpG oligonucleotides as adjuvants: polyguanosine runs enhance cellular uptake and improve immunostimulative activity of phosphodiester CpG oligonucleotides *in vitro* and *in vivo*. *Immunology*, **106**, 102-112.

90. Dausend, J., Musyanovych, A., Dass, M., Walther, P., Schrezenmeier, H., Landfester, K. and Mailander, V. (2008) Uptake mechanism of oppositely charged fluorescent nanoparticles in HeLa cells. *Macromolecular Bioscience*, **8**, 1135-1143.

91. Davidson, B.L. and Paulson, H.L. (2004) Molecular medicine for the brain: silencing of disease genes with RNA interference. *Lancet Neurology*, **3**, 145-149.

92. Davis, B.G. and Robinson, M.A. (2002) Drug delivery systems based on sugar-macromolecule conjugates. *Current Opinion in Drug Discovery & Development*, **5**, 279-288.

93. Davis, M.E., Zuckerman, J.E., Choi, C.H., Seligson, D., Tolcher, A., Alabi, C.A., Yen, Y., Heidel, J.D. and Ribas, A. (2010) Evidence of RNAi in humans from systemically administered siRNA via targeted nanoparticles. *Nature*, **464**, 1067-1070.

94.   De Clercq, E., Eckstein, E. and Merigan, T.C. (1969) [Interferon induction increased through chemical modification of a synthetic polyribonucleotide]. *Science*, **165**, 1137-1139.

95.   de Diesbach, P., N'Kuli, F., Delmee, M. and Courtoy, P.J. (2003) Infection by *Mycoplasma hyorhinis* strongly enhances uptake of antisense oligonucleotides: a reassessment of receptor-mediated endocytosis in the HepG2 cell line. *Nucleic Acids Research*, **31**, 886-892.

96.   de Martimprey, H., Vauthier, C., Malvy, C. and Couvreur, P. (2009) Polymer nanocarriers for the delivery of small fragments of nucleic acids: oligonucleotides and siRNA. *European Journal of Pharmaceutics and Biopharmaceutics: Official Journal of Arbeitsgemeinschaft fur Pharmazeutische Verfahrenstechnik e.V*, **71**, 490-504.

97.   De Paula, D., Bentley, M.V. and Mahato, R.I. (2007) Hydrophobization and bioconjugation for enhanced siRNA delivery and targeting. *RNA*, **13**, 431-456.

98.   Derossi, D., Calvet, S., Trembleau, A., Brunissen, A., Chassaing, G. and Prochiantz, A. (1996) Cell internalization of the third helix of the Antennapedia homeodomain is receptor-independent. *The Journal of Biological Chemistry*, **271**, 18188-18193.

99.   Derossi, D., Joliot, A.H., Chassaing, G. and Prochiantz, A. (1994) The third helix of the Antennapedia homeodomain translocates through biological membranes. *The Journal of Biological Chemistry*, **269**, 10444-10450.

100.   Deshayes, S., Gerbal-Chaloin, S., Morris, M.C., Aldrian-Herrada, G., Charnet, P., Divita, G. and Heitz, F. (2004) On the mechanism of non-endosomial peptide-mediated cellular delivery of nucleic acids. *Biochimica et Biophysica Acta*, **1667**, 141-147.

101.   Desigaux, L., Sainlos, M., Lambert, O., Chevre, R., Letrou-Bonneval, E., Vigneron, J.P., Lehn, P., Lehn, J.M. and Pitard, B. (2007) Self-assembled lamellar complexes of siRNA with lipidic aminoglycoside derivatives promote efficient siRNA delivery and interference. *Proceedings of the National Academy of Sciences USA*, **104**, 16534-16539.

102. Dewey, R.A., Morrissey, G., Cowsill, C.M., Stone, D., Bolognani, F., Dodd, N.J., Southgate, T.D., Klatzmann, D., Lassmann, H., Castro, M.G. *et al.* (1999) Chronic brain inflammation and persistent herpes simplex virus 1 thymidine kinase expression in survivors of syngeneic glioma treated by adenovirus-mediated gene therapy: implications for clinical trials. *Nature Medicine*, **5**, 1256-1263.

103. Dias, N., Dheur, S., Nielsen, P.E., Gryaznov, S., Van Aerschot, A., Herdewijn, P., Helene, C. and Saison-Behmoaras, T.E. (1999) Antisense PNA tridecamers targeted to the coding region of Ha-ras mRNA arrest polypeptide chain elongation. *Journal of Molecular Biology*, **294**, 403-416.

104. Dias, N. and Stein, C.A. (2002) Antisense oligonucleotides: basic concepts and mechanisms. *Molecular Cancer Therapeutics*, **1**, 347-355.

105. Doherty, G.J. and McMahon, H.T. (2009) Mechanisms of endocytosis. *Annual Review of Biochemistry*, **78**, 857-902.

106. Dominska, M. and Dykxhoorn, D.M. (2010) Breaking down the barriers: siRNA delivery and endosome escape. *Journal of Cell Science*, **123**, 1183-1189.

107. Donis-Keller, H. (1979) Site specific enzymatic cleavage of RNA. *Nucleic Acids Research*, **7**, 179-192.

108. dos Santos, T., Varela, J., Lynch, I., Salvati, A. and Dawson, K.A. (2011) Effects of transport inhibitors on the cellular uptake of carboxylated polystyrene nanoparticles in different cell lines. *PloS ONE*, **6**, e24438.

109. Dufes, C., Schatzlein, A.G., Tetley, L., Gray, A.I., Watson, D.G., Olivier, J.C., Couet, W. and Uchegbu, I.F. (2000) Niosomes and polymeric chitosan based vesicles bearing transferrin and glucose ligands for drug targeting. *Pharmaceutical Research*, **17**, 1250-1258.

110. Dwyer, D.S. (2001) Model of the 3-D structure of the GLUT3 glucose transporter and molecular dynamics simulation of glucose transport. *Proteins*, **42**, 531-541.

111. Edelstein, M.L., Abedi, M.R. and Wixon, J. (2007) Gene therapy clinical trials worldwide to 2007-an update. *The Journal of Gene Medicine*, **9**, 833-842.

112. Edelstein, M.L., Abedi, M.R., Wixon, J. and Edelstein, R.M. (2004) Gene therapy clinical trials worldwide 1989-2004-an overview. *The Journal of Gene Medicine*, **6**, 597-602.

113. Eder, P.S., DeVine, R.J., Dagle, J.M. and Walder, J.A. (1991) Substrate specificity and kinetics of degradation of antisense oligonucleotides by a 3' exonuclease in plasma. *Antisense Research and Development*, **1**, 141-151.

114. Egholm, M., Buchardt, O., Christensen, L., Behrens, C., Freier, S.M., Driver, D.A., Berg, R.H., Kim, S.K., Norden, B. and Nielsen, P.E. (1993) PNA hybridizes to complementary oligonucleotides obeying the Watson-Crick hydrogen-bonding rules. *Nature*, **365**, 566-568.

115. Elayadi, A.N. and Corey, D.R. (2001) Application of PNA and LNA oligomers to chemotherapy. *Current Opinion in Investigational Drugs*, **2**, 558-561.

116. Elbashir, S.M., Harborth, J., Lendeckel, W., Yalcin, A., Weber, K. and Tuschl, T. (2001b) Duplexes of 21-nucleotide RNAs mediate RNA interference in cultured mammalian cells. *Nature*, **411**, 494-498.

117. Elbashir, S.M., Lendeckel, W. and Tuschl, T. (2001c) RNA interference is mediated by 21- and 22-nucleotide RNAs. *Genes & Development*, **15**, 188-200.

118. Elbashir, S.M., Martinez, J., Patkaniowska, A., Lendeckel, W. and Tuschl, T. (2001a) Functional anatomy of siRNAs for mediating efficient RNAi in *Drosophila melanogaster* embryo lysate. *EMBO Journal*, **20**, 6877-6888.

119. Elmen, J., Thonberg, H., Ljungberg, K., Frieden, M., Westergaard, M., Xu, Y., Wahren, B., Liang, Z., Orum, H., Koch, T. *et al.* (2005) Locked nucleic acid (LNA) mediated improvements in siRNA stability and functionality. *Nucleic Acids Research*, **33**, 439-447.

120. Elsabahy, M., Nazarali, A. and Foldvari, M. (2011) Non-viral nucleic acid delivery: key challenges and future directions. *Current Drug Delivery*, **8**, 235-244.

121. Epa, W.R., Rong, P., Bartlett, P.F., Coulson, E.J. and Barrett, G.L. (1998) Enhanced downregulation of the p75 nerve growth factor receptor by cholesteryl and bis-cholesteryl antisense oligonucleotides. *Antisense & Nucleic Acid Drug Development*, **8**, 489-498.

122. Erbacher, P., Bousser, M.T., Raimond, J., Monsigny, M., Midoux, P. and Roche, A.C. (1996) Gene transfer by DNA/glycosylated polylysine complexes into human blood monocyte-derived macrophages. *Human Gene Therapy*, **7**, 721-729.

123. Esau, C., Davis, S., Murray, S.F., Yu, X.X., Pandey, S.K., Pear, M., Watts, L., Booten, S.L., Graham, M., McKay, R. *et al.* (2006) miR-122 regulation of lipid metabolism revealed by *in vivo* antisense targeting. *Cell Metabolism*, **3**, 87-98.

124. Famulok, M., Mayer, G. and Blind, M. (2000) Nucleic acid aptamers-from selection *in vitro* to applications *in vivo*. *Accounts of Chemical Research*, **33**, 591-599.

125. Farokhzad, O.C., Jon, S., Khademhosseini, A., Tran, T.N., Lavan, D.A. and Langer, R. (2004) Nanoparticle-aptamer bioconjugates: a new approach for targeting prostate cancer cells. *Cancer Research*, **64**, 7668-7672.

126. Farrell, L.L., Pepin, J., Kucharski, C., Lin, X., Xu, Z. and Uludag, H. (2007) A comparison of the effectiveness of cationic polymers poly-L-lysine (PLL) and polyethylenimine (PEI) for non-viral delivery of plasmid DNA to bone marrow stromal cells (BMSC). *European Journal of Pharmaceutics and Biopharmaceutics: Official Journal of Arbeitsgemeinschaft fur Pharmazeutische Verfahrenstechnik e.V*, **65**, 388-397.

127. Farsad, K. and De Camilli, P. (2003) Mechanisms of membrane deformation. *Current Opinion in Cell Biology*, **15**, 372-381.

128. Fawell, S., Seery, J., Daikh, Y., Moore, C., Chen, L.L., Pepinsky, B. and Barsoum, J. (1994) Tat-mediated delivery of heterologous proteins into cells. *Proceedings of the National Academy of Sciences USA*, **91**, 664-668.

129. Felgner, P.L., Gadek, T.R., Holm, M., Roman, R., Chan, H.W., Wenz, M., Northrop, J.P., Ringold, G.M. and Danielsen, M. (1987) Lipofection: a highly efficient, lipid-mediated DNA-transfection procedure. *Proceedings of the National Academy of Sciences USA*, **84**, 7413-7417.

130. Felgner, P.L. and Ringold, G.M. (1989) Cationic liposome-mediated transfection. *Nature*, **337**, 387-388.

131. Fennewald, S.M. and Rando, R.F. (1995) Inhibition of high affinity basic fibroblast growth factor binding by oligonucleotides. *The Journal of Biological Chemistry*, **270**, 21718-21721.

132. Fernando, H., Reszka, A.P., Huppert, J., Ladame, S., Rankin, S., Venkitaraman, A.R., Neidle, S. and Balasubramanian, S. (2006) A conserved quadruplex motif located in a transcription activation site of the human c-kit oncogene. *Biochemistry*, **45**, 7854-7860.

133. Fire, A., Xu, S., Montgomery, M.K., Kostas, S.A., Driver, S.E. and Mello, C.C. (1998) Potent and specific genetic interference by double-stranded RNA in *Caenorhabditis elegans*. *Nature*, **391**, 806-811.

134. Fisher, T.L., Terhorst, T., Cao, X. and Wagner, R.W. (1993) Intracellular disposition and metabolism of fluorescently-labeled unmodified and modified oligonucleotides microinjected into mammalian cells. *Nucleic Acids Research*, **21**, 3857-3865.

135. Fluiter, K., ten Asbroek, A.L., de Wissel, M.B., Jakobs, M.E., Wissenbach, M., Olsson, H., Olsen, O., Oerum, H. and Baas, F. (2003) *In vivo* tumor growth inhibition and biodistribution studies of locked nucleic acid (LNA) antisense oligonucleotides. *Nucleic Acids Research*, **31**, 953-962.

136. Fonseca, D.E. and Kline, J.N. (2009) Use of CpG oligonucleotides in treatment of asthma and allergic disease. *Advanced Drug Delivery Reviews*, **61**, 256-262.

137. Forsha, S.J., Panyutin, I.V., Neumann, R.D. and Panyutin, I.G. (2010) Intracellular traffic of oligodeoxynucleotides in and out of the nucleus: effect of exportins and DNA structure. *Oligonucleotides*, **20**, 277-284.

138. Fox, J.L. (2000) Gene-therapy death prompts broad civil lawsuit. *Nature Biotechnology*, **18**, 1136.

139. Frankel, A.D. and Pabo, C.O. (1988) Cellular uptake of the tat protein from human immunodeficiency virus. *Cell*, **55**, 1189-1193.

140. Fretz, M., Jin, J., Conibere, R., Penning, N.A., Al-Taei, S., Storm, G., Futaki, S., Takeuchi, T., Nakase, I. and Jones, A.T. (2006) Effects of Na+/H+ exchanger inhibitors on subcellular localisation of endocytic organelles and intracellular dynamics of protein transduction domains HIV-TAT peptide and octaarginine.

Journal of Controlled Release: Official Journal of the Controlled Release Society, **116**, 247-254.

141. Futaki, S., Suzuki, T., Ohashi, W., Yagami, T., Tanaka, S., Ueda, K. and Sugiura, Y. (2001) Arginine-rich peptides. An abundant source of membrane-permeable peptides having potential as carriers for intracellular protein delivery. *The Journal of Biological Chemistry*, **276**, 5836-5840.

142. Gabor, F., Bogner, E., Weissenboeck, A. and Wirth, M. (2004) The lectin-cell interaction and its implications to intestinal lectin-mediated drug delivery. *Advanced Drug Delivery Reviews*, **56**, 459-480.

143. Garbuzenko, O.B., Saad, M., Betigeri, S., Zhang, M., Vetcher, A.A., Soldatenkov, V.A., Reimer, D.C., Pozharov, V.P. and Minko, T. (2009) Intratracheal versus intravenous liposomal delivery of siRNA, antisense oligonucleotides and anticancer drug. *Pharmaceutical Research*, **26**, 382-394.

144. Garcia-Saez, A.J., Chiantia, S. and Schwille, P. (2007) Effect of line tension on the lateral organization of lipid membranes. *The Journal of Biological Chemistry*, **282**, 33537-33544.

145. Garcia-Saez, A.J. and Schwille, P. (2010) Surface analysis of membrane dynamics. *Biochimica et Biophysica Acta*, **1798**, 766-776.

146. Garzon, R., Pichiorri, F., Palumbo, T., Iuliano, R., Cimmino, A., Aqeilan, R., Volinia, S., Bhatt, D., Alder, H., Marcucci, G. *et al.* (2006) MicroRNA fingerprints during human megakaryocytopoiesis. *Proceedings of the National Academy of Sciences USA*, **103**, 5078-5083.

147. Gewirtz, A.M. (2000) Oligonucleotide therapeutics: a step forward. *Journal of Clinical Oncology: Official Journal of the American Society of Clinical Oncology*, **18**, 1809-1811.

148. Gewirtz, A.M., Sokol, D.L. and Ratajczak, M.Z. (1998) Nucleic acid therapeutics: state of the art and future prospects. *Blood*, **92**, 712-736.

149. Ghosh, P., Dahms, N.M. and Kornfeld, S. (2003) Mannose 6-phosphate receptors: new twists in the tale. *Nature reviews. Molecular Cell Biology*, **4**, 202-212.

150.   Gibbings, D.J., Ciaudo, C., Erhardt, M. and Voinnet, O. (2009) Multivesicular bodies associate with components of miRNA effector complexes and modulate miRNA activity. *Nature Cell Biology*, **11**, 1143-1149.

151.   Goldenberg, N.M., Grinstein, S. and Silverman, M. (2007) Golgi-bound Rab34 is a novel member of the secretory pathway. *Molecular Biology of the Cell*, **18**, 4762-4771.

152.   Gonzalez, H., Hwang, S.J. and Davis, M.E. (1999) New class of polymers for the delivery of macromolecular therapeutics. *Bioconjugate Chemistry*, **10**, 1068-1074.

153.   Goodchild, J. (2011) Therapeutic oligonucleotides. *Methods in Molecular Biology*, **764**, 1-15.

154.   Gordon, S.P., Berezhna, S., Scherfeld, D., Kahya, N. and Schwille, P. (2005) Characterization of interaction between cationic lipid-oligonucleotide complexes and cellular membrane lipids using confocal imaging and fluorescence correlation spectroscopy. *Biophysical Journal*, **88**, 305-316.

155.   Gosse, C., Boutorine, A., Aujard, I., Chami, M., Kononov, A., Cogne-Laage, E., Allemand, J.F., Li, J. and Jullien, L. (2004) Micelles of Lipid-Oligonucleotide Conjugates: Implications for Membrane Anchoring and Base Pairing. *The Journal of Physical Chemistry. B*, **108**, 6485-6497.

156.   Gottlieb, T.A., Ivanov, I.E., Adesnik, M. and Sabatini, D.D. (1993) Actin microfilaments play a critical role in endocytosis at the apical but not the basolateral surface of polarized epithelial cells. *The Journal of Cell Biology*, **120**, 695-710.

157.   Gould, G.W. and Lippincott-Schwartz, J. (2009) New roles for endosomes: from vesicular carriers to multi-purpose platforms. *Nature Reviews. Molecular Cell Biology*, **10**, 287-292.

158.   Green, M. and Loewenstein, P.M. (1988) Autonomous functional domains of chemically synthesized human immunodeficiency virus tat trans-activator protein. *Cell*, **55**, 1179-1188.

159.   Gregory, R.I. and Shiekhattar, R. (2005) MicroRNA biogenesis and cancer. *Cancer Research*, **65**, 3509-3512.

160. Grigoriev, M., Praseuth, D., Guieysse, A.L., Robin, P., Thuong, N.T., Helene, C. and Harel-Bellan, A. (1993) Inhibition of gene expression by triple helix-directed DNA cross-linking at specific sites. *Proceedings of the National Academy of Sciences USA*, **90**, 3501-3505.

161. Grijalvo, S., Ocampo, S.M., Perales, J.C. and Eritja, R. (2010) Synthesis of oligonucleotides carrying amino lipid groups at the 3'-end for RNA interference studies. *The Journal of Organic Chemistry*, **75**, 6806-6813.

162. Grijalvo, S., Ocampo, S.M., Perales, J.C. and Eritja, R. (2011) Synthesis of lipid-oligonucleotide conjugates for RNA interference studies. *Chemistry & Biodiversity*, **8**, 287-299.

163. Guerrier-Takada, C., Gardiner, K., Marsh, T., Pace, N. and Altman, S. (1983) The RNA moiety of ribonuclease P is the catalytic subunit of the enzyme. *Cell*, **35**, 849-857.

164. Guo, B., Zhang, Y., Luo, G., Li, L. and Zhang, J. (2009) Lentivirus-mediated small interfering RNA targeting VEGF-C inhibited tumor lymphangiogenesis and growth in breast carcinoma. *Anatomical Record (Hoboken)*, **292**, 633-639.

165. Guo, K., Pourpak, A., Beetz-Rogers, K., Gokhale, V., Sun, D. and Hurley, L.H. (2007) Formation of pseudosymmetrical G-quadruplex and i-motif structures in the proximal promoter region of the RET oncogene. *Journal of the American Chemical Society*, **129**, 10220-10228.

166. Guo, X., Geng, M. and Du, G. (2005) Glucose transporter 1, distribution in the brain and in neural disorders: its relationship with transport of neuroactive drugs through the blood-brain barrier. *Biochemical Genetics*, **43**, 175-187.

167. Guvakova, M.A., Yakubov, L.A., Vlodavsky, I., Tonkinson, J.L. and Stein, C.A. (1995) Phosphorothioate oligodeoxynucleotides bind to basic fibroblast growth factor, inhibit its binding to cell surface receptors, and remove it from low affinity binding sites on extracellular matrix. *The Journal of Biological Chemistry*, **270**, 2620-2627.

168. Hall, A.H., Wan, J., Shaughnessy, E.E., Ramsay Shaw, B. and Alexander, K.A. (2004) RNA interference using boranophosphate siRNAs: structure-activity relationships. *Nucleic Acids Research*, **32**, 5991-6000.

169. Hamasaki, M., Araki, N. and Hatae, T. (2004) Association of early endosomal autoantigen 1 with macropinocytosis in EGF-stimulated A431 cells. *The Anatomical Record. Part A, Discoveries in Molecular, Cellular and Evolutionary Biology*, **277**, 298-306.

170. Hamilton, A.J. and Baulcombe, D.C. (1999) A species of small antisense RNA in posttranscriptional gene silencing in plants. *Science*, **286**, 950-952.

171. Hanss, B., Leal-Pinto, E., Bruggeman, L.A., Copeland, T.D. and Klotman, P.E. (1998) Identification and characterization of a cell membrane nucleic acid channel. *Proceedings of the National Academy of Sciences USA*, **95**, 1921-1926.

172. Hanss, B., Leal-Pinto, E., Teixeira, A., Christian, R.E., Shabanowitz, J., Hunt, D.F. and Klotman, P.E. (2002) Cytosolic malate dehydrogenase confers selectivity of the nucleic acid-conducting channel. *Proceedings of the National Academy of Sciences USA*, **99**, 1707-1712.

173. Hartig, R., Shoeman, R.L., Janetzko, A., Grub, S. and Traub, P. (1998) Active nuclear import of single-stranded oligonucleotides and their complexes with non-karyophilic macromolecules. *Biology of the Cell/under the auspices of the European Cell Biology Organization*, **90**, 407-426.

174. Hashida, N., Ohguro, N., Yamazaki, N., Arakawa, Y., Oiki, E., Mashimo, H., Kurokawa, N. and Tano, Y. (2008) High-efficacy site-directed drug delivery system using sialyl-Lewis X conjugated liposome. *Experimental Eye Research*, **86**, 138-149.

175. Hashimoto, M., Morimoto, M., Saimoto, H., Shigemasa, Y., Yanagie, H., Eriguchi, M. and Sato, T. (2006) Gene transfer by DNA/mannosylated chitosan complexes into mouse peritoneal macrophages. *Biotechnology Letters*, **28**, 815-821.

176. Hattori, Y., Suzuki, S., Kawakami, S., Yamashita, F. and Hashida, M. (2005) The role of dioleoylphosphatidylethanolamine (DOPE) in targeted gene delivery with

mannosylated cationic liposomes via intravenous route. *Journal of Controlled Release: Official Journal of the Controlled Release Society*, **108**, 484-495.

177. Heasman, J. (2002) Morpholino oligos: making sense of antisense? *Developmental Biology*, **243**, 209-214.

178. Heidel, J.D., Yu, Z., Liu, J.Y., Rele, S.M., Liang, Y., Zeidan, R.K., Kornbrust, D.J. and Davis, M.E. (2007) Administration in non-human primates of escalating intravenous doses of targeted nanoparticles containing ribonucleotide reductase subunit M2 siRNA. *Proceedings of the National Academy of Sciences USA*, **104**, 5715-5721.

179. Heijnen, H.F., Oorschot, V., Sixma, J.J., Slot, J.W. and James, D.E. (1997) Thrombin stimulates glucose transport in human platelets via the translocation of the glucose transporter GLUT-3 from alpha-granules to the cell surface. *The Journal of Cell Biology*, **138**, 323-330.

180. Hempelmann, E., Schirmer, R.H., Fritsch, G., Hundt, E. and Groschel-Stewart, U. (1987) Studies on glutathione reductase and methemoglobin from human erythrocytes parasitized with *Plasmodium falciparum*. *Molecular and Biochemical Parasitology*, **23**, 19-24.

181. Herbert, B.S., Gellert, G.C., Hochreiter, A., Pongracz, K., Wright, W.E., Zielinska, D., Chin, A.C., Harley, C.B., Shay, J.W. and Gryaznov, S.M. (2005) Lipid modification of GRN163, an N3'-->P5' thio-phosphoramidate oligonucleotide, enhances the potency of telomerase inhibition. *Oncogene*, **24**, 5262-5268.

182. Hewlett, L.J., Prescott, A.R. and Watts, C. (1994) The coated pit and macropinocytic pathways serve distinct endosome populations. *The Journal of Cell Biology*, **124**, 689-703.

183. Higashi, T., Tamaki, N., Honda, T., Torizuka, T., Kimura, T., Inokuma, T., Ohshio, G., Hosotani, R., Imamura, M. and Konishi, J. (1997) Expression of glucose transporters in human pancreatic tumors compared with increased FDG accumulation in PET study. *Journal of Nuclear Medicine: Official Publication, Society of Nuclear Medicine*, **38**, 1337-1344.

184. Hirai, M., Minematsu, H., Kondo, N., Oie, K., Igarashi, K. and Yamazaki, N. (2007) Accumulation of liposome with Sialyl Lewis X to inflammation and tumor region: application to *in vivo* bio-imaging. *Biochemical and Biophysical Research Communications*, **353**, 553-558.

185. Hiraki, Y., Rosen, O.M. and Birnbaum, M.J. (1988) Growth factors rapidly induce expression of the glucose transporter gene. *The Journal of Biological Chemistry*, **263**, 13655-13662.

186. Hoekstra, D., Rejman, J., Wasungu, L., Shi, F. and Zuhorn, I. (2007) Gene delivery by cationic lipids: in and out of an endosome. *Biochemical Society Transactions*, **35**, 68-71.

187. Hogrefe, R.I. (1999) An antisense oligonucleotide primer. *Antisense & Nucleic Acid Drug Development*, **9**, 351-357.

188. Hollins, A.J., Benboubetra, M., Omidi, Y., Zinselmeyer, B.H., Schatzlein, A.G., Uchegbu, I.F. and Akhtar, S. (2004) Evaluation of generation 2 and 3 poly(propylenimine) dendrimers for the potential cellular delivery of antisense oligonucleotides targeting the epidermal growth factor receptor. *Pharmaceutical Research*, **21**, 458-466.

189. Holzer, A.K. and Howell, S.B. (2006) The internalization and degradation of human copper transporter 1 following cisplatin exposure. *Cancer Research*, **66**, 10944-10952.

190. Hou, Y., Xing, L., Fu, S., Zhang, X., Liu, J., Liu, H., Lv, B. and Cui, H. (2009) Down-regulation of inducible co-stimulator (ICOS) by intravitreal injection of small interfering RNA (siRNA) plasmid suppresses ongoing experimental autoimmune uveoretinitis in rats. *Graefe's Archive for Clinical and Experimental Ophthalmology = Albrecht von Graefes Archiv fur Klinische und Experimentelle Ophthalmologie*, **247**, 755-765.

191. Hudziak, R.M., Barofsky, E., Barofsky, D.F., Weller, D.L., Huang, S.B. and Weller, D.D. (1996) Resistance of morpholino phosphorodiamidate oligomers to enzymatic degradation. *Antisense & Nucleic Acid Drug Development*, **6**, 267-272.

192. Hudziak, R.M., Summerton, J., Weller, D.D. and Iversen, P.L. (2000) Antiproliferative effects of steric blocking phosphorodiamidate morpholino antisense agents directed against c-myc. *Antisense & Nucleic Acid Drug Development*, **10**, 163-176.

193. Hundal, R.S., Gomez-Munoz, A., Kong, J.Y., Salh, B.S., Marotta, A., Duronio, V. and Steinbrecher, U.P. (2003) Oxidized low density lipoprotein inhibits macrophage apoptosis by blocking ceramide generation, thereby maintaining protein kinase B activation and Bcl-XL levels. *The Journal of Biological Chemistry*, **278**, 24399-24408.

194. Hwang, H.W., Wentzel, E.A. and Mendell, J.T. (2007) A hexanucleotide element directs microRNA nuclear import. *Science*, **315**, 97-100.

195. Hwang, S.J., Bellocq, N.C. and Davis, M.E. (2001) Effects of structure of beta-cyclodextrin-containing polymers on gene delivery. *Bioconjugate Chemistry*, **12**, 280-290.

196. Iglina, A.A., Meschaninova, M.I. and Venyaminova, A.G. (2009) 5'-Lipophilic conjugates of oligonucleotides as components of cell delivery systems. *Nucleic Acids Symposium Series (Oxford)*, 121-122.

197. Ikeda, Y., Kubota, D. and Nagasaki, Y. (2010) Simple solid-phase synthesis and biological properties of carbohydrate-oligonucleotide conjugates modified at the 3'-terminus. *Bioconjugate Chemistry*, **21**, 1685-1690.

198. Ikeda, Y. and Taira, K. (2006) Ligand-targeted delivery of therapeutic siRNA. *Pharmaceutical Research*, **23**, 1631-1640.

199. Ivanov, A.I. (2008) Exocytosis and endocytosis. Preface. *Methods in Molecular Biology*, **440**, v-vi.

200. Iwabuchi, S. and Kawahara, K. (2011) Inducible astrocytic glucose transporter-3 contributes to the enhanced storage of intracellular glycogen during reperfusion after ischemia. *Neurochemistry International*, **59**, 319-325.

201. Jääskeläinen, I., Sternberg, B., Mönkkönen, J. and Urtti, A. (1998) Physicochemical and morphological properties of complexes made of cationic liposomes and oligonucleotides. *International Journal of Pharmaceutics*, **167**, 191-203.

202. Jackman, M.R., Shurety, W., Ellis, J.A. and Luzio, J.P. (1994) Inhibition of apical but not basolateral endocytosis of ricin and folate in Caco-2 cells by cytochalasin D. *Journal of Cell Science*, **107**, 2547-2556.

203. Jackson, A.L., Bartz, S.R., Schelter, J., Kobayashi, S.V., Burchard, J., Mao, M., Li, B., Cavet, G. and Linsley, P.S. (2003) Expression profiling reveals off-target gene regulation by RNAi. *Nature Biotechnology*, **21**, 635-637.

204. Janmey, P.A. and Kinnunen, P.K. (2006) Biophysical properties of lipids and dynamic membranes. *Trends in Cell Biology*, **16**, 538-546.

205. Jass, J., Tjarnhage, T. and Puu, G. (2000) From liposomes to supported, planar bilayer structures on hydrophilic and hydrophobic surfaces: an atomic force microscopy study. *Biophysical Journal*, **79**, 3153-3163.

206. Jekle, A., Keppler, O.T., De Clercq, E., Schols, D., Weinstein, M. and Goldsmith, M.A. (2003) *In vivo* evolution of human immunodeficiency virus type 1 toward increased pathogenicity through CXCR4-mediated killing of uninfected CD4 T cells. *Journal of Virology*, **77**, 5846-5854.

207. Jensen, K.K., Orum, H., Nielsen, P.E. and Norden, B. (1997) Kinetics for hybridization of peptide nucleic acids (PNA) with DNA and RNA studied with the BIAcore technique. *Biochemistry*, **36**, 5072-5077.

208. Jeong, J.H., Mok, H., Oh, Y.K. and Park, T.G. (2009) siRNA conjugate delivery systems. *Bioconjugate Chemistry*, **20**, 5-14.

209. Jiang, H.L., Kwon, J.T., Kim, E.M., Kim, Y.K., Arote, R., Jere, D., Jeong, H.J., Jang, M.K., Nah, J.W., Xu, C.X. *et al.* (2008) Galactosylated poly(ethylene glycol)-chitosan-graft-polyethylenimine as a gene carrier for hepatocyte-targeting. *Journal of Controlled Release: Official Journal of the Controlled Release Society*, **131**, 150-157.

210. Jin, Q., Agrawal, L., Vanhorn-Ali, Z. and Alkhatib, G. (2006) GLUT-1-independent infection of the glioblastoma/astroglioma U87 cells by the human T cell leukemia virus type 1. *Virology*, **353**, 99-110.

211. Joliot, A.H., Triller, A., Volovitch, M., Pernelle, C. and Prochiantz, A. (1991) alpha-2,8-Polysialic acid is the neuronal surface receptor of antennapedia homeobox peptide. *The New Biologist*, **3**, 1121-1134.

212. Jones, A.T., Gumbleton, M. and Duncan, R. (2003) Understanding endocytic pathways and intracellular trafficking: a prerequisite for effective design of advanced drug delivery systems. *Advanced Drug Delivery Reviews*, **55**, 1353-1357.

213. Juliano, R., Alam, M.R., Dixit, V. and Kang, H. (2008) Mechanisms and strategies for effective delivery of antisense and siRNA oligonucleotides. *Nucleic Acids Research*, **36**, 4158-4171.

214. Juliano, R.L., Ming, X. and Nakagawa, O. (2012) Cellular Uptake and Intracellular Trafficking of Antisense and siRNA Oligonucleotides. *Bioconjugate Chemistry*, **23**, 147-157.

215. Kalin, S., Amstutz, B., Gastaldelli, M., Wolfrum, N., Boucke, K., Havenga, M., DiGennaro, F., Liska, N., Hemmi, S. and Greber, U.F. (2010) Macropinocytotic uptake and infection of human epithelial cells with species B2 adenovirus type 35. *Journal of Virology*, **84**, 5336-5350.

216. Kalota, A., Shetzline, S.E. and Gewirtz, A.M. (2004) Progress in the development of nucleic acid therapeutics for cancer. *Cancer Biology & Therapy*, **3**, 4-12.

217. Katav, T., Liu, L., Traitel, T., Goldbart, R., Wolfson, M. and Kost, J. (2008) Modified pectin-based carrier for gene delivery: cellular barriers in gene delivery course. *Journal of Controlled Release: Official Journal of the Controlled Release Society*, **130**, 183-191.

218. Kawakami, S., Hattori, Y., Lu, Y., Higuchi, Y., Yamashita, F. and Hashida, M. (2004) Effect of cationic charge on receptor-mediated transfection using mannosylated cationic liposome/plasmid DNA complexes following the intravenous administration in mice. *Die Pharmazie*, **59**, 405-408.

219. Kawakami, S., Higuchi, Y. and Hashida, M. (2008) Nonviral approaches for targeted delivery of plasmid DNA and oligonucleotide. *Journal of Pharmaceutical Sciences*, **97**, 726-745.

220. Kawakami, S., Munakata, C., Fumoto, S., Yamashita, F. and Hashida, M. (2001) Novel galactosylated liposomes for hepatocyte-selective targeting of lipophilic drugs. *Journal of Pharmaceutical Sciences*, **90**, 105-113.

221. Keller, M., Harbottle, R.P., Perouzel, E., Colin, M., Shah, I., Rahim, A., Vaysse, L., Bergau, A., Moritz, S., Brahimi-Horn, C. *et al.* (2003) Nuclear localisation sequence templated nonviral gene delivery vectors: investigation of intracellular trafficking events of LMD and LD vector systems. *Chembiochem: a European Journal of Chemical Biology*, **4**, 286-298.

222. Khalil, I.A., Kogure, K., Akita, H. and Harashima, H. (2006) Uptake pathways and subsequent intracellular trafficking in nonviral gene delivery. *Pharmacological Reviews*, **58**, 32-45.

223. Khvorova, A., Reynolds, A. and Jayasena, S.D. (2003) Functional siRNAs and miRNAs exhibit strand bias. *Cell*, **115**, 209-216.

224. Kikin, O., D'Antonio, L. and Bagga, P.S. (2006) QGRS Mapper: a web-based server for predicting G-quadruplexes in nucleotide sequences. *Nucleic Acids Research*, **34**, W676-682.

225. Kim, D.H. and Rossi, J.J. (2007) Strategies for silencing human disease using RNA interference. *Nature Reviews. Genetics*, **8**, 173-184.

226. Kim, E.M., Jeong, H.J., Park, I.K., Cho, C.S., Moon, H.B., Yu, D.Y., Bom, H.S., Sohn, M.H. and Oh, I.J. (2005) Asialoglycoprotein receptor targeted gene delivery using galactosylated polyethylenimine-graft-poly(ethylene glycol): *in vitro* and *in vivo* studies. *Journal of Controlled Release: Official Journal of the Controlled Release Society*, **108**, 557-567.

227. Kim, H.G. and Miller, D.M. (1995) Inhibition of *in vitro* transcription by a triplex-forming oligonucleotide targeted to human c-myc P2 promoter. *Biochemistry*, **34**, 8165-8171.

228. Kim, H.G., Reddoch, J.F., Mayfield, C., Ebbinghaus, S., Vigneswaran, N., Thomas, S., Jones, D.E., Jr. and Miller, D.M. (1998) Inhibition of transcription of the human c-myc protooncogene by intermolecular triplex. *Biochemistry*, **37**, 2299-2304.

229. Kim, K.S., Lei, Y., Stolz, D.B. and Liu, D. (2007) Bifunctional compounds for targeted hepatic gene delivery. *Gene Therapy*, **14**, 704-708.

230. Kim, S.H., Mok, H., Jeong, J.H., Kim, S.W. and Park, T.G. (2006b) Comparative evaluation of target-specific GFP gene silencing efficiencies for antisense ODN, synthetic siRNA, and siRNA plasmid complexed with PEI-PEG-FOL conjugate. *Bioconjugate Chemistry*, **17**, 241-244.

231. Kim, T.H., Jin, H., Kim, H.W., Cho, M.H. and Cho, C.S. (2006a) Mannosylated chitosan nanoparticle-based cytokine gene therapy suppressed cancer growth in BALB/c mice bearing CT-26 carcinoma cells. *Molecular Cancer Therapeutics*, **5**, 1723-1732.

232. Kirsch, R., Jaffer, M.A., Woodburne, V.E., Sewell, T., Kelly, S.L., Kirsch, R.E. and Shephard, E.G. (2002) Fibrinogen is degraded and internalized during incubation with neutrophils, and fibrinogen products localize to electron lucent vesicles. *The Biochemical Journal*, **364**, 403-412.

233. Klug, W.S., Cummings, M.R., Spencer, C.A. and Palladino, M.A. (2008) *Concepts of Genetics*. 9th ed. Pearson Benjamin Cummings.

234. Kohyama, T., Kroll, D.M. and Gompper, G. (2003) Budding of crystalline domains in fluid membranes. *Physical Review. E, Statistical, Nonlinear and Soft Matter Physics*, **68**, 061905.

235. Koivusalo, M., Welch, C., Hayashi, H., Scott, C.C., Kim, M., Alexander, T., Touret, N., Hahn, K.M. and Grinstein, S. (2010) Amiloride inhibits macropinocytosis by lowering submembranous pH and preventing Rac1 and Cdc42 signaling. *The Journal of Cell Biology*, **188**, 547-563.

236. Köping-Höggård, M., Tubulekas, I., Guan, H., Edwards, K., Nilsson, M., Varum, K.M. and Artursson, P. (2001) Chitosan as a nonviral gene delivery system. Structure-property relationships and characteristics compared with polyethylenimine *in vitro* and after lung administration *in vivo*. *Gene Therapy*, **8**, 1108-1121.

237. Koziolkiewicz, M., Gendaszewska, E., Maszewska, M., Stein, C.A. and Stec, W.J. (2001) The mononucleotide-dependent, nonantisense mechanism of action of

phosphodiester and phosphorothioate oligonucleotides depends upon the activity of an ecto-5'-nucleotidase. *Blood*, **98**, 995-1002.

238. Kren, B.T., Wong, P.Y., Sarver, A., Zhang, X., Zeng, Y. and Steer, C.J. (2009) MicroRNAs identified in highly purified liver-derived mitochondria may play a role in apoptosis. *RNA Biology*, **6**, 65-72.

239. Krieg, A.M. (2002) CpG motifs in bacterial DNA and their immune effects. *Annual Review of Immunology*, **20**, 709-760.

240. Krieg, A.M., Yi, A.K., Matson, S., Waldschmidt, T.J., Bishop, G.A., Teasdale, R., Koretzky, G.A. and Klinman, D.M. (1995) CpG motifs in bacterial DNA trigger direct B-cell activation. *Nature*, **374**, 546-549.

241. Krützfeldt, J., Kuwajima, S., Braich, R., Rajeev, K.G., Pena, J., Tuschl, T., Manoharan, M. and Stoffel, M. (2007) Specificity, duplex degradation and subcellular localization of antagomirs. *Nucleic Acids Research*, **35**, 2885-2892.

242. Krützfeldt, J., Rajewsky, N., Braich, R., Rajeev, K.G., Tuschl, T., Manoharan, M. and Stoffel, M. (2005) Silencing of microRNAs *in vivo* with 'antagomirs'. *Nature*, **438**, 685-689.

243. Kubo, T., Yanagihara, K., Takei, Y., Mihara, K., Morita, Y. and Seyama, T. (2011) Palmitic acid-conjugated 21-nucleotide siRNA enhances gene-silencing activity. *Molecular Pharmaceutics*, **8**, 2193-2203.

244. Kulkarni, M., Ozgur, S. and Stoecklin, G. (2010) On track with P-bodies. *Biochemical Society Transactions*, **38**, 242-251.

245. Kumar, S., Aaron, J. and Sokolov, K. (2008) Directional conjugation of antibodies to nanoparticles for synthesis of multiplexed optical contrast agents with both delivery and targeting moieties. *Nature Protocols*, **3**, 314-320.

246. Kunath, K., von Harpe, A., Fischer, D. and Kissel, T. (2003) Galactose-PEI-DNA complexes for targeted gene delivery: degree of substitution affects complex size and transfection efficiency. *Journal of Controlled Release: Official Journal of the Controlled Release Society*, **88**, 159-172.

247. Kurreck, J. (2003) Antisense technologies. Improvement through novel chemical modifications. *European Journal of Biochemistry / FEBS*, **270**, 1628-1644.

248. Kurz, A., Bunge, A., Windeck, A.K., Rost, M., Flasche, W., Arbuzova, A., Strohbach, D., Muller, S., Liebscher, J., Huster, D. *et al.* (2006) Lipid-anchored oligonucleotides for stable double-helix formation in distinct membrane domains. *Angewandte Chemie International Edition in English*, **45**, 4440-4444.

249. Kuzmin, P.I., Akimov, S.A., Chizmadzhev, Y.A., Zimmerberg, J. and Cohen, F.S. (2005) Line tension and interaction energies of membrane rafts calculated from lipid splay and tilt. *Biophysical Journal*, **88**, 1120-1133.

250. Laing, B.M., Barrow-Laing, L., Harrington, M., Long, E.C. and Bergstrom, D.E. (2010) Properties of double-stranded oligonucleotides modified with lipophilic substituents. *Bioconjugate Chemistry*, **21**, 1537-1544.

251. Lares, M.R., Rossi, J.J. and Ouellet, D.L. (2010) RNAi and small interfering RNAs in human disease therapeutic applications. *Trends in Biotechnology*, **28**, 570-579.

252. Laufer, S.D. and Restle, T. (2008) Peptide-mediated cellular delivery of oligonucleotide-based therapeutics *in vitro*: quantitative evaluation of overall efficacy employing easy to handle reporter systems. *Current Pharmaceutical Design*, **14**, 3637-3655.

253. Lemaitre, M., Bayard, B. and Lebleu, B. (1987) Specific antiviral activity of a poly(L-lysine)-conjugated oligodeoxyribonucleotide sequence complementary to vesicular stomatitis virus N protein mRNA initiation site. *Proceedings of the National Academy of Sciences USA*, **84**, 648-652.

254. Lemarchand, C., Gref, R. and Couvreur, P. (2004) Polysaccharide-decorated nanoparticles. *European Journal of Pharmaceutics and Biopharmaceutics: Official Journal of Arbeitsgemeinschaft fur Pharmazeutische Verfahrenstechnik e.V*, **58**, 327-341.

255. Lennox, K.A. and Behlke, M.A. (2011) Chemical modification and design of anti-miRNA oligonucleotides. *Gene Therapy*, **18**, 1111-1120.

256. Leonetti, J.P., Mechti, N., Degols, G., Gagnor, C. and Lebleu, B. (1991) Intracellular distribution of microinjected antisense oligonucleotides. *Proceedings of the National Academy of Sciences USA*, **88**, 2702-2706.

257.   Leonetti, J.P., Rayner, B., Lemaitre, M., Gagnor, C., Milhaud, P.G., Imbach, J.L. and Lebleu, B. (1988) Antiviral activity of conjugates between poly(L-lysine) and synthetic oligodeoxyribonucleotides. *Gene*, **72**, 323-332.

258.   Letrou-Bonneval, E., Chevre, R., Lambert, O., Costet, P., Andre, C., Tellier, C. and Pitard, B. (2008) Galactosylated multimodular lipoplexes for specific gene transfer into primary hepatocytes. *The Journal of Gene Medicine*, **10**, 1198-1209.

259.   Leuschner, P.J., Ameres, S.L., Kueng, S. and Martinez, J. (2006) Cleavage of the siRNA passenger strand during RISC assembly in human cells. *EMBO Reports*, **7**, 314-320.

260.   Leventis, R. and Silvius, J.R. (1990) Interactions of mammalian cells with lipid dispersions containing novel metabolizable cationic amphiphiles. *Biochimica et Biophysica Acta*, **1023**, 124-132.

261.   Levin, A.A. (1999) A review of the issues in the pharmacokinetics and toxicology of phosphorothioate antisense oligonucleotides. *Biochimica et Biophysica Acta*, **1489**, 69-84.

262.   Lewis, B.P., Burge, C.B. and Bartel, D.P. (2005) Conserved seed pairing, often flanked by adenosines, indicates that thousands of human genes are microRNA targets. *Cell*, **120**, 15-20.

263.   Lindner, L.H., Brock, R., Arndt-Jovin, D. and Eibl, H. (2006) Structural variation of cationic lipids: minimum requirement for improved oligonucleotide delivery into cells. *Journal of Controlled Release: Official Journal of the Controlled Release Society*, **110**, 444-456.

264.   Lipowsky, R. (1992) Budding of membranes induced by intramembrane domains. *Journal de Physique II France*, **2**, 1825-1840.

265.   Lishko, V.K., Podolnikova, N.P., Yakubenko, V.P., Yakovlev, S., Medved, L., Yadav, S.P. and Ugarova, T.P. (2004) Multiple binding sites in fibrinogen for integrin alphaMbeta2 (Mac-1). *The Journal of Biological Chemistry*, **279**, 44897-44906.

266.   Lisziewicz, J., Sun, D., Weichold, F.F., Thierry, A.R., Lusso, P., Tang, J., Gallo, R.C. and Agrawal, S. (1994) Antisense oligodeoxynucleotide phosphorothioate

complementary to Gag mRNA blocks replication of human immunodeficiency virus type 1 in human peripheral blood cells. *Proceedings of the National Academy of Sciences USA*, **91**, 7942-7946.

267. Liu, H., Zhu, Z., Kang, H., Wu, Y., Sefan, K. and Tan, W. (2010) DNA-based micelles: synthesis, micellar properties and size-dependent cell permeability. *Chemistry*, **16**, 3791-3797.

268. Liu, J., Carmell, M.A., Rivas, F.V., Marsden, C.G., Thomson, J.M., Song, J.J., Hammond, S.M., Joshua-Tor, L. and Hannon, G.J. (2004) Argonaute2 is the catalytic engine of mammalian RNAi. *Science*, **305**, 1437-1441.

269. Loew, M., Springer, R., Scolari, S., Altenbrunn, F., Seitz, O., Liebscher, J., Huster, D., Herrmann, A. and Arbuzova, A. (2010) Lipid domain specific recruitment of lipophilic nucleic acids: a key for switchable functionalization of membranes. *Journal of the American Chemical Society*, **132**, 16066-16072.

270. Loke, S.L., Stein, C.A., Zhang, X.H., Mori, K., Nakanishi, M., Subasinghe, C., Cohen, J.S. and Neckers, L.M. (1989) Characterization of oligonucleotide transport into living cells. *Proceedings of the National Academy of Sciences USA*, **86**, 3474-3478.

271. Lonnberg, H. (2009) Solid-phase synthesis of oligonucleotide conjugates useful for delivery and targeting of potential nucleic acid therapeutics. *Bioconjugate Chemistry*, **20**, 1065-1094.

272. Lorenz, C., Hadwiger, P., John, M., Vornlocher, H.P. and Unverzagt, C. (2004) Steroid and lipid conjugates of siRNAs to enhance cellular uptake and gene silencing in liver cells. *Bioorganic & Medicinal Chemistry Letters*, **14**, 4975-4977.

273. Lorenz, P., Misteli, T., Baker, B.F., Bennett, C.F. and Spector, D.L. (2000) Nucleocytoplasmic shuttling: a novel *in vivo* property of antisense phosphorothioate oligodeoxynucleotides. *Nucleic Acids Research*, **28**, 582-592.

274. Love, K.T., Mahon, K.P., Levins, C.G., Whitehead, K.A., Querbes, W., Dorkin, J.R., Qin, J., Cantley, W., Qin, L.L., Racie, T. *et al.* (2010) Lipid-like materials for low-dose, *in vivo* gene silencing. *Proceedings of the National Academy of Sciences USA*, **107**, 1864-1869.

275. Lu, J., Qian, J., Chen, F., Tang, X., Li, C. and Cardoso, W.V. (2005) Differential expression of components of the microRNA machinery during mouse organogenesis. *Biochemical and Biophysical Research Communications*, **334**, 319-323.

276. Lubaroff, D.M. and Karan, D. (2009) CpG oligonucleotide as an adjuvant for the treatment of prostate cancer. *Advanced Drug Delivery Reviews*, **61**, 268-274.

277. MacKellar, C., Graham, D., Will, D.W., Burgess, S. and Brown, T. (1992) Synthesis and physical properties of anti-HIV antisense oligonucleotides bearing terminal lipophilic groups. *Nucleic Acids Research*, **20**, 3411-3417.

278. Mahato, R.I., Anwer, K., Tagliaferri, F., Meaney, C., Leonard, P., Wadhwa, M.S., Logan, M., French, M. and Rolland, A. (1998) Biodistribution and gene expression of lipid/plasmid complexes after systemic administration. *Human Gene Therapy*, **9**, 2083-2099.

279. Mahato, R.I., Cheng, K. and Guntaka, R.V. (2005) Modulation of gene expression by antisense and antigene oligodeoxynucleotides and small interfering RNA. *Expert Opinion on Drug Delivery*, **2**, 3-28.

280. Mahato, R.I., Smith, L.C. and Rolland, A. (1999) Pharmaceutical perspectives of nonviral gene therapy. *Advances in Genetics*, **41**, 95-156.

281. Mahato, R.I., Takemura, S., Akamatsu, K., Nishikawa, M., Takakura, Y. and Hashida, M. (1997) Physicochemical and disposition characteristics of antisense oligonucleotides complexed with glycosylated poly(L-lysine). *Biochemical Pharmacology*, **53**, 887-895.

282. Maier, M.A., Yannopoulos, C.G., Mohamed, N., Roland, A., Fritz, H., Mohan, V., Just, G. and Manoharan, M. (2003) Synthesis of antisense oligonucleotides conjugated to a multivalent carbohydrate cluster for cellular targeting. *Bioconjugate Chemistry*, **14**, 18-29.

283. Maiti, P.K., Çagin, T., Lin, S. and Goddard, W.A. (2005) Effect of Solvent and pH on the Structure of PAMAM Dendrimers. *Macromolecules*, **38**, 979-991.

284. Manche, L., Green, S.R., Schmedt, C. and Mathews, M.B. (1992) Interactions between double-stranded RNA regulators and the protein kinase DAI. *Molecular and Cellular Biology*, **12**, 5238-5248.

285. Maniak, M. (2001) Macropinocytosis. In Marsh, M. (ed.). *Endocytosis*. Oxford University Press, Oxford, United Kingdom, pp. 78-93.

286. Manoharan, M. (2001) In Crooke, R. M. (ed.), *Antisense Drug Technology*. Marcel Dekker Inc., New York, pp. 391-469.

287. Manoharan, M. (2002) Oligonucleotide conjugates as potential antisense drugs with improved uptake, biodistribution, targeted delivery, and mechanism of action. *Antisense & Nucleic Acid Drug Development*, **12**, 103-128.

288. Manoharan, M. (2004) RNA interference and chemically modified small interfering RNAs. *Current Opinion in Chemical Biology*, **8**, 570-579.

289. Marsh, D. (1996) Lateral pressure in membranes. *Biochimica et Biophysica Acta*, **1286**, 183-223.

290. Martinez, J., Patkaniowska, A., Urlaub, H., Luhrmann, R. and Tuschl, T. (2002) Single-stranded antisense siRNAs guide target RNA cleavage in RNAi. *Cell*, **110**, 563-574.

291. Maru, N., Shohda, K. and Sugawara, T. (2004) Assembling liposomes by means of an oligonucleotide tagged with a lipophilic unit. *Nucleic Acids Symposium Series (Oxford)*, 95-96.

292. Matranga, C., Tomari, Y., Shin, C., Bartel, D.P. and Zamore, P.D. (2005) Passenger-strand cleavage facilitates assembly of siRNA into Ago2-containing RNAi enzyme complexes. *Cell*, **123**, 607-620.

293. Matsukura, M., Shinozuka, K., Zon, G., Mitsuya, H., Reitz, M., Cohen, J.S. and Broder, S. (1987) Phosphorothioate analogs of oligodeoxynucleotides: inhibitors of replication and cytopathic effects of human immunodeficiency virus. *Proceedings of the National Academy of Sciences USA*, **84**, 7706-7710.

294. McIntosh, T.J. and Simon, S.A. (2007) Bilayers as protein solvents: role of bilayer structure and elastic properties. *The Journal of General Physiology*, **130**, 225-227.

295. McNamara, J.O., 2nd, Andrechek, E.R., Wang, Y., Viles, K.D., Rempel, R.E., Gilboa, E., Sullenger, B.A. and Giangrande, P.H. (2006) Cell type-specific delivery of siRNAs with aptamer-siRNA chimeras. *Nature Biotechnology*, **24**, 1005-1015.

296. Medina, R.A. and Owen, G.I. (2002) Glucose transporters: expression, regulation and cancer. *Biological Research*, **35**, 9-26.

297. Meidan, V.M., Cohen, J.S., Amariglio, N., Hirsch-Lerner, D. and Barenholz, Y. (2000) Interaction of oligonucleotides with cationic lipids: the relationship between electrostatics, hydration and state of aggregation. *Biochimica et Biophysica Acta*, **1464**, 251-261.

298. Meier, O., Boucke, K., Hammer, S.V., Keller, S., Stidwill, R.P., Hemmi, S. and Greber, U.F. (2002) Adenovirus triggers macropinocytosis and endosomal leakage together with its clathrin-mediated uptake. *The Journal of Cell Biology*, **158**, 1119-1131.

299. Meister, G., Landthaler, M., Patkaniowska, A., Dorsett, Y., Teng, G. and Tuschl, T. (2004) Human Argonaute2 mediates RNA cleavage targeted by miRNAs and siRNAs. *Molecular Cell*, **15**, 185-197.

300. Meister, G. and Tuschl, T. (2004) Mechanisms of gene silencing by double-stranded RNA. *Nature*, **431**, 343-349.

301. Midoux, P., Pichon, C., Yaouanc, J.J. and Jaffres, P.A. (2009) Chemical vectors for gene delivery: a current review on polymers, peptides and lipids containing histidine or imidazole as nucleic acids carriers. *British Journal of Pharmacology*, **157**, 166-178.

302. Miller, P.S., McParland, K.B., Jayaraman, K. and Ts'o, P.O. (1981) Biochemical and biological effects of nonionic nucleic acid methylphosphonates. *Biochemistry*, **20**, 1874-1880.

303. Miller, P.S., Yano, J., Yano, E., Carroll, C., Jayaraman, K. and Ts'o, P.O. (1979) Nonionic nucleic acid analogues. Synthesis and characterization of dideoxyribonucleoside methylphosphonates. *Biochemistry*, **18**, 5134-5143.

304. Mintzer, M.A. and Simanek, E.E. (2009) Nonviral vectors for gene delivery. *Chemical Reviews*, **109**, 259-302.

305. Miyagishi, M., Hayashi, M. and Taira, K. (2003) Comparison of the suppressive effects of antisense oligonucleotides and siRNAs directed against the same targets in mammalian cells. *Antisense & Nucleic Acid Drug Development*, **13**, 1-7.

306. Miyashita, T. (2004) Confocal microscopy for intracellular co-localization of proteins. *Methods in Molecular Biology*, **261**, 399-410.

307. Mologni, L., Nielsen, P.E. and Gambacorti-Passerini, C. (1999) *In vitro* transcriptional and translational block of the bcl-2 gene operated by peptide nucleic acid. *Biochemical and Biophysical Research Communications*, **264**, 537-543.

308. Monia, B.P., Lesnik, E.A., Gonzalez, C., Lima, W.F., McGee, D., Guinosso, C.J., Kawasaki, A.M., Cook, P.D. and Freier, S.M. (1993) Evaluation of 2'-modified oligonucleotides containing 2'-deoxy gaps as antisense inhibitors of gene expression. *The Journal of Biological Chemistry*, **268**, 14514-14522.

309. Monsigny, M., Midoux, P., Mayer, R. and Roche, A.C. (1999) Glycotargeting: influence of the sugar moiety on both the uptake and the intracellular trafficking of nucleic acid carried by glycosylated polymers. *Bioscience Reports*, **19**, 125-132.

310. Montanha, E.A., Pavinatto, F.J., Caseli, L., Kaczmarek, O., Liebscher, J., Huster, D. and Oliveira, O.N., Jr. (2010) Properties of lipophilic nucleoside monolayers at the air-water interface. *Colloids and Surfaces. B, Biointerfaces*, **77**, 161-165.

311. Montes, L.R., Alonso, A., Goni, F.M. and Bagatolli, L.A. (2007) Giant unilamellar vesicles electroformed from native membranes and organic lipid mixtures under physiological conditions. *Biophysical Journal*, **93**, 3548-3554.

312. Monticelli, S., Ansel, K.M., Xiao, C., Socci, N.D., Krichevsky, A.M., Thai, T.H., Rajewsky, N., Marks, D.S., Sander, C., Rajewsky, K. *et al.* (2005) MicroRNA profiling of the murine hematopoietic system. *Genome Biology*, **6**, R71.

313. Morimoto, K., Nishikawa, M., Kawakami, S., Nakano, T., Hattori, Y., Fumoto, S., Yamashita, F. and Hashida, M. (2003) Molecular weight-dependent gene transfection activity of unmodified and galactosylated polyethyleneimine on hepatoma cells and mouse liver. *Molecular Therapy: the Journal of the American Society of Gene Therapy*, **7**, 254-261.

314. Morishita, R., Higaki, J., Tomita, N. and Ogihara, T. (1998) Application of transcription factor "decoy" strategy as means of gene therapy and study of gene expression in cardiovascular disease. *Circulation Research*, **82**, 1023-1028.

315. Morris, M.C., Vidal, P., Chaloin, L., Heitz, F. and Divita, G. (1997) A new peptide vector for efficient delivery of oligonucleotides into mammalian cells. *Nucleic Acids Research*, **25**, 2730-2736.

316. Muratovska, A. and Eccles, M.R. (2004) Conjugate for efficient delivery of short interfering RNA (siRNA) into mammalian cells. *FEBS Letters*, **558**, 63-68.

317. Nag, A. and Ghosh, P.C. (1999) Assessment of targeting potential of galactosylated and mannosylated sterically stabilized liposomes to different cell types of mouse liver. *Journal of Drug Targeting*, **6**, 427-438.

318. Nagamatsu, S., Sawa, H., Wakizaka, A. and Hoshino, T. (1993) Expression of facilitative glucose transporter isoforms in human brain tumors. *Journal of Neurochemistry*, **61**, 2048-2053.

319. Nair, V. and Zavolan, M. (2006) Virus-encoded microRNAs: novel regulators of gene expression. *Trends in Microbiology*, **14**, 169-175.

320. Napoli, C., Lemieux, C. and Jorgensen, R. (1990) Introduction of a Chimeric Chalcone Synthase Gene into Petunia Results in Reversible Co-Suppression of Homologous Genes in trans. *Plant Cell*, **2**, 279-289.

321. Nelson, A.R., Borland, L., Allbritton, N.L. and Sims, C.E. (2007) Myristoyl-based transport of peptides into living cells. *Biochemistry*, **46**, 14771-14781.

322. Nelson, D.L. and Cox, M.M. (2008) *Lehninger Principles of Biochemistry*. 5th ed. W.H. Freeman.

323. Nielsen, P.E., Egholm, M., Berg, R.H. and Buchardt, O. (1991) Sequence-selective recognition of DNA by strand displacement with a thymine-substituted polyamide. *Science*, **254**, 1497-1500.

324. Nieva, J.L., Goni, F.M. and Alonso, A. (1989) Liposome fusion catalytically induced by phospholipase C. *Biochemistry*, **28**, 7364-7367.

325. Nishi, K. and Saigo, K. (2007) Cellular internalization of green fluorescent protein fused with herpes simplex virus protein VP22 via a lipid raft-mediated endocytic pathway independent of caveolae and Rho family GTPases but dependent on dynamin and Arf6. *The Journal of Biological Chemistry*, **282**, 27503-27517.

326. Nishina, K., Unno, T., Uno, Y., Kubodera, T., Kanouchi, T., Mizusawa, H. and Yokota, T. (2008) Efficient *in vivo* delivery of siRNA to the liver by conjugation of alpha-tocopherol. *Molecular Therapy: the Journal of the American Society of Gene Therapy*, **16**, 734-740.

327. Norbury, C.C., Hewlett, L.J., Prescott, A.R., Shastri, N. and Watts, C. (1995) Class I MHC presentation of exogenous soluble antigen via macropinocytosis in bone marrow macrophages. *Immunity*, **3**, 783-791.

328. Nossal, R. and Zimmerberg, J. (2002) Endocytosis: curvature to the ENTH degree. *Current Biology*, **12**, R770-772.

329. Oehlke, J., Scheller, A., Wiesner, B., Krause, E., Beyermann, M., Klauschenz, E., Melzig, M. and Bienert, M. (1998) Cellular uptake of an alpha-helical amphipathic model peptide with the potential to deliver polar compounds into the cell interior non-endocytically. *Biochimica et Biophysica Acta*, **1414**, 127-139.

330. Ohrt, T., Merkle, D., Birkenfeld, K., Echeverri, C.J. and Schwille, P. (2006) In situ fluorescence analysis demonstrates active siRNA exclusion from the nucleus by Exportin 5. *Nucleic Acids Research*, **34**, 1369-1380.

331. Oishi, M., Nagasaki, Y., Itaka, K., Nishiyama, N. and Kataoka, K. (2005) Lactosylated poly(ethylene glycol)-siRNA conjugate through acid-labile beta-thiopropionate linkage to construct pH-sensitive polyion complex micelles achieving enhanced gene silencing in hepatoma cells. *Journal of the American Chemical Society*, **127**, 1624-1625.

332. Opalinska, J.B. and Gewirtz, A.M. (2002) Nucleic-acid therapeutics: basic principles and recent applications. *Nature Reviews. Drug Discovery*, **1**, 503-514.

333. Opas, M. (1999) Fluorescence tracing of intracellular proteins. *Biotechnic & Histochemistry: Official Publication of the Biological Stain Commission*, **74**, 294-310.

334. Orlandi, P.A. and Fishman, P.H. (1998) Filipin-dependent inhibition of cholera toxin: evidence for toxin internalization and activation through caveolae-like domains. *The Journal of Cell Biology*, **141**, 905-915.

335. Orum, H. and Wengel, J. (2001) Locked nucleic acids: a promising molecular family for gene-function analysis and antisense drug development. *Current Opinion in Molecular Therapeutics*, **3**, 239-243.

336. Osaki, F., Kanamori, T., Sando, S., Sera, T. and Aoyama, Y. (2004) A quantum dot conjugated sugar ball and its cellular uptake. On the size effects of endocytosis in the subviral region. *Journal of the American Chemical Society*, **126**, 6520-6521.

337. Palumbo, S.L., Memmott, R.M., Uribe, D.J., Krotova-Khan, Y., Hurley, L.H. and Ebbinghaus, S.W. (2008) A novel G-quadruplex-forming GGA repeat region in the c-myb promoter is a critical regulator of promoter activity. *Nucleic Acids Research*, **36**, 1755-1769.

338. Park, T.G., Jeong, J.H. and Kim, S.W. (2006) Current status of polymeric gene delivery systems. *Advanced Drug Delivery Reviews*, **58**, 467-486.

339. Patel, L.N., Zaro, J.L. and Shen, W.C. (2007) Cell penetrating peptides: intracellular pathways and pharmaceutical perspectives. *Pharmaceutical Research*, **24**, 1977-1992.

340. Paterson, B.M., Roberts, B.E. and Kuff, E.L. (1977) Structural gene identification and mapping by DNA-mRNA hybrid-arrested cell-free translation. *Proceedings of the National Academy of Sciences USA*, **74**, 4370-4374.

341. Patil, S.D., Rhodes, D.G. and Burgess, D.J. (2005) DNA-based therapeutics and DNA delivery systems: a comprehensive review. *The Association of American Physicians and Surgeons Journal*, **7**, E61-77.

342. Peer, D., Karp, J.M., Hong, S., Farokhzad, O.C., Margalit, R. and Langer, R. (2007) Nanocarriers as an emerging platform for cancer therapy. *Nature Nanotechnology*, **2**, 751-760.

343. Penn, M.L., Grivel, J.C., Schramm, B., Goldsmith, M.A. and Margolis, L. (1999) CXCR4 utilization is sufficient to trigger CD4+ T cell depletion in HIV-1-infected

human lymphoid tissue. *Proceedings of the National Academy of Sciences USA*, **96**, 663-668.

344. Pestourie, C., Tavitian, B. and Duconge, F. (2005) Aptamers against extracellular targets for *in vivo* applications. *Biochimie*, **87**, 921-930.

345. Petrova, N.S., Chernikov, I.V., Meschaninova, M.I., Dovydenko, I.S., Venyaminova, A.G., Zenkova, M.A., Vlassov, V.V. and Chernolovskaya, E.L. (2012) Carrier-free cellular uptake and the gene-silencing activity of the lipophilic siRNAs is strongly affected by the length of the linker between siRNA and lipophilic group. *Nucleic Acids Research*, **40**, 2330-2344.

346. Pfeiffer, I. and Höök, F. (2004) Bivalent cholesterol-based coupling of oligonucletides to lipid membrane assemblies. *Journal of the American Chemical Society*, **126**, 10224-10225.

347. Pils, S., Schmitter, T., Neske, F. and Hauck, C.R. (2006) Quantification of bacterial invasion into adherent cells by flow cytometry. *Journal of Microbiological Methods*, **65**, 301-310.

348. Pirollo, K.F., Zon, G., Rait, A., Zhou, Q., Yu, W., Hogrefe, R. and Chang, E.H. (2006) Tumor-targeting nanoimmunoliposome complex for short interfering RNA delivery. *Human Gene Therapy*, **17**, 117-124.

349. Ponnappa, B.C. (2009) siRNA for inflammatory diseases. *Current Opinion in Investigational Drugs*, **10**, 418-424.

350. Pooga, M., Hallbrink, M., Zorko, M. and Langel, U. (1998) Cell penetration by transportan. *The FASEB Journal: Official Publication of the Federation of American Societies for Experimental Biology*, **12**, 67-77.

351. Postel, E.H., Flint, S.J., Kessler, D.J. and Hogan, M.E. (1991) Evidence that a triplex-forming oligodeoxyribonucleotide binds to the c-myc promoter in HeLa cells, thereby reducing c-myc mRNA levels. *Proceedings of the National Academy of Sciences USA*, **88**, 8227-8231.

352. Praseuth, D., Guieysse, A.L. and Helene, C. (1999) Triple helix formation and the antigene strategy for sequence-specific control of gene expression. *Biochimica et Biophysica Acta*, **1489**, 181-206.

353. Putnam, D. and Doody, A. (2006) RNA-interference effectors and their delivery. *Critical Reviews in Therapeutic Drug Carrier Systems*, **23**, 137-164.

354. Qi, P., Han, J.X., Lu, Y.Q., Wang, C. and Bu, F.F. (2006) Virus-encoded microRNAs: future therapeutic targets? *Cellular & Molecular Immunology*, **3**, 411-419.

355. Ray, A. and Norden, B. (2000) Peptide nucleic acid (PNA): its medical and biotechnical applications and promise for the future. *The FASEB journal: Official Publication of the Federation of American Societies for Experimental Biology*, **14**, 1041-1060.

356. Rejman, J., Bragonzi, A. and Conese, M. (2005) Role of clathrin- and caveolae-mediated endocytosis in gene transfer mediated by lipo- and polyplexes. *Molecular Therapy: The Journal of the American Society of Gene Therapy*, **12**, 468-474.

357. Resina, S., Prevot, P. and Thierry, A.R. (2009) Physico-chemical characteristics of lipoplexes influence cell uptake mechanisms and transfection efficacy. *PloS ONE*, **4**, e6058.

358. Rockwell, P., O'Connor, W.J., King, K., Goldstein, N.I., Zhang, L.M. and Stein, C.A. (1997) Cell-surface perturbations of the epidermal growth factor and vascular endothelial growth factor receptors by phosphorothioate oligodeoxynucleotides. *Proceedings of the National Academy of Sciences USA*, **94**, 6523-6528.

359. Rodriguez-Enriquez, S., Marin-Hernandez, A., Gallardo-Perez, J.C. and Moreno-Sanchez, R. (2009) Kinetics of transport and phosphorylation of glucose in cancer cells. *Journal of Cellular Physiology*, **221**, 552-559.

360. Ruffner, D.E., Dahm, S.C. and Uhlenbeck, O.C. (1989) Studies on the hammerhead RNA self-cleaving domain. *Gene*, **82**, 31-41.

361. Ruozi, B., Montanari, M., Vighi, E., Tosi, G., Tombesi, A., Battini, R., Restani, C., Leo, E., Forni, F. and Vandelli, M.A. (2009) Flow cytometry and live confocal analysis for the evaluation of the uptake and intracellular distribution of FITC-ODN into HaCaT cells. *Journal of Liposome Research*, **19**, 241-251.

362. Sakyo, T., Naraba, H., Teraoka, H. and Kitagawa, T. (2007) The intrinsic structure of glucose transporter isoforms Glut1 and Glut3 regulates their differential

distribution to detergent-resistant membrane domains in nonpolarized mammalian cells. *The FEBS Journal*, **274**, 2843-2853.

363. Sambrook, J., Fritsch, E.F. and Maniatis, T. (1989). *Molecular Cloning: A Laboratory Manual.* 2nd ed. Cold Spring Harbor, Cold Spring Harbor Laboratory Press.

364. Sannohe, Y. and Sugiyama, H. (2010) Overview of formation of G-quadruplex structures. *Current Protocols in Nucleic Acid Chemistry / edited by Serge L. Beaucage ... [et al.]*, **Chapter 17**, Unit 17.2. 1-17.

365. Santhakumaran, L.M., Thomas, T. and Thomas, T.J. (2004) Enhanced cellular uptake of a triplex-forming oligonucleotide by nanoparticle formation in the presence of polypropylenimine dendrimers. *Nucleic Acids Research*, **32**, 2102-2112.

366. Schiffelers, R.M., Ansari, A., Xu, J., Zhou, Q., Tang, Q., Storm, G., Molema, G., Lu, P.Y., Scaria, P.V. and Woodle, M.C. (2004) Cancer siRNA therapy by tumor selective delivery with ligand-targeted sterically stabilized nanoparticle. *Nucleic Acids Research*, **32**, e149.

367. Schmid, S.L. and Frolov, V.A. (2011) Dynamin: functional design of a membrane fission catalyst. *Annual Review of Cell and Developmental Biology*, **27**, 79-105.

368. Schmidt-Wolf, G.D. and Schmidt-Wolf, I.G. (2003) Non-viral and hybrid vectors in human gene therapy: an update. *Trends in Molecular Medicine*, **9**, 67-72.

369. Schnitzer, J.E., Oh, P., Pinney, E. and Allard, J. (1994) Filipin-sensitive caveolae-mediated transport in endothelium: reduced transcytosis, scavenger endocytosis, and capillary permeability of select macromolecules. *The Journal of Cell Biology*, **127**, 1217-1232.

370. Schroeder, A., Levins, C.G., Cortez, C., Langer, R. and Anderson, D.G. (2010) Lipid-based nanotherapeutics for siRNA delivery. *Journal of Internal Medicine*, **267**, 9-21.

371. Schwarz, D.S., Hutvagner, G., Du, T., Xu, Z., Aronin, N. and Zamore, P.D. (2003) Asymmetry in the assembly of the RNAi enzyme complex. *Cell*, **115**, 199-208.

372. Schwarze, S.R., Ho, A., Vocero-Akbani, A. and Dowdy, S.F. (1999) *In vivo* protein transduction: delivery of a biologically active protein into the mouse. *Science*, **285**, 1569-1572.

373. Selbach, M., Schwanhausser, B., Thierfelder, N., Fang, Z., Khanin, R. and Rajewsky, N. (2008) Widespread changes in protein synthesis induced by microRNAs. *Nature*, **455**, 58-63.

374. Sen, G.C. and Sarkar, S.N. (2007) The interferon-stimulated genes: targets of direct signaling by interferons, double-stranded RNA, and viruses. *Current Topics in Microbiology and Immunology*, **316**, 233-250.

375. Sengupta, P., Hammond, A., Holowka, D. and Baird, B. (2008) Structural determinants for partitioning of lipids and proteins between coexisting fluid phases in giant plasma membrane vesicles. *Biochimica et Biophysica Acta*, **1778**, 20-32.

376. Shea, R.G., Marsters, J.C. and Bischofberger, N. (1990) Synthesis, hybridization properties and antiviral activity of lipid-oligodeoxynucleotide conjugates. *Nucleic Acids Research*, **18**, 3777-3783.

377. Sheetz, M.P., Painter, R.G. and Singer, S.J. (1976) Biological membranes as bilayer couples. III. Compensatory shape changes induced in membranes. *The Journal of Cell Biology*, **70**, 193-203.

378. Sheetz, M.P. and Singer, S.J. (1974) Biological membranes as bilayer couples. A molecular mechanism of drug-erythrocyte interactions. *Proceedings of the National Academy of Sciences USA*, **71**, 4457-4461.

379. Shen, L.X., Kandimalla, E.R. and Agrawal, S. (1998) Impact of mixed-backbone oligonucleotides on target binding affinity and target cleaving specificity and selectivity by *Escherichia coli* RNase H. *Bioorganic & Medicinal Chemistry*, **6**, 1695-1705.

380. Shi, F. and Hoekstra, D. (2004) Effective intracellular delivery of oligonucleotides in order to make sense of antisense. *Journal of Controlled Release: Official Journal of the Controlled Release Society*, **97**, 189-209.

381. Shi, W., Gerster, K., Alajez, N.M., Tsang, J., Waldron, L., Pintilie, M., Hui, A.B., Sykes, J., P'ng, C., Miller, N. *et al.* (2011) MicroRNA-301 mediates proliferation and invasion in human breast cancer. *Cancer Research*, **71**, 2926-2937.

382. Shinoda, T., Maeda, A., Kojima, S., Kagatani, S., Konno, Y., Sonobe, T. and Akaike, T. (1999) Nanosphere Coated with Lactosyl-Polystyrene Polymer as a Targeting Carrier to Hepatocytes. *Drug Delivery*, **6**, 147-151.

383. Shnyrova, A.V., Frolov, V.A. and Zimmerberg, J. (2009) Domain-driven morphogenesis of cellular membranes. *Current Biology*, **19**, R772-780.

384. Siddiqui-Jain, A., Grand, C.L., Bearss, D.J. and Hurley, L.H. (2002) Direct evidence for a G-quadruplex in a promoter region and its targeting with a small molecule to repress c-MYC transcription. *Proceedings of the National Academy of Sciences USA*, **99**, 11593-11598.

385. Sierakowska, H., Sambade, M.J., Agrawal, S. and Kole, R. (1996) Repair of thalassemic human beta-globin mRNA in mammalian cells by antisense oligonucleotides. *Proceedings of the National Academy of Sciences USA*, **93**, 12840-12844.

386. Simeoni, F., Morris, M.C., Heitz, F. and Divita, G. (2003) Insight into the mechanism of the peptide-based gene delivery system MPG: implications for delivery of siRNA into mammalian cells. *Nucleic Acids Research*, **31**, 2717-2724.

387. Singh, Y., Murat, P. and Defrancq, E. (2010) Recent developments in oligonucleotide conjugation. *Chemical Society Reviews*, **39**, 2054-2070.

388. Singh, Y., Palombo, M. and Sinko, P.J. (2008) Recent trends in targeted anticancer prodrug and conjugate design. *Current Medicinal Chemistry*, **15**, 1802-1826.

389. Sliedregt, L.A., Rensen, P.C., Rump, E.T., van Santbrink, P.J., Bijsterbosch, M.K., Valentijn, A.R., van der Marel, G.A., van Boom, J.H., van Berkel, T.J. and Biessen, E.A. (1999) Design and synthesis of novel amphiphilic dendritic galactosides for selective targeting of liposomes to the hepatic asialoglycoprotein receptor. *Journal of Medicinal Chemistry*, **42**, 609-618.

390. Sonawane, N.D., Szoka, F.C., Jr. and Verkman, A.S. (2003) Chloride accumulation and swelling in endosomes enhances DNA transfer by polyamine-DNA polyplexes. *The Journal of Biological Chemistry*, **278**, 44826-44831.

391. Soomets, U., Lindgren, M., Gallet, X., Hallbrink, M., Elmquist, A., Balaspiri, L., Zorko, M., Pooga, M., Brasseur, R. and Langel, U. (2000) Deletion analogues of transportan. *Biochimica et Biophysica Acta*, **1467**, 165-176.

392. Soutschek, J., Akinc, A., Bramlage, B., Charisse, K., Constien, R., Donoghue, M., Elbashir, S., Geick, A., Hadwiger, P., Harborth, J. *et al.* (2004) Therapeutic silencing of an endogenous gene by systemic administration of modified siRNAs. *Nature*, **432**, 173-178.

393. Stahn, R., Grittner, C., Zeisig, R., Karsten, U., Felix, S.B. and Wenzel, K. (2001) Sialyl Lewis(x)-liposomes as vehicles for site-directed, E-selectin-mediated drug transfer into activated endothelial cells. *Cellular and Molecular Life Sciences*, **58**, 141-147.

394. Stein, C.A., Tonkinson, J.L., Zhang, L.M., Yakubov, L., Gervasoni, J., Taub, R. and Rotenberg, S.A. (1993) Dynamics of the internalization of phosphodiester oligodeoxynucleotides in HL60 cells. *Biochemistry*, **32**, 4855-4861.

395. Stephenson, M.L. and Zamecnik, P.C. (1978) Inhibition of Rous sarcoma viral RNA translation by a specific oligodeoxyribonucleotide. *Proceedings of the National Academy of Sciences USA*, **75**, 285-288.

396. Stewart, M.P., McDowall, A. and Hogg, N. (1998) LFA-1-mediated adhesion is regulated by cytoskeletal restraint and by a Ca2+-dependent protease, calpain. *The Journal of Cell Biology*, **140**, 699-707.

397. Summerton, J., Stein, D., Huang, S.B., Matthews, P., Weller, D. and Partridge, M. (1997) Morpholino and phosphorothioate antisense oligomers compared in cell-free and in-cell systems. *Antisense & Nucleic Acid Drug Development*, **7**, 63-70.

398. Summerton, J. and Weller, D. (1997) Morpholino antisense oligomers: design, preparation, and properties. *Antisense & Nucleic Acid Drug Development*, **7**, 187-195.

399. Sun, D., Guo, K., Rusche, J.J. and Hurley, L.H. (2005) Facilitation of a structural transition in the polypurine/polypyrimidine tract within the proximal promoter region of the human VEGF gene by the presence of potassium and G-quadruplex-interactive agents. *Nucleic Acids Research*, **33**, 6070-6080.

400. Sun, K., Wang, J., Zhang, J., Hua, M., Liu, C. and Chen, T. (2011) Dextran-g-PEI nanoparticles as a carrier for co-delivery of adriamycin and plasmid into osteosarcoma cells. *International Journal of Biological Macromolecules*, **49**, 173-180.

401. Sun, L.Q., Cairns, M.J., Saravolac, E.G., Baker, A. and Gerlach, W.L. (2000) Catalytic nucleic acids: from lab to applications. *Pharmacological Reviews*, **52**, 325-347.

402. Suzuki, T., Iwazaki, A., Katagiri, H., Oka, Y., Redpath, J.L., Stanbridge, E.J. and Kitagawa, T. (1999) Enhanced expression of glucose transporter GLUT3 in tumorigenic HeLa cell hybrids associated with tumor suppressor dysfunction. *European Journal of Biochemistry / FEBS*, **262**, 534-540.

403. Swanson, J.A. and Watts, C. (1995) Macropinocytosis. *Trends in Cell Biology*, **5**, 424-428.

404. Synnes, M., Prydz, K., Lovdal, T., Brech, A. and Berg, T. (1999) Fluid phase endocytosis and galactosyl receptor-mediated endocytosis employ different early endosomes. *Biochimica et Biophysica Acta*, **1421**, 317-328.

405. Szoka, F., Jr. and Papahadjopoulos, D. (1980) Comparative properties and methods of preparation of lipid vesicles (liposomes). *Annual Review of Biophysics and Bioengineering*, **9**, 467-508.

406. Taguchi, H. and Armarego, W.L. (1998) Glyceryl-ether monooxygenase [EC 1.14.16.5]. A microsomal enzyme of ether lipid metabolism. *Medicinal Research Reviews*, **18**, 43-89.

407. Takeshita, F. and Ochiya, T. (2006) Therapeutic potential of RNA interference against cancer. *Cancer Science*, **97**, 689-696.

408.   Taylor, M.F., Weller, D.D. and Kobzik, L. (1998) Effect of TNF-alpha antisense oligomers on cytokine production by primary murine alveolar macrophages. *Antisense & Nucleic Acid Drug Development*, **8**, 199-205.

409.   Teixeira, H., Rosilio, V., Laigle, A., Lepault, J., Erk, I., Scherman, D., Benita, S., Couvreur, P. and Dubernet, C. (2001) Characterization of oligonucleotide/lipid interactions in submicron cationic emulsions: influence of the cationic lipid structure and the presence of PEG-lipids. *Biophysical Chemistry*, **92**, 169-181.

410.   Thierry, A.R. and Dritschilo, A. (1992) Intracellular availability of unmodified, phosphorothioated and liposomally encapsulated oligodeoxynucleotides for antisense activity. *Nucleic Acids Research*, **20**, 5691-5698.

411.   Thoidis, G., Kupriyanova, T., Cunningham, J.M., Chen, P., Cadel, S., Foulon, T., Cohen, P., Fine, R.E. and Kandror, K.V. (1999) Glucose transporter Glut3 is targeted to secretory vesicles in neurons and PC12 cells. *The Journal of Biological Chemistry*, **274**, 14062-14066.

412.   Thorens, B. and Mueckler, M. (2010) Glucose transporters in the 21st Century. *American Journal of Physiology. Endocrinology and Metabolism*, **298**, E141-145.

413.   Tolia, N.H. and Joshua-Tor, L. (2007) Slicer and the argonautes. *Nature Chemical Biology*, **3**, 36-43.

414.   Tomita, N., Tomita, T., Yuyama, K., Tougan, T., Tajima, T., Ogihara, T. and Morishita, R. (2003) Development of novel decoy oligonucleotides: advantages of circular dumb-bell decoy. *Current Opinion in Molecular Therapeutics*, **5**, 107-112.

415.   Torres, A.G., Fabani, M.M., Vigorito, E., Williams, D., Al-Obaidi, N., Wojciechowski, F., Hudson, R.H., Seitz, O. and Gait, M.J. (2012) Chemical structure requirements and cellular targeting of microRNA-122 by peptide nucleic acids anti-miRs. *Nucleic Acids Research*, **40**, 2152-2167.

416.   Towbin, H., Staehelin, T. and Gordon, J. (1979) Electrophoretic transfer of proteins from polyacrylamide gels to nitrocellulose sheets: procedure and some applications. *Proceedings of the National Academy of Sciences USA*, **76**, 4350-4354.

417.   Trieu, A., Roberts, T.L., Dunn, J.A., Sweet, M.J. and Stacey, K.J. (2006) DNA motifs suppressing TLR9 responses. *Critical Reviews in Immunology*, **26**, 527-544.

418. Tuma, R.S., Beaudet, M.P., Jin, X., Jones, L.J., Cheung, C.Y., Yue, S. and Singer, V.L. (1999) Characterization of SYBR Gold nucleic acid gel stain: a dye optimized for use with 300-nm ultraviolet transilluminators. *Analytical Biochemistry*, **268**, 278-288.

419. Turner, J.J., Fabani, M., Arzumanov, A.A., Ivanova, G. and Gait, M.J. (2006) Targeting the HIV-1 RNA leader sequence with synthetic oligonucleotides and siRNA: chemistry and cell delivery. *Biochimica et Biophysica Acta*, **1758**, 290-300.

420. Ugarte-Uribe, B., Perez-Rentero, S., Lucas, R., Avino, A., Reina, J.J., Alkorta, I., Eritja, R. and Morales, J.C. (2010) Synthesis, cell-surface binding, and cellular uptake of fluorescently labeled glucose-DNA conjugates with different carbohydrate presentation. *Bioconjugate Chemistry*, **21**, 1280-1287.

421. Uline, M.J., Longo, G.S., Schick, M. and Szleifer, I. (2010) Calculating partition coefficients of chain anchors in liquid-ordered and liquid-disordered phases. *Biophysical Journal*, **98**, 1883-1892.

422. Usman, N. and Blatt, L.M. (2000) Nuclease-resistant synthetic ribozymes: developing a new class of therapeutics. *The Journal of Clinical Investigation*, **106**, 1197-1202.

423. Vaerman, J.L., Moureau, P., Deldime, F., Lewalle, P., Lammineur, C., Morschhauser, F. and Martiat, P. (1997) Antisense oligodeoxyribonucleotides suppress hematologic cell growth through stepwise release of deoxyribonucleotides. *Blood*, **90**, 331-339.

424. Valadi, H., Ekstrom, K., Bossios, A., Sjostrand, M., Lee, J.J. and Lotvall, J.O. (2007) Exosome-mediated transfer of mRNAs and microRNAs is a novel mechanism of genetic exchange between cells. *Nature Cell Biology*, **9**, 654-659.

425. Valberg, P.A., Brain, J.D. and Kane, D. (1981) Effects of colchicine or cytochalasin B on pulmonary macrophage endocytosis *in vivo*. *Journal of Applied Physiology: Respiratory, Environmental and Exercise Physiology*, **50**, 621-629.

426. van Duijvenbode, R.C., Borkovec, M. and Koper, G.J.M. (1998) Acid-base Properties of Poly(propylene imine) Dendrimers. *Polymers*, **39**, 2657-2664.

427. van Kooyk, Y. and Figdor, C.G. (2000) Avidity regulation of integrins: the driving force in leukocyte adhesion. *Current Opinion in Cell Biology*, **12**, 542-547.

428. van Meer, G. (2005) Cellular lipidomics. *EMBO Journal*, **24**, 3159-3165.

429. Vasquez, R.J., Howell, B., Yvon, A.M., Wadsworth, P. and Cassimeris, L. (1997) Nanomolar concentrations of nocodazole alter microtubule dynamic instability *in vivo* and *in vitro*. *Molecular Biology of the Cell*, **8**, 973-985.

430. Veldhoen, S., Laufer, S.D. and Restle, T. (2008) Recent developments in peptide-based nucleic acid delivery. *International Journal of Molecular Sciences*, **9**, 1276-1320.

431. Veldhoen, S., Laufer, S.D., Trampe, A. and Restle, T. (2006) Cellular delivery of small interfering RNA by a non-covalently attached cell-penetrating peptide: quantitative analysis of uptake and biological effect. *Nucleic Acids Research*, **34**, 6561-6573.

432. Vives, E., Brodin, P. and Lebleu, B. (1997) A truncated HIV-1 Tat protein basic domain rapidly translocates through the plasma membrane and accumulates in the cell nucleus. *The Journal of Biological Chemistry*, **272**, 16010-16017.

433. Wadia, J.S., Stan, R.V. and Dowdy, S.F. (2004) Transducible TAT-HA fusogenic peptide enhances escape of TAT-fusion proteins after lipid raft macropinocytosis. *Nature Medicine*, **10**, 310-315.

434. Wagner, E., Kircheis, R. and Walker, G.F. (2004) Targeted nucleic acid delivery into tumors: new avenues for cancer therapy. *Biomedicine & Pharmacotherapy = Biomedecine & Pharmacotherapie*, **58**, 152-161.

435. Wagner, H. (2001) Toll meets bacterial CpG-DNA. *Immunity*, **14**, 499-502.

436. Wahlestedt, C., Salmi, P., Good, L., Kela, J., Johnsson, T., Hokfelt, T., Broberger, C., Porreca, F., Lai, J., Ren, K. *et al.* (2000) Potent and nontoxic antisense oligonucleotides containing locked nucleic acids. *Proceedings of the National Academy of Sciences USA*, **97**, 5633-5638.

437. Wang, D.A., Narang, A.S., Kotb, M., Gaber, A.O., Miller, D.D., Kim, S.W. and Mahato, R.I. (2002) Novel branched poly(ethylenimine)-cholesterol water-soluble lipopolymers for gene delivery. *Biomacromolecules*, **3**, 1197-1207.

438. Wang, L.H., Rothberg, K.G. and Anderson, R.G. (1993) Mis-assembly of clathrin lattices on endosomes reveals a regulatory switch for coated pit formation. *The Journal of Cell Biology*, **123**, 1107-1117.

439. Wang, T.Y., Leventis, R. and Silvius, J.R. (2001) Partitioning of lipidated peptide sequences into liquid-ordered lipid domains in model and biological membranes. *Biochemistry*, **40**, 13031-13040.

440. Watanabe, M., Naraba, H., Sakyo, T. and Kitagawa, T. (2010) DNA damage-induced modulation of GLUT3 expression is mediated through p53-independent extracellular signal-regulated kinase signaling in HeLa cells. *Molecular Cancer Research*, **8**, 1547-1557.

441. Watson, P., Jones, A.T. and Stephens, D.J. (2005) Intracellular trafficking pathways and drug delivery: fluorescence imaging of living and fixed cells. *Advanced Drug Delivery Reviews*, **57**, 43-61.

442. Weiler, J., Hunziker, J. and Hall, J. (2006) Anti-miRNA oligonucleotides (AMOs): ammunition to target miRNAs implicated in human disease? *Gene Therapy*, **13**, 496-502.

443. Weiner, G.J. (2009) CpG oligodeoxynucleotide-based therapy of lymphoid malignancies. *Advanced Drug Delivery Reviews*, **61**, 263-267.

444. Weiner, G.J., Liu, H.M., Wooldridge, J.E., Dahle, C.E. and Krieg, A.M. (1997) Immunostimulatory oligodeoxynucleotides containing the CpG motif are effective as immune adjuvants in tumor antigen immunization. *Proceedings of the National Academy of Sciences USA*, **94**, 10833-10837.

445. Weisman, S., Hirsch-Lerner, D., Barenholz, Y. and Talmon, Y. (2004) Nanostructure of cationic lipid-oligonucleotide complexes. *Biophysical Journal*, **87**, 609-614.

446. Whitehead, K.A., Langer, R. and Anderson, D.G. (2009) Knocking down barriers: advances in siRNA delivery. *Nature Reviews. Drug Discovery*, **8**, 129-138.

447. Wickstrom, E. (1986) Oligodeoxynucleotide stability in subcellular extracts and culture media. *Journal of Biochemical and Biophysical Methods*, **13**, 97-102.

448. Wilhelmy, L. (1863) Ueber die abhangigkeit der capillaritats-constanten des alkohols von substanz und gestalt des benetzten festen korpers. *Annual Review of Physical Chemistry*, **119**, 177-217.

449. Wolff, J.A. and Rozema, D.B. (2008) Breaking the bonds: non-viral vectors become chemically dynamic. *Molecular Therapy: the Journal of the American Society of Gene Therapy*, **16**, 8-15.

450. Wolfrum, C., Shi, S., Jayaprakash, K.N., Jayaraman, M., Wang, G., Pandey, R.K., Rajeev, K.G., Nakayama, T., Charrise, K., Ndungo, E.M. *et al.* (2007) Mechanisms and optimization of *in vivo* delivery of lipophilic siRNAs. *Nature Biotechnology*, **25**, 1149-1157.

451. Wu, H., Lima, W.F. and Crooke, S.T. (1999) Properties of cloned and expressed human RNase H1. *The Journal of Biological Chemistry*, **274**, 28270-28278.

452. Wu, J., Liu, P., Zhu, J.L., Maddukuri, S. and Zern, M.A. (1998) Increased liver uptake of liposomes and improved targeting efficacy by labeling with asialofetuin in rodents. *Hepatology*, **27**, 772-778.

453. Wu, J., Nantz, M.H. and Zern, M.A. (2002) Targeting hepatocytes for drug and gene delivery: emerging novel approaches and applications. *Frontiers in Bioscience: a Journal and Virtual Library*, **7**, d717-725.

454. Wu, L., Tang, C. and Yin, C. (2010) Folate-mediated solid-liquid lipid nanoparticles for paclitaxel-coated poly(ethylene glycol). *Drug Development and Industrial Pharmacy*, **36**, 439-448.

455. Wu, R.P., Youngblood, D.S., Hassinger, J.N., Lovejoy, C.E., Nelson, M.H., Iversen, P.L. and Moulton, H.M. (2007) Cell-penetrating peptides as transporters for morpholino oligomers: effects of amino acid composition on intracellular delivery and cytotoxicity. *Nucleic Acids Research*, **35**, 5182-5191.

456. Wu-Pong, S., Weiss, T.L. and Hunt, C.A. (1994) Calcium dependent cellular uptake of a c-myc antisense oligonucleotide. *Cellular and Molecular Biology (Noisy-le-Grand)*, **40**, 843-850.

457. Xing, Z. and Whitton, J.L. (1992) Ribozymes which cleave arenavirus RNAs: identification of susceptible target sites and inhibition by target site secondary structure. *Journal of Virology*, **66**, 1361-1369.

458. Xu, L. and Anchordoquy, T. (2011) Drug delivery trends in clinical trials and translational medicine: challenges and opportunities in the delivery of nucleic acid-based therapeutics. *Journal of Pharmaceutical Sciences*, **100**, 38-52.

459. Yamaguchi, K., Papp, B., Zhang, D., Ali, A.N., Agrawal, S. and Byrn, R.A. (1997) The multiple inhibitory mechanisms of GEM 91, a gag antisense phosphorothioate oligonucleotide, for human immunodeficiency virus type 1. *AIDS Research and Human Retroviruses*, **13**, 545-554.

460. Yamazaki, N., Kojima, S. and Yokoyama, H. (2005) Biomedical nanotechnology for active drug delivery systems by applying sugar-chain molecular functions. *Current Applied Physics*, **5**, 112-117.

461. Yan, H. and Tram, K. (2007) Glycotargeting to improve cellular delivery efficiency of nucleic acids. *Glycoconjugate Journal*, **24**, 107-123.

462. Yanaihara, N., Caplen, N., Bowman, E., Seike, M., Kumamoto, K., Yi, M., Stephens, R.M., Okamoto, A., Yokota, J., Tanaka, T. *et al.* (2006) Unique microRNA molecular profiles in lung cancer diagnosis and prognosis. *Cancer Cell*, **9**, 189-198.

463. Yang, N., Ye, Z., Li, F. and Mahato, R.I. (2009) HPMA polymer-based site-specific delivery of oligonucleotides to hepatic stellate cells. *Bioconjugate Chemistry*, **20**, 213-221.

464. Ye, Z., Cheng, K., Guntaka, R.V. and Mahato, R.I. (2006) Receptor-mediated hepatic uptake of M6P-BSA-conjugated triplex-forming oligonucleotides in rats. *Bioconjugate Chemistry*, **17**, 823-830.

465. Ye, Z., Houssein, H.S. and Mahato, R.I. (2007) Bioconjugation of oligonucleotides for treating liver fibrosis. *Oligonucleotides*, **17**, 349-404.

466. Yi, R., O'Carroll, D., Pasolli, H.A., Zhang, Z., Dietrich, F.S., Tarakhovsky, A. and Fuchs, E. (2006) Morphogenesis in skin is governed by discrete sets of differentially expressed microRNAs. *Nature Genetics*, **38**, 356-362.

467. Yin, H., Moulton, H.M., Seow, Y., Boyd, C., Boutilier, J., Iverson, P. and Wood, M.J. (2008) Cell-penetrating peptide-conjugated antisense oligonucleotides restore systemic muscle and cardiac dystrophin expression and function. *Human Molecular Genetics*, **17**, 3909-3918.

468. You, J.O., Liu, Y.C. and Peng, C.A. (2006) Efficient gene transfection using chitosan-alginate core-shell nanoparticles. *International Journal of Nanomedicine*, **1**, 173-180.

469. Yu, W., Pirollo, K.F., Rait, A., Yu, B., Xiang, L.M., Huang, W.Q., Zhou, Q., Ertem, G. and Chang, E.H. (2004) A sterically stabilized immunolipoplex for systemic administration of a therapeutic gene. *Gene Therapy*, **11**, 1434-1440.

470. Zacharias, D.A., Violin, J.D., Newton, A.C. and Tsien, R.Y. (2002) Partitioning of lipid-modified monomeric GFPs into membrane microdomains of live cells. *Science*, **296**, 913-916.

471. Zamecnik, P.C. and Stephenson, M.L. (1978) Inhibition of Rous sarcoma virus replication and cell transformation by a specific oligodeoxynucleotide. *Proceedings of the National Academy of Sciences USA*, **75**, 280-284.

472. Zamore, P.D., Tuschl, T., Sharp, P.A. and Bartel, D.P. (2000) RNAi: double-stranded RNA directs the ATP-dependent cleavage of mRNA at 21 to 23 nucleotide intervals. *Cell*, **101**, 25-33.

473. Zaro, J.L., Rajapaksa, T.E., Okamoto, C.T. and Shen, W.C. (2005) Membrane transduction of oligoarginine in HeLa cells is not mediated by macropinocytosis. *Molecular Pharmaceutics*, **3**, 181-186.

474. Zatsepin, T.S. and Oretskaya, T.S. (2004) Synthesis and applications of oligonucleotide-carbohydrate conjugates. *Chemistry & Biodiversity*, **1**, 1401-1417.

475. Zelphati, O. and Szoka, F.C., Jr. (1996a) Intracellular distribution and mechanism of delivery of oligonucleotides mediated by cationic lipids. *Pharmaceutical Research*, **13**, 1367-1372.

476. Zelphati, O. and Szoka, F.C., Jr. (1996b) Mechanism of oligonucleotide release from cationic liposomes. *Proceedings of the National Academy of Sciences USA*, **93**, 11493-11498.

477.   Zhang, H., Ma, Y. and Sun, X.L. (2010) Recent developments in carbohydrate-decorated targeted drug/gene delivery. *Medicinal Research Reviews*, **30**, 270-289.

478.   Zhang, X., Jin, Y., Plummer, M.R., Pooyan, S., Gunaseelan, S. and Sinko, P.J. (2009) Endocytosis and membrane potential are required for HeLa cell uptake of R.I.-CKTat9, a retro-inverso Tat cell penetrating peptide. *Molecular Pharmaceutics*, **6**, 836-848.

479.   Zhao, Y., Samal, E. and Srivastava, D. (2005) Serum response factor regulates a muscle-specific microRNA that targets Hand2 during cardiogenesis. *Nature*, **436**, 214-220.

480.   Zhou, L., Lee, D.H., Plescia, J., Lau, C.Y. and Altieri, D.C. (1994) Differential ligand binding specificities of recombinant CD11b/CD18 integrin I-domain. *The Journal of Biological Chemistry*, **269**, 17075-17079.

Publications

Publications

Ugarte-Uribe, B., Perez-Rentero, S., Lucas, R., Avino, A., Reina, J.J., Alkorta, I., Eritja, R. and Morales, J.C. (2010) Synthesis, cell-surface binding, and cellular uptake of fluorescently labeled glucose-DNA conjugates with different carbohydrate presentation. *Bioconjugate Chemistry*, **21**, 1280-1287.

Manuscripts in preparation

Ugarte-Uribe, B., Grijalvo, S., Busto, J.V., Martín, C., Eritja, R., Goñi, F.M., Alkorta, I. "Synthesis, membrane incorporation in membrane model systems and cellular uptake of lipid-DNA conjugates with different alkyl presentations".

Ugarte-Uribe, B., Busto, J.V., Grijalvo, S., Eritja, R., Goñi, F.M., Alkorta, I. "Characterization of C_{28} lipid-DNA conjugate in membrane model systems of different lipid composition".

Ugarte-Uribe, B., Martín, C., Grijalvo, S., Eritja, R., Goñi, F.M., Alkorta, I. "Study of the celular uptake behaviours of C_{28} lipid-DNA conjúgate in different cell lines".

The ability of small nucleic acids to silence specific genes or inhibit the biological activity of specific proteins has generated great interest in their use as research tools and therapeutic agents. Unfortunately, biological applications of oligonucleotides meet with a huge limitation: their poor cellular accessibility. Thus, there is a big challenge for developing an appropriate delivery system in order to achieve their efficient cellular uptake.

Conjugation of appropriate molecules to small nucleic acids is advantageous over structural modifications because it could not only promote target specificity, but also improve their pharmacokinetic behaviours and cellular uptake efficiencies, endowing them with entirely new properties. In the present work different carbohydrate- and lipid-oligonucleotide conjugates have been studied as novel tools for targeted delivery and enhancement of cellular permeability.

According to the results obtained in this work, it was concluded that keeping a certain distance (15 to 18 atoms) between DNA and sugar modification could be important for a better incorporation of this type of conjugates into the target cell, being a useful requirement for further promising conjugate design. It was also confirmed that long or double-tailed lipid modifications are preferred for an enhanced incorporation into membrane-model and cell systems, being dual saturated lipid neighbouring modification (C_{28}) capable of inserting into both liquid-disordered and liquid-ordered phases of lipid bilayer systems. Interestingly, C_{28} lipid moiety provided efficient cellular incorporation mainly by macropinocytosis, without causing cytotoxicity in cells or altering the binding properties of the oligonucleotide part, thereby enabling binding to different molecules. All these features make C_{28} moiety a good conjugation candidate to be analysed in a wide range of nucleic acid-based molecules for improving oligonucleotide delivery.